

Feasibility of Granular Road and Shoulder Recycling

Final Report | April 2018



IOWA STATE UNIVERSITY
Institute for Transportation

Sponsored by
Iowa Highway Research Board
(IHRB Project TR-685)
Iowa Department of Transportation
(InTrans Project 15-526)

About the Institute for Transportation

The mission of the Institute for Transportation (InTrans) at Iowa State University is to develop and implement innovative methods, materials, and technologies for improving transportation efficiency, safety, reliability, and sustainability while improving the learning environment of students, faculty, and staff in transportation-related fields.

Disclaimer Notice

The contents of this report reflect the views of the authors, who are responsible for the facts and the accuracy of the information presented herein. The opinions, findings and conclusions expressed in this publication are those of the authors and not necessarily those of the sponsors.

The sponsors assume no liability for the contents or use of the information contained in this document. This report does not constitute a standard, specification, or regulation.

The sponsors do not endorse products or manufacturers. Trademarks or manufacturers' names appear in this report only because they are considered essential to the objective of the document.

Non-Discrimination Statement

Iowa State University does not discriminate on the basis of race, color, age, ethnicity, religion, national origin, pregnancy, sexual orientation, gender identity, genetic information, sex, marital status, disability, or status as a U.S. veteran. Inquiries regarding non-discrimination policies may be directed to Office of Equal Opportunity, Title IX/ADA Coordinator, and Affirmative Action Officer, 3350 Beardshear Hall, Ames, Iowa 50011, 515-294-7612, email eooffice@iastate.edu.

Iowa Department of Transportation Statements

Federal and state laws prohibit employment and/or public accommodation discrimination on the basis of age, color, creed, disability, gender identity, national origin, pregnancy, race, religion, sex, sexual orientation or veteran's status. If you believe you have been discriminated against, please contact the Iowa Civil Rights Commission at 800-457-4416 or the Iowa Department of Transportation affirmative action officer. If you need accommodations because of a disability to access the Iowa Department of Transportation's services, contact the agency's affirmative action officer at 800-262-0003.

The preparation of this report was financed in part through funds provided by the Iowa Department of Transportation through its "Second Revised Agreement for the Management of Research Conducted by Iowa State University for the Iowa Department of Transportation" and its amendments.

The opinions, findings, and conclusions expressed in this publication are those of the authors and not necessarily those of the Iowa Department of Transportation.

Technical Report Documentation Page

1. Report No. IHRB Project TR-685	2. Government Accession No.	3. Recipient's Catalog No.	
4. Title and Subtitle Feasibility of Granular Road and Shoulder Recycling		5. Report Date April 2018	
		6. Performing Organization Code	
7. Author(s) Cheng Li (orcid.org/0000-0003-0577-2117), Jeramy Ashlock (orcid.org/0000-0003-0677-9900), Bora Cetin (orcid.org/0000-0003-0415-7139), and Charles Jahren (orcid.org/0000-0003-2828-8483)		8. Performing Organization Report No. InTrans Project 15-526	
9. Performing Organization Name and Address Institute for Transportation Iowa State University 2711 South Loop Drive, Suite 4700 Ames, IA 50010-8664		10. Work Unit No. (TRAIS)	
		11. Contract or Grant No.	
12. Sponsoring Organization Name and Address Iowa Highway Research Board Iowa Department of Transportation 800 Lincoln Way Ames, IA 50010		13. Type of Report and Period Covered Final Report	
		14. Sponsoring Agency Code IHRB Project TR-685	
15. Supplementary Notes Visit www.intrans.iastate.edu for color pdfs of this and other research reports.			
16. Abstract <p>Granular-surfaced roads and shoulders frequently experience extensive surface damage caused by heavy agricultural traffic loads, freeze-thaw cycles, and wet-dry cycles, which increases maintenance requirements and reduces safety. The goal of this study was to cost-effectively recycle existing degraded granular surface materials while improving them to the optimum gradations and plasticity that will provide the best performance and durability. In this study, a series of laboratory tests was first conducted to quantify the influence of gradation and index properties on the mechanical performance of commonly used materials for granular-surfaced roads and shoulders. Using the optimum gradations and plasticity index ranges as design targets, field demonstration test sections were constructed and tested over the 2016-2017 seasonal freeze-thaw period to assess the performance of several selected materials and construction methods.</p> <p>Results of this study clearly demonstrate how index properties of granular materials, such as the maximum aggregate size, gradation, plasticity, and aggregate quality, significantly influence mechanical characteristics and field performance. Based on the laboratory and field evaluations, a performance-based free design method for determining the gradation and plasticity of granular surface materials was developed. To help secondary roads agencies implement the proposed method, a Microsoft Excel-based program was also developed to optimize the mixing ratios of two or three available quarry materials with a chosen thickness of existing surface material to reach the optimum gradation in terms of strength. To help secondary roads agencies more easily and accurately determine the plasticity of the existing granular surface materials to be recycled, various laboratory testing methods were statistically evaluated, and recommendations are provided. In addition to the optimized gradation and plasticity design, a new laboratory testing method was developed in this study to evaluate the quality, morphology changes, and compaction characteristics of granular materials under simulated compaction and traffic loading conditions.</p>			
17. Key Words design—gradation—granular-surfaced road—morphology—plasticity—recycling—specification—unpaved road		18. Distribution Statement No restrictions.	
19. Security Classification (of this report) Unclassified.	20. Security Classification (of this page) Unclassified.	21. No. of Pages 182	22. Price NA

FEASIBILITY OF GRANULAR ROAD AND SHOULDER RECYCLING

Final Report
April 2018

Principal Investigator

Jeremy C. Ashlock, Associate Professor
Institute for Transportation, Iowa State University

Co-Principal Investigators

Charles T. Jahren, Professor
Construction Management and Technology Program, Iowa State University

Bora Cetin, Assistant Professor
Institute for Transportation, Iowa State University

Research Assistant

Cheng Li

Authors

Cheng Li, Jeremy Ashlock, Bora Cetin, and Charles Jahren

Sponsored by
the Iowa Department of Transportation and
the Iowa Highway Research Board
(IHRB Project TR-685)

Preparation of this report was financed in part
through funds provided by the Iowa Department of Transportation
through its Research Management Agreement with the
Institute for Transportation
(InTrans Project 15-526)

A report from
Institute for Transportation
Iowa State University
2711 South Loop Drive, Suite 4700
Ames, IA 50010-8664
Phone: 515-294-8103 / Fax: 515-294-0467
www.intrans.iastate.edu

TABLE OF CONTENTS

ACKNOWLEDGMENTS	xiii
EXECUTIVE SUMMARY	xv
CHAPTER 1. INTRODUCTION	1
1.1 Statement of the Industrial and Technical Problems	1
1.2 Goal and Objectives of the Research	1
1.3 Organization of the Report.....	2
CHAPTER 2. ISSUES AND SPECIFICATIONS OF GRANULAR-SURFACED ROADS	3
2.1 Damage of Granular-Surfaced Roads in Iowa	3
2.2 Gradation and Plasticity of Granular Surface Materials	5
2.3 Specifications for Granular Surface Materials.....	9
2.4 Degradation and Morphology of Granular Materials	12
CHAPTER 3. LABORATORY EVALUATIONS OF GRADATION AND PLASTICITY EFFECTS	16
3.1 Introduction.....	16
3.2 Laboratory Testing Methods.....	16
3.3 Materials	19
3.4 Gradation Effects on the Soaked Bearing Capacity.....	22
3.5 Plasticity Effects on Undrained Shear Strength and Slaking Characteristics	30
3.6 Optimum Gradation and Plasticity Index for Granular Surface Materials	34
CHAPTER 4. DESIGN, CONSTRUCTION, AND PERFORMANCE OF FIELD TEST SECTIONS	36
4.1 Introduction.....	36
4.2 Field Testing Methods	38
4.3 Results of Pre-construction Tests and Visual Surveys	48
4.4 Design and Construction of the Test Sections	57
4.5 Performance of Granular-Surfaced Road Test Sections	70
4.6 Granular-surfaced Shoulder Sections	84
4.7 Conclusions.....	102
CHAPTER 5. STATISTICAL EVALUATION OF LABORATORY TESTS FOR DETERMINING SOIL PLASTICITY	104
5.1 Introduction.....	104
5.2 Various Tests for Determining Soil Consistency.....	105
5.3 Materials and Testing Methods.....	107
5.4 Correlations Between the Various Consistency Tests	110
5.5 Two-Way ANOVA-Based Repeatability and Reproducibility Analysis.....	114
5.6 Conclusions and Recommendations	119

CHAPTER 6. DEVELOPMENT OF A NEW LABORATORY TEST FOR EVALUATING QUALITY, MORPHOLOGY, AND COMPACTION CHARACTERISTICS OF GRANULAR MATERIALS	121
6.1 Introduction.....	121
6.2 Materials	122
6.3 Gyratory Compactor and Pressure Distribution Analyzer	122
6.4 Image Analysis.....	126
6.5 Image-Based Particle Size Analysis	127
6.6 Shortcomings of LA abrasion test.....	129
6.7 Particle Degradation and Morphology Changes Quantified by the GAIA Test.....	133
6.8 Compaction Characteristics and Changes in Shear Strength of the Five Materials	136
6.9 Conclusions.....	139
CHAPTER 7. CONCLUSIONS AND RECOMMENDATIONS.....	140
7.1 Key Findings of the Laboratory Study.....	140
7.2 Key Findings of the Field Study	140
7.3 Key Findings from the Statistical Evaluation of the Laboratory Testing Methods.....	141
7.4 Recommendations for Implementation of Research Results into Testing, Design, and Construction Procedures	142
7.5 Recommendations for Future Research and Further Implementation	143
REFERENCES	147
APPENDIX A. RESULTS OF SURVEY OF IOWA COUNTY ENGINEERS	155
APPENDIX B. FALL CONE LIQUID LIMIT AND BAR LINEAR SHRINKAGE TEST PROCEDURES.....	163

LIST OF FIGURES

Figure 2.1. Iowa map with the 46 counties that completed the web survey shown in blue.....	3
Figure 2.2. Percent of the 46 responding Iowa counties reporting a given granular road issue among their top three most observed	4
Figure 2.3. Number of the 46 responding Iowa counties ranking a given damage type as costing the most to mitigate	5
Figure 2.4. All counties responding to the survey highlighted, with those in gray reporting excessive fines caused by degradation of surface materials	7
Figure 2.5. All counties responding to the survey highlighted, with those in green reporting excessive fines that have migrated from the subgrade	7
Figure 2.6. All counties responding to the survey highlighted, with those in yellow reporting excessive fines from other sources	8
Figure 2.7. All counties responding to the survey highlighted, with those in orange reporting loss of fines.....	8
Figure 2.8. Surface course and shoulder material specifications used by counties that responded to survey	10
Figure 2.9. Relationship between shrinkage product, grading coefficient, and performance of surface course for gravel roads.....	11
Figure 2.10. Particle shape characterization at different scales	13
Figure 2.11. Comparison of computational geometry results to Krumbein and Sloss	14
Figure 3.1. Devices for (a) sieve analysis, (b) hydrometer analysis, (c) plastic limit, and (d) liquid limit tests	17
Figure 3.2. CBR test conducted on soaked specimens	18
Figure 3.3. Photographs of (a) UCS test and (b) slaking test after 1 minute and (c) 35 minutes on the control (C) and 4% bentonite-treated (B) 2-by-2 specimens	18
Figure 3.4. Particle size distribution curves of the existing surface material and virgin quarry materials relative to the Iowa DOT specifications	20
Figure 3.5. Proctor compaction curves for the existing surface and virgin quarry materials	21
Figure 3.6. Effect of (a) gravel content, (b) sand content, and (c) fines content on the soaked CBR of the existing surface aggregate specimens	24
Figure 3.7. Effect of (a) gravel content, (b) sand content, and (c) fines content on the soaked CBR for mixtures of existing (E) and virgin (V) surface materials.....	25
Figure 3.8. Particle size distribution curves of the 14 laboratory CBR test specimens compared to Iowa DOT Class A/B specification band.....	28
Figure 3.9. PSD curves generated using Fuller’s model with D_{max} of 1 in. and n value increasing from 0.1 to 0.7	28
Figure 3.10. Results of multiple regression analysis on soaked CBR test data: (a) 3D regression surface, (b) 2D contour map of regression surface.....	29
Figure 3.11. Schematics of particle packing states of a granular material with different gradations	30
Figure 3.12. Results of (a) UCS and (b) slaking tests conducted on 2-by-2 specimens of minus No. 40 materials treated with different percentages of bentonite.....	34
Figure 4.1. The selected granular-surfaced road section on County Road L66 in Pottawattamie County, Iowa	36

Figure 4.2. Shoulder test Site 1 on southbound T Ave. south of 205th St. in Boone County, Iowa	37
Figure 4.3. Shoulder test Site 2 on Exit 126 off-ramp of eastbound Highway 30 to D Ave. in Boone County, Iowa	38
Figure 4.4. DCP test performed on the Highway 30 off-ramp shoulder section	39
Figure 4.5. Example of DCP depth profiles; (a) cumulative blows, (b) DCPI, and (c) DCP-CBR	40
Figure 4.6. Zorn Model ZFG 3000 LWD used in this study	41
Figure 4.7. Dustometer test setup (a, b, and c) and a test conducted on the granular-surfaced road test sections (d)	44
Figure 4.8. Visualization of the Roadroid roughness test data collected on the L66 test sections on August 9, 2016	45
Figure 4.9. Cross-section profile of roadway and layout of the ground temperature sensors (not to scale)	47
Figure 4.10. Installation procedure for the subgrade temperature sensors	48
Figure 4.11. Particle size distributions of existing surface and subgrade materials of the selected granular-surfaced road section on CR L-66	49
Figure 4.12. Excavation performed on the test section to measure thickness of surface layer and identify the source of excessive fines	50
Figure 4.13. Depth profiles of gradation, Atterberg limit, and DCP-CBR values of excavated (a) Location 1 and (b) Location 2	51
Figure 4.14. Particle size distributions of existing surface and subgrade materials of T Ave. shoulder section	53
Figure 4.15. Survey photos of Highway 30 ramp section (granular shoulder test Site 2): (a) surface material on November 3, 2015, (b and c) edge drop-off on March 22, 2016.....	54
Figure 4.16. DCP depth profiles of Highway 30 ramp shoulder section; (a) cumulative blows, (b) DCPI, and (b) DCP-CBR.....	55
Figure 4.17. Particle size distributions of existing surface materials of Highway 30 ramp shoulder section (granular shoulder test Site 2)	56
Figure 4.18. Demonstration of using a vacuum street sweeper to remove fines of granular surface materials: (a) vacuum street sweeper, (b) vacuumed roadway surface with coarse material brushed to center and sides, (c) vacuum chute without a screen, (d) vacuum chute with screen installed to retain coarse material on road, (e) material in the hopper vacuumed without the screen, and (f) material in the hopper vacuumed with a screen	58
Figure 4.19. Particle size distributions of materials collected from street sweeper trial tests.....	59
Figure 4.20. Screenshot of the gradation optimization program	60
Figure 4.21. Nominal cross-section profiles of the granular-surfaced road test sections (not to scale).....	61

Figure 4.22. Construction procedures for the granular-surfaced road test sections: (a) placing virgin aggregate with dump trucks, (b) mixing the virgin and existing surface material with motor graders, (c) spreading water to increase water content for compaction, (d) incorporating bentonite powder with the tractor-powered soil reclaimer, (e) compacting the new surface layer with a vibratory smooth drum roller, and (f) the bentonite-treated surface material after compaction.....	62
Figure 4.23. Construction of Test Section 3: (a) mixing Virgin Aggregate 2 with existing surface material using FAE reclaimer, (b) checking plasticity of fine particles, (c) the new surface material after compaction, and (d) Virgin Aggregate 2 of the stockpile in the quarry	63
Figure 4.24. Gradations of Virgin Aggregate 2 provided by quarry and tested at ISU lab, and resulting gradation of the as-constructed mixture of Section 3.....	64
Figure 4.25. As-constructed gradations of representative samples from the granular surfaces of test sections.....	65
Figure 4.26. Performance predications based on the material selection chart developed by Paige-Green (1989) in South Africa	66
Figure 4.27. Nominal cross-section profiles (not to scale) of the shoulder test sections on (a) T Ave. and (b) Highway 30 EB off-ramp.....	67
Figure 4.28. Construction procedures of granular-surfaced shoulder test sections: (a) removing existing T Ave. shoulder surface material with a motor grader, (b) mixing virgin and existing material on road surface and placing back on the shoulder, (c) spreading bentonite powder on surface of Section 2 and spraying with water, (d) incorporating bentonite with a soil tiller, (e) shaping the treated material with a motor grader, and (f) compacting using a rubber tire roller.....	68
Figure 4.29. As-constructed gradations of representative samples of T Ave. shoulder test sections.....	69
Figure 4.30. As-constructed gradations of representative samples of Highway 30 off-ramp shoulder test sections	70
Figure 4.31. Ground temperature data of the center and shoulder locations of the granular-surfaced road test site on CR L-66	72
Figure 4.32. Temperature differences at the same depths between the center and shoulder locations	73
Figure 4.33. 2016-2017 subgrade freezing-thawing period of the CR L-66 site	73
Figure 4.34. Survey photos taken on July 22, 2016 by Pottawattamie County Engineer John Rasmussen	74
Figure 4.35. Survey photos taken during the 2016-2017 freezing and thawing period.....	76
Figure 4.36. Calculated IRI (cIRI) and average coefficient of friction (μ) values of test section surfaces as estimated by Roadroid smartphone app	77
Figure 4.37. (a) Average measured in situ DCP-CBR _{AGG} and predicted soaked CBR values, (b) average in situ composite modulus values of the four test sections (bars indicate range of measured values).....	79
Figure 4.38. Back-calculated elastic modulus values from MASW tests for (a) granular surface layer and (b) subgrade	80
Figure 4.39. Gradation and plasticity of the bentonite-treated Section 1 over 10-month time period	82

Figure 4.40. Gradation and plasticity of optimal gradation Section 2 over 10-month time period	83
Figure 4.41. Gradation and plasticity of finer gradation Section 3 over 10-month time period	84
Figure 4.42. Survey photos of T Ave. shoulder test sections taken on June 24, 2016	85
Figure 4.43. Survey photos of T Ave. shoulder test sections taken on August 30, 2016	86
Figure 4.44. Survey photos of T Ave. shoulder test sections taken on November 7, 2016.....	87
Figure 4.45. Survey photos of T Ave. shoulder test sections taken during thawing period on February 12, 2017	88
Figure 4.46. Survey photos of T Ave. shoulder test sections taken on April 20, 2017	89
Figure 4.47. Results of field tests on T Ave. shoulder test sections: (a) In situ CBR values from DCP tests, (b) in situ composite modulus values from FWD tests	90
Figure 4.48. Gradation and plasticity of the Class A control Section 1 over 10-month time period	91
Figure 4.49. Gradation and plasticity of bentonite-treated Section 2 over 10-month time period	92
Figure 4.50. Gradation and plasticity of optimal gradation Section 3 over 10-month time period	92
Figure 4.51. Survey photos of Highway 30 off-ramp shoulder sections from June 23, 2016.....	93
Figure 4.52. Survey photos of Highway 30 off-ramp shoulder sections from August 30, 2016.....	94
Figure 4.53. Survey photos of Hwy 30 off-ramp shoulder sections from November 7, 2016.....	95
Figure 4.54. Survey photos of Hwy 30 off-ramp shoulder sections from February 12, 2017.....	96
Figure 4.55. Survey photos of Hwy 30 off-ramp shoulder sections from April 20, 2017	97
Figure 4.56. As-constructed DCP depth profiles of the Highway 30 off-ramp shoulder test sections: (a and d) cumulative blows, (b and e) DCPI, and (c and f) DCP-CBR	98
Figure 4.57. Post-thawing DCP depth profiles of the Highway 30 off-ramp shoulder test sections: (a and d) cumulative blows, (b and e) DCPI, and (c and f) DCP-CBR	99
Figure 4.58. (a) In situ CBR values and (b) in situ composite modulus values of the Highway 30 ramp shoulder test sections.....	100
Figure 4.59. Gradation and plasticity changes of bentonite-treated ramp shoulder Section 1.....	101
Figure 4.60. Gradation and plasticity changes of ramp shoulder control Section 2	102
Figure 5.1. Example of using fall cone test results to determine LL and PI.....	106
Figure 5.2. Particle size distribution of the granular surface material from CR L-66	108
Figure 5.3. Test devices used in this study: (a) Casagrande LL test device, (b) PL rolling device, (c) fall cone test device, (d) BLS mold, and (e) BLS test specimen in the oven	109
Figure 5.4. Correlation between LL values determined using Casagrande cup and fall cone device (three operators times three replicates for each bentonite content).....	111
Figure 5.5. (a) PI and (b) PL values determined using the fall cone and ASTM-standardized methods	112

Figure 5.6. Correlation between BLS values and PI determined by ASTM methods (Casagrande cup for LL and plastic limit roller for PL) for five testing samples	114
Figure 6.1. (a) Photo of gyratory compactor and PDA, (b) schematic of the gyratory compactor, (c) schematic of the PDA	124
Figure 6.2. (a) Optical scanner used in this study, (b) example original scanned color image of gravel-size aggregates, (c) converted binary image with aggregate edges detected	127
Figure 6.3. Comparison of PSD curves for ESA material determined by sieve analysis and 2D image analysis using three different methods for estimating particle sizes, with tabulated data for other materials	128
Figure 6.4. Standard initial Gradings A and B of the LA abrasion test and gradations of specimens after testing	130
Figure 6.5. Comparison of percent abrasion loss in LA abrasion tests and gyratory compaction tests for the five specimens.....	131
Figure 6.6. PSD curves of gravel fraction of road rock specimen before and after gyratory compaction test, as determined by 2D image analyses	132
Figure 6.7. Correlation between initial gravel content of specimens and their total breakage caused by gyratory compaction tests, as measured by image analysis.....	133
Figure 6.8. (a) Pre- and post-test gradations and (b) sphericities of the gravel-size aggregates of the concrete stone specimen determined by 2D image analysis.....	134
Figure 6.9. (a) Pre- and post-test gradations and (b) sphericities of the gravel-size aggregates of the existing surface aggregate specimen determined by 2D image analysis.....	135
Figure 6.10. Changes in void ratio and shear resistance of the five material types during gyratory compaction tests	137
Figure 6.11. Density-shear resistance-compaction energy relationship for the road rock specimen.....	138

LIST OF TABLES

Table 2.1. DOT granular surface material specifications (percent passing) for Iowa and surrounding states	9
Table 2.2. Current granular surface material specifications used by the Iowa DOT and some of the surveyed counties	10
Table 3.1. Soil index properties of the two types of granular surface materials.....	19
Table 3.2. Laboratory as-compacted and soaked CBR test results of the existing surface and virgin quarry materials	21
Table 3.3 Chemical composition of the bentonite powder used in the laboratory study	22
Table 3.4. Results of laboratory soaked CBR tests on existing aggregate specimens with different gradations achieved by sieving minus No. 40 material.....	23
Table 3.5. Gradations, Fuller’s model parameters, and CBR test results of the 14 specimens tested in this study	27
Table 3.6. UCS test results for 2-by-2 specimens treated with different percentages of bentonite.....	32
Table 3.7. Slaking test results for 2-by-2 specimens treated with different percentages of bentonite.....	33
Table 4.1. Properties of the Zorn ZFG 3000 LWD.....	41
Table 4.2. Configuration used for the MASW test	42
Table 4.3. Unpaved road surface condition rating report	46
Table 4.4. Pre-construction DCP test results of the selected road section on CR L-66.....	49
Table 4.5. Pre-construction DCP test results of granular shoulder test Site 1	52
Table 4.6. Typical damage types, possible causes, and gradation issues for the existing surface materials of test sections.....	56
Table 4.7. Surface damage and maintenance activities of the test sections documented by the county motor grader operator.....	78
Table 4.8. Dustometer test results of the four granular-surfaced test sections	80
Table 5.1. Trough designs and drying methods for various BLS testing standards	107
Table 5.2. Chemical composition of the bentonite used in the laboratory study.....	108
Table 5.3. Correlations between the Casagrande cup and fall cone liquid limit test results	112
Table 5.4. Typical two-way ANOVA table for the gauge R&R study.....	115
Table 5.5. Laboratory testing matrix used in this study.....	117
Table 5.6. Repeatability and reproducibility results reported in ASTM D4318 and determined by two-way ANOVA-based analysis for the various laboratory tests.....	118
Table 6.1. Properties of the five granular materials tested in this study	122
Table 6.2. Equipment operation parameters of the gyratory compactor.....	124

ACKNOWLEDGMENTS

The research project was sponsored by the Iowa Highway Research Board (IHRB) and the Iowa Department of Transportation (DOT). The authors are grateful for this support. The authors would like to acknowledge the assistance of the Pottawattamie County and Iowa District I engineers (John Rasmussen, Jeff DeVries, Jeff Vander Zwaag, and Jesse Tibodeau) in constructing and monitoring the test sections. The assistance of the Iowa DOT Materials Testing Laboratory and undergraduate and graduate research assistants Yijun Wu, Sajjad Satvati, Raymond Kakala, HaSung Kim, Thomas Berry, Aleksei Hnastchenko, Ziqiang Xue, and Tiancheng Hu in performing laboratory and field testing are also greatly appreciated.

EXECUTIVE SUMMARY

When water receded from the massive 2011 Missouri River flood, granular-surfaced roads in Pottawattamie County, Iowa, were buried under layers of loessial silt, the fine-grained soil of western Iowa's scenic Loess Hills. To reopen the rural roads, the county desired a way to recover the existing aggregate from the contaminated surface materials rather than simply scraping the roads and starting over with all new materials. Not having a practical solution at the time, the county opted for the latter approach. However, the need remained for a practical and efficient solution to recycle existing contaminated or degraded granular-road surfacing materials to restore them to their original performance levels.

In this project, a laboratory study was first conducted to evaluate the feasibility of screening off the excessive fines in the contaminated granular surface materials to restore the roads to their original mechanical performance levels. Several potential types of large, specialized construction equipment that could help perform this task were evaluated in a desk study, and field trial tests using a vacuum street sweeper were conducted. Based on the laboratory soaked California Bearing Ratio (CBR) test results, it was determined that the undrained bearing capacity of granular surface materials does not simply increase with decreasing fines content or increasing top size. Instead, there is an optimum gradation (or particle size distribution and packing) that results in the greatest soaked bearing capacity.

In addition, the desk evaluation of the potential construction equipment and field trial tests revealed that the original concept of screening materials out of the road was not cost-effective due to the high equipment cost and low production rates. Furthermore, field and laboratory measurements revealed that the reconstructed roads in the county contained significant fines coming not from the loess subgrade soils, as initially suspected, but from degradation of the relatively low-strength limestone aggregate surfacing materials. The research focus therefore shifted from the relatively specialized scope of removing low-quality fines to a problem with much broader applicability to all gravel roads: keeping the existing high-quality materials and adding back only what is missing from the optimum gradation to deliver the best longevity and performance.

At the beginning of the project, a web survey was distributed to Iowa county engineers regarding the performance, maintenance issues, and specifications of their granular-surfaced roads. Based on the survey results, it was concluded that granular surface materials being worn down by traffic to a finer gradation is a widespread issue that can greatly influence the performance and longevity of the roads. A comprehensive literature review revealed that the mechanical performance and durability of granular surface materials is a function of four material properties: gradation, plasticity, quality, and particle morphology. Based on the needs identified in the survey, the project was then focused on developing performance-based design and testing methods to provide state secondary roads departments with more cost-effective solutions to build or reconstruct granular road systems with improved performance and durability while recycling as much of the existing materials as possible.

A series of laboratory tests was conducted to quantify the effects of gradation and plasticity on the mechanical performance of granular road surfacing materials. The laboratory soaked CBR test results revealed that there is an optimum gradation that can result in the greatest soaked bearing capacity. Multiple regression analyses conducted on the laboratory test results indicated that the optimal gradation in terms of the soaked CBR of a well-graded granular material can be predicted based on its top size and the shape parameter (n) of the particle size distribution (PSD) curve determined using Fuller's model. Laboratory tests were also conducted to determine the optimal plasticity index with respect to shear strength and slaking characteristics. The results showed that adding plastic fines to granular surface materials can reduce their shear strength under wet conditions but greatly improve their slaking performance and therefore reduce material loss. Based on these key findings, a complete set of testing, design, and construction procedures for building or reconstructing granular-surfaced roads was proposed.

To validate the proposed methods, field granular-surfaced road and shoulder test sections were designed and constructed in Pottawattamie County and Boone County, Iowa, in summer 2016. To help local roads agencies implement the proposed design methods and recycle existing degraded surface materials, a Microsoft Excel-based program was developed to optimize proportions of existing surface materials and two or three available quarry materials to reach the target optimal gradation. Performance-based field tests and visual surveys were conducted on the test sections following construction and after the 2016-2017 freeze-thaw season to compare the as-constructed performance and freeze-thaw durability of the various test sections.

The field test results further validated the performance of the proposed methods. The road section with the optimal gradation without bentonite showed better performance than the control section and yielded the smallest reduction in stiffness and strength among all the test sections after the freeze-thaw season. The test section with the optimal gradation and plasticity (by incorporating bentonite) yielded the best as-constructed performance and lowest dust emissions. However, visual observations and laboratory plasticity test results revealed that the bentonite content decreased significantly after one freeze-thaw season. For the shoulder test sections, the field and laboratory test results also showed that precipitation and traffic can quickly wash and blow away the small amount of incorporated bentonite, thus significantly reducing its beneficial binding effects. Based on the testing results and field observations, incorporating a greater concentration of low plasticity clay to achieve the target plasticity index of granular surface materials may be a better long-term solution.

During this project, several issues with current laboratory testing methods used to determine plasticity and aggregate quality were also identified, and alternative testing methods were evaluated and developed to address the issues. For the Atterberg limits tests, a two-way repeatability and reproducibility (R&R) analysis based on analysis of variance (ANOVA) revealed that the conventional Casagrande cup test used to determine the liquid limit is greatly influenced by the inter-operator variability, and the overall variation of the test results was 1.8%. The alternative fall cone liquid limit test showed much smaller overall variations than the Casagrande cup test, and results from the two test methods correlated very well ($R^2 = 0.98$). Additionally, the fall cone test was found to be easier to perform and less influenced by inter-operator variability. Therefore, use of the fall cone test is recommended for local roads agencies to more easily and reliably determine liquid limit compared to the Casagrande cup test. For the

plastic limit test, the ASTM roller method performs better than the conventional hand-rolling method in terms of repeatability and reproducibility.

In this study, a new laboratory testing method termed the “Gyratory Abrasion and Image Analysis (GAIA)” test was also developed to quickly evaluate the mechanical degradation, morphology, and shear strength of granular materials under simulated field loading conditions. Comparisons between the GAIA test and the Los Angeles (LA) abrasion test, which is commonly used for evaluating aggregate quality, revealed several shortcomings of the latter. The laboratory evaluation results demonstrated that the newly proposed GAIA test can address all of the identified issues. Additionally, various parameters determined by the GAIA test can be used to better understand the behavior of granular materials during compaction and to develop performance-based quality control/quality assurance (QC/QA) specifications for ensuring the quality and compaction of granular materials.

In addition to the recommendations provided for implementation of the research findings into testing, design, and construction procedures, several conclusions and recommendations for further research are identified in the final chapter of this report. It should be noted that the findings of this study were based upon evaluation of the crushed limestone materials local to Pottawattamie County. Further validations or calibrations of the proposed methods are recommended for materials having different morphology and mineralogy, such as rounded river gravels or higher strength dolomitic limestones occurring elsewhere throughout the state.

CHAPTER 1. INTRODUCTION

This project focused on improving the performance and durability of granular-surfaced roads and shoulders by recycling existing surface materials and blending them with fresh quarry aggregates to achieve optimum target gradations and plasticity indices. This chapter describes the industry and technical problems, presents the research objectives, and provides an overview of the report.

1.1 Statement of the Industrial and Technical Problems

Unpaved roads including granular-surfaced and gravel roads comprise 34% of the 4.2 million total miles of public roadways in the United States (FHWA 2014). In addition, damaged or aged paved low-volume roads in many states are sometimes converted to unpaved roads. Many agencies upgrade unpaved roads with little or no preparation of the foundation layers, which can lead to asphalt and portland cement concrete (PCC) surface courses that rapidly deteriorate and are more difficult and expensive to maintain (Fay et al. 2016). Compared to paved roads, granular-surfaced roads are more prone to extensive surface damage resulting from heavy agricultural traffic loads as well as freeze-thaw and wet-dry cycles. Current practice to address such damage typically involves covering the entire road surface with fresh aggregate followed by blading with little or no compaction. Furthermore, most state department of transportation (DOT) specifications for the gradation and plasticity of granular surface materials are neither performance based nor strictly followed. Consequently, sub-optimal gradations can be placed, leading to freshly placed aggregate material rapidly degrading to smaller particles and generating fugitive dust, which further contributes to a costly cycle of recurring maintenance.

Granular surface materials are quite different from pavement base materials in that the latter usually have a larger top size and contain a very low percentage of fines to provide sufficient drainage. If used as a granular surface course, typical pavement base materials would result in a surface that is unstable and difficult to maintain (Légère and Mercier 2004, Skorseth and Selim 2000). Therefore, granular-surfaced roads typically require a smaller top size for better stability and ride quality, and a small amount of plastic fines to bind the aggregate together and reduce aggregate loss. The importance of the index properties of granular road surface materials such as maximum aggregate size, gradation, plasticity, and abrasion characteristics has long been recognized (Hudson et al. 1986, Jones 2015, Paige-Green 1998, Skorseth and Selim 2000, Van Zyl et al. 2007). However, very few studies to date have focused on quantifying the effects of gradation and plasticity on the performance and durability of granular surface materials.

1.2 Goal and Objectives of the Research

The goal of this study was to develop an approach to cost-effectively recycle existing degraded granular surface materials by mixing them with fresh aggregates in optimized proportions to achieve a target gradation and plasticity that will maximize performance and durability. The specific objectives of this research are as follows:

1. Conduct a literature review and a web survey of county engineers to identify performance issues for granular-surfaced roads in the state of Iowa and evaluate current specifications for the gradation and plasticity of the granular surface course materials.
2. Conduct a laboratory study to quantify the effects of variations in gradation and plasticity on the mechanical characteristics of typical granular surface course materials.
3. Identify the optimum gradation and plasticity ranges that will lead to increased strength and reduced damage from freezing-thawing and wetting-drying cycles.
4. Construct granular-surfaced road and shoulder test sections using the optimum gradation and plasticity specifications to validate the laboratory test results and assess actual field performance through a seasonal winter-spring freeze-thaw period.
5. Conduct performance-based field tests to compare the pre-freezing and post-thawing performance of the test sections.
6. Develop laboratory and design tools to help county engineers rapidly assess the gradation and plasticity of existing surface materials to be recycled and to determine relative proportions of fresh aggregate materials to be added to achieve an optimized target gradation and plasticity.
7. Translate the research results into practice by developing technology transfer materials describing how the results can be implemented and by making presentations at county engineer meetings and workshops. To further this goal, the gradation optimization spreadsheet has been distributed to all county engineers on the Iowa County Engineers Service Bureau website. Several counties have begun using it and providing feedback.

1.3 Organization of the Report

This report consists of seven chapters. Chapter 2 summarizes the literature review and web survey results that identify current issues and specifications for granular surface materials. Chapter 3 presents the laboratory test results for quantifying the effects of gradation and plasticity on the shear strength and slaking characteristics of typical granular surface materials. Chapter 4 provides details on the design, construction, and field test results of the demonstration test sections. Chapter 5 compares the accuracy and repeatability of several laboratory tests that can be used to determine the consistency (i.e., liquid limit [LL], plastic limit [PL], and plasticity index [PI]) of soils. Chapter 6 presents a new laboratory testing method to evaluate the performance, morphology changes, and compaction characteristics of granular materials under simulated compaction and traffic loading conditions. Conclusions and recommendations for testing, design, and construction procedures to achieve optimum performance of granular-surfaced roads with or without recycling of existing aggregate surface course materials are provided in Chapter 7. Supporting materials are included as appendices.

CHAPTER 2. ISSUES AND SPECIFICATIONS OF GRANULAR-SURFACED ROADS

This chapter summarizes the literature review and results of a web survey distributed to Iowa county engineers regarding performance and maintenance issues and specifications of granular-surfaced roads. The complete survey results can be found in Appendix A.

2.1 Damage of Granular-Surfaced Roads in Iowa

Compared to paved roads, granular surfaces are more prone to severe surface damage, which significantly increases maintenance costs (DeVries 2012, Jahren et al. 2005, Li et al. 2015a). The types of surface damage commonly encountered include rutting, washboarding, potholes, surface deterioration, loss of crown, and dust, each of which can adversely affect traffic safety and require recurring maintenance.

In this study, a web survey was conducted to identify common issues for granular-surfaced roads in Iowa as well as the currently used specifications for surface materials. The survey was sent to all Iowa county engineers in May 2015. Staff for a total of 46 out of the 99 counties in Iowa completed the survey, as shown in Figure 2.1.

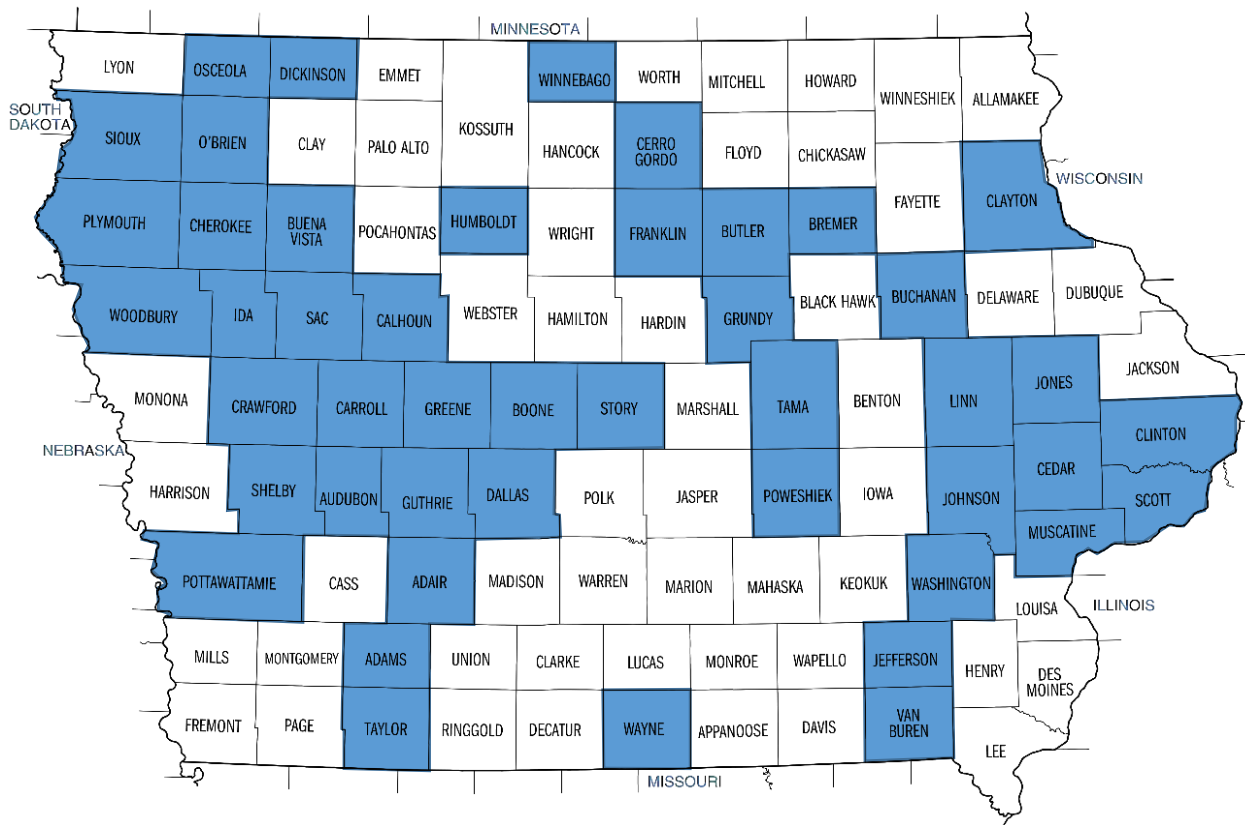


Figure 2.1. Iowa map with the 46 counties that completed the web survey shown in blue

Based on the responses received, over 80% of the 46 counties included raveling (washboarding) among the three issues observed most often on their granular roads, as shown in Figure 2.2. Rutting, potholes, frost boils, and dust (in decreasing rank order) were also identified as severe issues by more than 50% of the responding counties. Other issues identified in the survey responses were mainly attributed to heavy traffic loads and poor subgrade bearing capacity. These problems could be improved by use of thicker granular surface layers, subgrade stabilization methods, or higher quality aggregate materials.

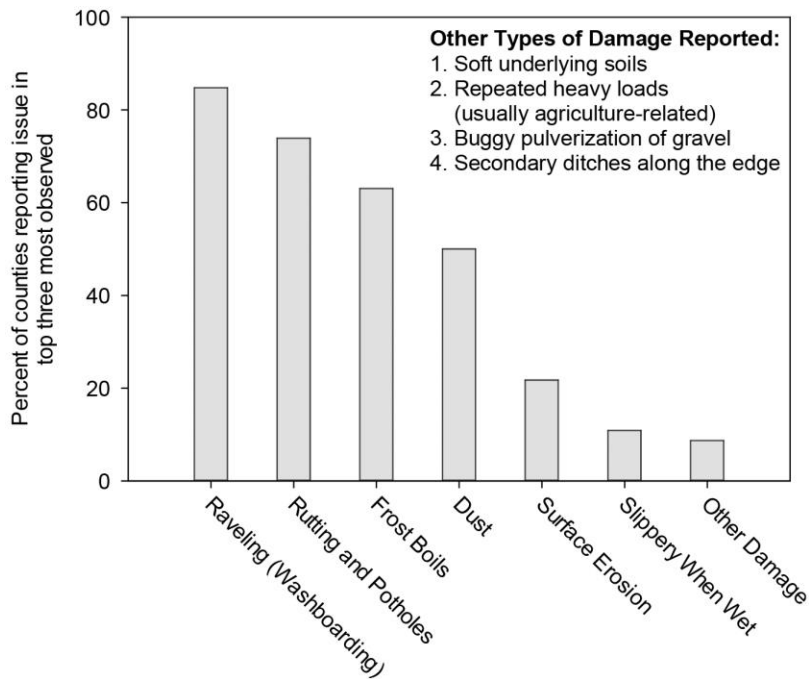


Figure 2.2. Percent of the 46 responding Iowa counties reporting a given granular road issue among their top three most observed

Based on the survey responses, among all the reported types of damage, frost boils occurring during relatively short thawing periods cost the most to mitigate, as shown in Figure 2.3. Frost boils are usually caused by frost-susceptible subgrade materials and a high ground water table. To repair the frost boil damage, the soft subgrade of the affected area is usually removed and replaced with granular or clean aggregate materials. Installing aggregate columns has also been found to be a very cost-effective method to prevent or mitigate frost boils (Li et al. 2017b).

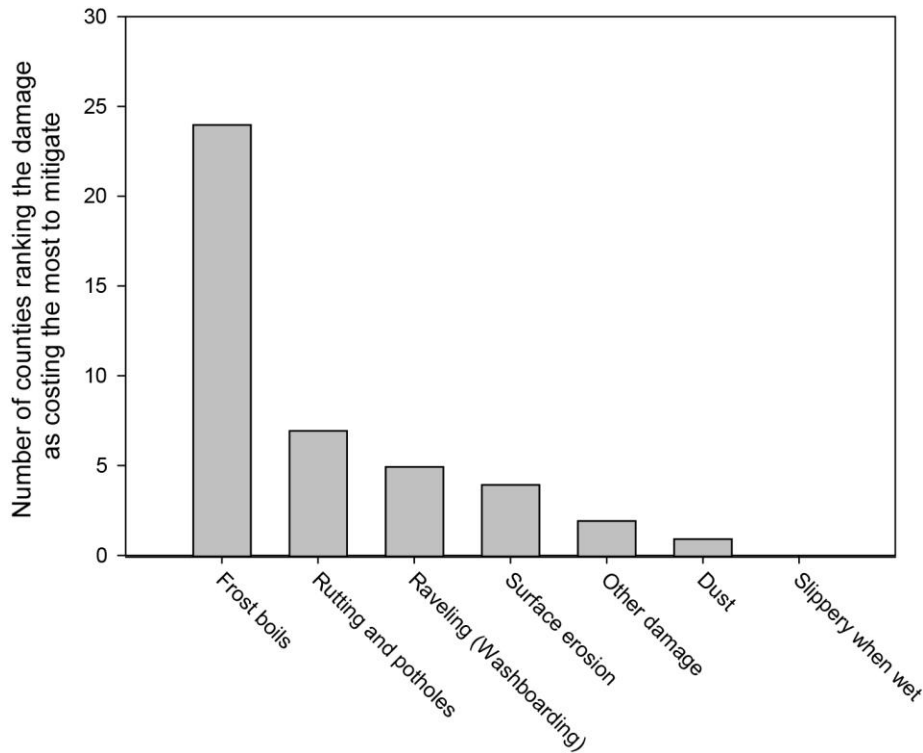


Figure 2.3. Number of the 46 responding Iowa counties ranking a given damage type as costing the most to mitigate

The survey responses indicated that the current maintenance practice typically involves covering the entire damaged area with fresh quarried (or virgin) aggregate without compaction, and materials pushed or kicked to the shoulders by traffic are retrieved using motor graders or discs.

The importance of the index properties of granular road surface materials, such as maximum aggregate size, gradation, plasticity, and quality, has long been recognized (Hudson et al. 1986, Jones 2015, Paige-Green 1998, Skorseth and Selim 2000, Van Zyl et al. 2007). However, most state DOT specifications for the gradation and plasticity of granular surface materials are neither performance based nor strictly executed. Consequently, considerable variation exists in the performance and durability of granular-surfaced roads, and substantial amounts of the freshly placed material for maintenance and repair rapidly degrade to smaller particles and dust (Jones and Paige-Green 2015).

2.2 Gradation and Plasticity of Granular Surface Materials

Raveling and washboarding issues are usually caused by poorly graded or gap-graded materials with a lack of fines and plasticity. The material particles do not bind together, ultimately resulting in significant gravel loss and recurring maintenance needs (Jones et al. 2013, Paige-Green 1989, Skorseth and Selim 2000). Granular surface materials are quite different from pavement base materials, which usually have a larger top size and contain a very small percentage of fines. These two characteristics can provide better drainage but result in a surface

layer that is unstable and difficult to maintain when used on granular-surfaced roads (Jones et al. 2013, Légère and Mercier 2004, Skorseth and Selim 2000).

Some studies in the literature suggest ranges for the top size, fines content (< No. 200 sieve), and plasticity index for general unpaved road surface materials, but most of the studies present conclusions without quantitative laboratory and field validations of the recommendations.

Berthelot and Carpentier (2003) concluded that gravel road surface materials with larger top sizes of 5/8 or 3/4 in. take longer to break down, and test sections with coarser gravel particles provide better traction and surface wearing durability than those with finer gravel under wet conditions. Jones et al. (2013) also suggest that unpaved road surface materials having a maximum particle size of 1.5 to 1.75 in. are preferable to provide adequate all-weather passability. For fines content, Anon (1988) recommends using materials with 12% to 16% fines and adding 3 to 5 yd³ of clay per mile to improve stability and reduce dust. Jones et al. (2013) concluded that materials with greater than 20% fines content (< No. 200 sieve) can be dusty when dry and may become slippery when wet, but fines contents below 10% may result in raveling.

The recently published Federal Highway Administration (FHWA) Gravel Roads Maintenance and Design Manual suggests that the plasticity index of good gravel road surface materials should be between 4 and 12 (FHWA 2015). Previous studies also found that bentonite (sodium-montmorillonite) can effectively reduce dust and increase stability of crushed limestone-surfaced roads because the negatively charged surfaces of the clay particles effectively bond the positively charged limestone particles (Bergeson et al. 1995, Bergeson and Wahbeh 1990). Field observations also showed that an appropriate amount of plastic fines can help to create a tighter and smoother roadway surface (Li et al. 2017b). However, the FHWA (2015) manual also warns that the amount of bentonite to be added must be very carefully controlled and that the bentonite must be mixed thoroughly because too much clay will cause rutting and slipperiness issues during prolonged wet periods.

In the web survey conducted for this study, 59% of the responding counties reported that existing surface materials typically have excessive fines caused by degradation of the surface aggregates (Figure 2.4), 25% reported excessive fines due to the migration of subgrade soils (Figure 2.5), and 14% reported excessive fines due to other sources, including quarries and off-road sources (Figure 2.6). However, some counties (18%) are also suffering a loss of fines, as shown in Figure 2.7.

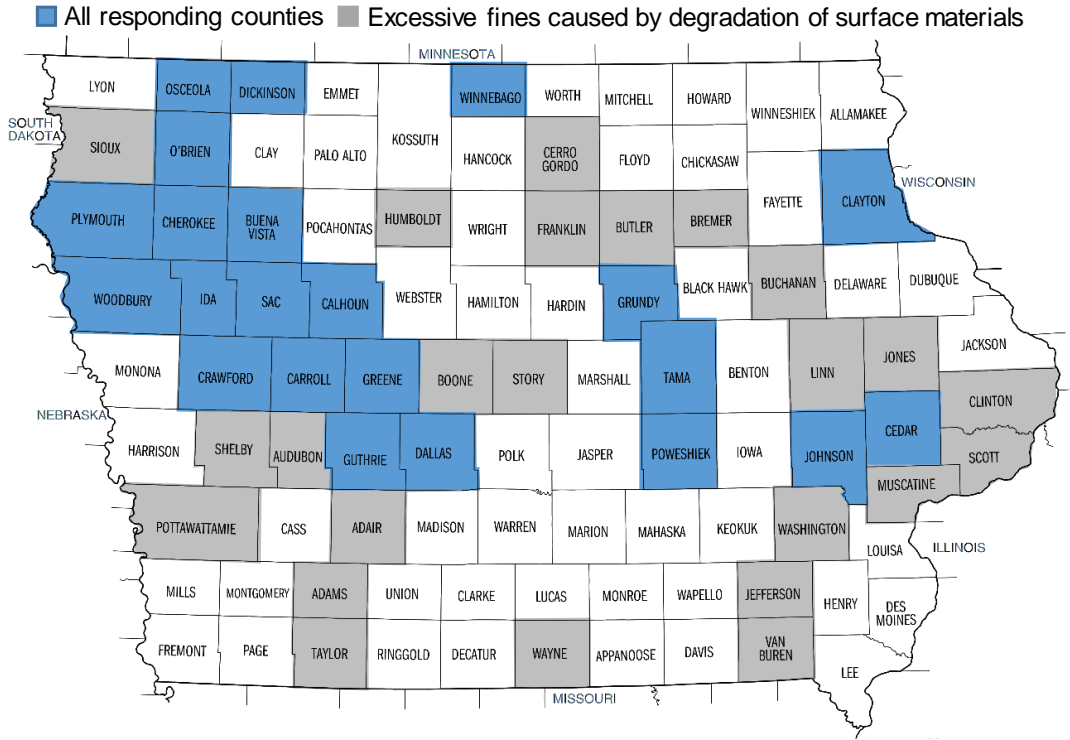


Figure 2.4. All counties responding to the survey highlighted, with those in gray reporting excessive fines caused by degradation of surface materials

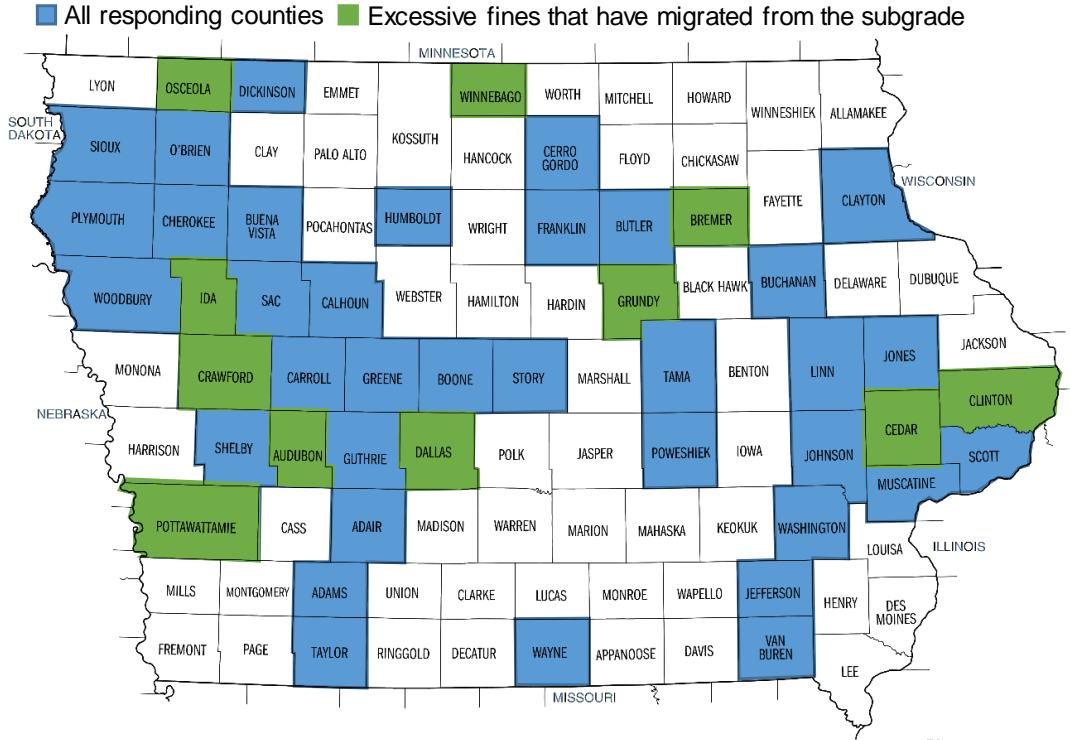


Figure 2.5. All counties responding to the survey highlighted, with those in green reporting excessive fines that have migrated from the subgrade

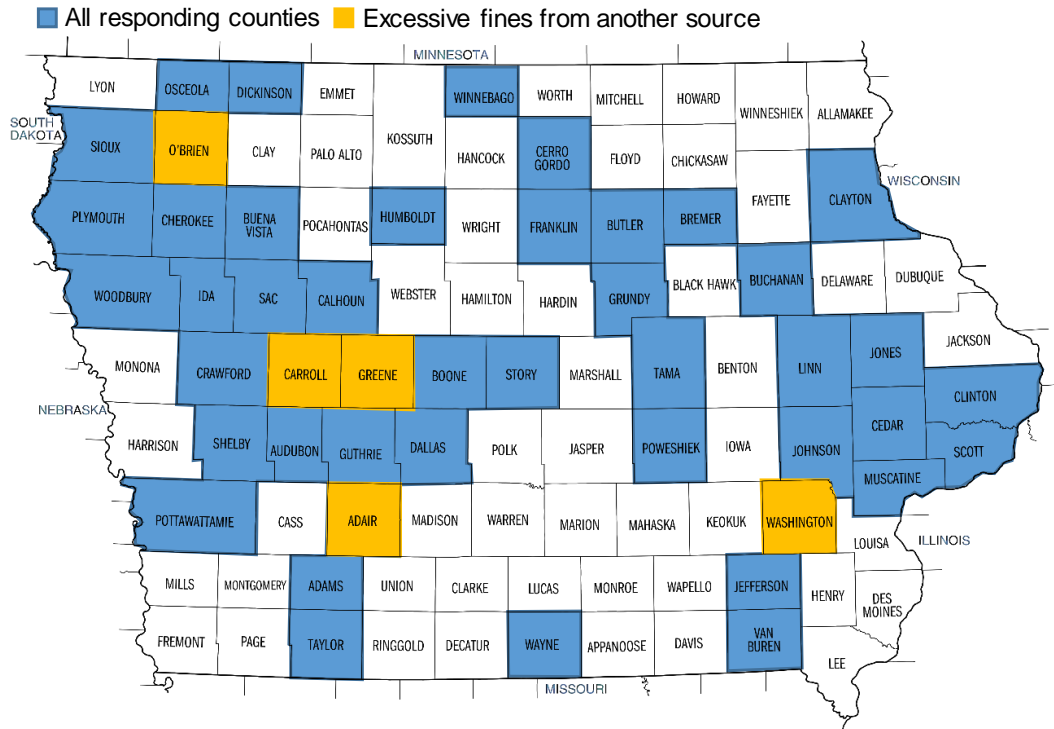


Figure 2.6. All counties responding to the survey highlighted, with those in yellow reporting excessive fines from other sources

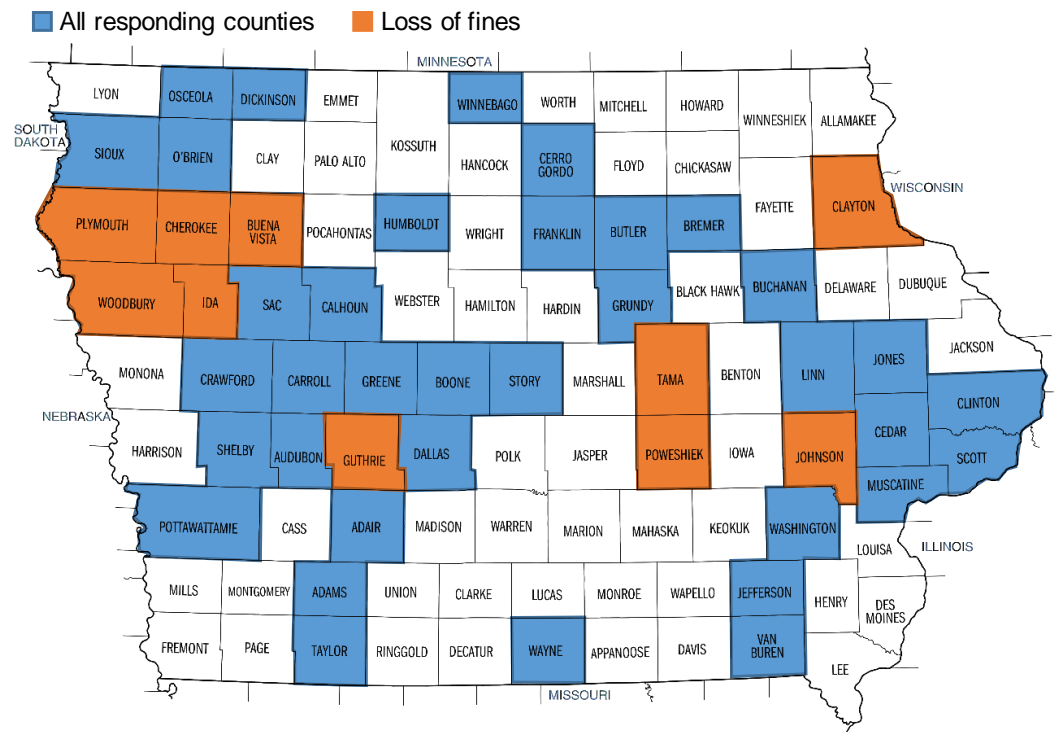


Figure 2.7. All counties responding to the survey highlighted, with those in orange reporting loss of fines

2.3 Specifications for Granular Surface Materials

2.3.1 State DOT and Iowa County Specifications

Specifications for the gradation and plasticity index of granular surface materials vary among state DOTs. Several specifications used by the Iowa DOT and neighboring state DOTs are compared in Table 2.1. However, all of the specifications were established based on arbitrary gradation bands with (at most) six control points, which are not performance related. In addition, most of the states, except for South Dakota and Illinois, do not specify the plastic index.

Table 2.1. DOT granular surface material specifications (percent passing) for Iowa and surrounding states

Sieve	Iowa Class A or B	South Dakota	Illinois CA-6	Minnesota Class 1	Nebraska Rock	Missouri Grade B
1.5 in.			100			
1 in.	100		100-90		100	100
3/4 in.	100-95	100		100		
1/2 in.	90-70		90-60			
3/8 in.				95-65		< 65
No. 4	55-30	78-50	56-30	85-40	60-20	
No. 8	40-15	67-37				
No. 10				70-25	30-0	25-5
No. 16			40-10			
No. 40		35-13		45-10		
No. 200	16-6	15-4	12-4	15-8	10-0	
Plastic Index	NA	12-4	9-2	NA	NA	NA

Based on the web survey responses, most of the responding counties (74%) reported that they follow Iowa DOT Class A and B crushed stone specifications for granular surface materials, as shown in Figure 2.8. However, 36% of the responding counties have also set up their own specifications, which are summarized and compared with the Iowa DOT specifications in Table 2.2.

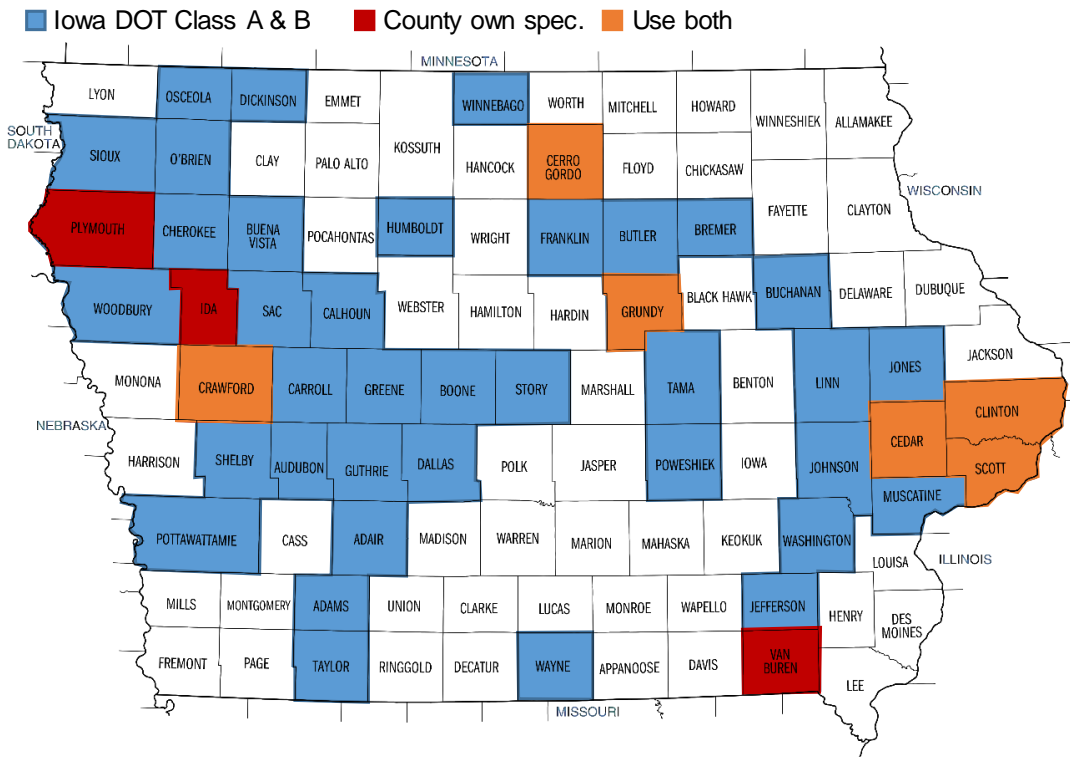


Figure 2.8. Surface course and shoulder material specifications used by counties that responded to survey

Table 2.2. Current granular surface material specifications used by the Iowa DOT and some of the surveyed counties

Iowa DOT Spec. /County Name	1-1/4 in. (%)	1.0 in. (%)	3/4 in. (%)	1/2 in. (%)	No. 4 (%)	No. 8 (%)	No. 30 (%)	No. 200 (%)	Plasticity Index
Iowa DOT Class A		100	100-95	90-70	55-30	40-15		16-6	
Iowa DOT Class B		100	100-95	90-70	55-30	40-15		16-6	
Iowa DOT Class C			100		80-50	60-25		6	
Cedar County	100	100-97			65-20	30-15		15-6	
Cerro Gordo County		100	100-95	90-70	55-30	40-15		12-6	
Clinton County	100					30-15		16-6	NA
Ida County		100-98	98-85		67-50	55-35	28-10	10-4	
Plymouth County		100		100-85	70-50	55-25	28-10	10-0	
Scott County	100	100-90				30-10		12-5	
Van Buren County	100	98-90	90-70	70-40	40-18	30-10		10-3	
Crawford County	100		98-85		67-50	55-35	28-10	7-0	

To cope with heavy traffic loads or soft subgrade conditions, specifications with a larger top size of 1¼ in. are used by several counties. Some survey respondents also indicated that the binding properties of clayey fines can help reduce dust and provide a tighter roadway surface for

granular-surfaced or gravel roads. However, none of the specifications in Table 2.2 stipulate a range of plasticity index for granular surface materials. In addition, due to the limited availability and high costs of high-quality granular materials, some counties reported that they could not strictly meet the material specifications for granular-surfaced roads. As noted above, excessive plastic fines can lead to excessive dust in dry conditions and rutting and slippery road surfaces in wet conditions. Therefore, it is important to empirically determine the useful range of application rates for incorporating plastic material such as clayey subgrade or bentonite powder and to identify effective methods to thoroughly mix the clayey and granular materials.

2.3.2 A Performance-Related Specification

Paige-Green (1989) developed a performance-related material selection chart for determining the gradation and plasticity of unpaved road surface materials, shown in Figure 2.9, based on testing and monitoring 110 unpaved road sections for more than three years in South Africa. The author explained that the surface material needs adequate cohesion to resist raveling and the formation of corrugations under traffic loading.

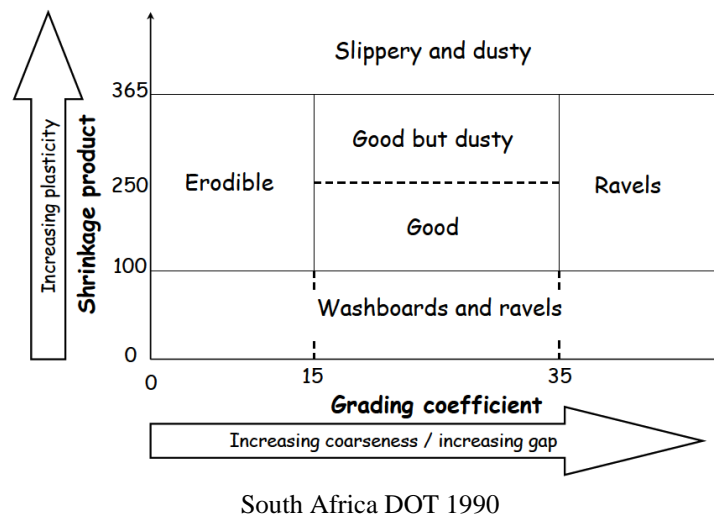


Figure 2.9. Relationship between shrinkage product, grading coefficient, and performance of surface course for gravel roads

In this chart, the grading coefficient and shrinkage product are calculated using the results of sieve analyses and bar linear shrinkage (BLS) tests on the granular surface materials. These quantities are then related to the observed performance of the corresponding road sections. The grading coefficient and shrinkage product in the figure are calculated as follows:

$$\text{Grading Coefficient} = \frac{(\% \text{ passing } 26.5 \text{ mm} - \% \text{ passing } 2.0 \text{ mm}) \times \% \text{ passing } 4.75 \text{ mm}}{100} \quad (2.1)$$

$$\text{Shrinkage Product} = \text{Bar Linear Shrinkage} \times \% \text{ passing } 0.425 \text{ mm} \quad (2.2)$$

The bar linear shrinkage test is described in the South African Technical Methods for Highways (TMH1-A4). In the present study, the bar linear shrinkage test method was statistically evaluated and compared to other laboratory testing methods for determining the plasticity of soils. The comparison results are presented in Chapter 5.

Based on the performance-related material selection chart in Figure 2.9, Paige-Green (1989) concluded that the grading coefficient of good performing surface materials should be between 15 and 35, and the shrinkage product should be between 100 and 365, or below 250 for reduced dust. Jones et al. (2013) also stated that “although not directly measured in the grading coefficient formula, a fines content (material passing the No. 200 sieve) of between 12 and 15 percent is typically required to meet the grading coefficient requirements.” However, Jones and Paige-Green (2015) noted that “local calibrations of the grading coefficient and shrinkage product ranges may be needed” to use this chart.

2.4 Degradation and Morphology of Granular Materials

2.4.1 Degradation of Granular Materials

Mechanical degradation or abrasion of granular materials used for granular-surfaced roads or pavement bases can significantly influence their mechanical properties, drainage conditions, and freeze-thaw durability (Cho et al. 2006, Nurmikolu 2005, Vallejo et al. 2006, White and Vennapusa 2014). As detailed in several previous studies, the degradation and abrasion of a granular material is a function of its mineral composition, gradation, morphology, and loading conditions, including compaction during construction and traffic loading over the service life of a roadway (Hardin 1985, Lade et al. 1996, Lees and Kennedy 1975, Marsal 1967, Nurmikolu 2005, White et al. 2004, Zeghal 2009). Zeghal (2009) found that the mechanical degradation of granular materials can decrease the resilient modulus by up to 50% and increase permanent deformations by 100% to 300%, resulting in significant rutting and cracking on roadway surfaces. Other previous studies have also illustrated the effects of gradation and loading conditions on the degradation of aggregate, railroad ballast, and soils using static or cyclic triaxial tests (Chen and Zhang 2016, Hardin 1985, Indraratna et al. 2005, Nurmikolu 2005).

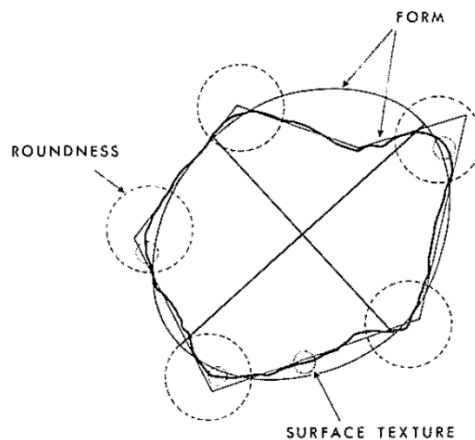
It is widely known that uniformly graded or gap-graded aggregates can experience significantly more degradation than well-graded aggregates because the lower void ratio of well-graded materials results in lower interparticle contact stresses. As a result, well-graded materials tend to break down more slowly than uniformly graded materials under a given set of loading conditions (Airey et al. 2008, Lade et al. 1996, Nurmikolu 2005). For example, the effects of maximum particle size and coefficient of uniformity (C_u) on the permanent deformation and degradation of railroad ballast were examined using large-scale cyclic triaxial tests in Indraratna et al. (2016). It was reported that particle breakage was significantly reduced when C_u was larger than 1.8. Particle breakage was also significantly influenced by load duration, with reported values of breakage index under creep loading greater than 1.5 times those of monotonic loading (Chen and Zhang 2016). Based on the results of cyclic triaxial tests, an optimum range of confining pressures in terms of minimizing degradation of railway ballasts exists for a given deviator stress (Lackenby et al. 2007).

To practically evaluate abrasion and degradation characteristics or create specifications for the quality of granular materials, most transportation agencies rely on the Los Angeles (LA) abrasion and Micro-Deval tests, which require specimens to be prepared to standard gradings and tested in a rotating steel drum containing steel spheres (ASTM C131, ASTM D6928). However, these two testing methods do not simulate the actual traffic loading conditions responsible for the degradation and performance of the materials and do not test their full gradations, which strongly affect their performance in the field.

The Iowa DOT specifications for Class A and Class B crushed stone require less than 45% and 55% LA abrasion loss, respectively (Iowa DOT 2012). Based on the responses to the web survey, only 24% of the responding counties request LA abrasion test results for their virgin granular materials.

2.4.2 *Quantification of Particle Morphology*

Aggregate particle morphology has long been recognized as an important factor affecting the engineering properties and degradation of granular materials (Cheung and Dawson 2002, Cho et al. 2006, Pan et al. 2006). Various parameters have been proposed to quantify the external morphology of particles (Barrett 1980, Ozen 2007). Barrett (1980) conducted a literature review to evaluate the relationships among these parameters and concluded that the various parameters can be categorized into a three-tiered hierarchy of observational scales with respect to particle size: form, roundness, and surface texture. The hierarchy is shown in Figure 2.10.



Barrett 1980, Copyright © 1980, John Wiley and Sons

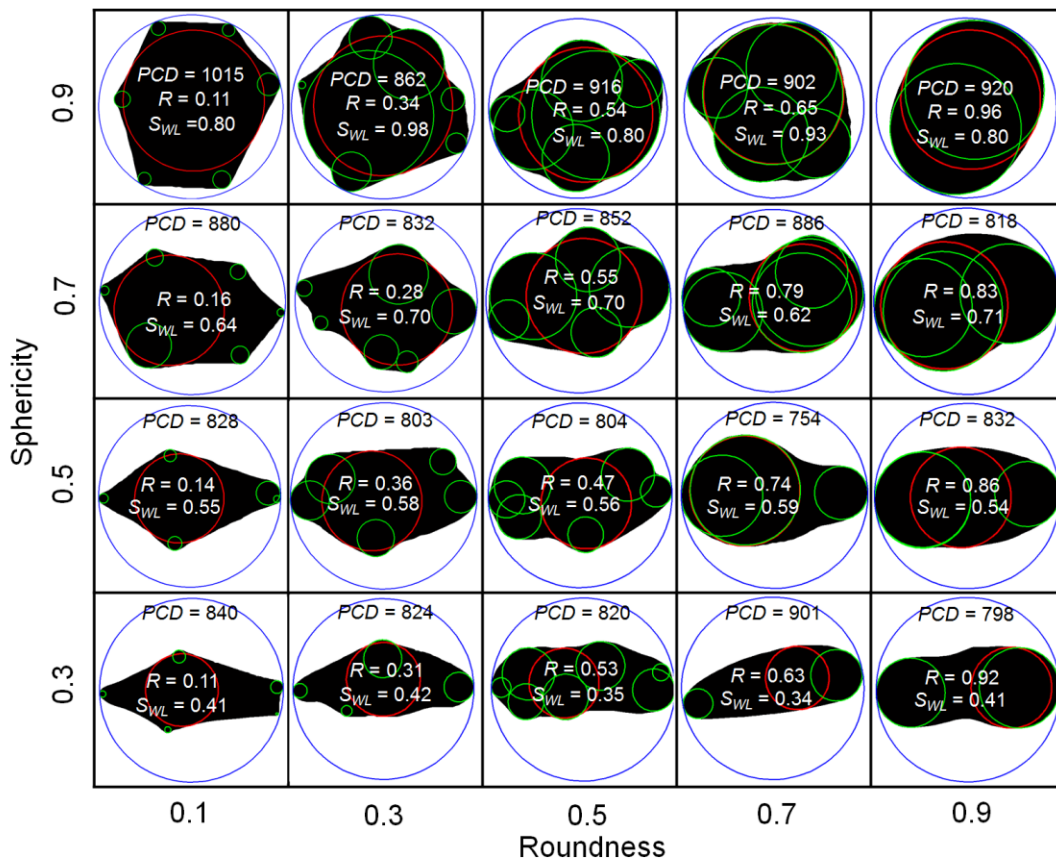
Figure 2.10. Particle shape characterization at different scales

For the first observational scale, also called the global form of a particle, almost all parameters (e.g., flatness, elongation, sphericity, and oblate-prolate index) are calculated using the ratio of the largest inscribed circle and the smallest circle circumscribing the projected area of the particle, or the shortest and intermediate orthogonal axes, which are independent of the particle size. Sphericity is the most commonly used parameter to describe the form of a particle. It is defined as the ratio of the surface area of a sphere with same volume as the particle to the surface

area of the particle (Wadell 1932). The Rittenhouse chart is traditionally used to quantify the sphericity of particles (Rittenhouse 1943). For two-dimensional (2D) calculations, the sphericity (Ψ) can also be calculated using the diameter (r_i) of the largest inscribed sphere divided by the diameter (r_c) of the smallest circle circumscribing the project area, as shown in the equation below (Wadell 1932):

$$\Psi = \frac{r_i}{r_c} \quad (2.3)$$

For the second observational scale-level parameters, there are three types of roundness measurements: average roundness of corners, roundness of the sharpest corner(s), and convexity in the particle outline. These are not independent and should be used for different purposes (Barrett 1980). Krumbein and Sloss (1951) also developed a chart, which has been widely used to date, for visual quantification of the sphericity and roundness of a particle (e.g., Figure 2.11).



Zheng and Hryciw 2015, Copyright © ICE Publishing, all rights reserved. *Géotechnique* by INSTITUTION OF CIVIL ENGINEERS (GREAT BRITAIN); THOMPSON, ANN E. Reproduced with permission of THOMAS/TELFORD LTD. in the format Republish in other published product via Copyright Clearance Center.

Figure 2.11. Comparison of computational geometry results to Krumbein and Sloss

To quantify the roundness of a particle, Wadell (1932) defined a corner as “every such part of the outline of an area (projection area) which has a radius of curvature equal to or less than the

radius of curvature of the maximum inscribed circle of the same area.” However, Barrett (1980) noted that “if the limit were a straight part of the outline, all particles with convex outlines would consist entirely of corners, some of which would have a radius of curvature of almost infinite size.” Using advancements in image analysis technology, Zheng and Hryciw (2015) developed a numerical method based on computational geometry to determine the particle roundness from 2D images of particles, as shown in Figure 2.11. The roundness of a corner can be calculated as the radius of curvature of the corner divided by the maximum inscribed circle of the 2D projected area of the particle. The total (also called average) roundness of a particle can be calculated by taking the arithmetic mean of the roundness of the individual corners.

Roundness of granular materials has been recognized as a significant factor influencing the performance of granular-surfaced roads. Jones et al. (2013) suggest checking the roundness of the aggregate in the materials used on unpaved roads because the roundness can greatly influence the particle interlocking, and rounded aggregates should be crushed to obtain at least two fracture faces to prevent raveling. Skorseth and Selim (2000) also discussed the benefits gained from processing the material by crushing, which causes the broken stones to embed into the unpaved road surface much better than natural rounded stones.

As developments in imaging and computational techniques have advanced, image-based particle morphological analysis has become a more rapid, objective, and repeatable means of classification (Al-Rousan et al. 2007). For example, high-definition cameras and scanners have been used to collect 2D image data of aggregates. Automated three-dimensional (3D) image analysis systems, including the University of Illinois Aggregate Image Analyzer (UI-AIA) and the Aggregate Imaging System (AIMS), have also been developed for determining morphological parameters at multiple length scales (Fletcher et al. 2003, Liu et al. 2016, Rao et al. 2001). The accuracy and capabilities of several image analysis methods have also been assessed by comparing their results to the Rittenhouse and Krumbein charts (Al-Rousan et al. 2007). However, Barrett (1980) recommends that “selecting parameters to characterize particle shapes with different level of precision will depend on the problem being studied.”

In the following chapters, the laboratory and field performances of various mixtures of virgin aggregates and recycled existing aggregate materials are evaluated. A new performance-based gradation design method and spreadsheet tool is presented to help county engineers determine the mixing ratios of fresh and existing materials to optimize strength and performance, and construction procedures are recommended. Various laboratory methods for determining the consistency of soils (liquid and plastic limits) were evaluated in a statistical laboratory study, and recommendations are made for obtaining faster, more repeatable results. A new test method named the Gyratory Abrasion and Image Analysis (GAIA) test was developed in this research to overcome some limitations of the LA abrasion and Micro-Deval test methods by more closely simulating traffic loading and the resulting abrasion loss. The GAIA test includes analysis of 2D images of gravel-size particles to automatically quantify particle roundness and sphericity, as well as particle size distribution (PSD). The GAIA test results can be used to develop more efficient and economical performance-based compaction specifications.

CHAPTER 3. LABORATORY EVALUATIONS OF GRADATION AND PLASTICITY EFFECTS

3.1 Introduction

The main objectives of the laboratory study were to quantify the effects of gradation and plasticity on the soaked shear strength and slaking characteristics of granular road surface materials and to identify the optimum gradation and plasticity index of materials from southwest Iowa that would be used in the field test sections. To meet these objectives, a series of laboratory California Bearing Ratio (CBR), unconfined compressive strength (UCS), and slaking tests were performed. Based on the results of the laboratory tests and statistical analyses, a new performance-based design method is proposed for specifying the gradation and plasticity of materials for new granular roadway construction as well as the recycling of existing surface materials by mixing with virgin aggregate and plastic fines.

3.2 Laboratory Testing Methods

Granular-surfaced roads are most prone to damage during spring thaws and rainy seasons, when the thawing water or infiltrating water cannot drain efficiently and the nearly saturated surface materials can easily lose strength under heavy agricultural traffic loads. Therefore, the laboratory evaluations in this study were focused on quantifying the gradation and plasticity effects on the post-saturation performance of surface materials. The sample preparation methods and testing procedures used in the laboratory tests are detailed in the following sections.

3.2.1 Soil Index Property Tests

Particle size analysis and Atterberg limits tests were conducted in accordance with ASTM D422 and ASTM D4318. The standardized testing devices used are shown in Figure 3.1. Representative specimens of the granular surface materials were obtained using a riffle sample splitter and prepared in accordance with ASTM D421.

Particle size analysis consists of two parts: the sieve analysis (Figure 3.1[a]) and hydrometer test (Figure 3.1[b]). Sieve analyses were used for material retained on the No. 200 sieve, and hydrometer tests were used for determining proportions of silt and clay for particle sizes smaller than the No. 200 sieve. The testing specimen was first split using a No. 10 sieve, and particles retained on the No. 10 sieve were washed thoroughly and oven dried at 110°C before the sieve analysis test. A representative portion of particles passing the No. 10 sieve (50 g for clayey material and 100 g for silty material) was collected for the hydrometer test. The specimen was soaked in a 40 g/L sodium metaphosphate solution for at least 16 hours and then dispersed before the test using the air-jet dispersion apparatus. After completing the hydrometer test, the suspended material was washed through a No. 200 sieve. The material retained on the No. 200 sieve was then oven dried at 110°C overnight to complete the of the rest of the sieve analysis test for the medium and fine sand-size particle sizes between No. 10 and No. 200.

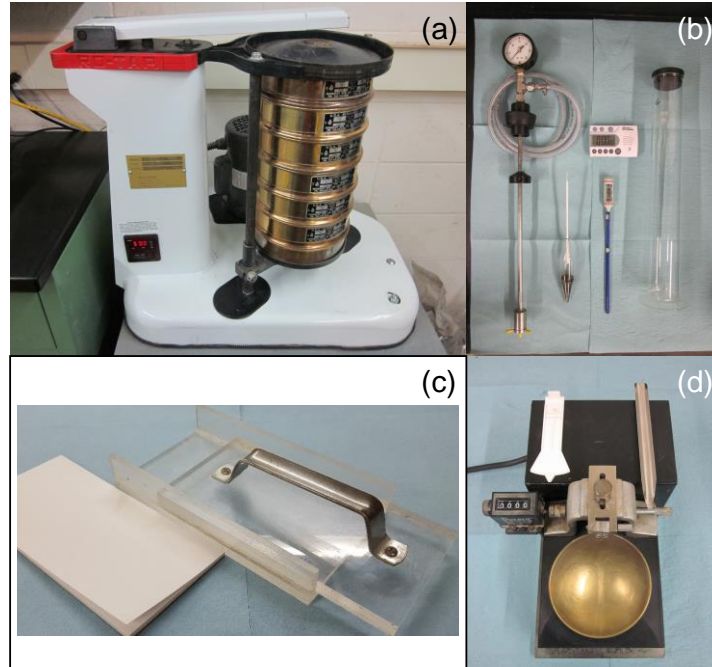


Figure 3.1. Devices for (a) sieve analysis, (b) hydrometer analysis, (c) plastic limit, and (d) liquid limit tests

The liquid limit, plastic limit, and plasticity index of the testing specimens were determined in accordance with ASTM D4318. The wet preparation method was followed for preparing representative specimens for the tests. Distilled water was used to avoid alteration of the results due to cation exchange. Liquid limit tests were performed according to the multi-point liquid limit method, and at least three points were measured for each specimen. Plastic limit tests were performed using the ASTM-recommended roller (Figure 3.1[c]) to provide more repeatable test results than the conventional hand test method. The liquid limit test was performed using the Casagrande cup, as shown in Figure 3.1[d]. Both LL and PL were rounded to whole numbers for calculating PI. According to ASTM D4318, if either the LL or PL could not be determined, or if the PL was equal to or greater than the LL, the material was reported as nonplastic (NP).

Based on the sieve analysis and Atterberg limits test results, the collected samples were classified following the Unified Soil Classification System (USCS) and American Association of State Highway and Transportation Officials (AASHTO) classification system in accordance with ASTM D2487-10 and ASTM D3282-09.

3.2.2 California Bearing Ratio Test

To evaluate how gradation influences the shear strength of granular surface materials under wet conditions, soaked CBR tests were conducted in accordance with ASTM D1883. The gradations of test specimens were adjusted manually as stipulated in the standard. All of the specimens were compacted to standard Proctor maximum dry unit weight and soaked for 48 hours before testing. During the CBR test, the specimens were submerged in a water tub, as shown in Figure 3.2.

After the CBR tests, sieve analysis tests were performed on the specimens in accordance with ASTM C136.



Figure 3.2. CBR test conducted on soaked specimens

3.2.3 Unconfined Compressive Strength and Slaking Tests

To evaluate the effects of plasticity on the undrained shear strength and slaking behavior of the granular surface materials, UCS and slaking tests were performed on specimens consisting of the minus No. 40 fraction of the samples, as shown in Figure 3.3. For the UCS and slaking tests, cylindrical specimens with a diameter and height both equal to 2 in. were prepared using the 2-by-2 compaction apparatus developed at Iowa State University (ISU). Previous studies have demonstrated that the 2-by-2 compaction device can achieve moisture-density results similar to those obtained by standard Proctor compaction tests (Oflaherty et al. 1963).

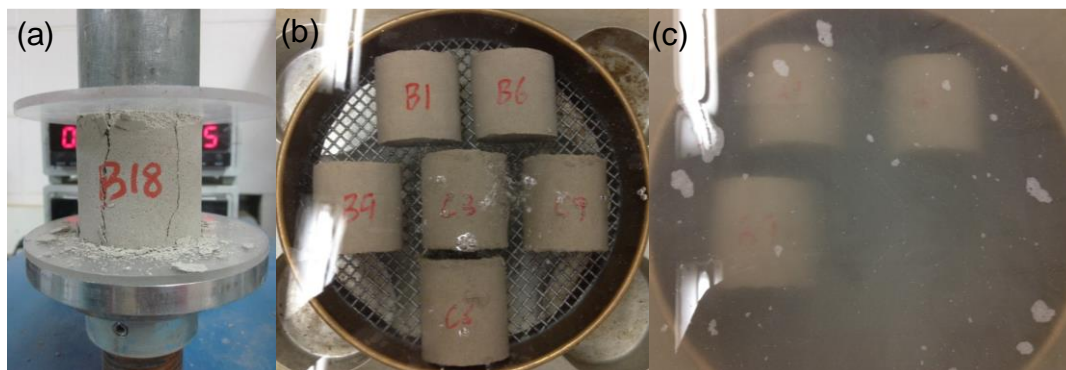


Figure 3.3. Photographs of (a) UCS test and (b) slaking test after 1 minute and (c) 35 minutes on the control (C) and 4% bentonite-treated (B) 2-by-2 specimens

The plasticity of the specimens was adjusted by incorporating different percentages of bentonite powder (sodium montmorillonite). The slaking test was used to evaluate the long-term water susceptibility of the specimens by placing them on a No. 4 sieve and submerging them in a water tub, as shown in Figure 3.3(b). The time for the specimens to disintegrate and pass through the No. 4 sieve was then recorded (Figure 3.3[c]).

3.3 Materials

In this study, two types of granular surface materials were collected from an existing granular-surfaced road (County Road L-66) and a quarry (Macedonia Quarry) in Pottawattamie County, Iowa. A quantity of bentonite clay (sodium montmorillonite) was purchased from American Colloid Company in East Colony, Wyoming, to adjust the plasticity of the testing specimens.

3.3.1 Granular Surface Materials

The experimentally determined soil index properties and classifications of the existing surface materials and virgin quarry granular surface materials are summarized in Table 3.1. Compared to the virgin aggregate, the existing surface material has much higher sand and fines contents due to material degradation caused by traffic.

Table 3.1. Soil index properties of the two types of granular surface materials

Parameter	Existing Surface Material	Virgin Quarry Material
Particle size analysis results (ASTM D422-03)		
Gravel content (%)	24.0	68.7
Sand content (%)	50.0	22.8
Silt content (%)	18.5	6.0
Clay content (%)	7.5	2.5
D ₁₀ (mm)	0.0038	0.2121
D ₃₀ (mm)	0.1147	4.4371
D ₆₀ (mm)	0.8146	12.1874
Coefficient of uniformity, c_u	213.67	57.45
Coefficient of curvature, c_c	4.23	7.61
Atterberg limits test results (ASTM D4318-10e1)		
Liquid limit (%)	17	25
Plastic limit (%)	15	16
AASHTO and USCS soil classification (ASTM D2487-11 and D3282-09)		
AASHTO classification	A-2-4(0)	A-2-4(0)
USCS classification	SM	GP-GC
USCS group name	Silty sand with gravel	Poorly graded gravel

The particle size distribution curves of the existing and quarry materials are also compared to the Iowa DOT specification for granular surface materials in Figure 3.4. The existing degraded

surface material contains too much sand and fines and therefore does not meet the Iowa DOT specification, while the virgin quarry material is at the lower boundary of the DOT specification but has a slightly larger top size.

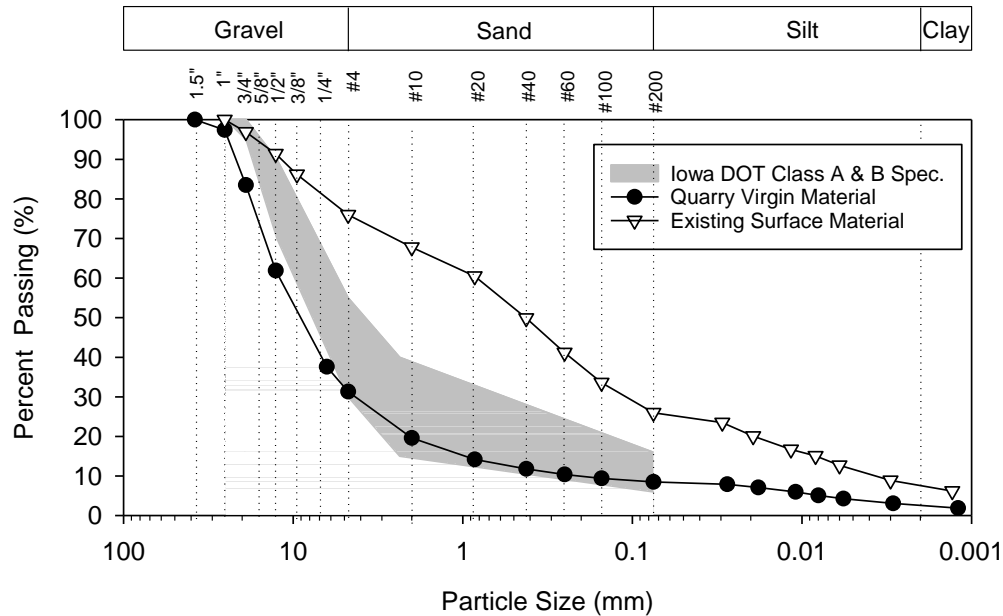


Figure 3.4. Particle size distribution curves of the existing surface material and virgin quarry materials relative to the Iowa DOT specifications

The standard Proctor test was performed in accordance with ASTM D698 to determine the optimum moisture contents and maximum dry unit weights of the two materials for preparing the CBR test specimens. The resulting moisture-density relationships of the two materials are shown in Figure 3.5. The optimum moisture contents and maximum dry unit weights of the two materials are very similar, but the shapes of the curves are quite different. For the virgin quarry material, a bulking moisture content that can result in the lowest dry unit weight due to capillary attraction was observed between 6% and 8% moisture content. The compaction curve of the existing surface material is relatively flat as moisture content increases from 2% to 6%.

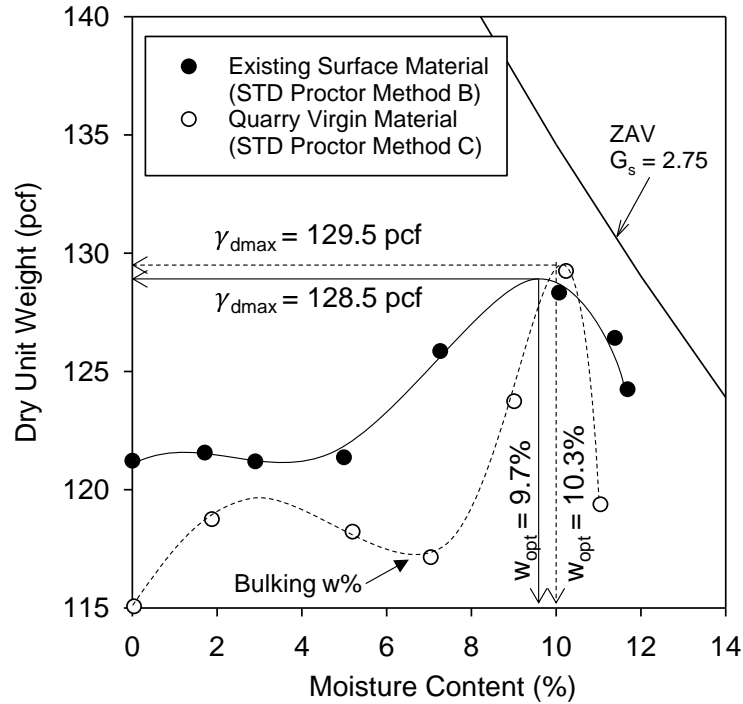


Figure 3.5. Proctor compaction curves for the existing surface and virgin quarry materials

Laboratory CBR tests were first performed on the specimens with their original gradations to compare the shear strength of two types of materials. The CBR tests were conducted on both as-compacted and soaked specimens for comparison. Neither of the materials showed significant strength reductions after soaking, as shown in Table 3.2. However, the CBR values of the virgin quarry material were about nine times higher than those of the existing surface material.

Table 3.2. Laboratory as-compacted and soaked CBR test results of the existing surface and virgin quarry materials

Material (Testing condition)	Dry Unit Weight (pcf)	Moisture Content (%)	CBR (%)
Existing surface aggregate (as-compacted)	132.7	9.2	5.9
Existing surface aggregate (soaked)	131.8	8.9	4.8
Virgin quarry aggregate (as-compacted)	121.6	9.2	47.5
Virgin quarry aggregate (soaked)	122.3	9.2	42.2

3.3.2 Bentonite

The chemical composition and mineralogy of the bentonite powder were determined in a previous project using X-ray fluorescence (XRF) and x-ray diffraction (XRD) analyses, respectively (Li et al. 2015a). The XRD results showed that the bentonite used in this project was sodium montmorillonite ($\text{Na}_{0.3}(\text{Al},\text{Mg})_2\text{Si}_4\text{O}_{10}(\text{OH})_2 \cdot 4\text{H}_2\text{O}$) with calcite (CaCO_3) and quartz

(SiO₂). The XRF results showed that the main chemical components of the bentonite were SiO₂ and Al₂O₃ (Table 3.3).

Table 3.3 Chemical composition of the bentonite powder used in the laboratory study

Chemical Composition	Percent
SiO ₂	58.77
Al ₂ O ₃	20.66
Fe ₂ O ₃	3.81
SO ₃	0.86
CaO	2.42
MgO	3.61
Na ₂ O	2.45
K ₂ O	0.62
P ₂ O ₅	0.08
TiO ₂	0.18
SrO	0.03
BaO	0.02
Total	93.50
LOI	6.15
Bulk Moisture	7.60

3.4 Gradation Effects on the Soaked Bearing Capacity

3.4.1 Existing Surface Materials

To evaluate the influence of gradation on the bearing capacity of the granular surface materials under wet conditions, laboratory soaked CBR tests were first conducted on the existing surface material specimens with various gradations (Table 3.4). The gradations were obtained by sieving out different percentages of the minus No. 40 material. The nine testing specimens covered a wide range of gradations. The gravel contents (> No. 4 sieve) of the specimens varied from 20.8% to 50.1%, while the corresponding fines contents (< No. 200 sieve) varied from 30.3% to 1.2%. However, the sand content of all the specimens varied within 2%. The CBR test results show that the maximum CBR of the specimens is 51.3%, which is more than five times the minimum value of 8.9%. Based on these results, it can be concluded that the gradation of the existing granular surface material greatly influences its saturated bearing capacity. This may result in significant variations in the performance of granular-surfaced roads under prolonged wet conditions.

Table 3.4. Results of laboratory soaked CBR tests on existing aggregate specimens with different gradations achieved by sieving minus No. 40 material

Specimen No.	Compaction Moisture Content (%)	Dry Unit Weight (pcf)	Gravel (%)	Sand (%)	Fines (%)	Soaked CBR (%)
1	9.0	136.6	20.8	48.9	30.3	8.9
2	9.3	134.6	25.5	49	25.5	30.5
3	9.5	137.6	27.5	48.5	24	26
4	9.6	130.5	28.5	49.5	22	41
5	10.2	133.7	33.2	48.2	18.6	41.2
6	9.7	130.7	34.4	48.5	17.1	51.3
7	9.0	124.5	41	48.2	10.8	50.7
8	9.0	131.4	44.5	49.7	5.8	37.8
9	9.0	135.0	50.1	48.7	1.2	20.7

It is also important to note from Table 3.4 that the soaked CBR does not simply increase with increasing gravel content or decreasing fines content. Instead, there is an optimum combination of the gravel, sand, and fines particle size ranges that results in the greatest bearing capacity. To evaluate in more detail how the different particle size ranges play an important role in the saturated shear strength of the granular surface materials, the relationships between the soaked CBR and the gravel, sand, and fines contents of the specimens are plotted in Figure 3.6.

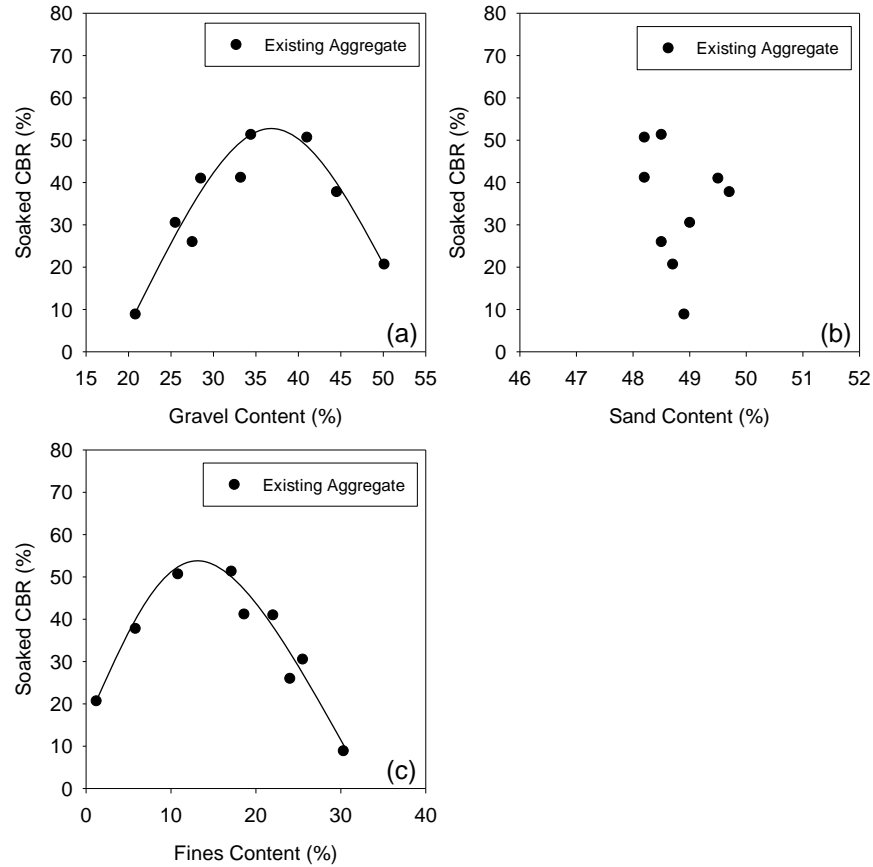


Figure 3.6. Effect of (a) gravel content, (b) sand content, and (c) fines content on the soaked CBR of the existing surface aggregate specimens

The effect of sand content cannot be clearly determined due to its small range ($< 2\%$) for the specimens. However, clear trends for the gravel and fines contents can be fit by bell-shaped curves, indicating that both can significantly influence the soaked CBR values. Also, optimum percentages of the gravel and fines contents in terms of the soaked shear strength can be clearly identified from the plots. These test results, therefore, indicate that there is an optimum gradation (particle size distribution) that can provide the highest soaked shear strength for this particular granular surface material. It is also probable that materials from other quarries with hardness, angularity, and other mineralogical properties sufficiently different from those tested in this study will have different optimum gradations.

3.4.2 Mixture of Existing and Virgin Surface Materials

To further validate the conclusion that an optimum gradation exists in terms of soaked shear strength, another series of soaked CBR tests was performed on several specimens prepared by mixing the existing (E) surface material from the roadway with virgin (V) quarry materials in varied proportions (Figure 3.7). In this series of tests, the sand content of the mixtures covered a wider range from 22% to 50%.

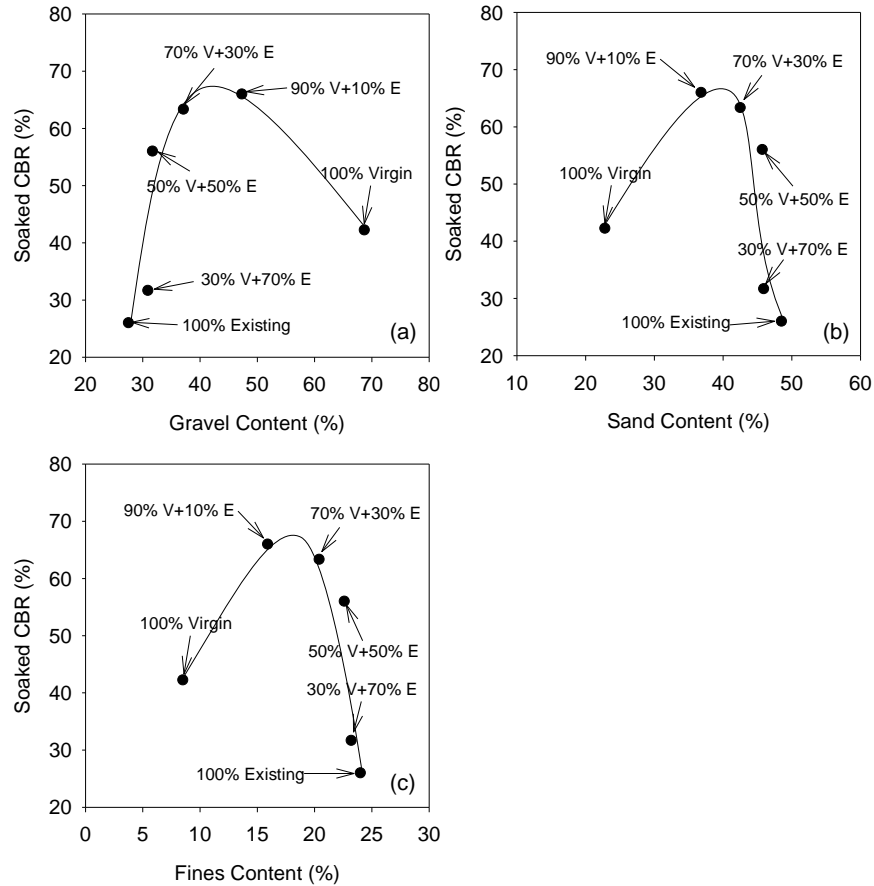


Figure 3.7. Effect of (a) gravel content, (b) sand content, and (c) fines content on the soaked CBR for mixtures of existing (E) and virgin (V) surface materials

The test results show that the CBR values of the specimens increased from a minimum of 26% for the existing material to a maximum of slightly over 68% for a V:E mixture somewhere between 70:30 and 90:10, as shown in Figure 3.7. These results confirm that the soaked strengths of granular materials depend more strongly on their gradation or particle packing than whether the particles fall within a specific range.

3.4.3 Fuller's Model for Parametrization of Particle Size Distribution Curves

It is expected that the influence of gradation on the soaked bearing capacity of granular surface materials can be quantified using the laboratory CBR and sieve analysis data generated in this study. To this end, parameters or models that can quantify the material's PSD and packing are needed. Various parameters and models were compared for the present study, and it was determined that Fuller's model (Equation 3.1) is the simplest mathematical model for quantifying the PSD of well-graded granular materials (Fuller and Thompson 1907);

$$p_i = \left(\frac{D_i}{D_{\max}} \right)^n \times 100 \quad (3.1)$$

where

the subscript i represents a particular sieve size

p_i is the percentage passing sieve number i

D_i is the corresponding sieve opening size

D_{\max} is the maximum particle size (top size) of the gradation

n is a shape factor

In Fuller's model, the gradation of a material can thus be represented by only two parameters: the maximum aggregate size (D_{\max}) and the shape factor of the PSD curve (n). Previous studies demonstrated that the coefficient of determination (R^2) values of Fuller's model are usually higher than 0.97 for well-graded materials, but the model may not be appropriate for gap-graded materials.

The PSD curves of the 14 laboratory CBR specimens tested in this study were fit by Fuller's model, giving the D_{\max} , n , and R^2 values listed in Table 3.5. The gradation and CBR test results are also summarized in Table 3.5 in descending order of fines content (percent passing No. 200) of the specimens. The maximum aggregate size varies from 20.7 to 26.4 mm, and the n value varies from 0.17 to 0.64.

Table 3.5. Gradations, Fuller’s model parameters, and CBR test results of the 14 specimens tested in this study

Specimen No.	Gradation			Parameters of Fuller’s Model			Water Content after Soaking (%)	As-compacted Dry Unit Weight (lb/ft ³)	Soaked CBR (%)
	% Gravel	% Sand	% Fines	D_{max} (in.)	n	R^2			
1	20.8	48.9	30.3	0.82	0.17	0.97	11.1	124.5	8.9
2	25.5	49.0	25.5	1.00	0.20	0.98	9.0	129.7	30.5
3	27.5	48.5	24.0	0.93	0.20	0.98	10.8	130.7	26.0
4	30.9	45.9	23.2	0.92	0.23	1.00	9.4	130.9	31.7
5	31.7	45.7	22.6	0.91	0.25	1.00	8.8	133.2	56.0
6	28.5	49.5	22.0	0.81	0.24	0.99	8.5	134.6	41.0
7	37.1	42.5	20.4	0.92	0.29	1.00	9.0	132.0	63.3
8	33.2	48.2	18.6	0.85	0.28	0.99	10.1	135.7	41.2
9	34.4	48.5	17.1	0.84	0.30	0.99	9.4	137.3	51.3
10	47.3	36.8	15.9	1.04	0.36	1.00	8.4	129.6	66.0
11	41.0	48.2	10.8	0.86	0.36	0.99	9.0	136.0	50.7
12	68.7	22.8	8.5	1.02	0.64	0.98	9.2	122.4	42.2
13	44.5	49.7	5.8	0.84	0.43	0.98	8.2	131.4	37.8
14	50.1	48.7	1.2	0.83	0.51	0.98	8.8	130.8	20.7

The PSD curves of the 14 testing specimens are also compared to the current Iowa DOT gradation specification band for unpaved road surface materials in Figure 3.8. The gradation curves cover a wide range from coarse graded to well graded, and a few of the curves are inside the Iowa DOT specification band.

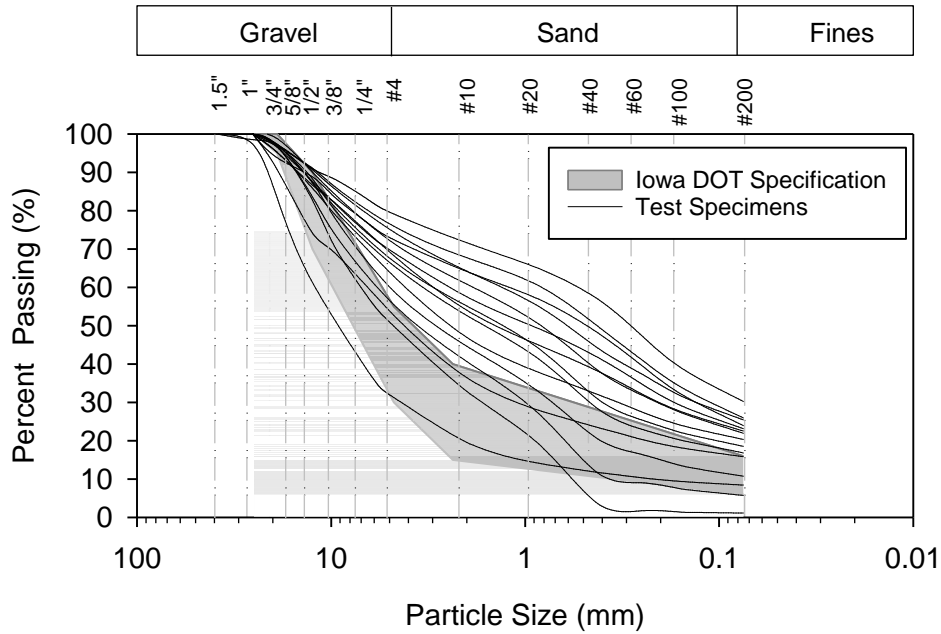


Figure 3.8. Particle size distribution curves of the 14 laboratory CBR test specimens compared to Iowa DOT Class A/B specification band

For granular road surface materials, the most commonly used top sizes are 3/4 in. and 1 in. Additionally, n values between 0.1 and 0.7 in Fuller’s model can cover a wide range of gradations, as demonstrated in Figure 3.9. The n value increases as the coarseness of the material increases, and the material becomes more well graded as n decreases.

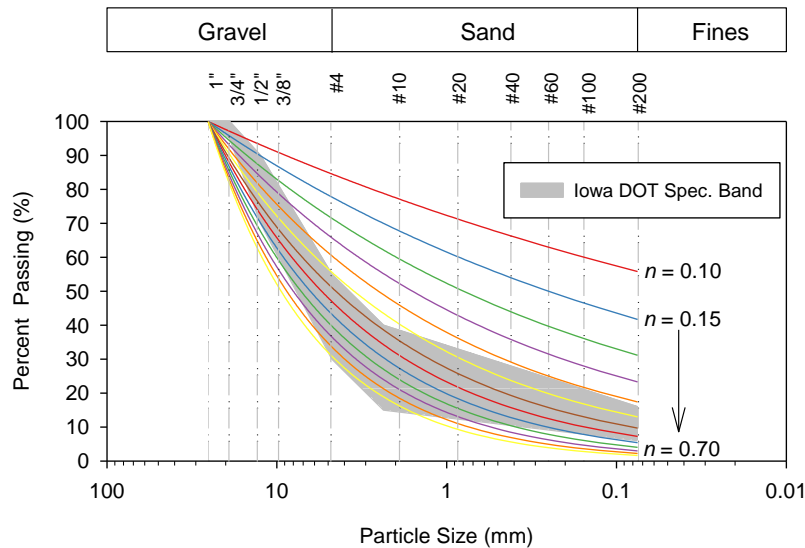


Figure 3.9. PSD curves generated using Fuller’s model with D_{max} of 1 in. and n value increasing from 0.1 to 0.7

3.4.4 Statistical Analysis of Laboratory Test Data

A multiple regression analysis was performed on the test data in Table 3.5 to quantify how changes in gradation influence the soaked CBR strength of the tested material. The resulting regression model equation, shown in Figure 3.10, has an R^2 of 0.80, and all variables of the model are statistically significant with a 95% confidence interval (p values < 0.05 and t values < -2 or > 2).

$$\text{Soaked CBR (\%)} = 78.72 - 933.39(n)^2 - 85.22(n) + 34.53(n)(D_{\max}) - 6.74(D_{\max}),$$

$R^2 = 0.80$, Number of specimens = 14, D_{\max} is in mm.

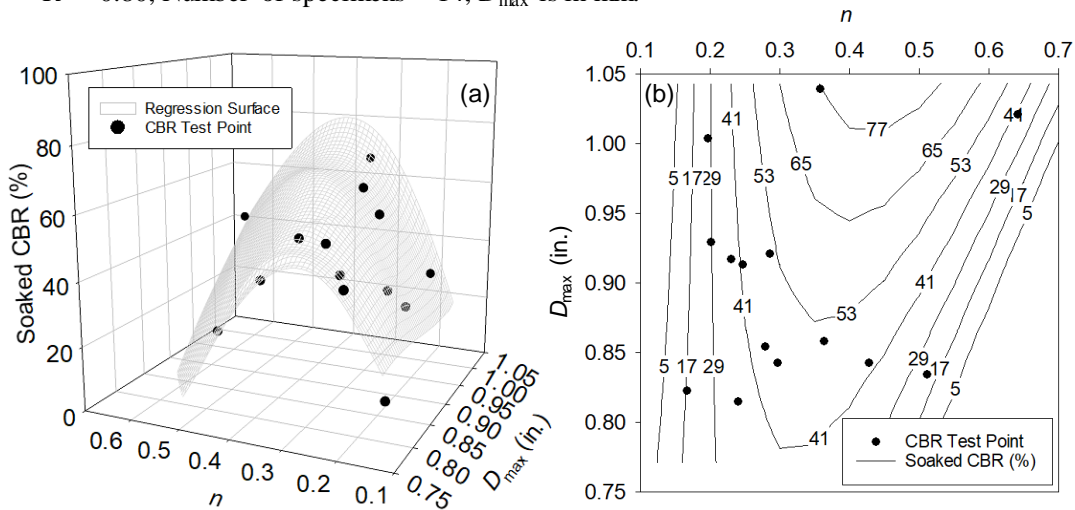


Figure 3.10. Results of multiple regression analysis on soaked CBR test data: (a) 3D regression surface, (b) 2D contour map of regression surface

A 3D surface plot of the regression model equation is compared to the laboratory testing results in Figure 3.10 (a). In general, the soaked CBR value increases as D_{\max} increases, and a bell-shape trend is exhibited for a given D_{\max} as n varies between 0.1 and 0.7. These results indicate that the undrained bearing capacity of a well-graded granular material increases as top size increases, and an optimal gradation in terms of the soaked CBR can be quantified by a particular value of the shape parameter n for a given top size.

The regression surface is also plotted as a 2D contour map in Figure 3.10(b), which more clearly shows that the optimal n value increases from 0.28 to 0.4 as D_{\max} increases from 0.77 in. to 1 in. Because CBR is commonly used for designing the thickness of granular surface layers, and each CBR data point in Figure 3.10(b) represents a specific PSD curve (see Table 3.5), this contour plot can be used to develop performance-based design criteria that specify acceptable or target gradation ranges for granular surface materials.

Compared to the Iowa DOT specification in Figure 3.9, it can be seen that materials with a top size of 1 in. and any n values between 0.35 and 0.65 can meet the specification band. However, the 2D contour plot (Figure 3.10[b]) reveals that the corresponding soaked CBR values of this range of materials decreases by an order of magnitude (from 65% to 5%) as n increases from

0.35 to 0.65. This clearly demonstrates that an arbitrary gradation band is not sufficient to ensure the strength and performance of granular road surface materials.

For a material with a given top size, Figure 3.10(b) also indicates that as the n value decreases beyond the optimal value, the soaked CBR decreases rapidly and becomes practically independent of D_{\max} . This may be explained by particle packing characteristics, as shown in Figure 3.11; when the coarseness of a material decreases (n decreases) below a certain level, the coarse aggregates eventually float in a matrix of finer particles (Figure 3.11[c]), and the particle interlocking between the coarse aggregates is thereby greatly reduced, significantly lowering the shear strength of the material.

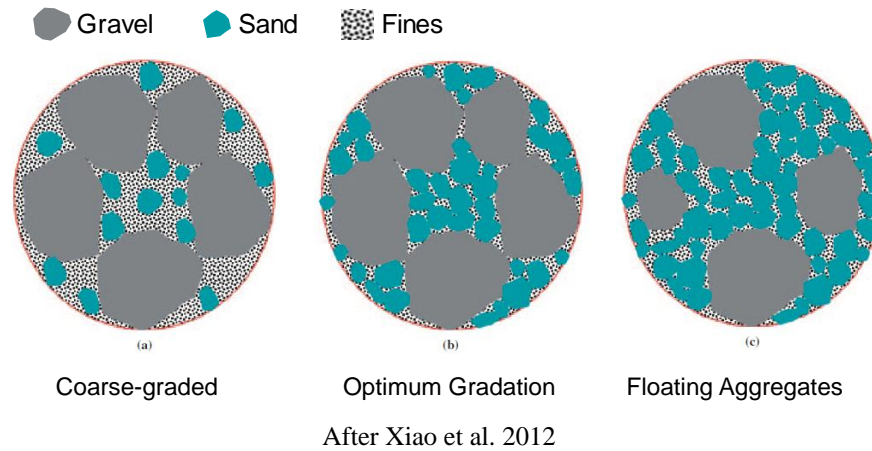


Figure 3.11. Schematics of particle packing states of a granular material with different gradations

The saturated mechanical properties of the material are then governed by those of the fine matrix (i.e., sands and fines). Conversely, when the coarseness of the material increases (n increases), the material becomes more coarse graded (Figure 3.11[a]), and the CBR for a given top size also decreases as n increases above the optimum value, but CBR remains somewhat proportional to top size, as previously shown in Figure 3.10(b).

3.5 Plasticity Effects on Undrained Shear Strength and Slaking Characteristics

Previous studies have reported that the plasticity of granular road surface materials is related to the severity of washboarding, potholes, aggregate loss, and dust emissions, as discussed in Chapter 2. In the present study, laboratory UCS and slaking tests were conducted on the 2-by-2 specimens of minus No. 40 material treated with different percentages of bentonite clay to determine the optimal plasticity index for granular road surface materials with respect to shear strength and slaking characteristics.

The granular materials were sieved through a No. 40 sieve, and the minus No. 40 materials were then treated with 2%, 4%, and 6% bentonite by dry weight. To disperse the bentonite and reach a more uniform consistency, a 0.5% sodium carbonate (i.e., soda ash) solution was used to

increase the water content of the bentonite-treated specimens, as recommended by Bergeson and Wahbeh (1990). The UCS and slaking test results including the dry unit weights and moisture contents of the specimens are summarized in Table 3.6 and Table 3.7, respectively.

Table 3.6. UCS test results for 2-by-2 specimens treated with different percentages of bentonite

Percent Bentonite	Dry Unit Weight (pcf)	Moisture Content (%)	UCS (psi)
0%	124.0	0.5	617.8
	121.5	0.5	619.4
	123.0	0.5	548.1
	112.0	8.6	42.0
	111.8	8.6	46.8
	111.6	8.8	44.9
2%	122.5	0.3	940.6
	123.1	0.3	954.9
	123.1	0.3	972.4
	122.7	0.3	907.5
	123.1	0.3	971.2
	123.2	0.4	906.9
	122.8	0.4	875.4
	121.3	0.4	885.9
	122.2	0.5	906.5
	120.5	11.4	35.7
	122.2	11.5	34.1
	120.2	11.5	38.2
4%	118.4	1.1	404.3
	117.0	1.1	390.9
	116.8	1.1	450.4
	117.1	1.3	381.3
	117.2	1.4	394.1
	116.9	1.4	371.8
	120.2	13.6	24.5
	117.6	13.7	22.9
	119.0	13.7	19.7
	120.3	13.7	22.0
	117.2	13.7	23.6
	117.2	13.8	20.7
	118.2	13.8	17.5
	116.7	13.8	21.6
117.5	14.0	19.1	
6%	114.5	1.5	449.5
	114.7	1.6	432.9
	108.4	1.7	400.1
	114.5	15.4	8.9
	115.0	15.4	8.3
	115.3	15.4	7.6

Table 3.7. Slaking test results for 2-by-2 specimens treated with different percentages of bentonite

Percent Bentonite	Dry Unit Weight (pcf)	Moisture Content (%)	Slaking Time (min)
0%	118.1	0.5	35
	118.4	0.5	33
	113.7	8.6	8
	113.9	8.6	8
	113.0	8.6	10
2%	121.1	0.3	39
	122.1	0.3	60
	122.0	0.3	110
	121.3	0.3	50
	120.8	0.3	50
	121.1	0.4	40
	121.9	11.5	22
	122.4	11.5	29
	120.4	11.5	29
	120.8	11.5	27
4%	117.7	1.1	1080
	119.6	1.1	990
	119.1	1.1	1150
	118.1	13.7	420
	117.0	13.7	450
	115.7	13.7	540
	118.5	13.7	840
	118.5	13.7	420
	116.6	13.7	720
	107.6	13.8	300
	120.0	13.8	269
	117.9	13.8	300
6%	115.5	1.6	2980
	114.8	1.6	2680
	114.5	15.4	210
	114.5	15.4	240

The UCS and slaking tests were conducted on specimens that were compacted at approximately the optimum moisture contents and on similar specimens that were oven dried 24 hours at 40°C. These two moisture contents approximate the upper and lower bounds of the moisture content range observed in the field.

Results of the UCS and slaking tests are summarized in Figure 3.12(a) and Figure 3.12(b) respectively, which both have logarithmic scales on the y-axes.

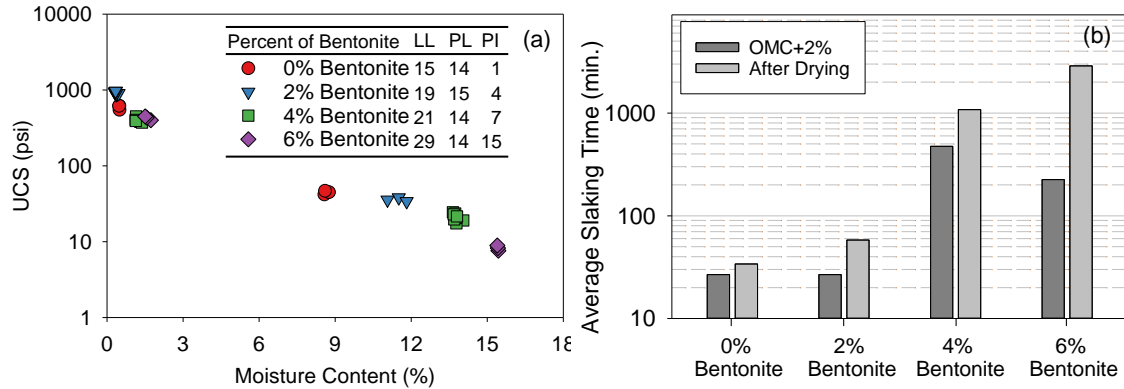


Figure 3.12. Results of (a) UCS and (b) slaking tests conducted on 2-by-2 specimens of minus No. 40 materials treated with different percentages of bentonite

Atterberg limits tests were also conducted on the untreated and bentonite-treated materials from which the specimens were prepared. As detailed in the figure, the PI of the specimens increased from 1 to 15 as the bentonite content increased from 0% to 6%.

Figure 3.12 (a) shows that the UCSs of the dried specimens are roughly similar for the range of bentonite percentages used, but the UCS is reduced by one to two orders of magnitude as moisture content is increased to near OMC. Additionally, the specimens with 6% bentonite (by dry mass of minus No. 40 material) generally show the greatest reductions in strength. These results suggest that adding excessive plastic fines such as bentonite may lead to rutting and skidding issues under wet conditions.

For slaking behavior, Figure 3.12(b) shows that the oven-dried specimens yielded longer disintegration times than the specimens with as-compacted (OMC+2%) water contents, as expected, and the 4% bentonite-treated specimens yielded the best slaking behavior among the specimens with as-compacted water contents. Based on these results, 4% bentonite by dry mass of particles passing the No. 40 sieve may be the optimal percentage for treating crushed limestone granular surface materials. Also, a target plasticity index range between 7 and 15 is recommended for the minus No. 40 fraction of treated materials.

3.6 Optimum Gradation and Plasticity Index for Granular Surface Materials

The laboratory study presented in this chapter focused on evaluating the effects of gradation and plasticity on the mechanical properties of granular road surfacing materials. Based on the results of the laboratory tests and statistical analyses, a theoretical optimal gradation in terms of maximizing the predicted soaked CBR for a given material with known top size can be determined using the statistical model presented in Figure 3.10.

It is well known that particle packing is also influenced by the material's morphology, whereas the statistical model and corresponding optimum range of n values for Fuller's model presented here are based on test results of crushed limestone materials from southwest Iowa. Based on the

authors' visual observations, most granular road surface materials, except for those consisting of rounded river gravel, have very similar morphologies to those tested in this study. The statistical model is therefore likely to be useful for examining the typical crushed limestone materials with top sizes of 3/4 to 1 in. commonly used for granular road surfacing. However, the statistical model requires further validation for other aggregate morphologies, for example, river gravel, which has more rounded particle shapes.

Comparing the proposed method of using Fuller's model with an optimum shape parameter n for a given top size to several current DOT specifications in the form of arbitrary gradation bands, the proposed method is more performance related and can be used to develop specifications with more precise target gradation curves rather than a wide gradation band that can actually encompass a large range of CBR strengths. For the plasticity effect, the laboratory test results showed that adding plastic fines can reduce the shear strength under wet conditions, but greatly improve the slaking performance. Based on the slaking test results, 4% bentonite by dry mass of the particles passing the No. 40 sieve is recommended for use with crushed limestone, and the recommended range of plasticity index is between 7 and 15.

CHAPTER 4. DESIGN, CONSTRUCTION, AND PERFORMANCE OF FIELD TEST SECTIONS

4.1 Introduction

The effects of gradation and plasticity on the soaked shear strength and slaking characteristics of granular surface materials were evaluated by means of laboratory tests in the previous chapter. To study the actual field performance of roadways constructed using the laboratory-determined optimal gradation and bentonite content, an existing granular-surfaced road section in Pottawattamie County and two granular-surfaced shoulder sections in Boone County, Iowa, were selected for constructing field test sections. The design, construction methods, and observed performance of the test sections are detailed in this chapter.

According to the Iowa County Traffic Map (DOT 2011), the annual average daily traffic (AADT) of the selected road section on County Road (CR) L66 in Pottawattamie County was 80 in the year 2016. The width of the road was approximately 28 ft, with a very flat vertical profile, as shown in Figure 4.1.

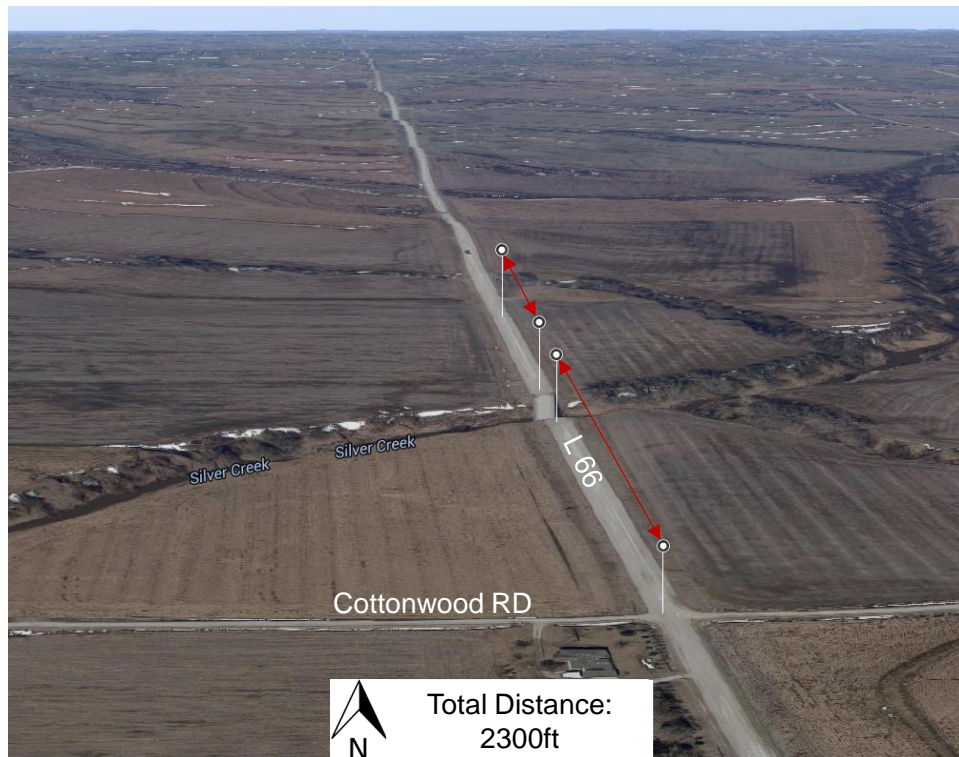


Figure 4.1. The selected granular-surfaced road section on County Road L66 in Pottawattamie County, Iowa

Shoulder test Site 1 is located on T Ave., a paved two-lane road with granular-surfaced shoulders (Figure 4.2). The southbound shoulder was selected for building test sections. The AADT of this road was 2,630 in the year 2015.



Figure 4.2. Shoulder test Site 1 on southbound T Ave. south of 205th St. in Boone County, Iowa

Shoulder test Site 2 is located on the Exit 126 off-ramp of Highway 30 eastbound (EB) to D Ave., shown in Figure 4.3. The AADT of the ramp was not available, but significant truck traffic was observed.

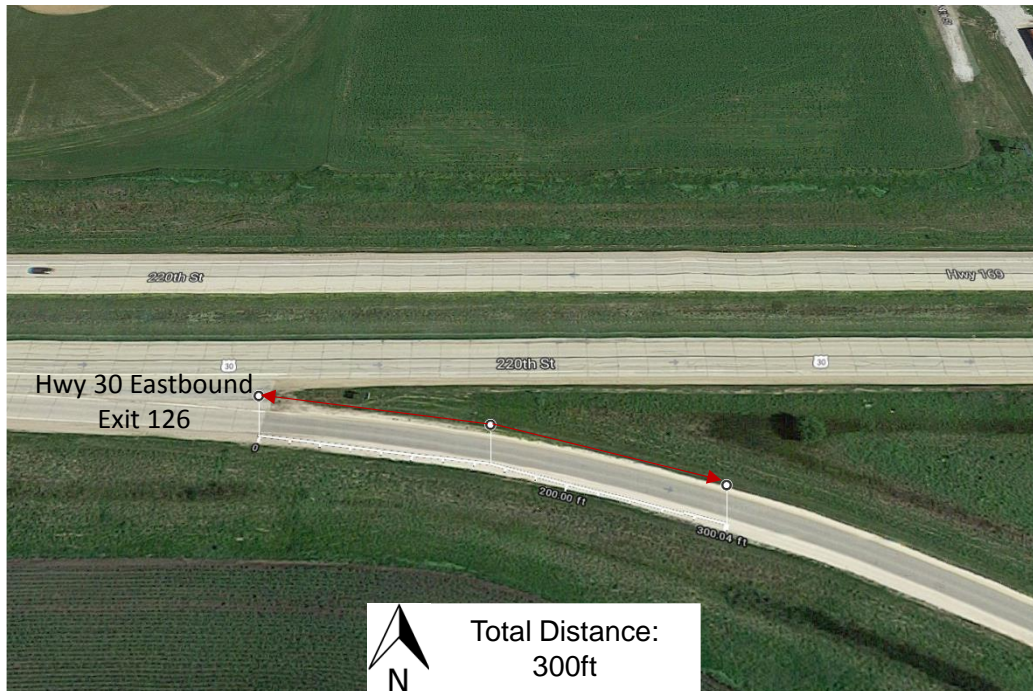


Figure 4.3. Shoulder test Site 2 on Exit 126 off-ramp of eastbound Highway 30 to D Ave. in Boone County, Iowa

4.2 Field Testing Methods

To evaluate the performance of the various control and test sections, three series of performance-based field tests and visual surveys were conducted. First, pre-construction field tests were conducted to assess the initial conditions of the existing road and shoulder sections. Samples were taken at this time to allow the optimum target gradations to be determined in the laboratory. Using the gradation optimization spreadsheet, the quantities and proportions of various virgin materials to add to the existing materials in order to reach the target gradations were determined. Second, a series of as-constructed (pre-freezing) field tests were conducted to determine the initial performance of the newly constructed sections prior to a winter freeze-thaw season. Third, post-thawing field tests were conducted after the spring thaw to determine the resulting changes in the stiffness, strength, and performance of the sections. This chapter describes the test setups and data analysis methods of the various field testing methods.

4.2.1 Dynamic Cone Penetrometer Test

The dynamic cone penetrometer (DCP) test was performed in accordance with ASTM D6951-09, Standard Test Method for Use of the Dynamic Cone Penetrometer in Shallow Pavement Applications, to estimate the in situ bearing capacity of the surface and subgrade materials. The test involves driving a conical point with a diameter at the base of 0.79 in., using a 17.6 lb hammer dropped a distance of 22.6 in., and measuring the penetration distance per blow, as shown in Figure 4.4.



Figure 4.4. DCP test performed on the Highway 30 off-ramp shoulder section

The penetration distance per blow, with units of inches per blow, is referred to as the dynamic cone penetration index (DCPI). In situ CBR values (referred to as DCP-CBR) of both the surface and subgrade materials can be estimated based on the DCPI values using the empirical correlations of Equations (4.1) through (4.3):

for all soils except CL soils with CBR < 10 and CH soils,

$$DCP-CBR = 292 / (DCPI \times 25.4)^{1.12} \quad (4.1)$$

for CL soils with CBR < 10,

$$DCP-CBR = 1 / (0.432283 \times DCPI)^2 \quad (4.2)$$

for CH soils,

$$DCP-CBR = 1 / (0.072923 \times DCPI) \quad (4.3)$$

Based on the DCP test results, the boundary between the surface and subgrade layers can be estimated by jumps or sudden changes in the slopes of the depth profiles, as shown in Figure 4.4.

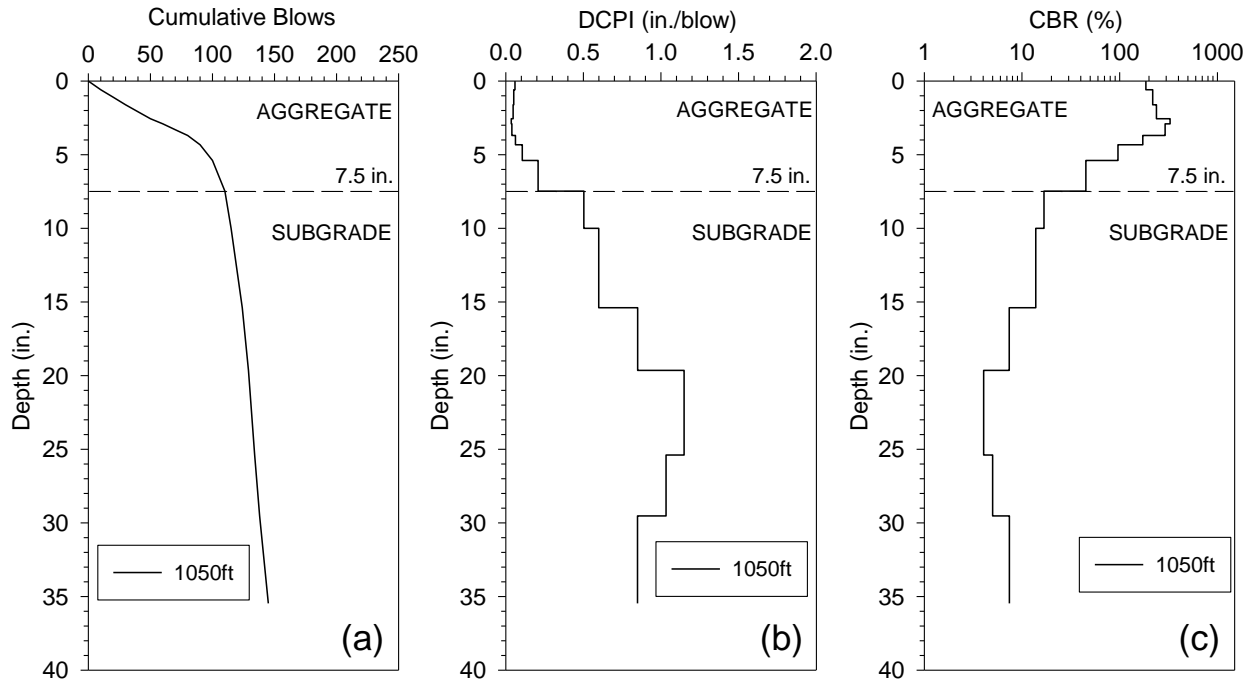


Figure 4.5. Example of DCP depth profiles; (a) cumulative blows, (b) DCPI, and (c) DCP-CBR

The weighted-average CBR of each material layer can then be calculated using Equation (4.4):

$$\text{Weighted - average CBR} = \frac{(CBR_i \times H_i) + (CBR_{i+1} \times H_{i+1}) \cdots (CBR_n \times H_n)}{\sum_i^n H_i} \quad (4.4)$$

The notation DCP-CBR_{AGG} will be used to denote the weighted-average CBR of the aggregate surface layer, and DCP-CBR_{SG} will represent the weighted-average CBR of the subgrade to a depth of 18 in. below the interface with the overlying aggregate surface layer.

4.2.2 Light Weight Deflectometer Test

The light weight deflectometer (LWD) test was used to rapidly evaluate the composite elastic modulus of the test sections. The test involves dropping a mass onto a circular loading plate and measuring the peak ground surface deflection underneath the plate using an embedded accelerometer. In this study, the LWD test was conducted using a Zorn Model ZFG 3000 device, shown in Figure 4.6.



Figure 4.6. Zorn Model ZFG 3000 LWD used in this study

The configuration of the device provide by the manufacturer is shown in Table 4.1. The manufacturer recommends using the device on stiff cohesive soils, mixed soils, and coarse-grained soils with maximum particle size less than 2.5 in.

Table 4.1. Properties of the Zorn ZFG 3000 LWD

Parameter	Value
Falling weight (kg)	10
Drop height (mm)	710
Maximum applied force (kN)	7.07
Total load pulse (ms)	18 ± 2
Deflection transducer	Accelerometer in plate
Measuring range (mm)	0.2 to 30 (± 0.02)
Plate diameter (mm)	300
Plate thickness (mm)	20
Type of buffers	Steel spring

For each testing location, the LWD test was performed by applying three seating drops of the weight to improve contact between the loading plate and roadway surface and then measuring the deflections for three subsequent load pulses. Based on Boussinesq's solution (elasticity theory), the elastic modulus (E_{LWD}) can be calculated from the average peak deflection for the three load pulses using Equation (4.5):

$$E_{LWD} = \frac{(1 - \nu^2) \sigma_0 A}{d_0} \times f \quad (4.5)$$

where d_0 is the measured average peak deflection at the center of the loading plate (mm); ν is the Poisson's ratio (assumed to be 0.4); σ_0 is the normalized applied peak stress (MPa); A is the radius of the plate (mm); and f is a shape factor that depends on the assumed contact stress distribution. In this study, a shape factor of 2 was assumed, which corresponds to a uniform stress distribution. The measurement influence depth of an LWD device is approximately equal to the diameter of its loading plate (Vennapusa et al. 2012).

4.2.3 Multi-channel Analysis of Surface Waves Test

The multi-channel analysis of surface waves (MASW) test was evaluated for determining elastic moduli of multi-layered granular-surfaced road systems in previous Iowa DOT projects (Li and Ashlock 2017, Li et al. 2017a, Li et al. 2015a). Compared to the FWD test, the MASW test evaluates the stiffness of the material layers at much lower strain levels. To generate the surface waves, a 2 lb ball-peen hammer with an attached accelerometer for triggering was used as a seismic source to impact a 6 in. square by 1 in. thick aluminum plate resting on the road surface. The vertical motion of the generated surface waves was measured using an array of 24 4.5 Hz geophone receivers installed on a custom-built land streamer with 6 in. spacing. The lower amount of energy (compared to the energy produced by a larger 10 lb sledgehammer used in some tests) and close receiver spacing were selected to focus the measurements on the surface aggregate layer and top few inches of subgrade. The MASW test configuration is summarized in Table 4.2.

Table 4.2. Configuration used for the MASW test

Test Setup Parameter	Value
Source-to-first-receiver offset (x1)	12 in.
Receiver spacing (dx)	6 in.
Total number of receivers (N)	24
Total length of receiver spread (XT)	11.5 ft

The MASW test measures the seismic Rayleigh-wave velocity as a function of frequency, from which the shear-wave velocity, or, alternatively, the small-strain modulus, can be determined for both of the surface and subgrade layers. Data from the MASW tests were used to back-calculate the shear-wave velocity (V_s) profile through an inversion procedure that uses the measured dispersion characteristics of the surface (Rayleigh) wave velocity (V_R) as input.

The MASW back-calculation procedure typically involves specifying layer unit weights and Poisson's ratios, after which the optimization procedure automatically searches over ranges of layer thicknesses and shear-wave velocities to find a best match between the measured and theoretical dispersion images. In this study, however, the thicknesses of the surface layers were

set equal to the values determined from the DCP test data, which enabled the back-calculation procedure to search only over a range of layer shear-wave velocities, thus reducing the computation time. The laboratory-determined standard Proctor maximum dry unit weights of the surface aggregate (130 pcf) and subgrade (96 pcf) were used for all sections in the back-calculations. The Poisson's ratios of the surface aggregate and subgrade material were assumed to be 0.3 and 0.4, respectively.

4.2.4 Dustometer Test

A dust measurement device developed at Colorado State University (Sanders and Addo 2000) was used to evaluate the fugitive dust emissions of the test sections. The test setup is shown in Figure 4.7. The dustometer is a metal filter box mounted on the rear bumper of a 1/2-ton pickup truck and connected by a 2 in. hose to a 1/3-horsepower high-volume suction pump. The suction pump is powered by a gas generator secured to the truck bed. The 10 by 10 in. opening of the metal filter box is covered with a 200 μm mesh metal grid and is horizontally aligned with the left rear wheel of the test vehicle. For each test, a pre-weighed glass fiber filter paper (0.3 μm) is placed inside of the filter box to collect dust. The vehicle is driven at a speed of 45 miles per hour (mph) during the test, and the suction hose is connected and disconnected from the running vacuum pump at the beginning and end of the test section. After the test, the filter paper is removed from the box and stored in a pre-weighed zip-top plastic bag for later weighing. The test results are reported in grams of dust collected per mile.

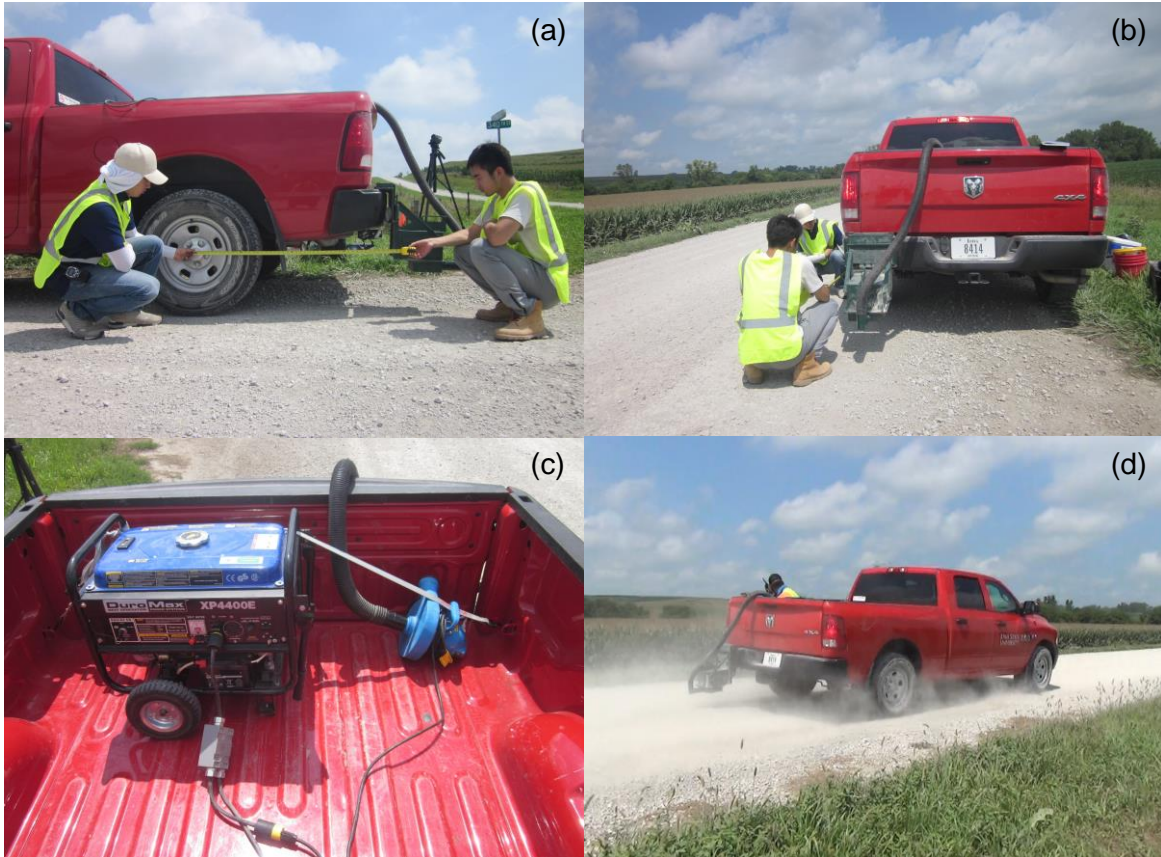


Figure 4.7. Dustometer test setup (a, b, and c) and a test conducted on the granular-surfaced road test sections (d)

4.2.5 Surface Conditions by Roadroid Smartphone App and Visual Ratings

Roadroid is an Android smartphone application developed by a Swedish company to evaluate roadway surface roughness and friction by using the built-in accelerometers and GPS sensors in modern smartphones (Jones and Forslof 2015). The app was used in this study to measure the roughness and friction coefficients of the test and control sections.

For the roughness test, the smartphone was mounted to the windshield of a 1/2-ton truck using a rigid windshield cellphone mount. The driving speed of the testing vehicle was controlled between 38 and 56 mph. During the test, the app can also automatically take photos or videos of the tested road sections. The collected testing data and photos were uploaded to the company's website for the further data processing and visualization (Figure 4.8).

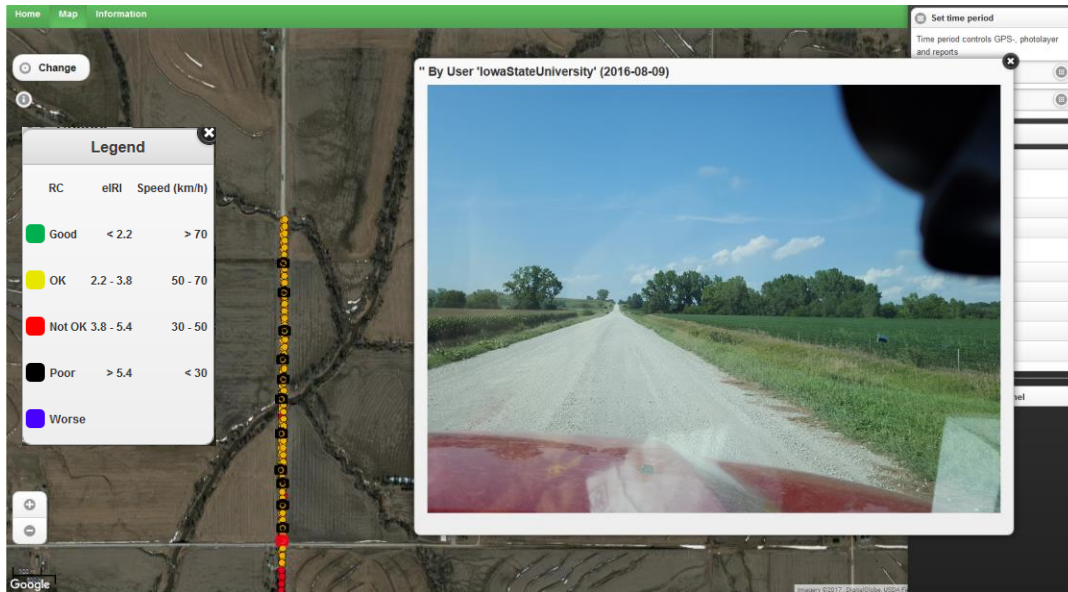


Figure 4.8. Visualization of the Roadroid roughness test data collected on the L66 test sections on August 9, 2016

According to Sayers et al. (1986), there are four classes of road roughness measuring methods: Class 1 – precision profiles, Class 2 – other profilometric methods, Class 3 – International Roughness Index (IRI) estimates from correlation equations, and Class 4 – subjective ratings and uncalibrated measures. The Roadroid app can provide two types of IRI values at the Class 3 level: (1) estimated IRI (eIRI) values, which are determined based on correlations between the cellphone vibration data and Swedish laser measurements on paved roads, and (2) calculated IRI (cIRI) values, which are calculated based on the quarter-car simulation model (Jones and Forslof 2015). In this study, the cIRI was used to compare the surface roughness of the test sections.

The Roadroid app was also used to evaluate the braking friction of the testing vehicle on the test sections. According to the instructions for the friction test, the vehicle should first reach a speed of at least 30 mph and then brake as hard as possible for at least 3 to 4 seconds, or until the vehicle fully stops. If the vehicle does not stop in this time period, the brake pedal should be released. The vehicle deceleration data is automatically analyzed, and the calculated friction coefficient (μ) of the roadway surface is immediately displayed and recorded.

A visual rating report form (Table 4.3) was developed so that grader operators could record their visual evaluations of the test section surface conditions. The rating report was created following the “Visual Assessment System for Rating Unsealed Roads” proposed by Huntington and Ksaibati (2015). The major distress types, including rutting, washboarding, potholes, loose surface aggregate, dust, and loss of crown, can be quantitatively evaluated using the form. In this study, a county motor grader operator used the rating report to document maintenance activities and visual evaluations of the test section surface conditions on different dates during the freeze-thaw period.

Table 4.3. Unpaved road surface condition rating report

Road Name		Section Name			Inspector Name	
Length of Section (ft)		Width of Section (ft)			Road Condition (e.g. Wet or Dry)	
Notes: (examples: Dust was not assessed due to moisture in surface material. Two blading passes were performed.)						
Score	Rutting	Washboarding	Potholes	Loose Aggregate	Dust	Crown
9	No or negligible ruts	No or negligible corrugations	No or negligible potholes	No or negligible loose aggregate;		
8	Ruts less than 1" deep and less than 5% of the roadway surface	Less than 1" deep; less than 10% of roadway surface area	Most small potholes less than 1" deep and less than 1' diameter	Berms <1" deep; Loose aggregate. <3/4" thick		
7						
6	Ruts between 1"-3" deep and 5% to 15% of the roadway surface	1"-2" deep; 10%-25% of roadway surface	Considerable potholes less than 3" deep and less than 2' diameter	Berms <2" deep; Loose aggregate <1.5" thick		
5						
4	Ruts between 3"-6" deep and 10% to 40% of the roadway surface	2"-3" deep; over 25% of roadway surface	Many potholes up to 4" deep and 3' in diameter	berms between 2"- 4" deep;	No visible dust	
3					Minor dust and no visible obstruction	Cross-slope >3%; good rooftop shape
2	Ruts between 6"-12" deep	Deeper than 3"; over 30% of roadway surface	Up to 8" deep and > 4' in diameter	berms >4" deep	Significant dust; Dust loss is major concern	1% to 3%
1	Ruts over 12" deep	Impassable	Impassable	Sand dunes	Heavy dust and obscures vision	<1%

4.2.6 Ground Temperature Monitoring

To monitor the ground temperature and frost depth of the granular-surfaced road test site in Pottawattamie County, two vertical arrays of thermocouples were installed on November 23, 2017 and monitored continuously through the 2016-2017 seasonal freeze-thaw period. One array was installed under the centerline and the other near the west shoulder (Figure 4.9).

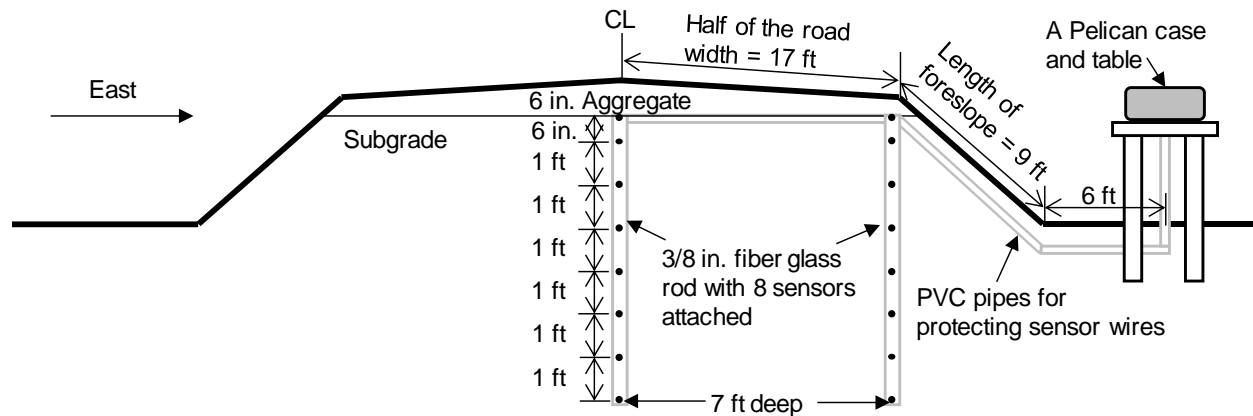


Figure 4.9. Cross-section profile of roadway and layout of the ground temperature sensors (not to scale)

A total of eight thermocouples were embedded in each hole. The top sensors were positioned at the boundary between the surface aggregate and subgrade, approximately 6 in. below the road surface. The remaining sensors from 1 to 7 ft below the road surface were spaced at 1 ft intervals. The ground temperature data was recorded at 15-minute intervals using two Omega OM-CP-OctTemp2000 data loggers. The sensor installation procedure is shown in Figure 4.10. A trench was first dug using an automatic chain trencher. Two holes were then created by pushing a custom-fabricated steel rod with a 1/2 in. conical tip into the ground with the aid of a small amount of water. A hammer drill with a 12 in. long bit was used to help start the hole near the centerline. The sensors were attached to the 3/8 in. fiberglass rods using Gorilla tape, and the rods were then easily pushed into the holes, resulting in very good contact with the surrounding subgrade soil. The thermocouple wires were routed along the trench to a wooden table through 1 in. PVC pipes filled at the end with expanding spray foam to keep pests out, and then the wires were connected to the data loggers, which are sealed in a weatherproof Pelican case.



Figure 4.10. Installation procedure for the subgrade temperature sensors

4.3 Results of Pre-construction Tests and Visual Surveys

The pre-construction field tests and visual surveys were conducted to determine the mechanical properties, road geometries, and thicknesses of the granular surface layers of the selected road and shoulder sections. Representative surface and subgrade samples were collected for laboratory determination of the soil index properties.

4.3.1 Granular-surfaced Road Section

Two sets of visual surveys and field tests were conducted on the selected road section, on April 14, 2015 and March 29, 2016. The DCP test results are summarized in Table 4.4. The average thickness of the surface layer decreased from 3.9 in. to 3.7 in. after one year, and the CBR values of both the surface and subgrade materials decreased significantly. Based on the visual surveys, the existing surface material had a top size of 3/4 in. and contained excessive sands and fines. The roadway surfaces were dry for both testing periods.

Table 4.4. Pre-construction DCP test results of the selected road section on CR L-66

Testing Date	Distance from South End (ft)	Surface Layer Thickness (in.)	Weighted-Average CBR _{AGG} (%)	Weighted-Average CBR _{SG} (%)
4/14/2015	250	3.0	33.7	14.9
	450	4.0	90.2	25.0
	650	3.0	72.8	17.6
	850	5.7	174.9	14.7
	1,050	6.5a	178.4	11.7
3/29/2016	300	3.1	38.4	6.5
	600	4.1	44.7	5.0
	900	4.4	73.3	8.6
	1,800	4.4	35.8	14.5
	2,100	3.3	32.7	3.5
	2,400	3.1	22.3	2.2

^a The testing location close to the bridge approach had a much thicker aggregate surface layer. This location is not included in the calculation of the average thickness of the aggregate surface layer.

The sieve and hydrometer analysis tests were conducted on representative surface-course and subgrade samples collected on March 29, 2016. The subgrade material contained 99% fines, consisting of 66% silt and 33% clay, with an AASHTO classification of A-7-6(26) (USCS: CL). The existing granular surface course had an AASHTO classification of A-1-b (USCS: SM), and contained much more sand and fines than both the Iowa DOT specification and the optimal gradation determined in the laboratory study using Fuller’s model ($D_{max} = 1$ in. and $n = 0.4$), as shown in Figure 4.11.

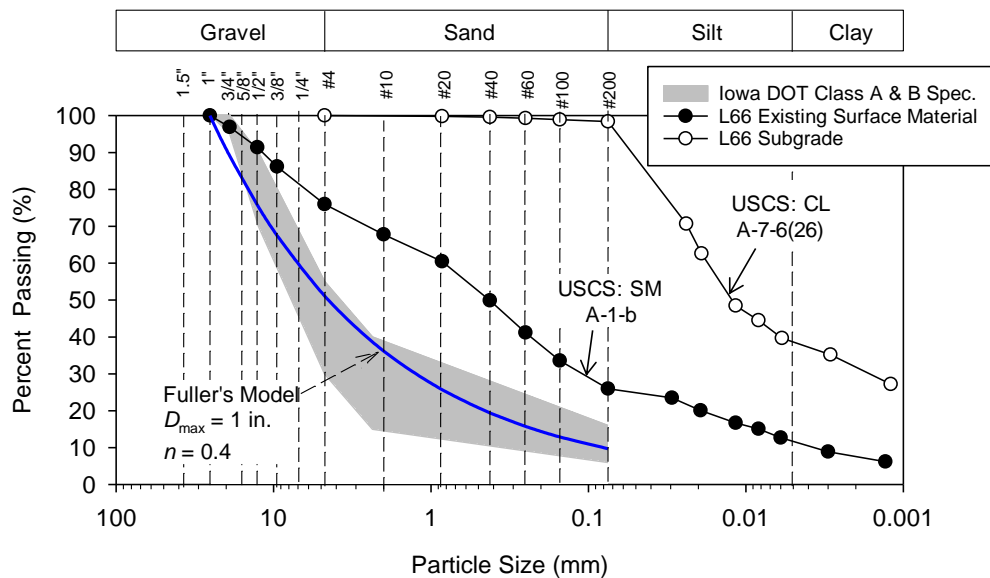


Figure 4.11. Particle size distributions of existing surface and subgrade materials of the selected granular-surfaced road section on CR L-66

To identify the sources of the excessive sand and fines in the surface material and measure the actual thickness of the surface layer, excavations were performed using a hammer drill at two of the DCP test locations on April 14, 2015 (Figure 4.12).



Figure 4.12. Excavation performed on the test section to measure thickness of surface layer and identify the source of excessive fines

Based on the DCP test data, the first test location at 650 ft from the south end of the road section is representative of the average road condition. The second location at 1,050 ft from the south end was very close to the bridge abutment and had a much thicker aggregate surface layer, likely due to repeated settlement and placement of fresh aggregate (the “bump at the end of the bridge” problem). During excavation, the materials for each inch of depth were removed and stored in zip-top bags to determine the profiles of gradation and plasticity with depth through laboratory testing. The gradation and Atterberg limits test results of the samples collected at the different depths are shown in Figure 4.13.

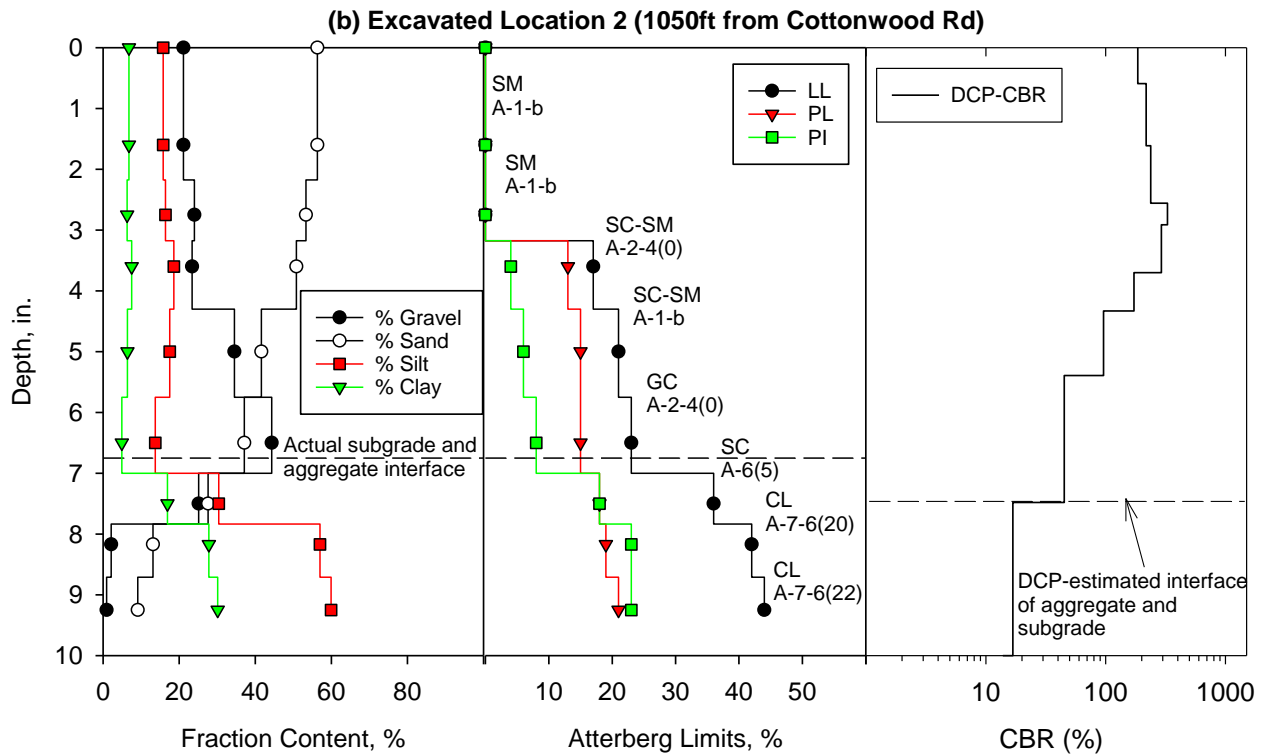
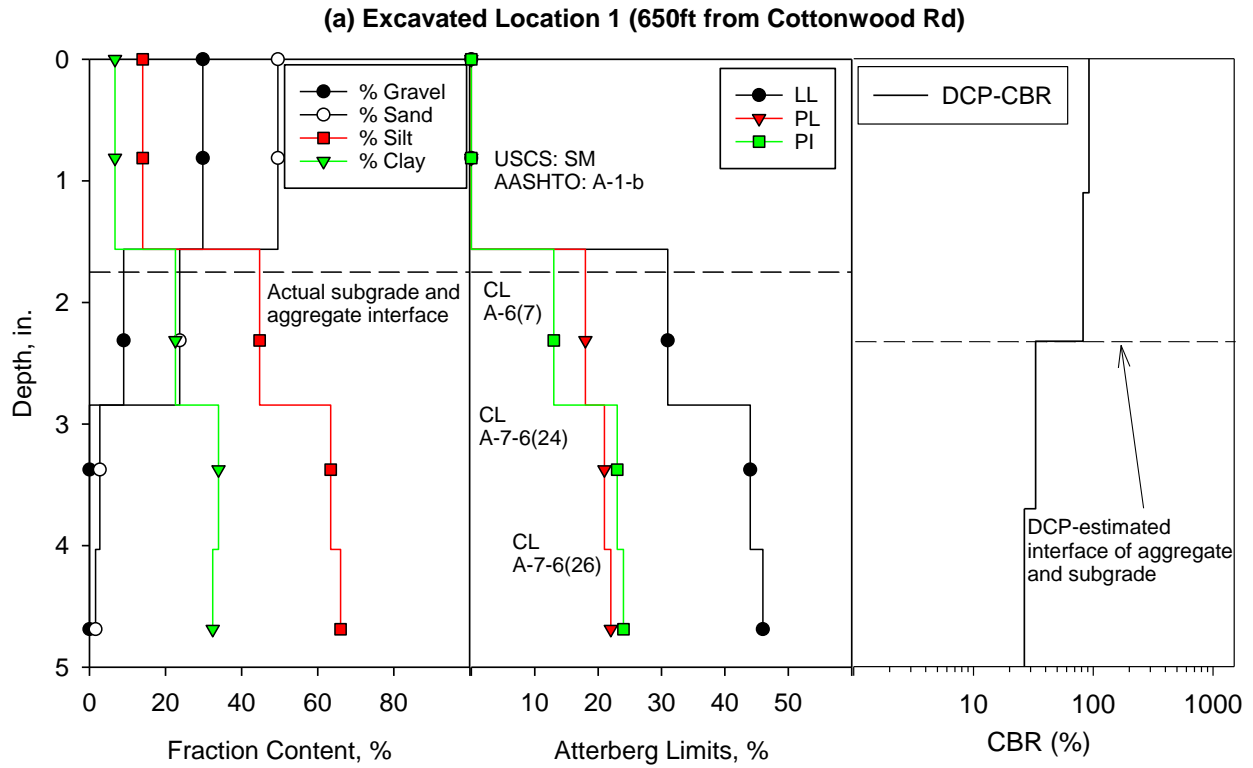


Figure 4.13. Depth profiles of gradation, Atterberg limit, and DCP-CBR values of excavated (a) Location 1 and (b) Location 2

The laboratory test results show that the surface material of Location 1 was nonplastic and contained more gravel and sand than the subgrade material (Figure 4.13 [a]). The CBR of the surface material was approximately 70%, while that of the subgrade was approximately 20%. The top inch of subgrade also had higher gravel and sand contents due to mixing with the overlying surface course materials. Based on the field observations, the interface between the surface and subgrade layers was very clear, which indicates that the excessive amounts of fines and sand-size particles in the surface material were primarily caused by material degradation of the crushed limestone due to heavy traffic loading and not by migration of the subgrade into the surface course.

For Location 2 near the bridge, the gravel content of the surface material remained relatively constant in the top 4.3 in. and then increased with depth, as shown in Figure 4.13 (b). The plasticity of the surface material also increased with depth. These results indicate that the top layer of surface aggregate degraded more than the bottom layer, and the bottom layer may also have been contaminated due to subgrade intrusion.

The actual thicknesses of the surface aggregate layers measured during the hand excavations were approximately 0.5 in. less than those estimated by the DCP tests. These discrepancies may be due to the fact that the top layer of subgrade was compacted by traffic, giving it a similar shear resistance to the surface material under dry conditions.

4.3.2 Granular-Surfaced Shoulder Sections

The pre-construction visual survey and field tests were conducted on the T Ave. shoulder section (granular shoulder test Site 1) on April 19, 2016. The district maintenance crews reported that this section typically suffered significant rutting and edge drop-off issues during thawing and rainy periods. However, no significant damage was observed during the pre-construction visual survey.

The pre-construction DCP test results for shoulder Site 1 are summarized in Table 4.5. The surface-subgrade interface could not be clearly determined from the results because of the similar CBR values for the two materials. Additionally, field excavations revealed that the surface and subgrade materials were mixed together, resulting in a gradual transition between their CBR values.

Table 4.5. Pre-construction DCP test results of granular shoulder test Site 1

Distance from North 205th St (ft)	Weighted-Average CBR _{AGG} (%)	Weighted-Average CBR _{SG} (%)
200	19.9	15.9
400	25.5	13.2
600	7.9	13.3
800	39.1	8.6
1000	38.1	11.0

Representative pre-construction surface and subgrade shoulder materials were also sampled for laboratory tests. The particle size distributions of the samples are shown in Figure 4.14. The surface material had a top size of 3/4 in. and contained excessive fine gravel and coarse sand-size particles compared to the Iowa DOT specifications. The subgrade consisted of well-graded soils containing about 60% sand and 40% fines.

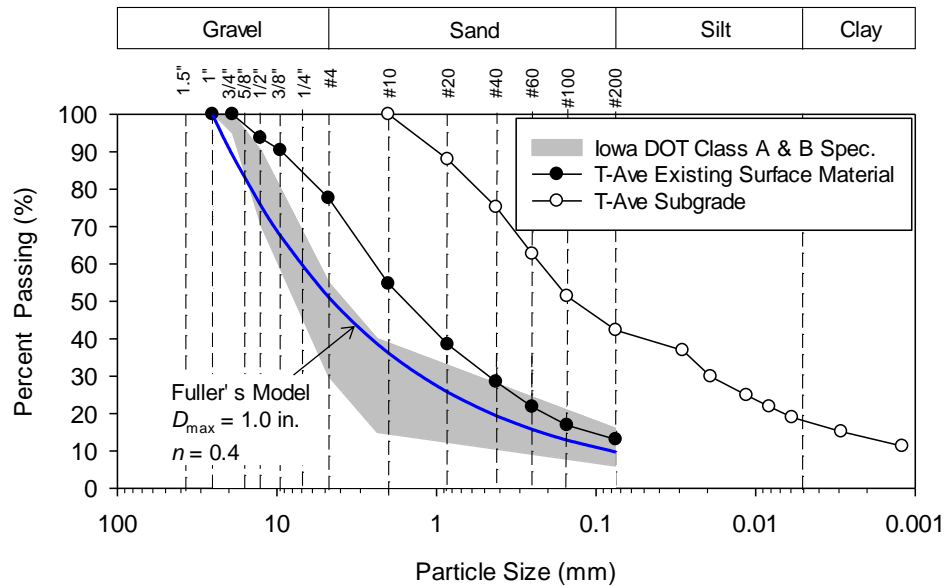
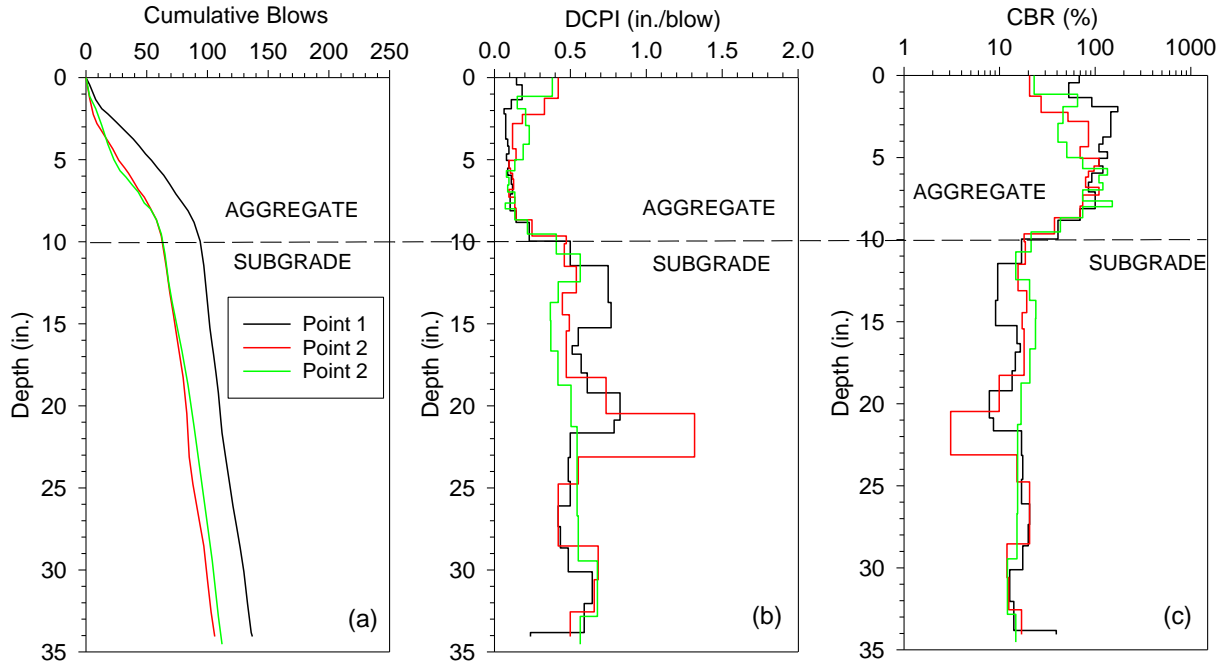




Figure 4.15. Survey photos of Highway 30 ramp section (granular shoulder test Site 2): (a) surface material on November 3, 2015, (b and c) edge drop-off on March 22, 2016

The DCP test results show that the granular-surface layer of the highway ramp section was approximately 10 in. thick with an average CBR of 71.3%, but the top 2 in. of the aggregate surface layer had lower CBR values than the lower part of the aggregate layer, as shown in Figure 4.16.



**Figure 4.16. DCP depth profiles of Highway 30 ramp shoulder section;
 (a) cumulative blows, (b) DCPI, and (b) DCP-CBR**

For this test site, the loose surface aggregate in the top 2 in. and deeper materials from 2 to 4 in. depths were sampled for laboratory testing. The gradation of the loose upper aggregate was coarser and contained approximately 0% fines, while the PSD of the lower material was close to the optimal PSD determined in the laboratory study using Fuller's model (Figure 4.17).

that would result in a gradation of the mixture as close as possible to the optimal gradation characterized in terms of the Fuller's model parameters.

4.4 Design and Construction of the Test Sections

In this study, an investigation was conducted to identify potential construction equipment to cost-effectively modify the gradation of existing granular surface materials. Based on the laboratory and field test results, test sections were designed and constructed.

4.4.1 Investigation of Potential Construction Equipment for Recycling Granular Surface Materials

Based on the web survey results and field observations, most granular surface materials contained excessive fines. Several types of equipment that can potentially be used to process existing granular surface materials to enable removing the fines were evaluated in a desk study. However, most of the commercial equipment included crushing, milling, and full-depth reclamation machines that are typically used to crush large size rocks or pavement surfaces but cannot easily control the material gradations or fines contents. Some types of on-site or mobile screeners, including railway ballast cleaners and mobile screeners, could be used to screen out large aggregates and remove finer particles, but the opening sizes of the screeners are too large for processing granular surface materials (the smallest opening is usually 1/8 in.), and the process could be very time-consuming and expensive.

As an alternative, the feasibility of using a vacuum street sweeper to reduce fines contents of existing unpaved road materials was briefly evaluated in this study. A field demonstration test was conducted on a granular-surfaced parking lot at Iowa State University. A commercial vacuum street sweeper (Green Machines Model 636) owned by ISU was used to remove fine particles of the existing surface material, as shown in Figure 4.18. The field test showed that the street sweeper can rapidly and effectively remove fines of the loose surface material, but without any modifications, the mechanical brooms cannot break through the surface crust to disturb deeper materials, as shown in Figure 4.18(b).

For the field evaluation, two tests were conducted. The first test was conducted using the street sweeper without any modification. It can be observed that the larger size particles were vacuumed into the hopper, as shown in Figure 4.18(c) and Figure 4.18(e). To keep the larger particles on the roadway surface, a No. 10 screen (0.079 in.) was installed at the entrance of the hopper, as shown in Figure 4.18(d), and a second test was conducted. With the screen installed at the entrance of the hopper, the large size aggregates were effectively prevented from being vacuumed into the hopper (Figure 4.18[f]).



Figure 4.18. Demonstration of using a vacuum street sweeper to remove fines of granular surface materials: (a) vacuum street sweeper, (b) vacuumed roadway surface with coarse material brushed to center and sides, (c) vacuum chute without a screen, (d) vacuum chute with screen installed to retain coarse material on road, (e) material in the hopper vacuumed without the screen, and (f) material in the hopper vacuumed with a screen

The gradation of the existing and vacuumed surface materials as well as the processed materials from the hopper are compared in Figure 4.19. The results show that the vacuum street sweeper effectively reduced the sand and fines contents, and the screen installed at the entrance of the hopper kept more of the large particles on the road. However, the smallest size of the screen that can be used without damage was not determined.

Gradation Optimization for Granular Surface Materials
Developed in Iowa Highway Research Board Project TR-685

Purpose:

This program was developed based on a performance-based free-design approach used to recycle existing degraded surface materials of granular-surfaced roads by mixing in fresh quarry materials with or without subgrade to achieve an optimized target gradation. This program was developed in the IHRB Project TR-685 sponsored by the Iowa DOT.

Theory:

This program calculates the target optimal gradation based on the maximum aggregate size (D_{max}) and particle size distribution shape factor (n) of Fuller's model. The optimal range of the n value is recommended based on experimental and field test results obtained in Project TR-685. The gradation of representative existing surface and/or subgrade materials need to be accurately determined by users. If the subgrade will be incorporated to improve the plasticity of the surface material, the gradation of the existing surface plus subgrade mixture will be calculated in the program and compared to the theoretical optimal gradation, and then the missing size ranges will be identified. Since the resulting target virgin material gradation may not be locally available, the program can also optimize the proportion of two or three locally available materials to provide the closest gradation to the target virgin material gradation.

Inputs:

The green color cells are the inputs that need to be provided by users. The dry unit weights of the surface and subgrade materials can be adjusted based on users' experience. The average thicknesses and representative gradations of the existing surface aggregate and/or subgrade need to be measured. If the subgrade will not be incorporated, enter 0 for the thickness and gradation of the subgrade. The target final thickness of the surface aggregate layer must be more than four times the top size of the virgin material.

Instructions:

1. Click "Enable Editing" and then "Enable Contents" in the yellow security warning ribbon above.
2. Fill in the green cells.
3. Enter the gradations of the available virgin materials.
4. If using only two materials, enter zeros in the Quarry Material C column.
5. Click the 'INSTALL SOLVER' button to activate the Excel Solver Add-in.
6. Click the "RUN" button.
7. The optimized proportions and quantities of the virgin materials are shown in the blue cells.

District		Project	Granular Surfaced Road	Date	9/3/2017
County	Cass County	Note	This is a trial version of the program	Designer	Cheng Li

Road Geometry		Properties of Existing Materials	
Road Length	5280 ft	Thickness of Existing Surface Material	1.50 in.
Average Road Width	26 ft	Dry Unit Weight of the Virgin Material	125 pcf
		Thickness of Subgrade to be Incorporated into the Surface	1.00 in.
		Dry Unit Weight of the Subgrade	90 pcf
		Total Thickness of the Existing Surface and Subgrade	2.50 in.

Final Design Parameter		Final Design Parameter										
Target Final Thickness	5.00 in.	0.35 to 0.40 is recommended. The coarseness increases as the n value increases.										
Target Maximum Aggregate Size (D_{max})	1.00 in.											
Target Gradation Shape Factor (n)	0.35											

Sieve No.	Sieve size (mm)	Optimal Gradation (%)	Existing Surface Material Gradation (%)	Subgrade Gradation (%)	Calculated Gradation of the Existing Surface and Subgrade Mixture (%)	Quarry Material A (%)	Quarry Material B (%)	Quarry Material C (%)	Optimized Quarry Virgin Gradation (%)	Target Virgin Material Gradation (%)	Final Gradation with Target Virgin Material (%)	Final Gradation with Optimized Virgin Material (%)
2	50.8	100.0	100.0	100.0	100.0	100.0	100.0	0.0	100.0	100.0	100.0	100.0
1.5	38.1	100.0	100.0	100.0	100.0	100.0	100.0	0.0	100.0	100.0	100.0	100.0
1	25.4	100.0	100.0	100.0	100.0	100.0	99.0	0.0	94.3	100.0	100.0	97.1
3/4	19.0	90.3	93.0	100.0	95.3	77.0	78.0	0.0	77.8	85.4	90.3	86.5
1/2	12.7	78.5	88.9	98.8	92.1	36.0	60.0	0.0	55.0	64.8	78.5	73.5
3/8	9.51	70.9	84.8	97.1	88.8	18.0	51.0	0.0	44.1	53.0	70.9	66.4
#4	4.76	55.7	70.8	95.4	78.8	16.0	36.0	0.0	31.8	32.5	55.7	55.3
#8	2.38	43.7	56.3	93.8	68.5	13.0	28.0	0.0	24.8	18.9	43.7	46.7
#16	1.19	34.3	44.7	92.3	60.1	11.0	21.0	0.0	18.9	8.4	34.3	39.5
#30	0.595	26.9	35.5	91.2	53.6	9.6	16.0	0.0	14.7	0.2	26.9	34.1
#50	0.297	21.1	27.0	90.3	47.5	5.4	13.0	0.0	11.4	0.0	23.8	29.5
#100	0.149	16.6	20.4	88.0	42.3	3.2	11.0	0.0	9.4	0.0	21.2	25.8
#200	0.075	13.0	16.6	87.1	39.5	0.0	9.6	0.0	7.6	0.0	19.7	23.5
Proportion (%)						21	79	0	100	100		
Quantity (tons)						375.9	1411.6	0.0	1787.5	1787.5		

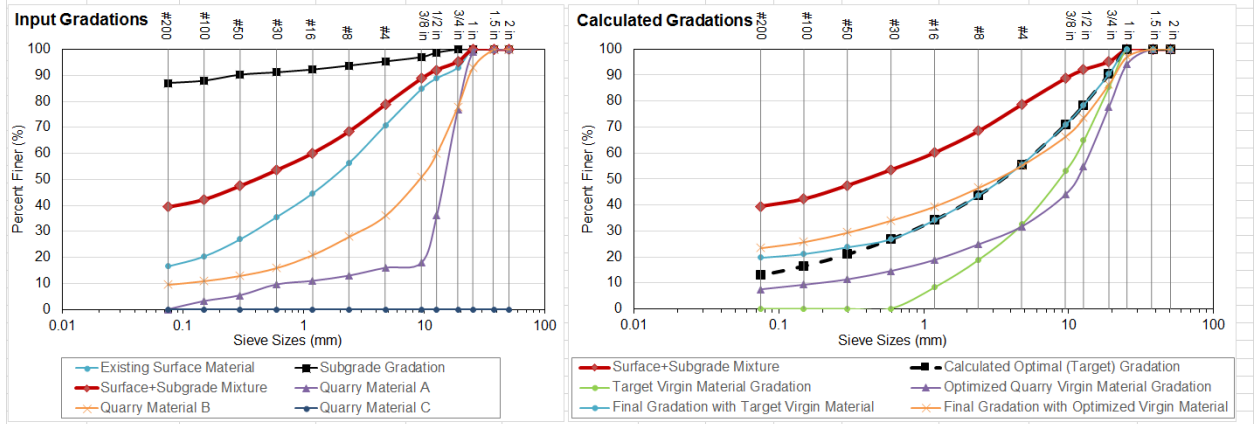


Figure 4.20. Screenshot of the gradation optimization program

According to the AASHTO 1993 aggregate-surfaced road design catalog (AASHTO 1993), a surface thickness of 7 in. is recommended for roads in climatic Region 3 with fair- or good-quality subgrades and low traffic volumes. Therefore, the sections were designed with a thickness of 7 in. The lengths and nominal as-built cross-section profiles of the four granular-

surfaced road test sections determined based on the as-constructed DCP test data are shown in Figure 4.21.

For Section 1, the existing surface material was recycled by mixing in Virgin Aggregate 1 (quarry road rock) to reach to the optimal target gradation ($n = 0.4$, $D_{max} = 1$ in.) based on the findings from the laboratory study, and bentonite was added to increase plasticity. To account for material loss during construction, the target rate of bentonite application was increased from 2% to 3% by dry mass of the entire gradation. To evaluate the influence of the plasticity of the granular surface material, Section 2 was constructed with the same materials, but without the bentonite. For Section 3, a different type of material termed Virgin Aggregate 2 (quarry road rock containing excessive fines) was mixed with the existing aggregate without adding bentonite. Section 4 was a control section featuring existing aggregate and current maintenance practices for comparison.

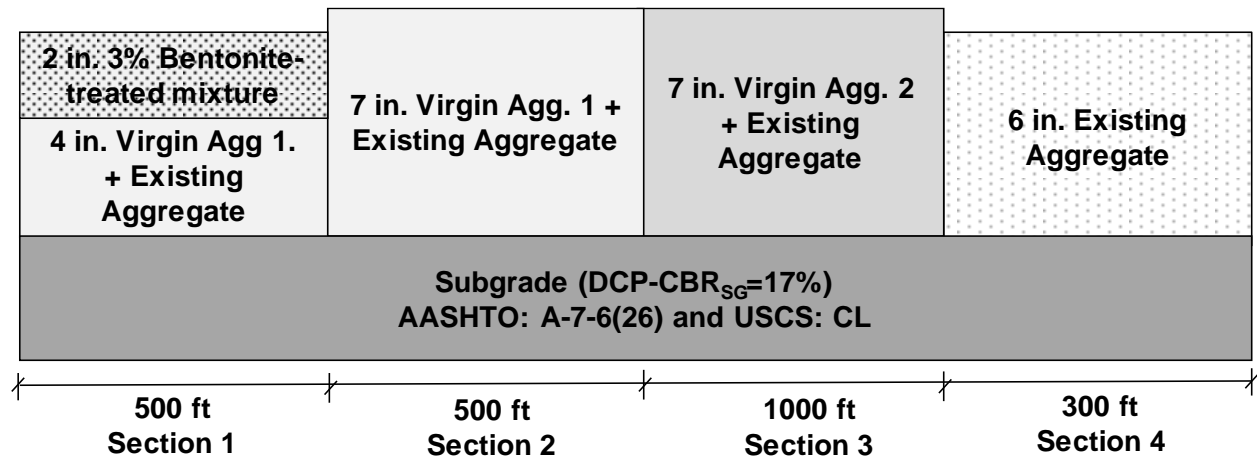


Figure 4.21. Nominal cross-section profiles of the granular-surfaced road test sections (not to scale)

The construction procedures and equipment used for building the test sections are shown in Figure 4.22. For Sections 1 and 2, the Virgin Aggregate 1 material was dumped on the roadway surface and mixed with the existing surface material by windrowing using motor graders, as shown in Figure 4.22(a) and (b). To aid compaction, the water content of the mixtures was increased using a water truck during the mixing process (Figure 4.22[c]). The field moisture contents of the mixtures were adjusted in the field by hand-feel to be close to the optimum moisture contents from laboratory standard Proctor tests. For Section 1, the 3% bentonite (Table 3.3) was incorporated into the top 2 in. of material using the FAE tractor-powered soil reclaimer shown in Figure 4.22(d). To disperse the bentonite to reach to a better consistency, 0.5% sodium carbonate (i.e., soda ash) by dry mass was added to the water tanker, as recommended by Bergeson and Wahbeh (1990). A 15,000 lb vibratory smooth drum roller was used to compact the surface materials using four machine passes (Figure 4.22[e]). The bentonite-treated surface material after compaction was very hard and smooth, as shown in Figure 4.22(f).



Figure 4.22. Construction procedures for the granular-surfaced road test sections:
(a) placing virgin aggregate with dump trucks, (b) mixing the virgin and existing surface material with motor graders, (c) spreading water to increase water content for compaction, (d) incorporating bentonite powder with the tractor-powered soil reclaimer, (e) compacting the new surface layer with a vibratory smooth drum roller, and (f) the bentonite-treated surface material after compaction

For Section 3, the Virgin Aggregate 2 material was mixed with the existing surface material to a depth of 6 in. using the reclaimer, as shown in Figure 4.23(a). Similar to Sections 1 and 2, the original plan was to incorporate 3% bentonite over the first 500 ft to create two test sections. However, it was observed during construction that the virgin quarry materials contained much more fines than expected according to the quarry’s provided gradation. The plasticity of the fine particles was evaluated by hand in the field, as shown in Figure 4.23(b); the evaluation indicated a low plasticity index. Incorporating the bentonite would have resulted in a mixture with excessive fines content leading to a muddy and slippery surface. The bentonite was therefore eliminated from the first half of Section 3, resulting in a single 1,000 ft long test section (Figure 4.21). The new surface mixture of the existing and virgin quarry aggregates containing natural

finer is shown in Figure 4.23(c) after compaction. To verify whether the excessive fine particles in the final surface were from the virgin quarry aggregate or stirred up from the subgrade during construction, the color of the excessive fines was compared to that of the subgrade during construction, and Virgin Aggregate 2 was also sampled from the quarry immediately after construction; the comparison revealed that the excessive fines came from the virgin quarry pile that was used (Figure 4.23[d]).



Figure 4.23. Construction of Test Section 3: (a) mixing Virgin Aggregate 2 with existing surface material using FAE reclaimer, (b) checking plasticity of fine particles, (c) the new surface material after compaction, and (d) Virgin Aggregate 2 of the stockpile in the quarry

Laboratory tests were also conducted on the quarry sample to determine its actual gradation, and the results confirmed that the Virgin Aggregate 2 contained much more gravel and fines than the gradation provided by the quarry, as shown in Figure 4.24. The quarry-provided gradation for Virgin Aggregate 2 had 8% fines, but ISU test results showed that the sample from the stockpile contained 18% fines, and the resulting final surface mixture of Section 3 had 28% fines. This issue can greatly influence the performance of the proposed design method. To ensure performance, field quality control/quality assurance (QC\QA) testing methods and equipment for the rapid determination of the gradation and plasticity of quarry materials are needed.

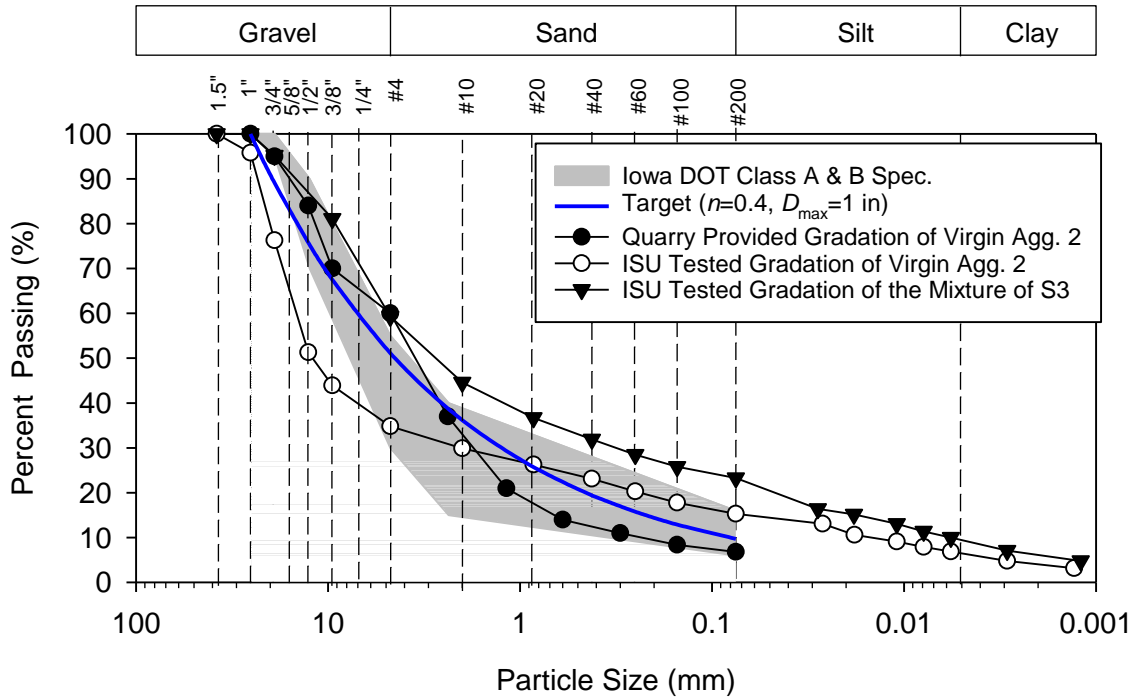


Figure 4.24. Gradations of Virgin Aggregate 2 provided by quarry and tested at ISU lab, and resulting gradation of the as-constructed mixture of Section 3

Sieve and hydrometer analyses and Atterberg limits tests were performed on representative samples collected from the surface materials of all test sections during construction, and their particle size distributions are compared in Figure 4.25.

Based on the PSD data, the gradation parameters for Fuller’s model were also calculated. The top size (D_{max}) of the as-constructed materials in Sections 1 through 3 was 1 in., while that of the unmodified control section was 0.9 in. The PSD shape factor (n) of the surface materials ranged between 0.16 and 0.39, and the gradation of Section 2 ($n = 0.39$) was closest to the theoretical optimal gradation ($n = 0.4$). The bentonite-treated Section 1 contained approximately 8% higher fines content than that of the optimal target gradation. The PSD of Section 3 was very similar to Section 1, but with more sands and fines. The gradation of the control Section 4 was the finest among the four test sections because the material had already been abraded by traffic for some time. The plasticity index values of the surface samples are also listed in Figure 4.25. The bentonite-treated sample of Section 1 yielded a PI of 28, which is above the range of 7 to 15 recommended in Section 3.5. The PI of the Section 3 sample was 8, and the samples of Sections 2 and 4 were nonplastic.

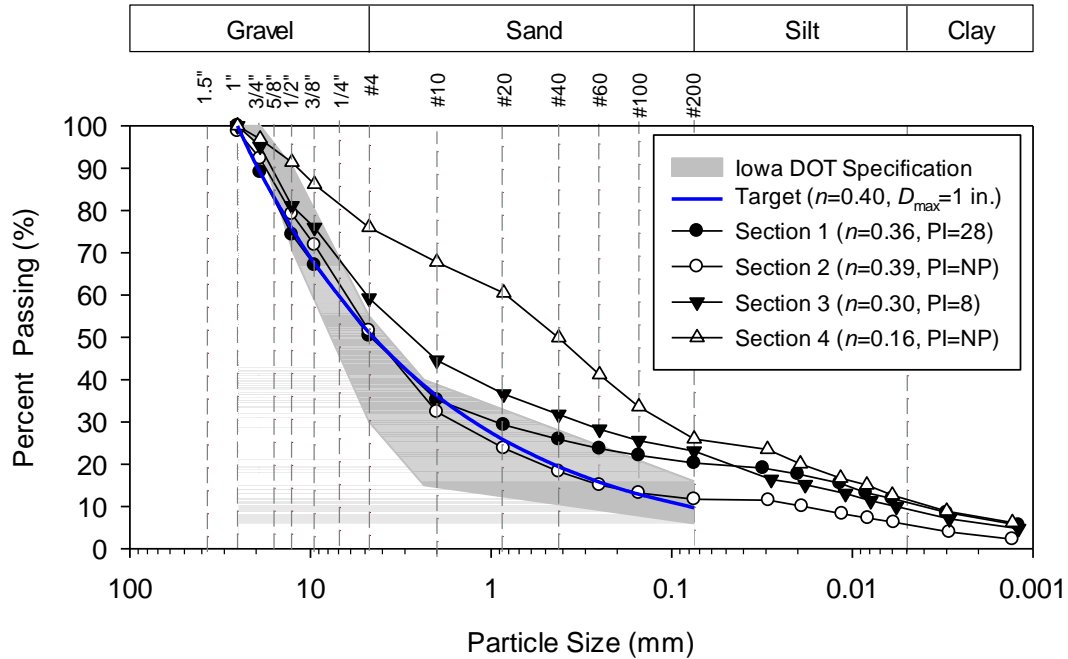


Figure 4.25. As-constructed gradations of representative samples from the granular surfaces of test sections

The gradation and plasticity test results were also used to predict the field performance of the different materials based on the unpaved road surface material selection chart developed by Paige-Green (1989) in South Africa (see Section 2.3.2). According to chart (Figure 4.26), Sections 1 and 3 are predicted to perform well, but Sections 2 and 4 may suffer washboarding and raveling issues because of the low plasticity of the fine particles (< No. 40 sieve).

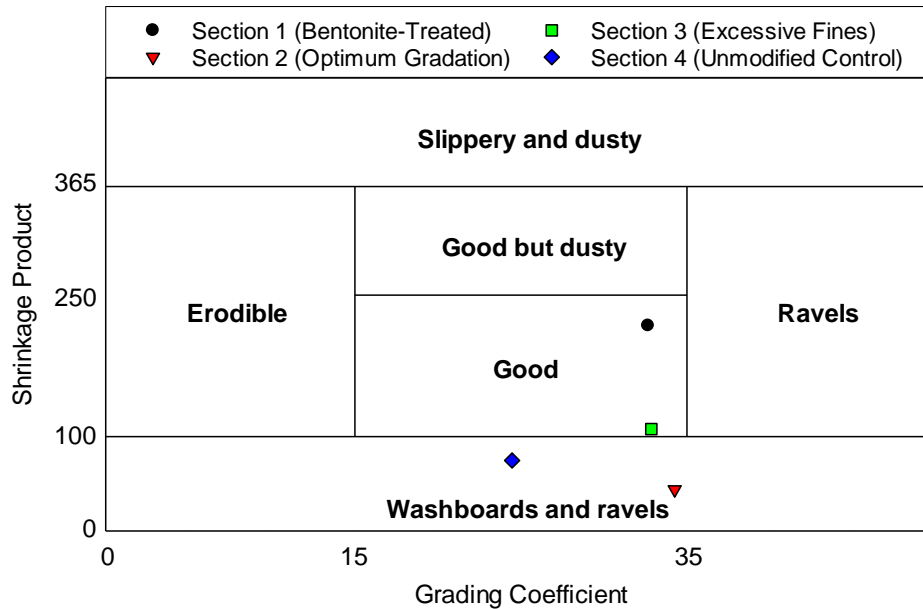


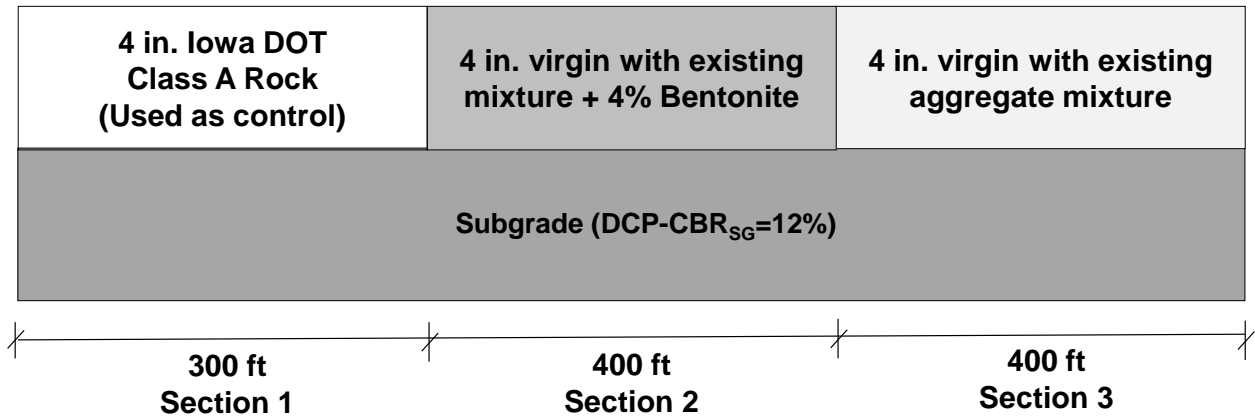
Figure 4.26. Performance predications based on the material selection chart developed by Paige-Green (1989) in South Africa

4.4.3 Design and Construction of the Granular-Surfaced Shoulder Sections

The shoulder test sections were also designed with the goal of determining whether the optimal gradation and plasticity specifications developed in Chapter 3 can minimize the rutting and edge drop-off issues and improve performance for granular-surfaced shoulders. The nominal cross-section profiles of the test sections on T Ave. (shoulder Site 1) and the Highway 30 off-ramp (shoulder Site 2) are shown in Figure 4.28. Considering that shoulders usually experience much less traffic than granular-surfaced roads, the slaking behavior should be a more significant influence factor on performance than shear strength. Therefore, the bentonite incorporation rate of 3% used on the granular-surfaced road test sections was increased to 4% for the shoulder sections.

The construction procedures and equipment used in building the T Ave. shoulder sections on June 14 and 15, 2016 are shown in Figure 4.28. The existing surface material was first removed and pushed onto the roadway surface (Figure 4.28[a]). For the Class A rock Section 1, the Iowa DOT-specified Class A aggregate material was used to replace the existing material, and the section was then considered as a newly constructed control section. For Section 3, the optimal gradation was achieved by mixing two available virgin quarry materials (1 in. concrete stone and concrete sand) with the Class A rock in proportions determined using the gradation optimization program described in Section 4.4.2. The resulting mixture was blended using a motor grader (Figure 4.28[b]). Section 2 was constructed the same as Section 3, but the 4% bentonite by dry mass was incorporated using a soil tiller, as shown in Figure 4.28(c) and (d). The sections were all compacted with a rubber tire roller, as shown in Figure 4.28(e).

(a) T-Ave Shoulder Test Sections



(b) Highway Ramp Shoulder Test Sections

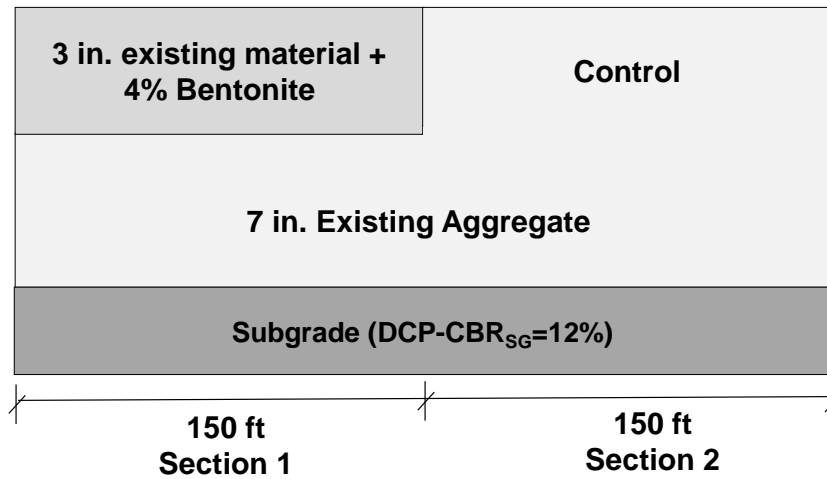


Figure 4.27. Nominal cross-section profiles (not to scale) of the shoulder test sections on (a) T Ave. and (b) Highway 30 EB off-ramp



Figure 4.28. Construction procedures of granular-surfaced shoulder test sections: (a) removing existing T Ave. shoulder surface material with a motor grader, (b) mixing virgin and existing material on road surface and placing back on the shoulder, (c) spreading bentonite powder on surface of Section 2 and spraying with water, (d) incorporating bentonite with a soil tiller, (e) shaping the treated material with a motor grader, and (f) compacting using a rubber tire roller

The as-constructed gradations of the surface materials of the T Ave. test sections are shown in Figure 4.29. The Section 1 Class A material nearly met the Iowa DOT specification and was closer than Sections 2 and 3 to the target optimal gradation in the sand-size range but was

slightly further from the target in the gravel range. The gradations of Sections 2 and 3 were similar, with lower gravel and sand contents than the target. The PI of the bentonite-treated Section 2 material was 19, whereas the other two materials were nonplastic.

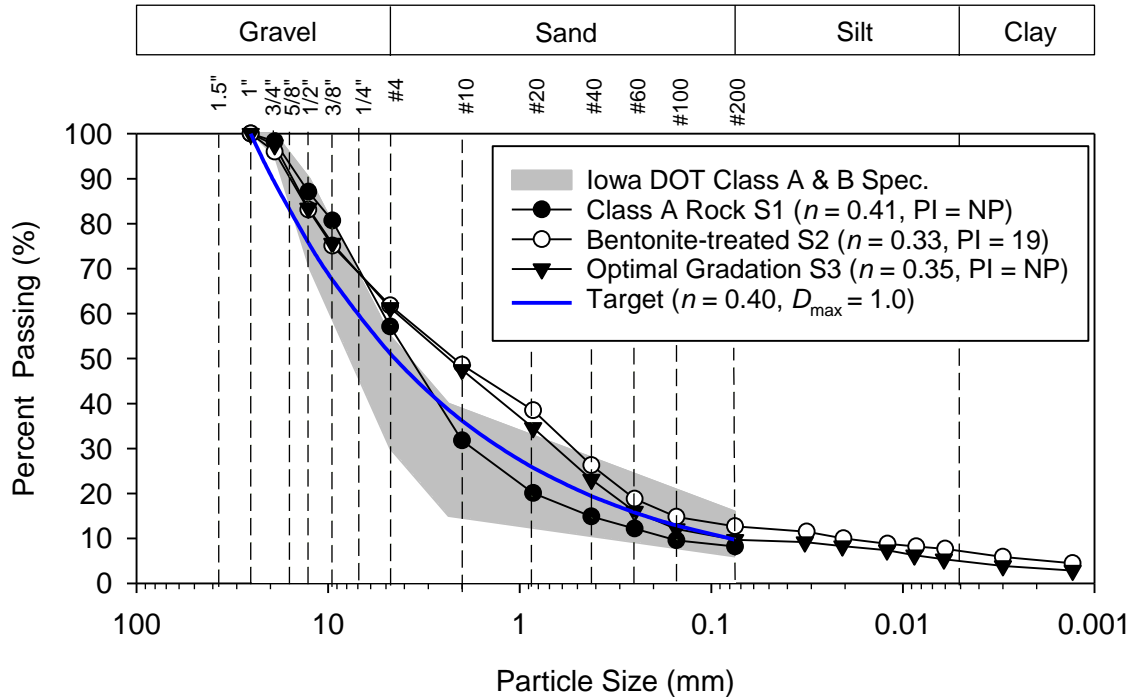


Figure 4.29. As-constructed gradations of representative samples of T Ave. shoulder test sections

For the Highway 30 ramp shoulder sections, which were constructed on June 15, 2016, no virgin aggregate material was added because the gradation of the existing material was very close to the optimal target gradation, as shown in Figure 4.17. For the bentonite Section 1, the 4% bentonite was incorporated into the top 3 in. of existing material using the soil tiller. For the control Section 2, the edge drop-off damage was repaired during construction. The as-constructed gradations shown in Figure 4.30 were approximately the same and very close to the target. However, the bentonite-treated surface material had a PI of 49.

The temperature differences at the same depths between the center and shoulder locations are shown in Figure 4.32. The maximum difference reached 7°F at 6 in. depth, and the difference decreased as depth increased; the temperature difference also exhibited a seasonal fluctuation. The center was colder than the shoulder in winter and warmer than the shoulder in summer. The temperature differences may have been caused by several factors, such as the different surface exposures to wind and solar radiation, the uniformity of the surface aggregate thickness, different subgrade properties and moisture profiles, heat transfer over the fore-slope surface of the ditch, and the insulating properties of vegetation or snow on the ditch surface.

Based on the long-term temperature data, the maximum frost penetration depths and freezing and thawing periods of the subgrade were determined as shown in Figure 4.33. The 2016-2017 winter was relatively mild. The maximum frost penetration of the center location was approximately 2 ft, which was slightly deeper than that of the shoulder location. The freezing period was about 71 days, and the thawing period was 5 days. The last portion of frozen subgrade thawed at a depth of approximately 1.25 ft around February 20, 2017.

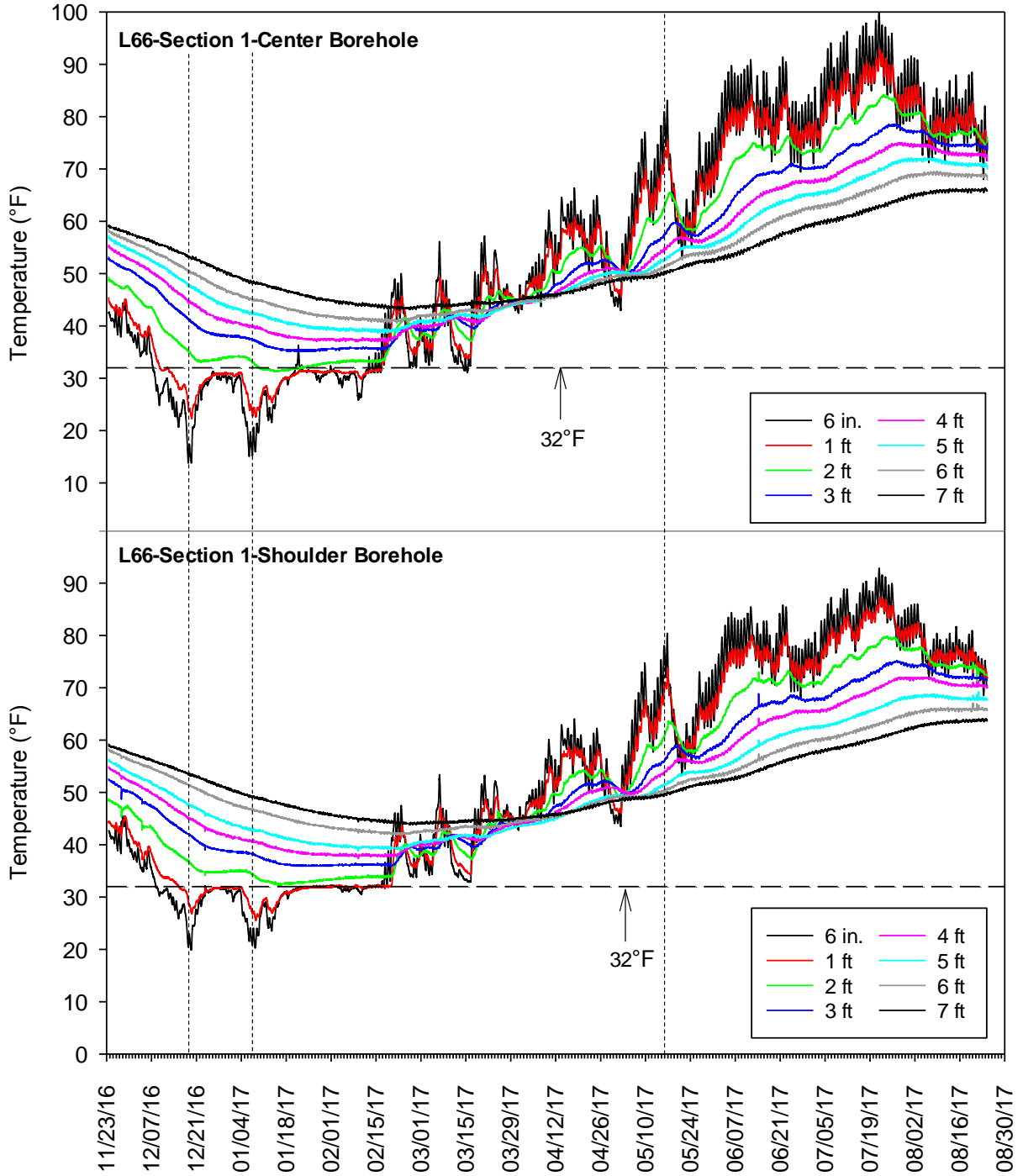


Figure 4.31. Ground temperature data of the center and shoulder locations of the granular-surfaced road test site on CR L-66

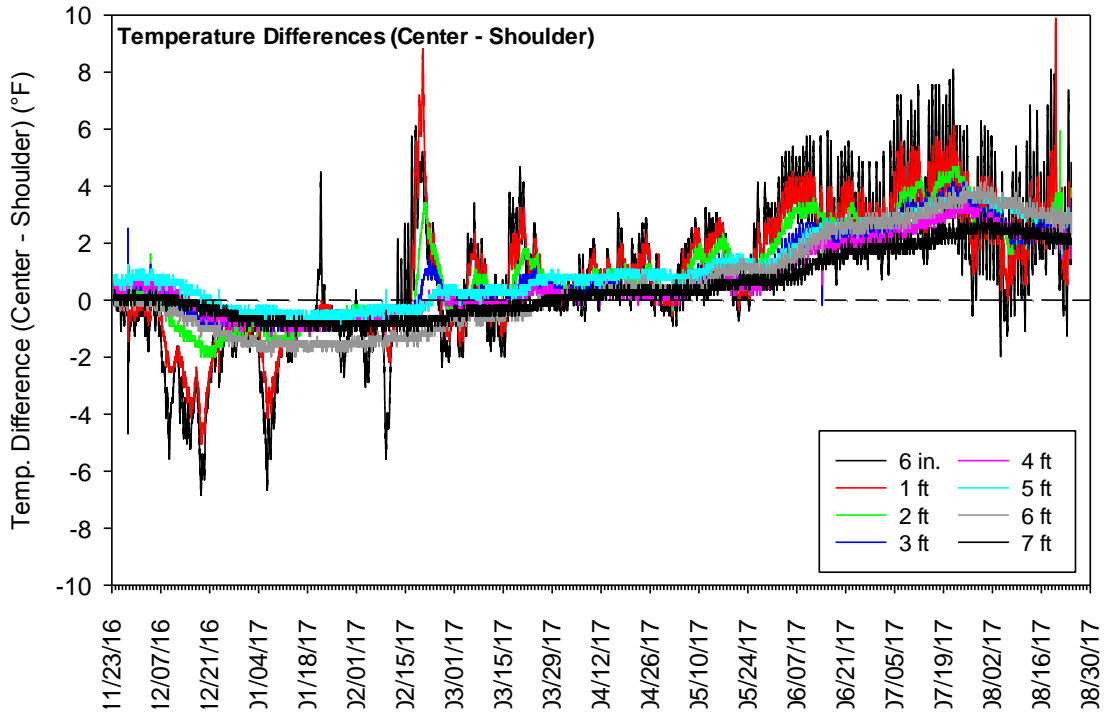


Figure 4.32. Temperature differences at the same depths between the center and shoulder locations

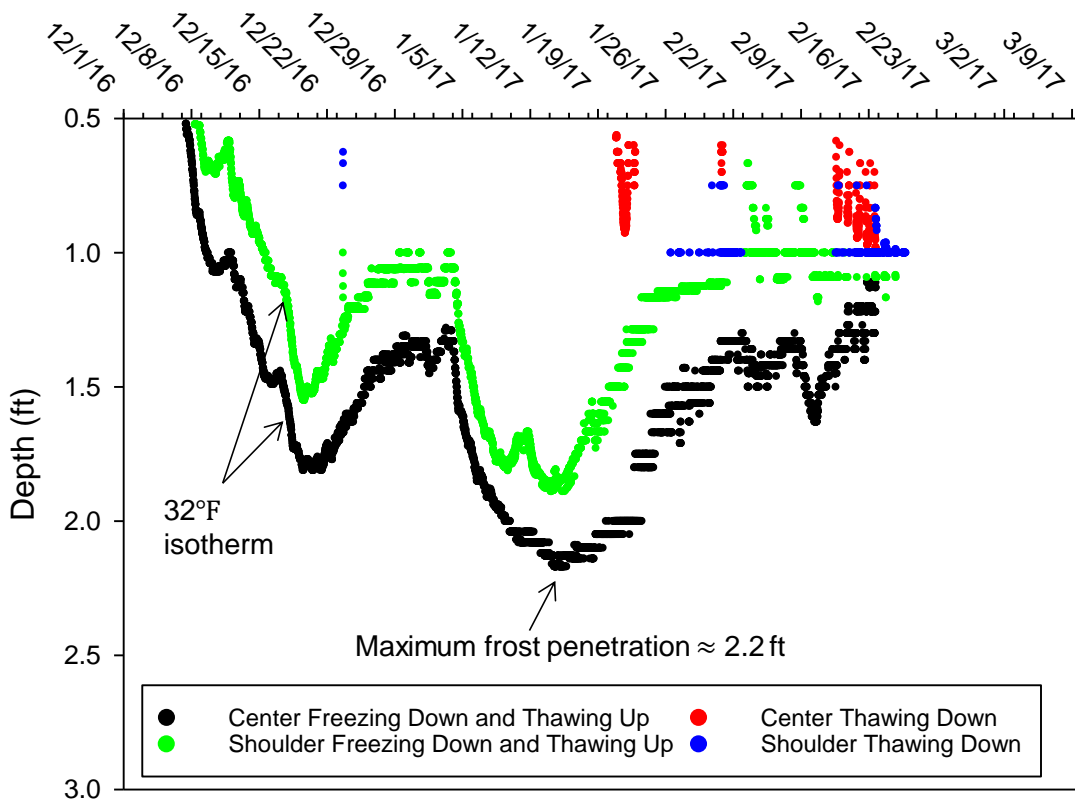


Figure 4.33. 2016-2017 subgrade freezing-thawing period of the CR L-66 site

4.5.2 Surface Conditions

During the project, several groups of survey photos were taken to monitor the surface conditions of the test sections. Approximately 5 in. of rain fell on the site two weeks after construction. A group of survey photos taken the next day by the county engineer revealed that the bentonite-treated Section 1 yielded a much tighter and smoother surface than the other two sections (Figure 4.34). Larger aggregate accumulating on the shoulders and between the wheel tracks can be observed for Sections 2 and 3. A survey photo was not taken on this date for the control section, but more dust and damage was observed away from the test sections by the county engineer.



Figure 4.34. Survey photos taken on July 22, 2016 by Pottawattamie County Engineer John Rasmussen

Survey photos taken during the 2016-2017 freezing and thawing period are shown in Figure 4.35. No significant rutting was observed in any of the test sections, but the control Section 4 and finer gradation Section 3 suffered more potholes and wheel tracks.

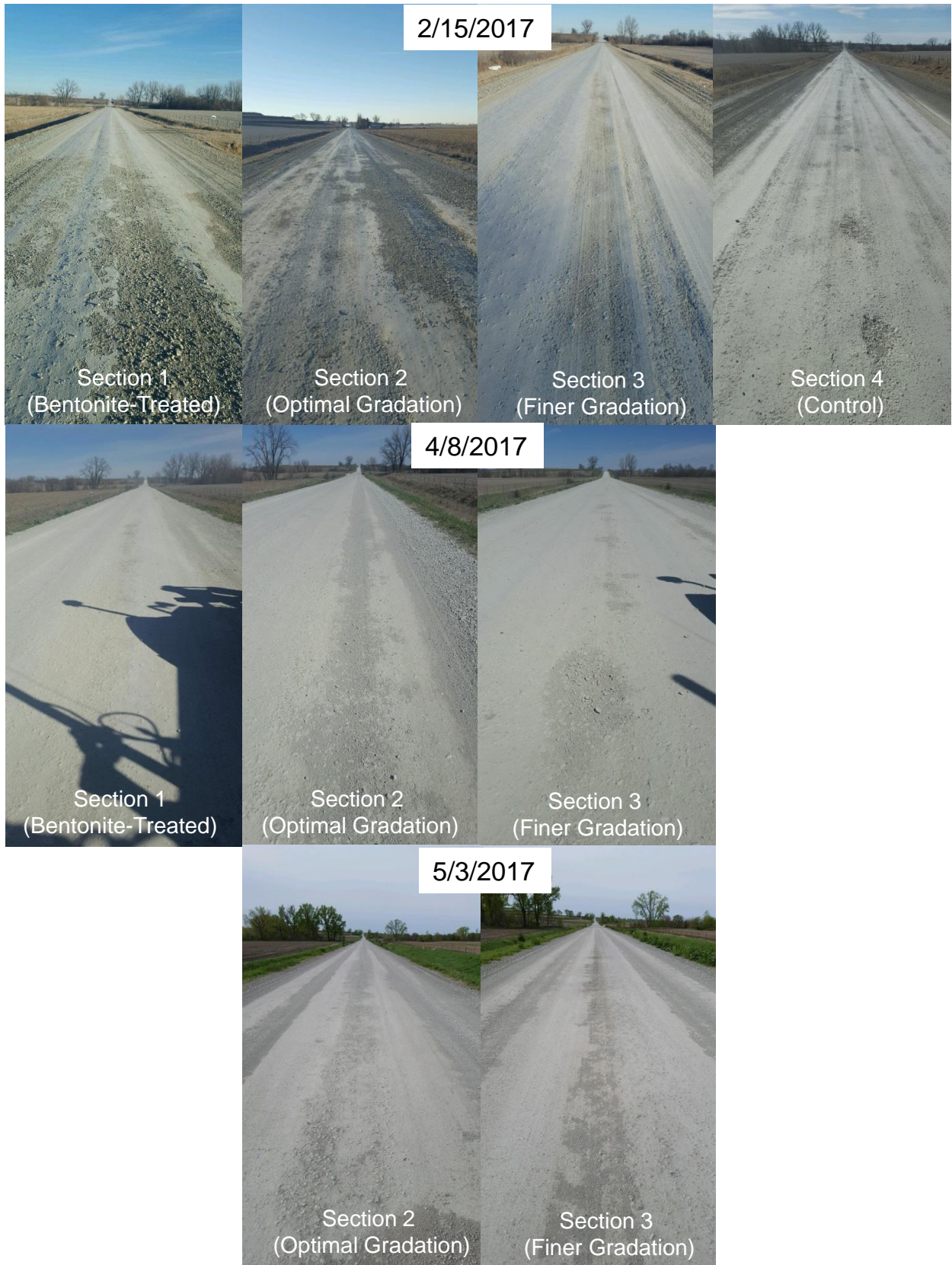


Figure 4.35. Survey photos taken during the 2016-2017 freezing and thawing period

The roughness and friction of the roadway surfaces of the various test sections were evaluated using the Roadroid smartphone app. The results of three groups of IRI tests conducted at different periods showed that the average trends are relatively consistent (Figure 4.36). The as-constructed cIRI values (July 25, 2016) are higher than those measured pre-freezing (August 9, 2016) and post-thawing (May 5, 2017). The two latter groups of tests showed that the cIRI values of the test and control sections were approximately at the same level.

The average coefficient of friction ($\bar{\mu}$) values of the test sections are also summarized in Figure 4.36. According to the Roadroid app's manual, friction coefficients larger than 0.3 are considered good. The test results indicate that the friction provided by the different materials were all similar and exceeded 0.3.

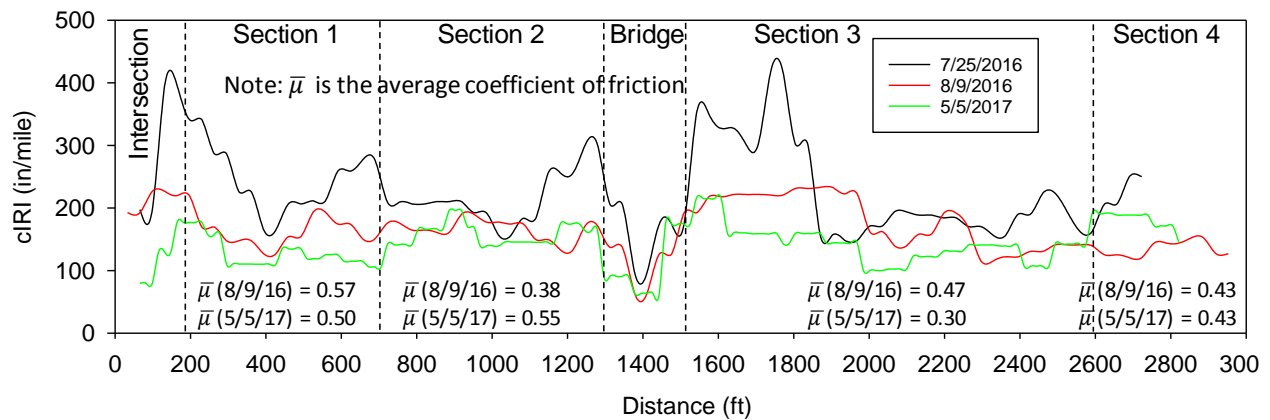


Figure 4.36. Calculated IRI (cIRI) and average coefficient of friction ($\bar{\mu}$) values of test section surfaces as estimated by Roadroid smartphone app

The roadway surface damage and maintenance activities documented by the county motor grader operator are summarized in Table 4.7. No documentation was performed for the control Section 4 during the first two groups of visual surveys. Based on the visual rating reports, potholes were the issue suffered most often by the test sections, indicating that controlling the gradation and plasticity alone are not sufficient to prevent potholes. In addition, the visual surveys indicated that Section 3, with excessive low-plasticity fines, suffered more severe potholes than the other three sections and yielded more severe rutting during the thawing period.

Table 4.7. Surface damage and maintenance activities of the test sections documented by the county motor grader operator

Date	Road Condition	Section 1	Section 2	Section 3	Section 4
9/14/2016	Wet	Repair one pothole (4" deep and 3" in diameter)	None	Repair several potholes (4" deep and 3" in diameter)	Not documented
2/15/2017	Dry and Frozen	None	Cut out potholes (2" deep and 6" in diameter)	Cut out potholes (3" deep and 2" in diameter)	Not documented
4/8/2017	Dry and Hard	Repair 1" deep wheel track rutting and many potholes (4" deep and 3" in diameter)	Repair 1" deep wheel track rutting and several potholes (3" deep and 2" in diameter)	Repair 1-3" deep rutting and many potholes (4" deep and 3" in diameter)	None
5/3/2017	Moist and Hard	None	None	Repair small potholes (1" deep and 1" in diameter)	Repair small potholes (1" deep and 1" in diameter)

4.5.3 Strength and Stiffness

Field DCP and LWD tests were conducted to evaluate the in situ shear strength and stiffness of the surface materials in the four test sections before and after the 2016-2017 freeze-thaw season. The in situ DCP-CBR values are compared in Figure 4.37(a) to the soaked CBR values predicted using the statistical model in Figure 3.10. The in situ values are much higher because the field DCP tests were conducted under dry conditions, whereas the statistical model was developed based on soaked laboratory CBR test results. However, the relative CBR ratios between the different sections are somewhat similar for the model predictions and in situ tests, with the exception of the ratios for Section 4. The statistical model predicts a much lower CBR for Section 4 than Section 3, but the average values measured in the field were similar for these two sections. Additionally, more severe surface damage was observed for the control Section 4 after heavy rain events, which supports the previous hypothesis that due to this section's low shape factor of $n = 0.16$, the bearing capacity of the existing surface material greatly decreases under wet conditions. The measured CBR values decreased for the newly constructed test Sections 1 through 3 after the first freeze-thaw period but slightly increased for the control section during the same timeframe.

The comparison between the predicted and in situ CBR values may indicate that the gradation has a greater effect on bearing capacity as water content increases. However, when the material's gradation is at the optimum or coarser than the optimum, the bearing capacity may not be greatly influenced by water content because the skeleton of the material mainly consists of large

aggregate or sand particles, which are not as susceptible to water. For the material comprising the fine matrix, the water content can greatly influence its bearing capacity.

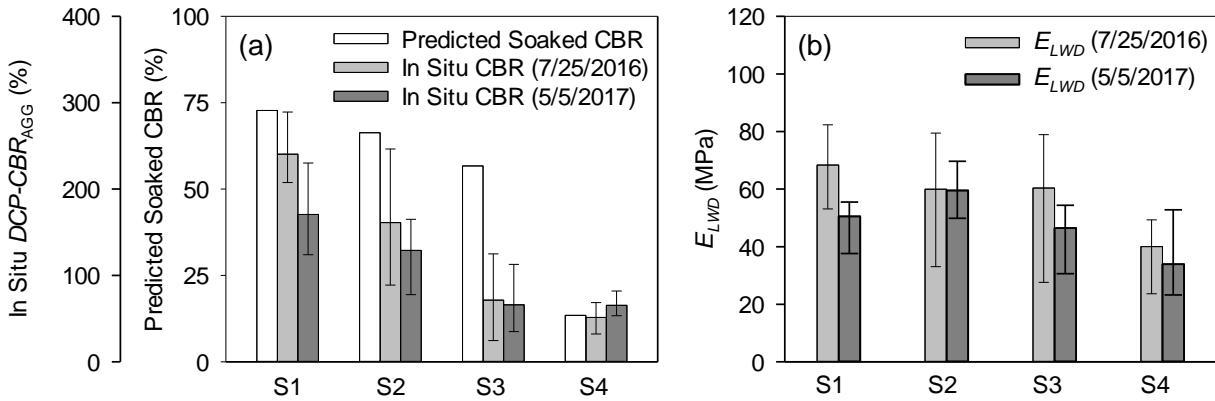


Figure 4.37. (a) Average measured in situ DCP-CBR_{AGG} and predicted soaked CBR values, (b) average in situ composite modulus values of the four test sections (bars indicate range of measured values)

The LWD test results in Figure 4.37 (b) show that the as-constructed composite modulus values (E_{LWD}) of the three test sections were approximately the same and were all higher than that of the control Section 4. After one seasonal freeze-thaw period, the modulus values of all sections decreased by 12% to 25% except for Section 2, for which the gradation was the closest to the theoretical optimal target gradation, as shown in Figure 4.25. This observation also supports the hypothesis that the granular roadway performs best the closer the material is to the theoretical optimum gradation as determined by the statistical model developed from the laboratory CBR tests.

Series of MASW tests were also conducted after construction and after the 2016-2017 seasonal freeze-thaw period to estimate the in situ modulus of the surface and subgrade layers of the test sections. The results from the two series of MASW tests are shown in Figure 4.38. For the surface aggregate layers ($E_{MASW-AGG}$), the average elastic modulus of the pre-existing control Section 4 was higher than those of the newly reconstructed test Sections 1 and 2 and was approximately equal to that of Section 3. However, after 10 months and one freeze-thaw season, the values for the three reconstructed and optimized test sections all increased beyond that of the control section, which itself suffered a decrease of approximately 25%. The increase in stiffness for the newly constructed surface layers could have resulted from their further compaction by traffic. The optimal gradation Section 2 had the lowest average surface layer modulus after construction, but the values for all three reconstructed test sections increased to similar levels after the 2016-2017 freeze-thaw period, with Section 2 stiffer than Section 1.

The average modulus values of the subgrade layers ($E_{MASW-SG}$) were similar and remained relatively unchanged between the two test periods, with the exception of Section 2, which exhibited a decrease of approximately 30%.

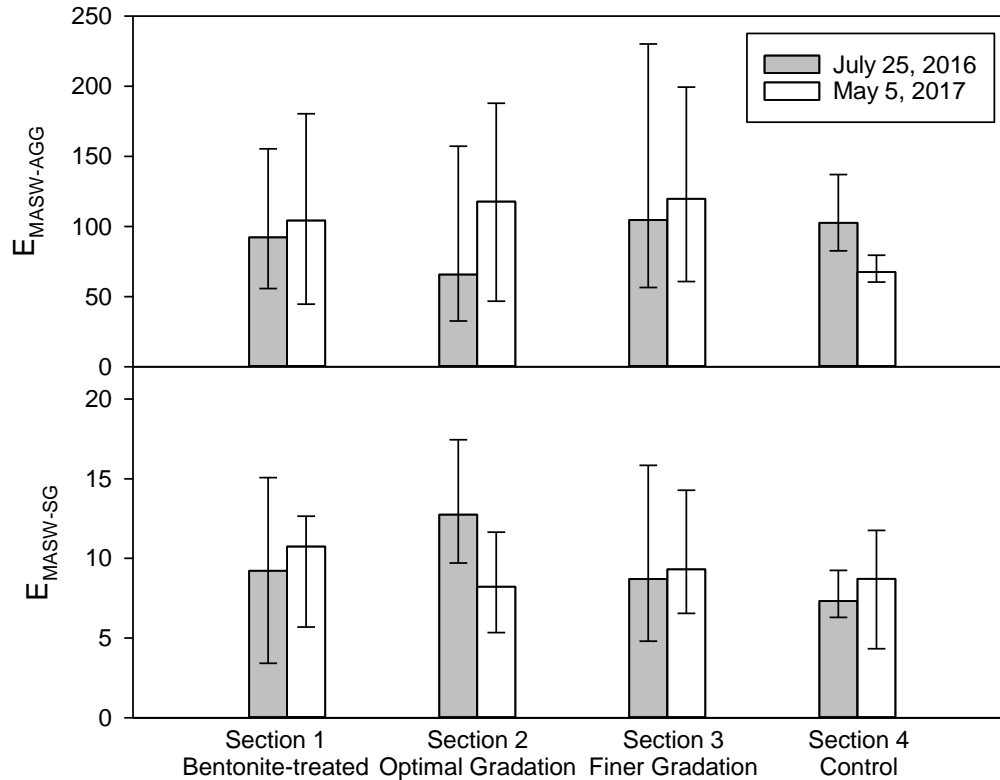


Figure 4.38. Back-calculated elastic modulus values from MASW tests for (a) granular surface layer and (b) subgrade

4.5.4 Dust Emissions

Two groups of dustometer tests were also conducted to compare the dust emissions of the test sections. The test results are summarized in Table 4.8. The bentonite-treated test Section 1 yielded the least amount of dust for both of the test periods, which indicates that the incorporated bentonite was still effective after one seasonal freeze-thaw period. The optimal gradation Section 2 performed nearly as well as the bentonite-treated section in terms of dust emissions. The finer gradation Section 3 also yielded low dust emissions due to the natural fines in the surface material, which had a PI of 8. The dust emissions for control Section 4 were three to four times those of the first three sections with optimized target gradations.

Table 4.8. Dustometer test results of the four granular-surfaced test sections

Section Number (Name)	Fugitive Dust Emission (g/mile)	
	7/25/2016	5/5/2017
1 (Bentonite-Treated)	4.5	4.8
2 (Optimal Gradation)	4.8	5.4
3 (Finer Gradation)	6.1	8.1
4 (Unmodified Control)	17.1	22.0

During the field tests, it was also observed that a nearby road section treated with calcium chloride generated much less dust under traffic than the bentonite-treated section. Indeed, Bergeson and Wahbeh (1990) concluded that “[s]oda ash dispersed bentonite treatment is approximately 10 times more cost effective per percent dust reduction than conventional chloride treatments with respect to time. However, the disadvantage is that there is not the initial dramatic reduction in dust generation as with the chloride treatment. Although dust is reduced 30-40% after treatment there is still dust being generated and the traveling public or residents may not perceive the reduction.”

4.5.5 Changes in Gradation and Plasticity over Time

To evaluate the longevity of the bentonite’s aggregate binding and dust control effects, representative surface samples were collected from the test sections to study how the gradation and plasticity index change over time. The samples were collected from the three reconstructed test sections on the following three dates: during construction on July 8, 2016, before freezing on November 23, 2016, and after the 2016-2017 freeze-thaw period on May 5, 2017. The particle size distributions, Fuller’s model gradation parameters, and plasticity index values for these dates are compared in Figure 4.39 through Figure 4.41.

For the bentonite-treated Section 1, the gradation of the samples became slightly finer with time for the gravel and sand size ranges, but the fines content remained relatively constant. The small differences between the three PSD curves indicate that the gradation of the surface material remained approximately the same 10 months after construction. The n value of Fuller’s model is a more sensitive parameter to changes in the PSD curve. Its value for Section 1 decreased from 0.36 to 0.30 over the 10-month timeframe, corresponding to a slightly finer and more well-graded PSD. During the same timeframe, the PI values of the samples decreased significantly from 28 to 8, which may indicate a large reduction in the bentonite content.

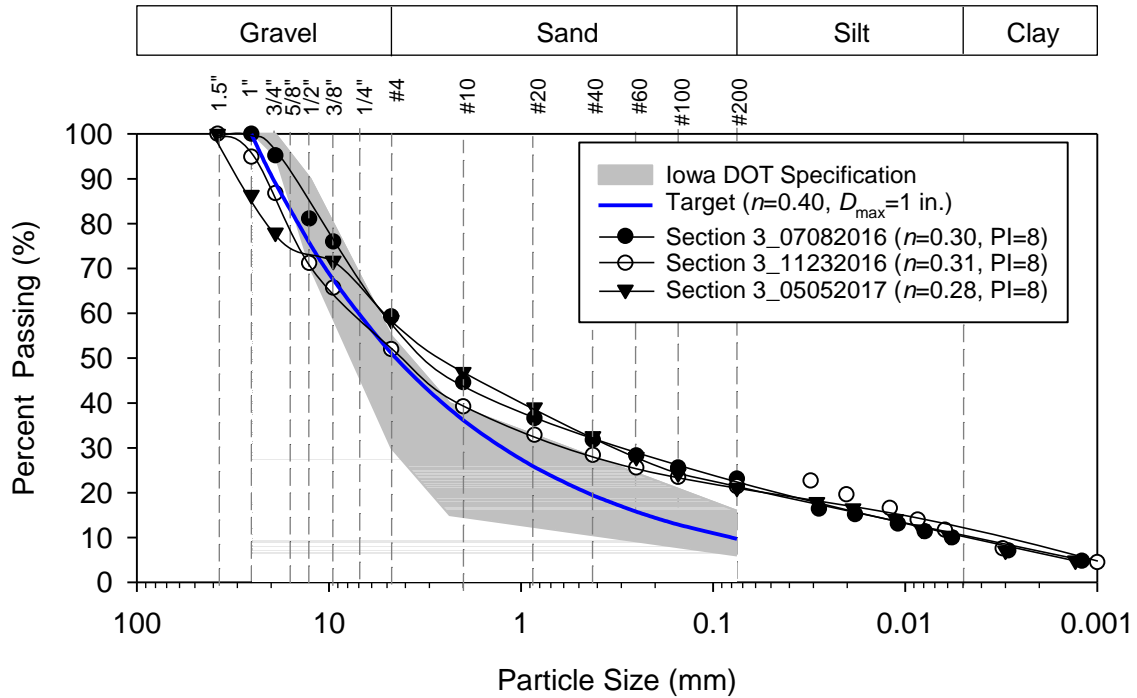


Figure 4.41. Gradation and plasticity of finer gradation Section 3 over 10-month time period

4.6 Granular-surfaced Shoulder Sections

Survey photos and field DCP and LWD tests were also conducted on the shoulder test sections to evaluate their performance. The field tests were performed after construction and after one seasonal freeze-thaw cycle, and survey photos were taken at several times throughout the year.

4.6.1 T Ave. Shoulder Test Sections

The first set of survey photos was taken 10 days after construction of the T Ave. shoulder sections (Figure 4.42). The photos illustrate that the bentonite-treated Section 2 had a smoother and better-sealed surface than the other sections, while the Class A control Section 1 and the optimal gradation Section 3 both suffered minor wheel tracks.



Figure 4.42. Survey photos of T Ave. shoulder test sections taken on June 24, 2016

Another set of survey photos taken two months after construction (Figure 4.43) show that both the bentonite-treated Section 2 and optimal gradation Section 3 performed well, but the Class A control Section 1 yielded an edge drop-off of approximately 0.5 in.



Figure 4.43. Survey photos of T Ave. shoulder test sections taken on August 30, 2016

Survey photos taken five months after construction show that the bentonite-treated Section 2 had more coarse aggregates on the shoulder surface than the other two sections. A few weeks prior to this set of photos, the test sections were all bladed and compacted using a rubber tire roller in October because of the edge drop-off in the Class A control Section 1 as well as damage caused by heavy agricultural equipment parked on the bentonite-treated Section 2.



Figure 4.44. Survey photos of T Ave. shoulder test sections taken on November 7, 2016

Survey photos taken during the 2017 spring thawing period (Figure 4.45) show that the optimal gradation Section 3 yielded much less rutting than the bentonite-treated Section 2 and the Class A control Section 1.



Figure 4.45. Survey photos of T Ave. shoulder test sections taken during thawing period on February 12, 2017

Survey photos taken 10 months after construction on April 20, 2017 (Figure 4.46) show that all three test sections performed well and that the surface of the bentonite-treated Section 2 was better sealed, which indicates that the incorporated bentonite was still effective. Compared to the previous survey photos taken on February 12, 2017, much less coarse aggregate was observed on the surfaces of all three sections. This may have been due to maintenance that involved one motor grader blading and one pass of a rubber tire roller conducted on all of the test sections 8 days prior to the survey photos.



Figure 4.46. Survey photos of T Ave. shoulder test sections taken on April 20, 2017

Results of DCP and LWD tests performed after construction and after the 2016-2017 seasonal freeze-thaw period are shown in Figure 4.47. The average as-constructed DCP-CBR of the Class A control Section 1 (with $n = 0.41$) was higher than those of Sections 2 and 3, as shown in Figure 4.47(a). The as-constructed DCP-CBR of Sections 2 and 3 were approximately the same. After thawing, the DCP-CBR values of all three sections did not yield significant changes.

For the LWD stiffness values, the average composite modulus of the bentonite-treated Section 2 was slightly lower than those of Sections 1 and 3, as shown in Figure 4.47(b). After thawing, modulus reductions of approximately 20% occurred for all three test sections.

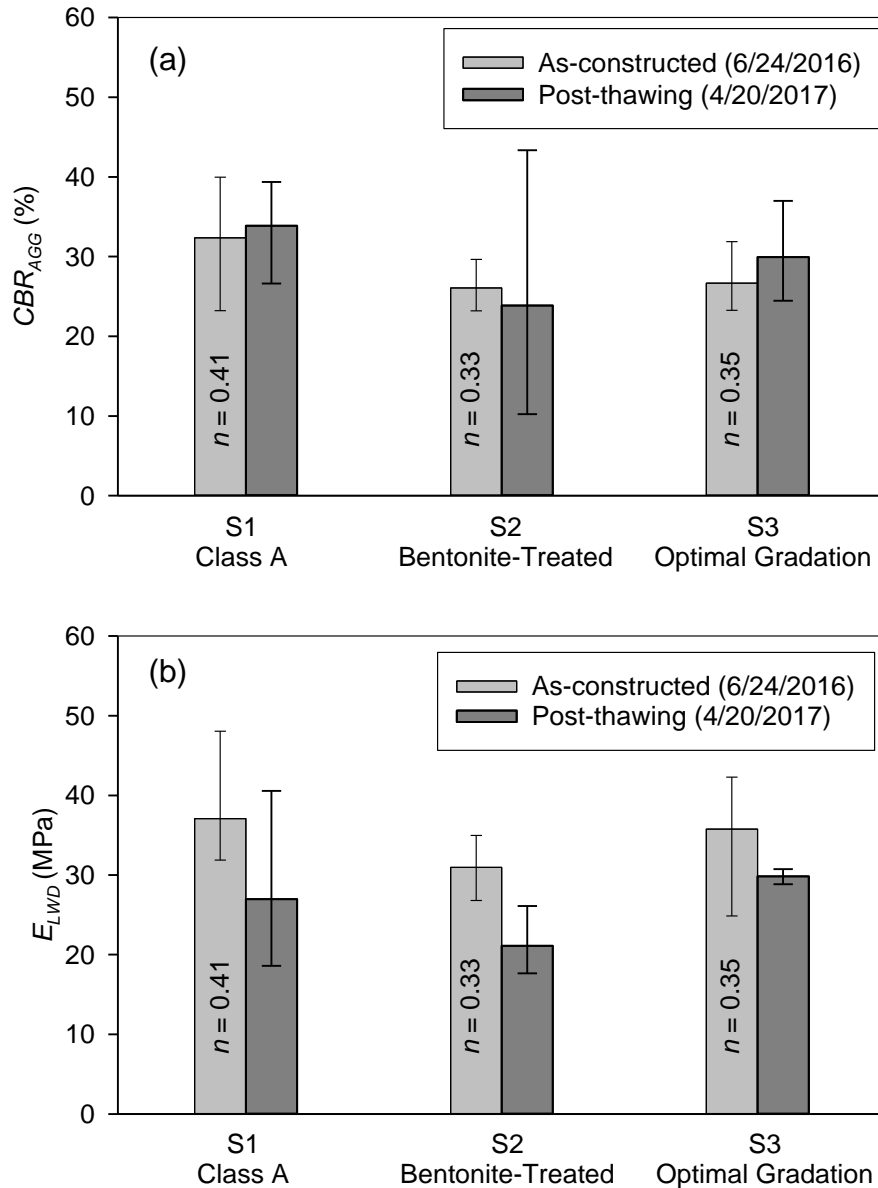
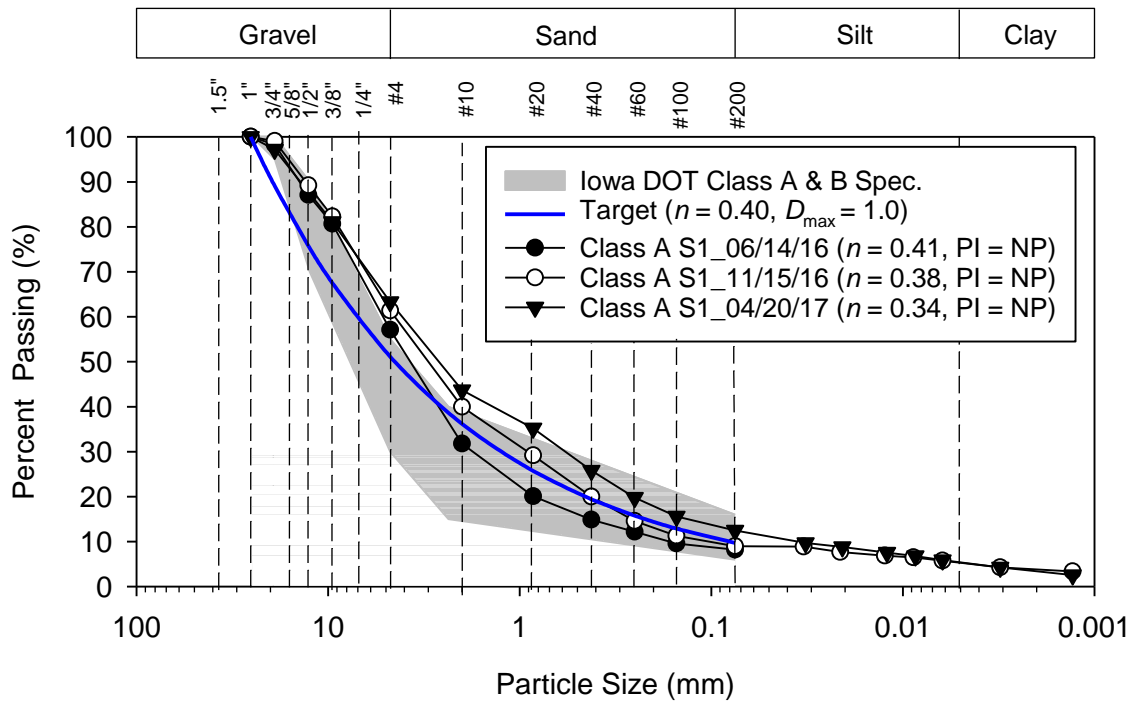


Figure 4.47. Results of field tests on T Ave. shoulder test sections: (a) In situ CBR values from DCP tests, (b) in situ composite modulus values from FWD tests

Representative samples were collected from the shoulder test sections during construction, before freezing, and after the 2016-2017 freeze-thaw period. The changes in gradation and plasticity with time for the different shoulder section surface materials are shown in Figure 4.48 through Figure 4.51.

For the Class A control Section 1, the as-constructed n value was 0.41, which was closest to the target n value among the three test sections, as shown in Figure 4.29. The gradation of the material became finer with time, and the n value decreased from 0.41 to 0.34 after 10 months service, as shown in Figure 4.48. The Class A rock material was nonplastic, which indicates that the surface material was not contaminated by the subgrade intrusion. However, the nonplastic characteristic of the material may cause edge drop-off issues (Figure 4.43[a] and [b]) because the fine particles close to the pavement edge do not bind and can be easily blown by traffic.



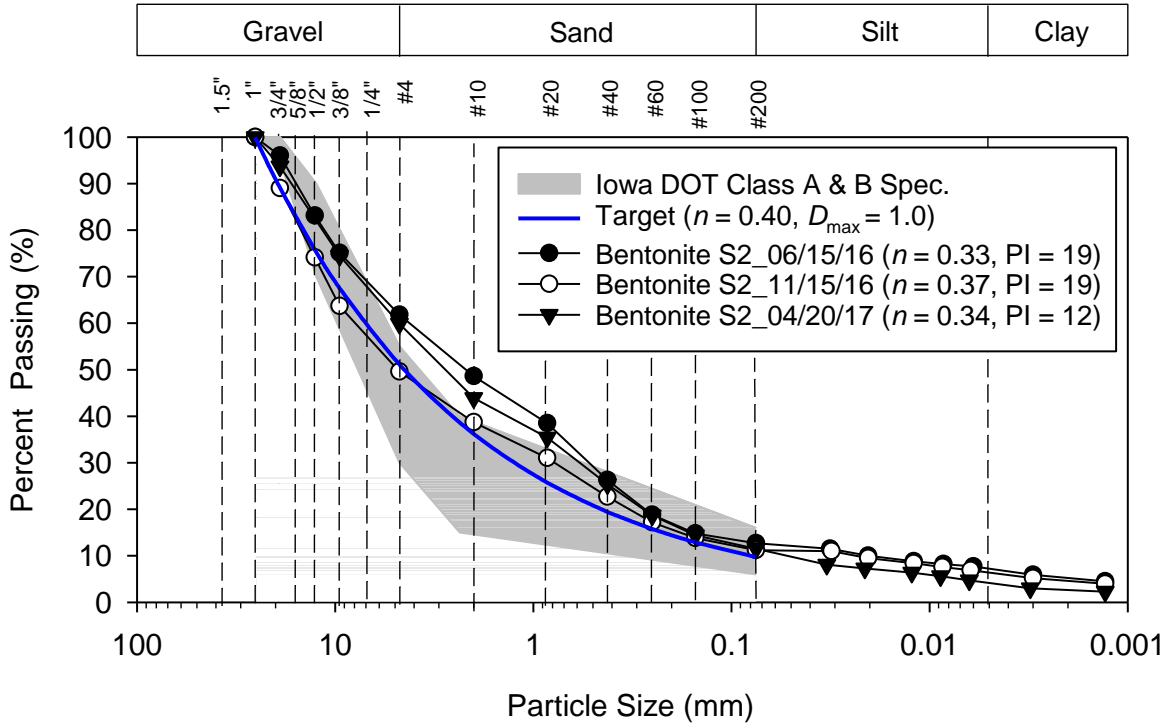


Figure 4.49. Gradation and plasticity of bentonite-treated Section 2 over 10-month time period

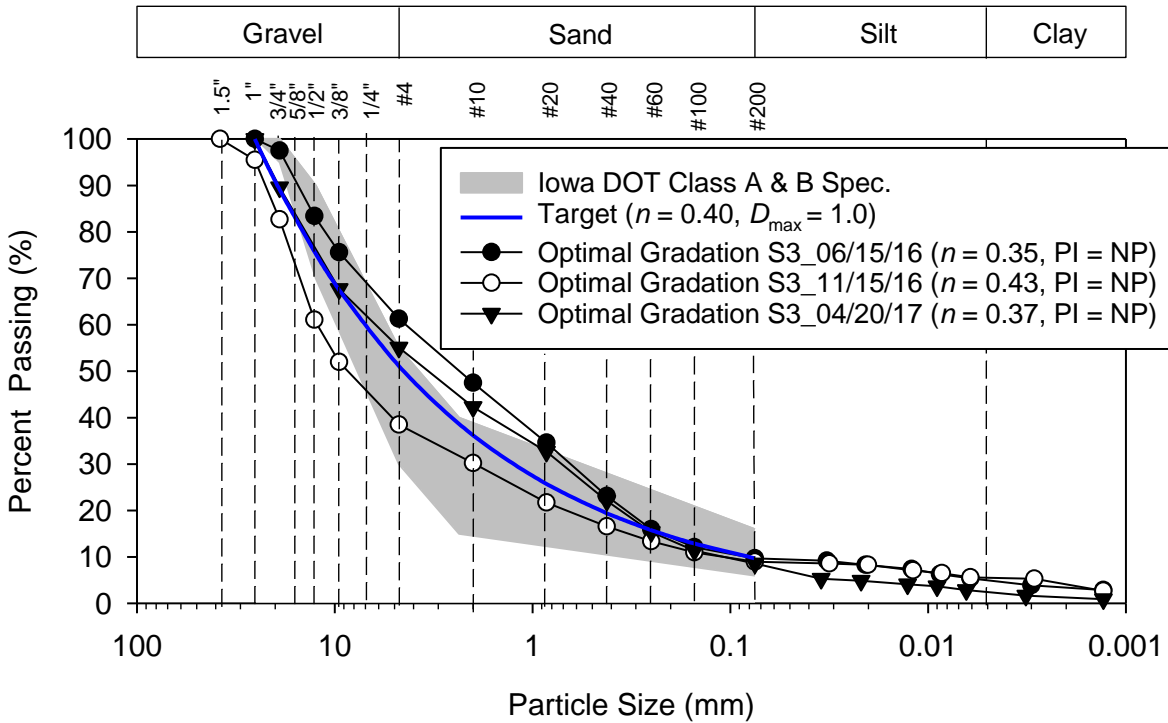


Figure 4.50. Gradation and plasticity of optimal gradation Section 3 over 10-month time period

4.6.2 Highway 30 Off-Ramp Shoulder Test Sections

Survey photos were also taken for the Highway 30 off-ramp shoulder sections 10 days after construction (Figure 4.51). The bentonite-treated section clearly showed a much smoother and better-sealed surface than the control section. No edge drop-off was observed for the bentonite-treated section, whereas the control section yielded approximately 0.5 in. of edge drop-off and had more loose aggregates on the surface.



Figure 4.51. Survey photos of Highway 30 off-ramp shoulder sections from June 23, 2016

However, survey photos taken approximately three months after construction show that most of the incorporated bentonite had been washed or blown away (Figure 4.52). Approximately 1 in. of edge drop-off can be observed for both the bentonite-treated and control sections.

Survey photos taken on various dates throughout the 2016-2017 seasonal freeze-thaw period show that the bentonite-treated section performed approximately the same as the control section (Figure 4.52 through Figure 4.55). These observations indicate that incorporating bentonite into the surface material of a granular-surfaced shoulder is not a cost-effective long-term solution to the edge drop-off issue because the large amount of runoff from the pavement surface and heavy traffic loads and volume are too harsh for the bond between the bentonite and aggregate particles to survive for any great length of time.

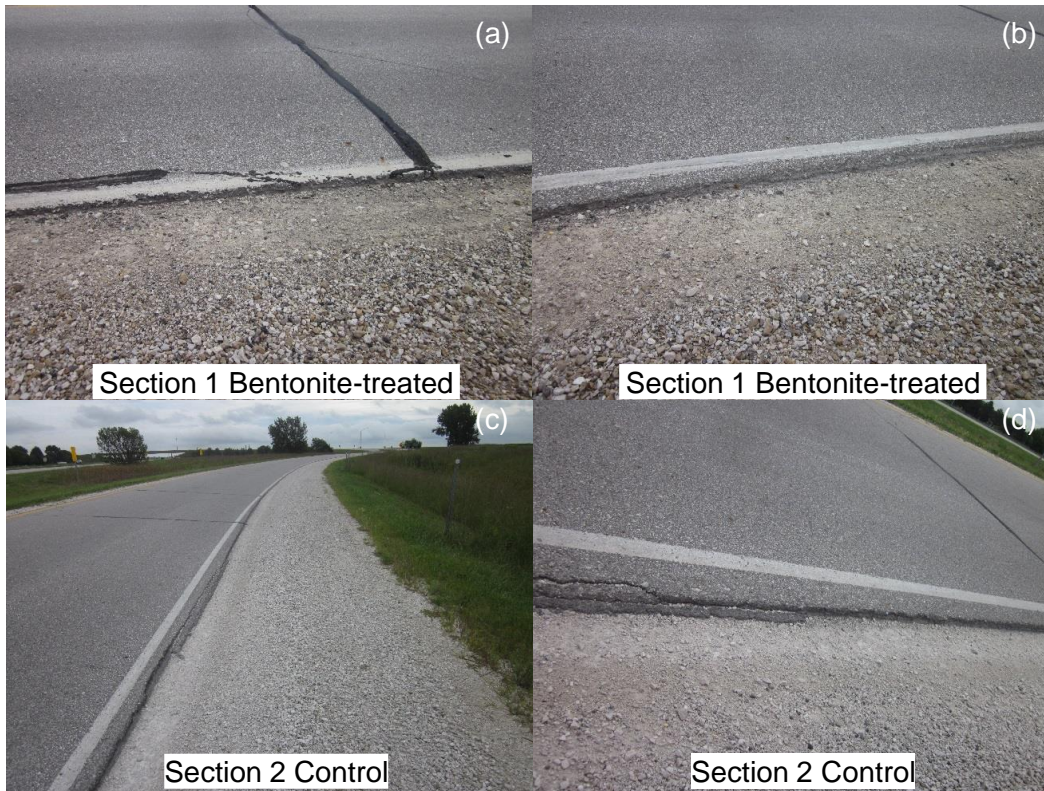


Figure 4.52. Survey photos of Highway 30 off-ramp shoulder sections from August 30, 2016

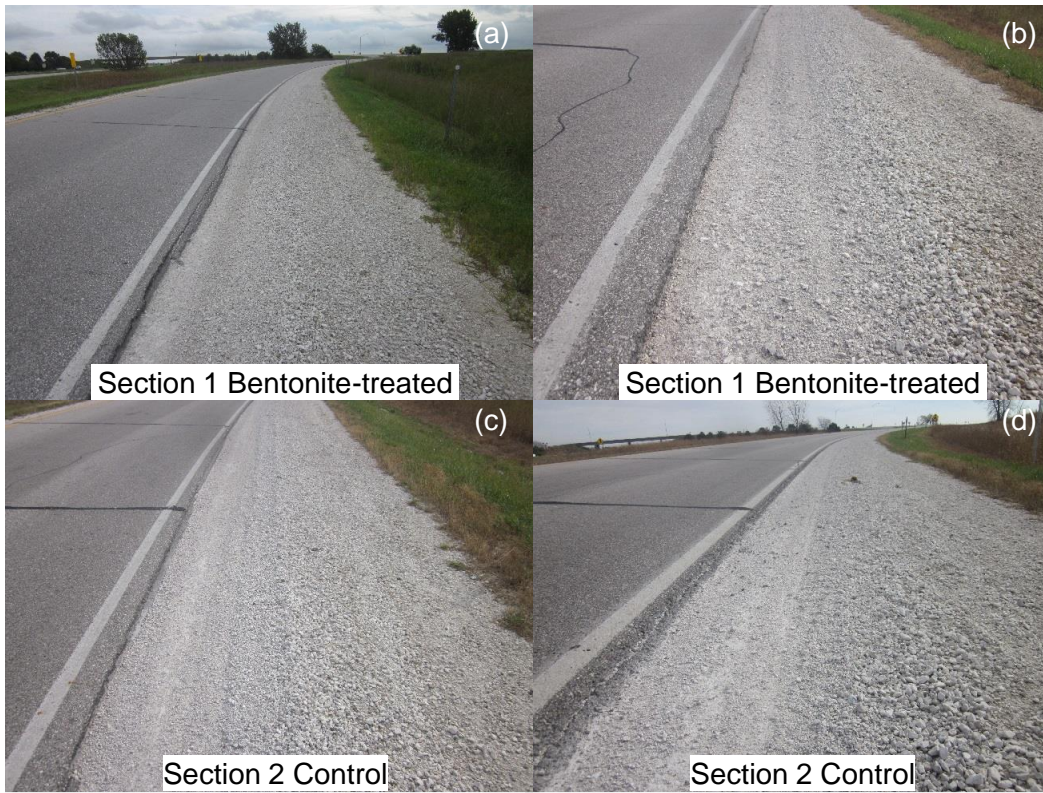


Figure 4.53. Survey photos of Hwy 30 off-ramp shoulder sections from November 7, 2016



Figure 4.54. Survey photos of Hwy 30 off-ramp shoulder sections from February 12, 2017



Figure 4.55. Survey photos of Hwy 30 off-ramp shoulder sections from April 20, 2017

The DCP tests conducted two weeks after construction showed that the top 2 in. of the surface aggregate materials were much softer than the bottom materials for both the bentonite-treated and control sections, as shown in Figure 4.56. The average thicknesses of the surface layers of the two sections were about 9 in., and the DCP-CBR values of the two sections were approximately the same.

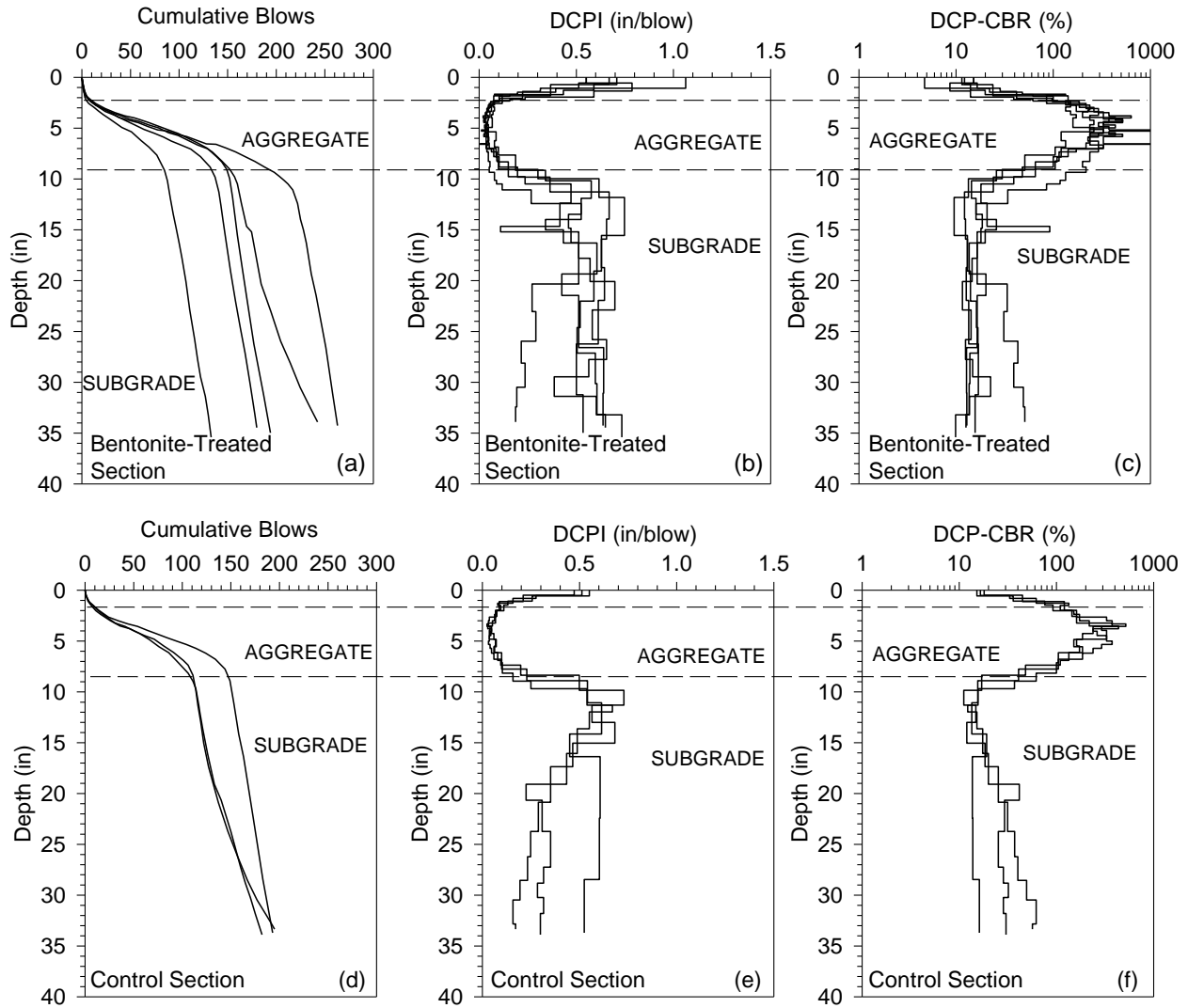


Figure 4.56. As-constructed DCP depth profiles of the Highway 30 off-ramp shoulder test sections: (a and d) cumulative blows, (b and e) DCPI, and (c and f) DCP-CBR

DCP tests were also conducted on the ramp shoulder sections after thawing. The test results are shown in Figure 4.57. Unlike the as-constructed DCP test results, the top and bottom of the aggregate surface layers showed much closer CBR values.

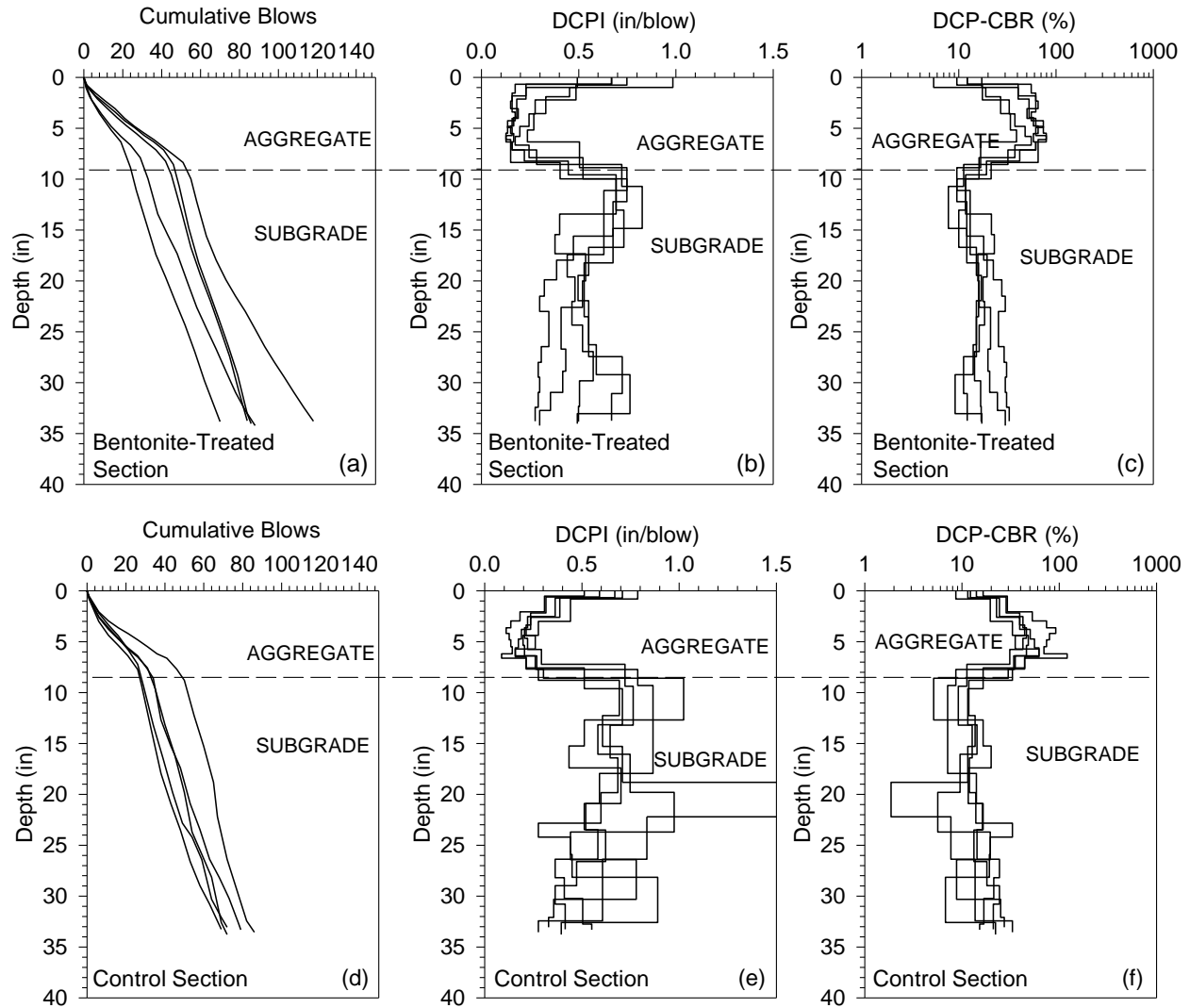


Figure 4.57. Post-thawing DCP depth profiles of the Highway 30 off-ramp shoulder test sections: (a and d) cumulative blows, (b and e) DCPI, and (c and f) DCP-CBR

Compared to the as-constructed DCP-CBR values, both of the sections yielded significant reductions in CBR after the thawing period, as shown in Figure 4.58(a). Similar trends can also be observed for the LWD test results, as shown in Figure 4.58(a), which indicate that the bentonite treatment did not improve the mechanical performance of the ramp shoulder section.

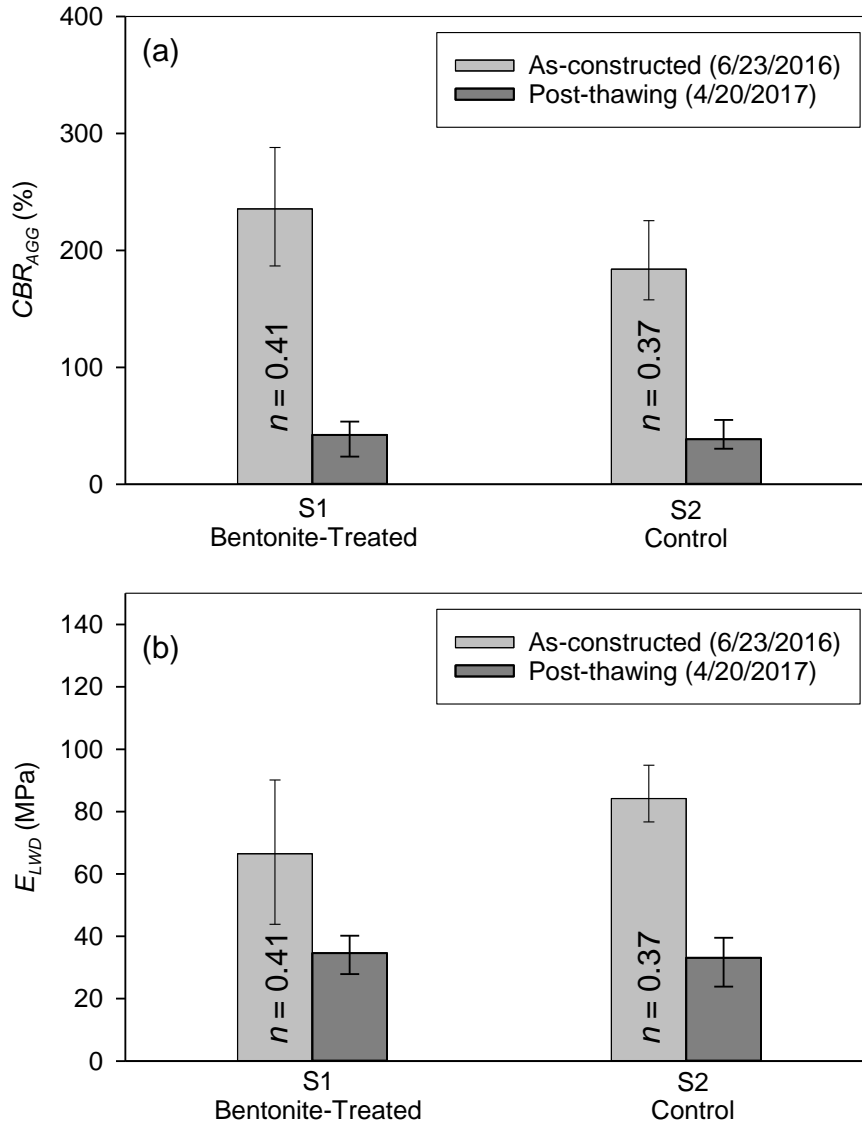
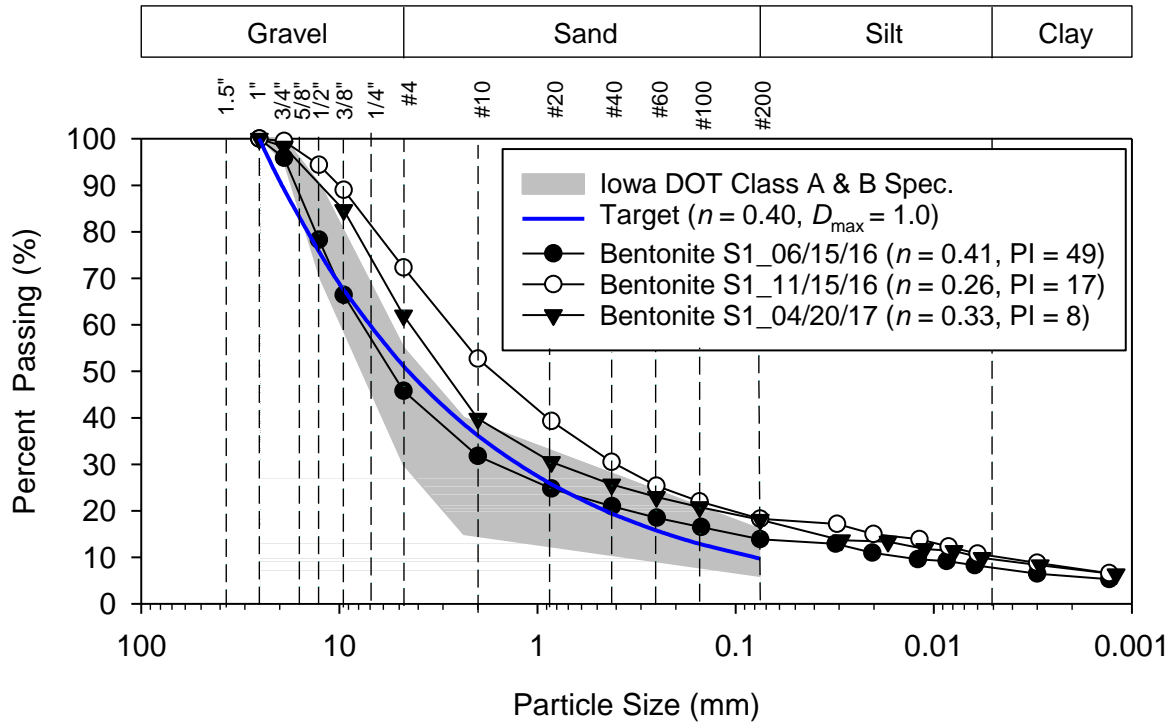


Figure 4.58. (a) In situ CBR values and (b) in situ composite modulus values of the Highway 30 ramp shoulder test sections

The changes in the gradation and plasticity of the ramp shoulder test sections are summarized for the bentonite-treated and control sections in Figure 4.59 and Figure 4.60, respectively. The gradation of the bentonite-treated section became much finer after five months. However, the maintenance conducted to repair the edge drop-off made the gradation of the material coarser in April 2017. The PI of the bentonite-treated material decreased from 49 to 8 after 10 months of service, which further supports the visual survey conclusions that most of the incorporated fines were washed away by runoff from the pavement surface and/or blown away by the heavy traffic load and volume.

The material gradations of the control section are shown in Figure 4.60. A sample was not collected after the thawing period because it had been concluded that incorporating bentonite

into the granular surface material of the highway shoulder was not a cost-effective method to address the edge drop-off issue of shoulder sections with such heavy traffic.



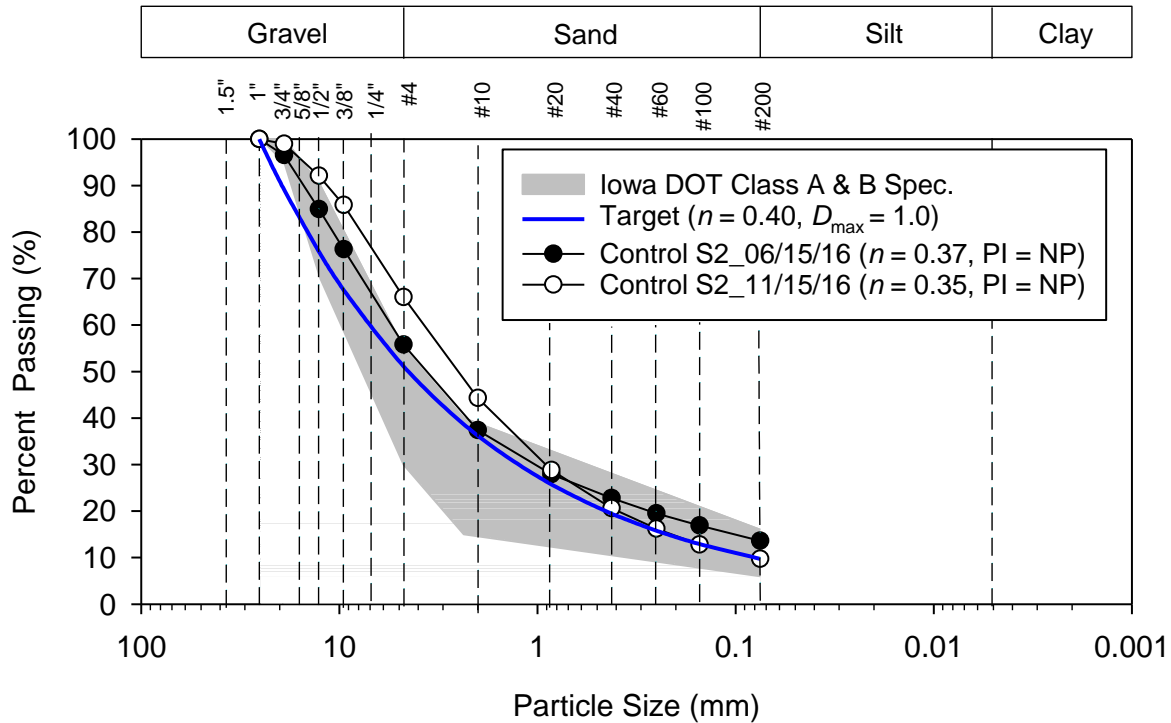


Figure 4.60. Gradation and plasticity changes of ramp shoulder control Section 2

4.7 Conclusions

The field study presented in this chapter focused on validating the optimal gradation and plasticity (by incorporating bentonite powder) for granular surface materials. The optimal gradations were determined based on the laboratory study presented in Chapter 3. One granular-surfaced road test site in Pottawattamie County and two granular-surfaced shoulder test sites in Boone County were selected for construction of the test and control sections. Pre-construction field tests and visual surveys were conducted to identify the sources of the excessive fines in the existing surface materials and determine the common damage types for the selected test sites.

The thickness, gradation, and plasticity of the existing surface materials of the selected test sites were determined for the design of the new test sections. To help the local road agencies implement the proposed design method and recycle the existing degraded surface materials, a Microsoft Excel-based program was developed to optimize the proportions of the existing surface materials along with two or three quarry materials available for mixing to reach the optimal target gradation.

Performance-based field tests were performed on the test sections following construction and before and after one seasonal freeze-thaw period to compare the as-constructed performance and evaluate the freeze-thaw durability of the various test sections. To monitor the ground temperature and frost depth of the granular-surfaced road test site in Pottawattamie County, two vertical arrays of thermocouples were installed under the centerline and west side shoulder.

Several groups of visual survey photos were also taken to compare the surface conditions of the various sections.

Field test results further validated the performance of the proposed design method developed based on the findings of the laboratory study. The granular-surfaced road section closest to the optimal gradation and plasticity yielded the best overall performance and lowest dust emissions. However, the visual observations and laboratory plasticity tests conducted on the surface samples collected from the test sections at different periods indicate that the content of the incorporated bentonite significantly decreased after one seasonal freeze-thaw period. The road section with the optimal gradation without bentonite also yielded better performance than the control section and the smallest reduction in stiffness and strength among all the test sections. For the shoulder test sections, the field and laboratory test results also showed that the optimal gradation can improve the mechanical performance of granular surface materials, but the binding effect of the incorporated bentonite decreased significantly after one seasonal freeze-thaw cycle, indicating that the small amount of incorporated bentonite (3%) was washed away by precipitation runoff or blown away by traffic.

CHAPTER 5. STATISTICAL EVALUATION OF LABORATORY TESTS FOR DETERMINING SOIL PLASTICITY

5.1 Introduction

Swedish soil scientist Albert Atterberg defined moisture content limits to delineate transitions in the consistency of fine-grained soils (Atterberg 1911). Since Terzaghi introduced Atterberg's limits into modern soil mechanics practice and Casagrande standardized the testing devices, the liquid and plastic limit tests have been extensively performed in geotechnical engineering and soil science fields worldwide (Wroth and Wood 1978). To date, Atterberg limits remain a requirement for most soil classification systems, and they are used in many empirical models for predicting soil engineering properties. However, many previous studies have demonstrated that the conventional Atterberg limits tests are highly operator dependent and thus produce significant variations in the test results (Di Matteo 2012, Haigh 2012, Sherwood and Ryley 1970, Sowers et al. 1960, Wroth and Wood 1978).

To provide more repeatable and reproducible test results, different devices and testing methods, including the fall cone and bar linear shrinkage tests, have been proposed and evaluated (Paige-Green and Ventura 1999, Sherwood and Ryley 1970, Sowers et al. 1960). The repeatability (i.e., the single-operator or intralaboratory precision) and reproducibility (the interlaboratory precision) of a measurement are important characteristics that can be quantified to enable users to understand the variability of test results. The ASTM E691 standard practice on interlaboratory testing states that "ASTM standard regulations require precision statements in all test methods in terms of repeatability and reproducibility." It also specifies a one-way ANOVA (i.e., a simple standard deviation across all measurements) to quantify the single-operator or multilaboratory errors. However, the R&R statistics from a one-way ANOVA analysis cannot quantify the contributions of multiple error sources to the overall variation in a measurement. Such information would be useful for identifying potential ways to further improve the test methods. For example, the design of the testing device may need to be improved or the training of operators may need to be enhanced. The capacity of a measurement, defined as the ratio of precision to tolerance, is also an important parameter for determining whether a measurement is useful for checking conformance of a measured characteristic to engineering specifications. The ASTM standards use the 95% limits on the difference between two test results, referred to as the d_{2s} limit (i.e., $1.960\sqrt{2} \cdot 1s$, where $1s$ is one standard deviation) to determine the acceptable range of two test results (ASTM E177). However, for a given testing method, the acceptable ranges calculated using the method are usually different between the single-operator and multilaboratory test results due to their different standard deviations. Therefore, it is useful to quantify the capacity of a measurement, which considers errors arising from both the device and different operators.

To address these issues, the authors proposed to use a two-way ANOVA-based R&R analysis to determine the repeatability, reproducibility, and capacity of various testing methods. In this study, several Atterberg limits tests, which are highly operator dependent, were employed for comparisons and demonstration of the statistical analysis. The ASTM-standardized Atterberg limits tests, fall cone tests, and bar linear shrinkage tests were conducted on specimens prepared

by incorporating different percentages of pure bentonite into the minus No. 40 fraction of crushed limestone samples from granular roadways. The R&R and capacity of the testing methods were determined using the two-way ANOVA-based analysis and compared to those determined using the ASTM-standardized methods (ASTM E691, ASTM E177). Based on the results of the laboratory tests and statistical analyses, the correlations between the different tests are provided and discussed in this chapter, and the testing methods with the best R&R are identified.

5.2 Various Tests for Determining Soil Consistency

Atterberg initially set up five limits to describe the consistency of a soil at different water contents: (1) the upper limit of fluidity, (2) the lower limit of fluidity (flow limit), (3) the sticky limit, (4) the roll-out limit, and (5) the cohesion limit. Based on his laboratory evaluations, Atterberg established that a soil is plastic between the flow limit (liquid limit) and roll-out limit (plastic limit) and that the plasticity number (plasticity index), which is the difference between the flow and roll-out limits, is the best measure of the plasticity of soils (Bauer 1960).

5.2.1 Liquid Limit Test

In 1932, Arthur Casagrande developed a device to standardize the liquid limit test and in 1949 further refined the design to overcome inherent shortcomings (Casagrande 1958). The later design of the device is standardized in the current ASTM D4318. Although the Casagrande device has become ubiquitous in geotechnical testing, many previous studies have demonstrated that the device yields large variations in LL values. Some of the factors responsible for the large variation are a strong dependency of the results on operator judgment, wear of the grooving tool, and variations in the hardness of the base materials of different devices (Di Matteo 2012, Haigh 2012, Sherwood and Ryley 1970, Sowers et al. 1960). Since the late 1950s, many studies have focused on alternative LL measurement methods, and several have concluded that the fall cone device originally developed for testing bitumen materials can eliminate most of the shortcomings of the Casagrande device and provide more consistent test results (Sherwood and Ryley 1970, Sowers et al. 1960). Sowers et al. (1960) evaluated the effects of cone angle, cone mass, and penetration time on the test results and concluded that the fall cone test is a promising method for measurement of LL. Haigh (2012) reported that the fall cone test is a measure of specific strength that corresponds to a soil shear strength of ~ 1.7 kPa, but the Casagrande cup test corresponds to a mean specific strength of ~ 1.07 m²/s². These are clearly different physical properties. However, many studies have reported strong linear correlations between LL values determined by the Casagrande and fall cone test devices for a range of material types (Belviso et al. 1985, Di Matteo 2012, Dragoni et al. 2008, Fojtová et al. 2009, Sherwood and Ryley 1970, Spagnoli 2012, Wasti and Bezirci 1986, Özer 2009).

5.2.2 Plastic Limit Test

The fall cone test device was also evaluated for determination of the plastic limit of soils by Kodikara et al. (2006) and Wroth and Wood (1978). The data interpretations used in these studies were developed based on three assumptions: (1) the undrained shear strength (C_u) of a

soil at its PL is approximately 100 times that at its LL (Skempton and Northey 1952); (2) the relationship between moisture content (w) and $\ln(C_u)$ is linear based on critical state soil mechanics concepts (Hansbo 1957, Wroth and Wood 1978); and (3) $C_u d^2/W$ is constant for the same cone geometry, where d is the fall cone penetration depth and W is the weight of the fall cone (Hansbo 1957, Wroth and Wood 1978). Based on these three assumptions, Wroth and Wood (1978) proposed to determine the plasticity index of a soil by conducting fall cone tests with two different cone weights (W_1 and W_2) to determine the water content separation (Δ) of the two parallel flow lines, as shown in Figure 5.1, from which the PI of the specimen can be calculated using the following equation:

$$PI = \frac{\Delta \log(100)}{\log\left(\frac{W_1}{W_2}\right)} \quad (4.6)$$

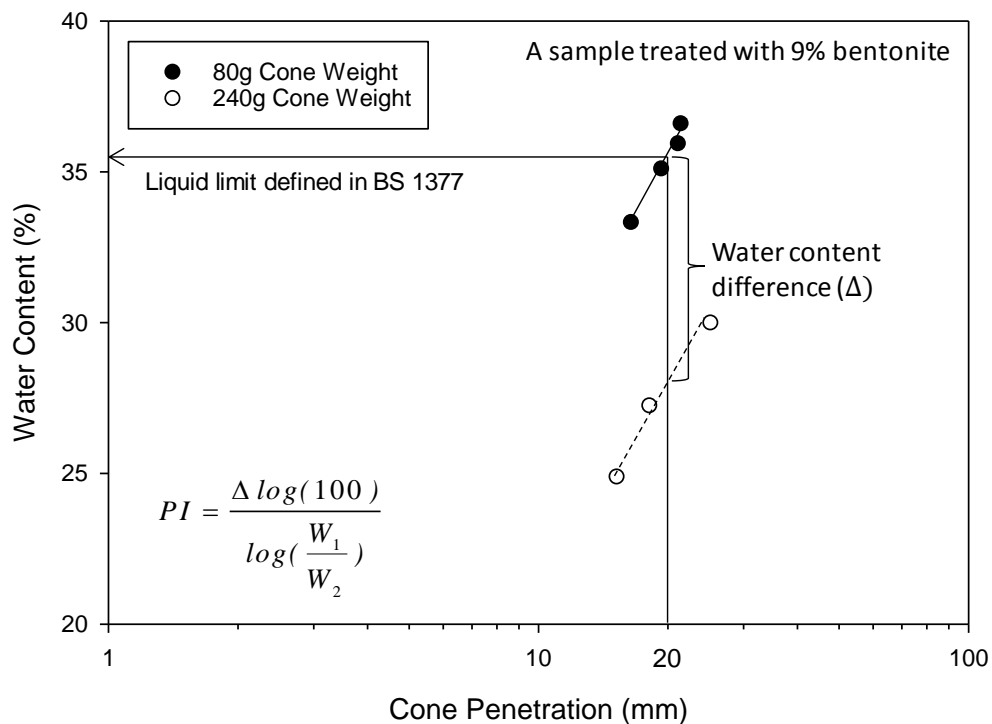


Figure 5.1. Example of using fall cone test results to determine LL and PI

5.2.3 Bar Linear Shrinkage Test

Paige-Green and Ventura (1999) concluded that the bar linear shrinkage test result is a good indicator of the plasticity of soils. The BLS specimen is prepared by mixing minus No. 40 material at a water content close to its LL, then transferring the material to a 150 mm long by 10 mm square trough and oven drying at 110°C until shrinkage stops. The shrinkage of the specimen is then measured and expressed as a percentage of the original specimen length, which is defined as the BLS value. To improve repeatability and reduce uneven shrinkage leading to

bowing (bending) of the specimens, Sampson et al. (1992) recommended using a mold with openings on two sides, instead of a trough, and placing the specimen into the oven immediately after filling to reduce cracking. Paige-Green and Ventura (1999) observed a linear correlation between BLS values and PI, with the PI values approximately two times the corresponding BLS values. Paige-Green and Ventura (1999) found that the BLS test is less susceptible to operator error and is much quicker and easier to learn and perform than the conventional Atterberg limits tests. Similar bar shrinkage tests can be found in several different testing standards, which are summarized in Table 5.1 along with their various trough dimensions, drying methods, and oven temperatures.

Table 5.1. Trough designs and drying methods for various BLS testing standards

Parameter	South Africa TMH1 A4	British Standard BS1377	Australia P6A/1	Texas 107-E	California CTM-228
Cross-Section Shape	Square	Semi-circular	Semi-circular	Square	Tapered
Cross-Section Dimension (mm)	10×10	25 Diameter	25 Diameter	19×19	Top width 19.05, bottom width 17.48
Length (mm)	150	140	135 or 250	127	127
Drying method	Oven dry (110°C)	Air dry + Oven dry (65°C and 110°C) ^a	Air dry (24h) + Oven dry (110°C)	Air dry ^b + Oven dry (110°C)	Air dry ^b + Oven dry (110°C)

^a Place the mold where the soil/water can air dry slowly in a position free from drafts until the soil has shrunk away from the walls of the mold. Then complete the drying, first at a temperature not exceeding 65°C until shrinkage has largely ceased, and then at 105°C to 110°C to complete the drying.

^b Air dry the soil bar at room temperature until color changes slightly.

5.3 Materials and Testing Methods

5.3.1 Materials

In this study, a total of five samples were prepared by incorporating different percentages of pure bentonite powder into the minus No. 40 fraction of existing crushed limestone granular-road surfacing materials that had been abraded by traffic loading on County Road L66 in Pottawattamie County, Iowa. The incorporated bentonite content by dry mass of the minus No. 40 material was increased from 0% to 12% in 3% increments. The sieve and hydrometer analysis results of the initial full granular surface material gradation are shown in Figure 5.2.

The bentonite used in this study was purchased from American Colloid Company in East Colony, Wyoming. The chemical composition and mineralogy of the bentonite were determined at Iowa State University using x-ray fluorescence and x-ray diffraction analyses, respectively. The XRD results showed that the bentonite was sodium montmorillonite ($\text{Na}_{0.3}(\text{Al},\text{Mg})_2\text{Si}_4\text{O}_{10}(\text{OH})_2 \cdot 4\text{H}_2\text{O}$) with calcite (CaCO_3) and quartz (SiO_2). The chemical composition determined by the XRF results is shown in Table 5.2 and indicates that the primary chemical components are SiO_2 and Al_2O_3 .

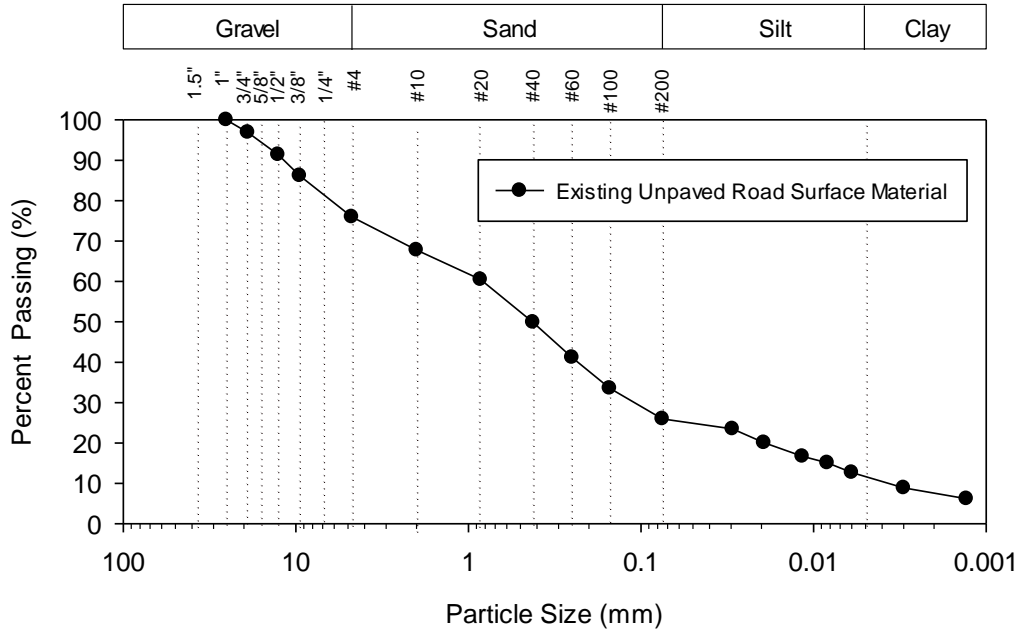


Figure 5.2. Particle size distribution of the granular surface material from CR L-66

Table 5.2. Chemical composition of the bentonite used in the laboratory study

Chemical Component	Percent
SiO ₂	58.77
Al ₂ O ₃	20.66
Fe ₂ O ₃	3.81
SO ₃	0.86
CaO	2.42
MgO	3.61
Na ₂ O	2.45
K ₂ O	0.62
P ₂ O ₅	0.08
TiO ₂	0.18
SrO	0.03
BaO	0.02
Total	93.50
LOI	6.15
Bulk Moisture	7.60

The liquid and plastic limits of the bentonite determined using the methods of ASTM D4318-10 were 297% and 35%, respectively. Following the recommendation from Bergeson and Wahbeh (1990), a 0.5% sodium carbonate (i.e., soda ash) solution was used to increase the water content of the bentonite-treated samples in order to disperse the bentonite particles and reach a more uniform consistency.

5.3.2 Testing Methods

The conventional LL and PL tests were performed in accordance with ASTM D4318-10. The testing devices used in this study are shown in Figure 5.3(a) and (b).

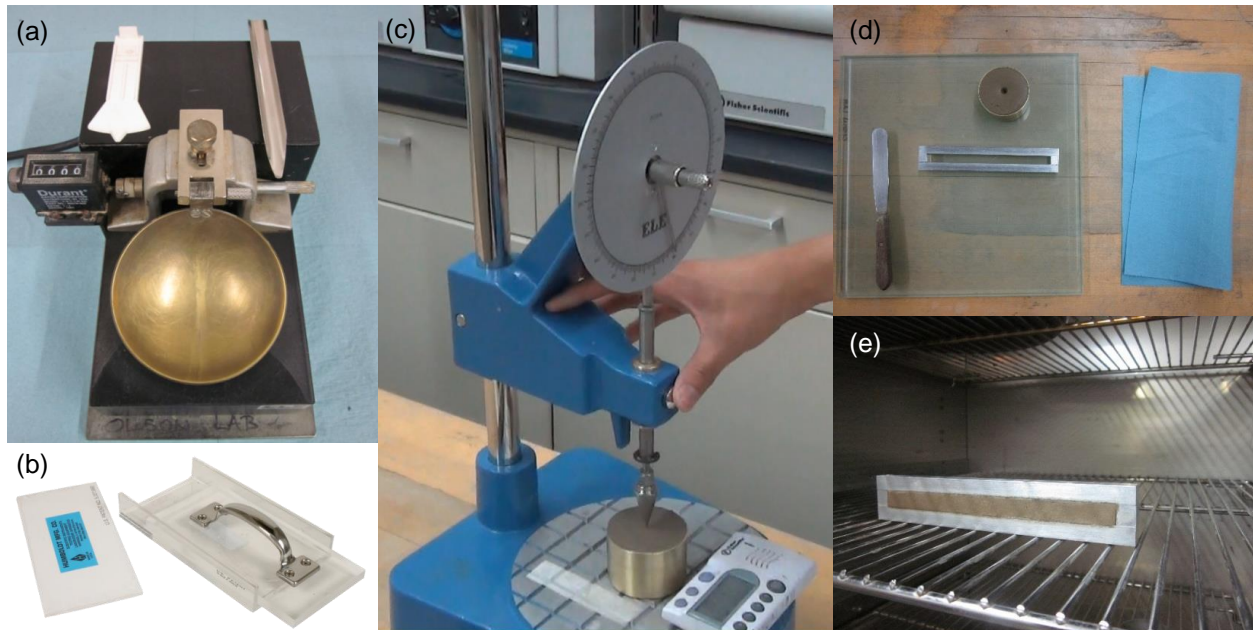


Figure 5.3. Test devices used in this study: (a) Casagrande LL test device, (b) PL rolling device, (c) fall cone test device, (d) BLS mold, and (e) BLS test specimen in the oven

The fall cone LL test was conducted in accordance with British Standard BS 1377 (1990) using the ELE fall cone device shown in Figure 5.3(c). The cone weighs 80 g and has an apex angle of 30 degrees. The testing procedure is simpler and less operator dependent than the Casagrande cup test. At the beginning of the test, the tip of the cone is lowered until it just touches the surface of the specimen and barely marks the surface with slight movement. The cone is then allowed to fall freely for 5 seconds. The penetration depth of the cone is measured using the dial gauge, and the water content of the specimen is then determined using the oven-dry method of ASTM D2216-10. For each soil specimen being tested, four measured penetration values uniformly distributed between 15 and 25 mm should be obtained. The LL is determined as the moisture content corresponding to a cone penetration of 20 mm using a best-fit straight line through the data points of moisture content versus cone penetration, plotted on linear scales. A detailed laboratory testing procedure for the fall cone liquid limit test is provided in Appendix B.

To determine the PI using the fall cone device, the testing and calculation methods recommended by Wroth and Wood (1978) were followed. As illustrated in Figure 5.1, the PI of the sample can be calculated based on two known cone weights (W_1 and W_2) and the water content separation (Δ) of the two flow lines at a cone penetration of 20 mm. Along with the fall cone LL tests using the 80 g cone, another set of tests were performed on the same samples using a 240 g cone for this purpose.

The BLS test specimens were also prepared during the fall cone LL tests because the initial water content of the BLS specimens should be close to the LL that results in a cone penetration of 20 mm. As recommended by Sampson et al. (1992), the aluminum BLS molds custom-fabricated for this study are open on two sides, with a length of 150 mm and a 10 mm by 10 mm square cross-section (Figure 5.3[d] and [e]). The molds were first oven heated at 110°C and then lubricated using a wax bar to reduce friction between the inside walls of the mold and soil specimen, which helps eliminate cracking and uneven or incomplete shrinkage. The wax-lined molds were filled with the soil specimens at moisture contents close to their LL and were immediately placed in the oven at 110°C. After drying for 24 hours, the lengths of the specimens were measured using calipers. If a specimen was bowed, the arc height and chord length of the specimen were measured to calculate the average specimen length.

In this study, a total of five samples were prepared by mixing the minus No. 40 granular road surface material with five different percentages of bentonite. All five samples were prepared at the same time to minimize possible variations caused by sample preparation. For each of the samples, three well-trained operators performed three replicate tests each. The three operators were all trained on all the different tests at the same time in order to minimize errors associated with the inter-operator variability.

5.4 Correlations Between the Various Consistency Tests

5.4.1 Liquid Limit by Fall Cone versus Casagrande Cup

The correlation between the liquid limits determined using the Casagrande cup (LL_{cup}) and the fall cone (LL_{cone}) was determined using a total of 45 tests for each device (five bentonite contents times three operators times three replicates per operator). For each bentonite content, the average LL values from the replicate tests are shown in Figure 5.4, with error bars indicating the maximum and minimum values.

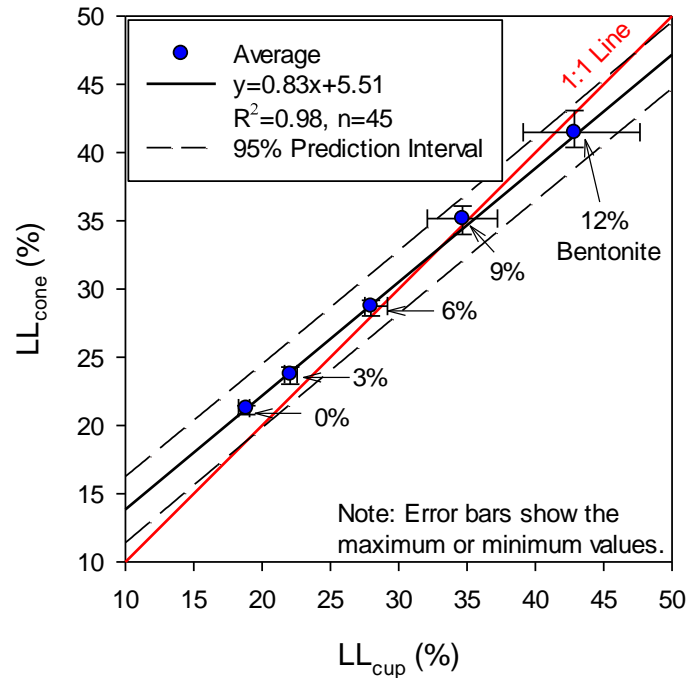


Figure 5.4. Correlation between LL values determined using Casagrande cup and fall cone device (three operators times three replicates for each bentonite content)

A strong linear correlation can be observed between the two testing methods. The best-fit line is very close to the 1:1 line, but on average the fall cone test yields higher LL_{cone} values for LL_{cup} values below 33 and lower LL_{cone} values for LL_{cup} values above 33. Both tests yield progressively larger variations with the increasing LL values that result from increasing the bentonite content. However, the variations in the fall cone test results are much smaller than those of the Casagrande cup, as clearly demonstrated by the smaller range of the vertical error bars compared to the horizontal ones.

The linear correlations determined in the present and previous studies for different types of materials are summarized in Table 5.3. These linear correlations indicate that using the fall cone test to determine LL is promising, and the test results are very close to those of the conventional Casagrande cup test despite the different mechanisms of the two testing methods.

Table 5.3. Correlations between the Casagrande cup and fall cone liquid limit test results

Reference	Material	LL range (%)	Number of specimens	Correlations
Sherwood and Ryley (1970)	Various clays	30-76	25	$LL_{\text{cone}} = 0.95 LL_{\text{cup}} + 0.95$
Belviso et al. (1985)	Natural soils, Southern Italian	34-134	16	$LL_{\text{cone}} = 0.97 LL_{\text{cup}} + 1.19$
Wasti and Bezirci (1986)	Natural soils, Turkey	27-110	15	$LL_{\text{cone}} = 1.01 LL_{\text{cup}} + 4.92$
Dragoni et al. (2008)	Clayey soils, Central Italy	28-74	41	$LL_{\text{cone}} = 1.02 LL_{\text{cup}} + 2.87$
Ozer (2009)	Natural soils, Turkey	29-104	32	$LL_{\text{cone}} = 0.90 LL_{\text{cup}} + 6.04$
Fojtová et al. (2009)	Ostrava Basin clay, Czech Republic	20-50	52	$LL_{\text{cone}} = 1.00 LL_{\text{cup}} + 2.44$
Di Matteo (2012)	Database of various soils	24-50	>50	$LL_{\text{cone}} = 1.00 LL_{\text{cup}} + 2.20$
Spagnoli (2012)	Kaolinite and illitic clay	20-61	50	$LL_{\text{cone}} = 0.99 LL_{\text{cup}} + 1.05$
Present study	Crushed limestone material plus bentonite	20-45	45	$LL_{\text{cone}} = 0.85 LL_{\text{cup}} + 5.51$

5.4.2 Plastic Limit and Plasticity Index by Fall Cone versus Conventional Method

Fall cone tests were also performed on the five bentonite-treated samples using a heavier cone to determine the PI, and thereby the PL, using the previously described method of Wroth and Wood (1978). The relationships between the PI determined using the fall cone (PI_{cone}) and the ASTM-standardized (PI_{ASTM}) testing methods, the latter of which involves rolling specimens into 1/8 in. diameter threads, are shown in Figure 5.5(a).

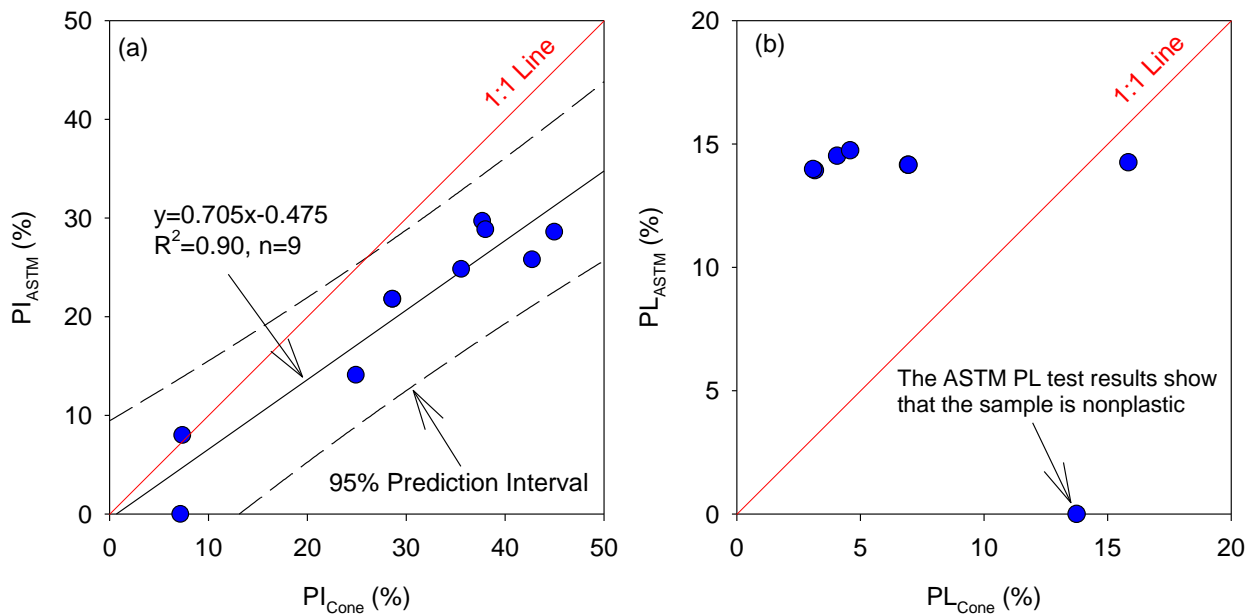


Figure 5.5. (a) PI and (b) PL values determined using the fall cone and ASTM-standardized methods

A linear correlation can be observed between the two testing methods, but the PI_{cone} values are approximately 40% greater than those determined by the ASTM test method using the plastic roller device. For the fall cone device, the plastic limit (PL_{cone}) was calculated by subtracting the PI_{cone} values from the LL_{cone} values. The resulting plastic limits are compared with those from the conventional ASTM-standardized rolling device in Figure 5.5(b). Interestingly, the PL_{roller} values are approximately the same for the samples treated with different percentages of bentonite (from 0% to 12%), whereas the PL_{cone} values vary over a much wider range. This phenomenon may indicate that the PL determined using the conventional method is governed by the dominant material of the samples (i.e., the minus No. 40 sieved granular limestone material) and that the fall cone test is more sensitive to the bentonite content. This observation warrants further study.

5.4.3 Plasticity Index versus Bar Linear Shrinkage Values

In this study, the BLS test was also conducted on the five samples with bentonite contents varying from 0% to 12%. The BLS test results are compared with the PI values determined using the ASTM plastic roller device in Figure 5.6. A linear correlation can be observed between the two parameters, and the variation of the BLS test results generally increases as the bentonite content increases.

However, as the bentonite content increases from 0% to 12%, the PI determined by the ASTM methods varies from 0% to 28%, whereas the BLS values vary over a much smaller range of 2% to 8%. This indicates that BLS values are much less sensitive than PI values to changes in plasticity. More importantly, the ranges of maximum and minimum values of PI (vertical error bars) for the different bentonite contents do not overlap, whereas most of the BLS ranges (horizontal error bars) do overlap. This means that a BLS measurement on the high end of the range for a bentonite content of 3%, for example, could have the same value as the BLS measurement on the low end of the range for a bentonite content of 12%. In both cases, plugging the BLS value into the linear equation for converting BLS to PI in Figure 5.6 would result in a significant error in the estimated PI. For this reason, the use of BLS as an alternative test method to directly obtain PI instead of measuring LL and PL separately is not recommended in this study.

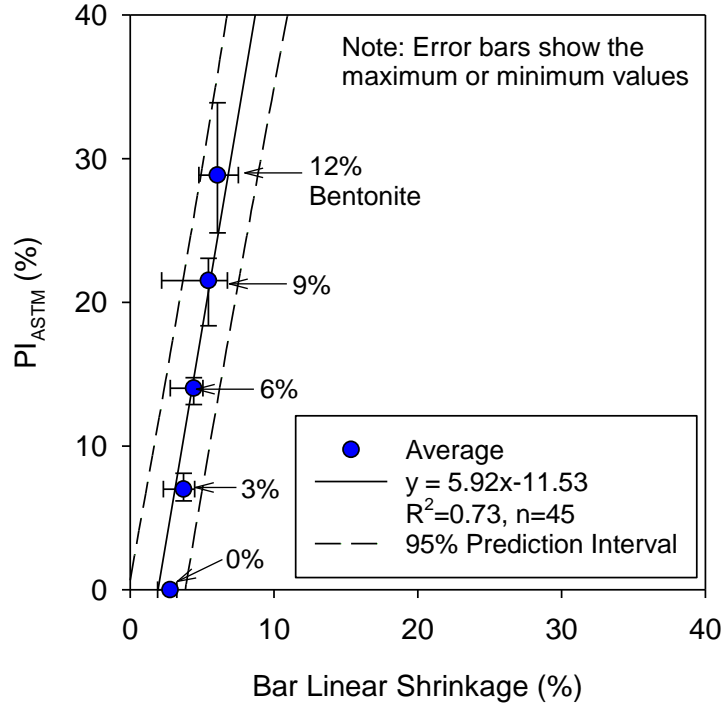


Figure 5.6. Correlation between BLS values and PI determined by ASTM methods (Casagrande cup for LL and plastic limit roller for PL) for five testing samples

5.5 Two-Way ANOVA-Based Repeatability and Reproducibility Analysis

5.5.1 Description of the Statistical Analysis Method

In this study, a two-way ANOVA-based R&R analysis was used to statistically quantify the repeatability, reproducibility, overall variability, and error sources of the various laboratory plasticity tests. This statistical analysis method is detailed in Vardeman and Jobe (1998).

The input data for the analysis requires J different operators to measure each of I different parts a total of m times. The two-way random effects model is represented by Equation (5.1):

$$y_{ijk} = \mu + \alpha_i + \beta_j + \alpha\beta_{ij} + \varepsilon_{ijk} \quad (5.1)$$

where

y_{ijk} = the k^{th} measurement made by operator j on part i

μ = a measurement averaged over all possible operators and all possible parts

α_i = random effects of different parts

β_j = random effects of different operators

$\alpha\beta_{ij}$ = random joint effects specific to combinations of particular parts and operators

ε_{ijk} = random measurement error

The corresponding variances (σ_α^2 , σ_β^2 , $\sigma_{\alpha\beta}^2$, and σ^2) of the parameters in the model, called “variance components,” govern the variability of the measurements.

According to the random effects model, the only difference between different measurements for a specific combination of part and operator is the measurement error (ε), so its standard deviation (σ) is a measure of the repeatability in the model:

$$\sigma_{\text{Repeatability}} = \sigma \quad (5.2)$$

For a fixed part i , the value $\mu + \alpha_i$ is constant for different measurements, so the measure of operator bias for a fixed part, i.e., $\sqrt{\sigma_\beta^2 + \sigma_{\alpha\beta}^2}$, is an appropriate measure of reproducibility, which can be expressed as

$$\sigma_{\text{Reproducibility}} = \sqrt{\sigma_\beta^2 + \sigma_{\alpha\beta}^2} \quad (5.3)$$

Therefore, the overall variation due to repeatability and reproducibility ($\sigma_{R\&R}$) can be calculated as

$$\sigma_{R\&R} = \sqrt{\sigma_{\text{Repeatability}}^2 + \sigma_{\text{Reproducibility}}^2} \quad (5.4)$$

To obtain the parameters used in this model, a two-way ANOVA table such as Table 5.4 can be determined based on the test data using a statistical software package.

Table 5.4. Typical two-way ANOVA table for the gauge R&R study

Source	Sum of Squares (SS)	Degrees of Freedom (df)	Mean Square (MS)
Part (I)	SSA	$I-1$	$MSA = SSA/(I-1)$
Operator (J)	SSB	$J-1$	$MSB = SSB/(J-1)$
Part \times Operator ($I \times J$)	SSAB	$(I-1)(J-1)$	$MSAB = SSAB/((I-1)(J-1))$
Error	SSE	$IJ(m-1)$	$MSE = SSE/IJ(m-1)$
Total	SSTot	$IJm - 1$...

The number of parts (I) and number of operators (J) should be set as nominal variables for the two-way ANOVA analysis. The three standard deviations can then be calculated as follows:

$$\sigma_{\text{Repeatability}} = \sigma = \sqrt{MSE} \quad (5.5)$$

$$\sigma_{Reproducibility} = \sqrt{\max\left(0, \frac{MSB}{mI} + \frac{(I-1)MSAB}{mI} - \frac{MSE}{m}\right)} \quad (5.6)$$

$$\sigma_{R\&R} = \sqrt{\frac{MSB}{mI} + \frac{(I-1)MSAB}{mI} - \frac{(m-1)MSE}{m}} \quad (5.7)$$

The degrees of freedom of the three quantities can be approximately determined using the Satterthwaite method (Satterthwaite 1946) as

$$v_{Repeatability} = IJ(m-1) \quad (5.8)$$

$$v_{Reproducibility} = \frac{\sigma_{Reproducibility}^4}{\frac{1}{m^2} \left(\frac{MSB^2}{I^2(J-1)} + \frac{(I-1)MSAB^2}{I^2(J-1)} + \frac{MSE^2}{IJ(m-1)} \right)} \quad (5.9)$$

$$v_{R\&R} = \frac{\sigma_{R\&R}^4}{\frac{1}{m^2} \left(\frac{MSB^2}{I^2(J-1)} + \frac{(I-1)MSAB^2}{I^2(J-1)} + \frac{(m-1)MSE^2}{IJ} \right)} \quad (5.10)$$

The corresponding confidence limits for each of the quantities can be calculated based on the Chi-squared distribution (χ_v^2) using

$$\sigma \sqrt{\frac{v}{\chi_{upper}^2}} \text{ and } \sigma \sqrt{\frac{v}{\chi_{lower}^2}} \quad (5.11)$$

The contributions of $\sigma_{Repeatability}$ and $\sigma_{Reproducibility}$ to $\sigma_{R\&R}$ are quantified using Equations (5.12) and (5.13):

$$\text{Fraction of } \sigma_{R\&R} \text{ due to } \sigma_{Repeatability} = \frac{\sigma_{Repeatability}^2}{\sigma_{R\&R}^2} \quad (5.12)$$

$$\text{Fraction of } \sigma_{R\&R} \text{ due to } \sigma_{Reproducibility} = \frac{\sigma_{Reproducibility}^2}{\sigma_{R\&R}^2} \quad (5.13)$$

5.5.2 Results of Repeatability and Reproducibility Analysis

The two-way ANOVA-based R&R analysis was conducted on the results of the various laboratory plasticity tests detailed in the preceding sections. The testing matrix used for the R&R analysis is shown in Table 5.5. For each of the test methods, each operator conducted three replicate tests on the five samples. Hence, the data collected for the analysis of each test method are from three different operators (J) measuring each of the five different parts (I) a total of three times (m).

Table 5.5. Laboratory testing matrix used in this study

Test Method	No. of Soil Samples (I)	No. of Operators (J)	No. of Replicate Tests Per Operator (m)
Casagrande Cup LL	5 ^a	3	3
Fall Cone LL			
ASTM PL			
Bar Linear Shrinkage			

^a Minus No. 40 sieved granular road surface material with 0%, 3%, 6%, 9%, and 12% added bentonite.

The results of the analyses are summarized and compared to the R&R values reported in ASTM D4318 in Table 5.6. For the Casagrande cup LL test, the R&R values determined using the two-way ANOVA-based method presented herein (0.6% and 1.7%) are close to those reported in ASTM D4318 (0.5% and 1.3%). The results also show that the overall variation ($\sigma_{R\&R}$) of the fall cone LL tests is 0.7%, which is less than half that of the Casagrande cup test (1.8%).

The analysis results also can identify the sources of error inherent in the test methods. For the fall cone test, the fraction of $\sigma_{R\&R}$ due to $\sigma_{Reproducibility}$ (i.e., between-operator error) is 50%. However, for the Casagrande cup test 89% of the overall $\sigma_{R\&R}$ is contributed by the between-operator error, even though all three operators were trained at the same time. Based on the two-way ANOVA results, it can be concluded that the fall cone test used for measuring the LL is more consistent and less operator dependent than the Casagrande cup test.

For the PL test conducted using the ASTM rolling device, $\sigma_{R\&R}$ determined using the two-way ANOVA-based method is 0.7%, which is close to the multilaboratory value reported in ASTM D4318. The between-operator error of the PL test is still the main source of the overall variation (73%), which is expected because the testing method is somewhat subjective. The use of the ASTM PL rolling device produces more consistent 1/8 in. diameter threads compared to rolling by hand, which improves both the repeatability and reproducibility of the PL test results. However, the R&R analysis was not specifically performed on the hand rolling method in this study.

For the BLS test, $\sigma_{R\&R}$ is 1%, and the between-operator error accounts for 57% of the overall variation. As discussed in the previous section on correlations, however, the conventional PL and BLS test results were not sensitive to the bentonite content of the mixtures. Therefore, the five

different samples (parts) prepared in this study could be regarded as nearly the same for these two tests, which may result in the favorably smaller $\sigma_{reproducibility}$ values.

Table 5.6. Repeatability and reproducibility results reported in ASTM D4318 and determined by two-way ANOVA-based analysis for the various laboratory tests

Parameters	Liquid Limit		Plastic Limit		Bar Linear Shrinkage
	Casagrande Cup	Fall Cone	ASTM Roller ^b	Fall Cone	
<i>Repeatability and Reproducibility (R&R)^a Reported in ASTM D4318</i>					
Single-Operator Standard Deviation (%) (Within-Laboratory Repeatability)	0.5		0.3		
Multilaboratory Standard Deviation (%) (Between-Laboratory Reproducibility)	1.3	NA	0.9	NA	NA
<i>Two-way ANOVA-based R&R Analysis Results</i>					
$\sigma_{Reproducibility}$ (%)	0.6	0.5	0.4		0.6
$\nu_{Repeatability}$	30	30	24		30
95% Confidence Interval (%)	0.5–0.8	0.4–0.6	0.3–0.5		0.5–0.9
$\sigma_{Reproducibility}$ (%)	1.7	0.5	0.6		0.7
$\nu_{Reproducibility}$	6	3	5		3
95% Confidence Interval (%)	1.1–3.8	0.3–1.7	0.4–1.5	NA	0.4–2.7
$\sigma_{R\&R}$ (%)	1.8	0.7	0.7		1.0
$\nu_{R\&R}$	8	10	11		10
95% Confidence Interval (%)	1.3–3.5	0.5–1.1	0.5–1.2		0.7–1.7
Fraction of $\sigma_{R\&R}$ due to $\sigma_{Repeatability}$	11%	50%	27%		43%
Fraction of $\sigma_{R\&R}$ due to $\sigma_{Reproducibility}$	89%	50%	73%		57%

^a The R&R analysis was conducted on a USCS:ML soil.

^b The ASTM PL test was conducted on four samples because the 0% bentonite sample was nonplastic.

5.5.3 Measurement Capacity Ratio

The ASTM standards typically use the d_{2s} limit (i.e., $1.960\sqrt{2} \cdot 1s$) to determine the acceptable range of two test results (ASTM E691, ASTM E177), which are calculated based on either the single-operator or multilaboratory standard deviations, s . Based on the two-way ANOVA R&R analysis results, the measurement capacity ratio (MCR), which is the precision-to-tolerance ratio of a measurement, can be used to quantify the errors from both the testing device and multiple operators.

The MCR can be used to determine whether a measurement is suitable for verifying the conformance of a measured characteristic to engineering specifications. The MCR can also be considered when setting specification ranges based on measurements. For example, if the lower (L) and upper (U) boundaries of a specification for the LL of a material are 30% and 45%, and

the $\sigma_{R\&R}$ of the fall cone LL device is 0.7%, the MCR of the device can be calculated using Equation (5.14), which gives a value of 0.28.

$$MCR = \frac{6\sigma_{R\&R}}{U - L} \quad (5.14)$$

According to Vardeman and Jobe (1998), “[t]he hope is that measurement uncertainty is at least an order of magnitude smaller than the spread in specifications,” which requires that the MCR should be no larger than 0.1 in order to use the measurements to check conformance to such specifications. However, this target MCR value of 0.1 may be too strict for geotechnical applications and needs to be reevaluated for different materials and testing methods.

5.6 Conclusions and Recommendations

In this study, several laboratory tests for measuring Atterberg limits were evaluated and statistically compared. Correlations between the fall cone and Casagrande cup tests determined in the present and previous studies demonstrated that the fall cone test can be used to determine the LL of a material with reduced variability between repeated tests. The two-way ANOVA-based repeatability and reproducibility analysis also revealed that the fall cone test can result in smaller overall variation than the Casagrande cup test, which is more prone to inter-operator errors.

In measuring PL and PI, the fall cone test and conventional test method using the ASTM plastic roller yielded significant discrepancies for the abraded crushed limestone granular materials with small percentages of bentonite incorporated. The fall cone test showed a dependence of PL on the bentonite content, whereas the conventional method was practically insensitive to the bentonite content. Further studies need to be conducted to evaluate the influence of the different testing mechanisms and whether PL is governed by the dominant minerals of a soil mixture.

The bar linear shrinkage results exhibited a linear correlation with the PI determined by conventional ASTM testing methods. However, as the PI increased significantly from 0% to 28% by incorporating bentonite, the corresponding BLS values were much less sensitive, exhibiting a change of only 6%. Moreover, the ranges of measured BLS values for the different bentonite contents overlapped, prohibiting a reasonably accurate correlation between BLS and PI.

This study also demonstrated the use of a two-way ANOVA-based R&R analysis to evaluate the repeatability, reproducibility, overall variation, and capacity of a testing method. Such an analysis can also identify the error sources and thus provide useful suggestions for improving a testing method. The MCR was demonstrated based on the two-way ANOVA R&R analysis results, which considers errors from both the device and the inter-operator variability, and it should therefore be considered when selecting QC/QA testing methods.

Based on the findings of this study, the authors suggest the following: (1) include the fall cone test as an alternative method for determining the liquid limit of soils, (2) use the two-way ANOVA-based analysis presented herein to determine the R&R and identify the sources of measurement error, and (3) consider the MCR of a measurement when setting specifications or selecting QA/QC testing methods.

CHAPTER 6. DEVELOPMENT OF A NEW LABORATORY TEST FOR EVALUATING QUALITY, MORPHOLOGY, AND COMPACTION CHARACTERISTICS OF GRANULAR MATERIALS

Note: the contents of this chapter were originally published in the following journal paper and are re-used in this report with permission:

Li, C., J. C. Ashlock, D. J. White, C. T. Jahren, and B. Cetin. 2017. Gyrotory Abrasion with 2D Image Analysis Test Method for Evaluation of Mechanical Degradation and Changes in Morphology and Shear Strength of Compacted Granular Materials. *Construction & Building Materials*, Vol. 152, 547–557. <https://doi.org/10.1016/j.conbuildmat.2017.07.013>.

6.1 Introduction

Mechanical degradation or abrasion of granular materials used for granular-surfaced roads and pavement base layers can significantly influence their mechanical properties, drainage conditions, and freeze-thaw durability (Cho et al. 2006, Nurmikolu 2005, Vallejo et al. 2006, White and Vennapusa 2014). To more practically evaluate degradation characteristics or create specifications for granular materials, most researchers and transportation agencies rely on the Los Angeles abrasion and Micro-Deval tests, which require specimens to be prepared to standard gradings and tested in a rotating steel drum containing steel spheres. However, these two testing methods do not simulate the actual loading conditions responsible for the degradation and performance of the materials and do not test their full gradations.

Aggregate morphology has long been recognized as an important factor affecting the engineering properties and particle degradation of granular materials (Cheung and Dawson 2002, Cho et al. 2006, Pan et al. 2006). Various parameters have been proposed to quantify the external morphology of particles. However, the conventional procedure using Rittenhouse and Krumbein charts to visually classify the sphericity and roundness of particles can be very time-consuming and subjective (Krumbein 1941, Rittenhouse 1943).

To address these deficiencies, a new laboratory testing method is proposed and developed herein that employs the gyrotory compaction device and 2D image analyses to evaluate the mechanical degradation and changes in morphology and shear strength of granular materials under simulated field compaction and traffic loads. The new method, named the Gyrotory Abrasion and Image Analysis method, aims to more accurately predict the actual degradation of granular materials after compaction or traffic loading and to rapidly establish the density-strength-compaction energy relationship for a material. The latter can be used to develop performance-based specifications that ensure field performance, minimize material degradation, and save time and energy. This chapter details the new testing method and associated analyses, compares the results with those of conventional LA abrasion tests using five types of granular materials, explains the behavior of the granular materials during the gyrotory compaction tests, and demonstrates how the test results can be used to develop performance-based specifications for field compaction of granular surface layers or pavement base layers.

6.2 Materials

In this study, five granular materials typically used for granular-surfaced roads and pavement foundation layers were collected from a granular-surfaced road section and from two quarries having different geological diagenesis in Iowa. The sieve analysis test results and USCS and AASHTO soil classifications of the five materials are summarized in Table 6.1.

Table 6.1. Properties of the five granular materials tested in this study

Parameters	Existing Surface Aggregate	Virgin Surface Aggregate	Road Rock	Class A Stone	Concrete Stone
Abbreviation	ESA	VSA	RR	CAS	CS
Source	Granular road	Quarry 1	Quarry 1	Quarry 2	Quarry 2
Gravel content (%) (> 4.75mm)	24.0	68.7	65.2	42.9	96.3
Sand content (%) (4.75 mm – 75 μ m)	50.0	22.8	19.5	48.9	2.9
Fines content (%) (< 75 μ m)	26.0	8.5	15.3	8.2	0.8
Maximum aggregate size (mm)	25.4	38.1	38.1	25.4	25.4
Coefficient of curvature, C_c	4.23	7.61	18.32	3.99	1.08
Coefficient of uniformity, C_u	213.67	57.45	970.27	31.39	2.25
Plastic limit (%)	15	25	NP	NP	NP
Liquid limit (%)	17	16			
AASHTO Classification	A-2-4(0)	A-2-4(0)	A-1-a	A-1-a	A-1-a
USCS Symbol	SM	GP-GC	GM	SP-SM	GP

NP = nonplastic

The existing surface aggregate (ESA) had the lowest gravel content (> No. 4 sieve) because this material had already been abraded by traffic for some time. Compared to the concrete stone (CS) material, which consisted of a uniformly graded clean aggregate, the virgin surface aggregate (VSA), road rock (RR), and Class A stone (CAS) were all more well graded.

6.3 Gyrotory Compactor and Pressure Distribution Analyzer

The gyrotory compaction test was originally developed for mix design of hot-mix asphalt (HMA) mixtures (Harman et al. 2002). In this test, two compaction mechanisms, namely, a constant vertical pressure and gyrotory shear stresses induced by eccentric loadings, are used to simulate field compaction and traffic loads (Bahia and Faheem 2007, Delrio-Prat et al. 2011). Previous studies have demonstrated that the gyrotory compactor is also useful for evaluating the compaction characteristics of soils ranging from coarse aggregates to high-plasticity clays (Cerni and Camilli 2011, Li et al. 2015b, Ping et al. 2002). The effects of the four equipment operational parameters, which are the vertically applied pressure and the angle, frequency, and number of gyrations, have been well studied for both HMA and soils (Butcher 1998, Mokwa and

Cuelho 2008). Compared to other laboratory compaction methods, such as impact and vibratory compaction, it has been reported that the gyratory compaction curves for soils can better replicate field compaction results (Ping et al. 2003).

A pressure distribution analyzer (PDA) was also developed in a prior study to monitor changes in the shear resistance of HMA specimens during gyratory compaction (Guler et al. 2000). The PDA uses three load cells to measure the applied vertical load and changes in eccentricity of the load during the test. Based on the PDA data and equipment operational parameters, the theoretical compaction energy applied to the specimen can also be calculated (Delrio-Prat et al. 2011). The repeatability of using the PDA to measure shear resistance of a granular material (Ottawa sand) was reported to be less than 7 kPa, and a strong linear correlation ($R^2 = 0.89$) was found between the PDA-measured shear resistance and unconfined compressive strength for a fine-grained granular material possessing some apparent cohesion (Li et al. 2015b).

6.3.1 Sample Preparation and Testing Procedures

A gyratory compactor was used to compact the specimens under a constant vertical pressure, with the PDA on top of the specimens to measure changes in their shear resistance throughout the tests, as shown in Figure 6.1.

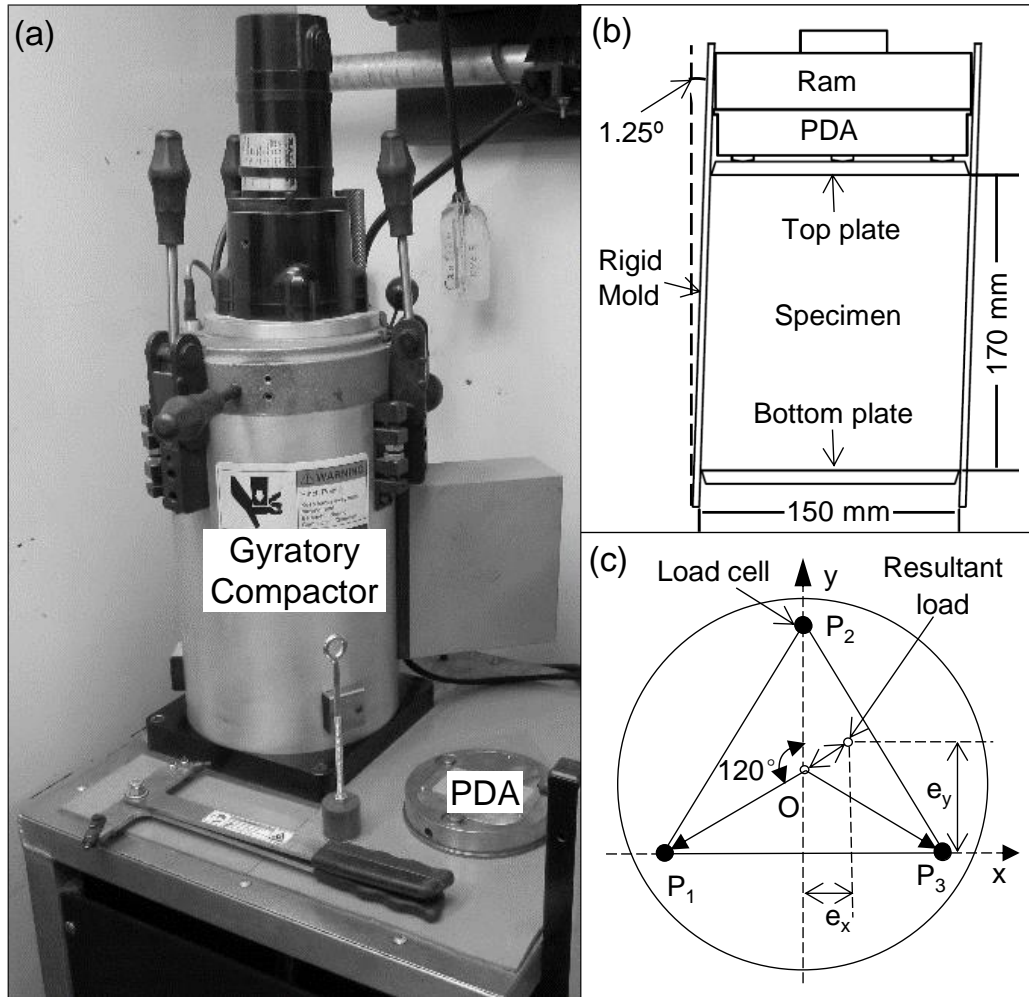


Figure 6.1. (a) Photo of gyrotory compactor and PDA, (b) schematic of the gyrotory compactor, (c) schematic of the PDA

In this study, the operational parameters of the gyrotory equipment specified for testing asphalt mixtures in ASTM D6925 were followed and are summarized in Table 6.2.

Table 6.2. Equipment operation parameters of the gyrotory compactor

Parameter	Value
Vertical applied pressure	600 ± 10 kPa
Number of gyrations	500 *
Angle of gyration	1.25 ± 0.02 degrees
Frequency of gyration	30 ± 0.5 gyrations/min
Number of dwell gyrations	2

* Applied in two consecutive tests having 250 gyrations each

For each material type, a representative specimen of approximately 4,500 g was prepared using a riffle splitter and then oven dried at 110°C for 24 hours. During the test, a total of 500 gyrations

were applied to each specimen. Due to the compactor's limitation of a maximum of 299 gyrations per test, the device was temporarily stopped after 250 gyrations and then manually restarted. However, after the first 250 gyrations, the compactor automatically released the vertical pressure and applied two dwell gyrations to remove the angle of gyration and square the specimen. This procedure may have introduced some slight disturbance of the specimens and possibly resulted in varying degrees of dilation.

6.3.2 Data Analysis

The changes in the volume of the specimens during the gyratory compaction tests were calculated from specimen heights measured using the system's integral displacement transducer. Based on the dry mass and volume of the specimen, the dry unit weight (γ_d) can be easily determined for each gyration, and the void ratio (e) can be calculated by assuming or measuring the specific gravity (G_s) of the material as

$$e = \frac{G_s \gamma_w}{\gamma_d} - 1 \quad (6.1)$$

where γ_w is the unit weight of water (9.81 kN/m³).

The shear resistance of the specimens can be determined for each gyration using the PDA data. The three load cells embedded in the PDA give the resultant vertical load applied to the specimen, as well as the eccentricity of the load relative to the center (O) of the PDA from moment equilibrium equations along two perpendicular axes, as shown in Figure 6.1(c). Based on energy conservation principles, the energy of the external forces can be equated to the strain energy of the specimen, assuming that energy due to surface traction is negligible (Guler et al. 2000). The effective moment can then be calculated for a direct measure of the shear resistance of the specimen as

$$\tau_G = \frac{R_i e_i}{AH_i} \quad (6.2)$$

where A is the cross-sectional area of the compaction mold, H_i is the specimen height at a given gyration number, R_i is the resultant vertical load applied on the specimen for the same gyration number, and e_i is the eccentricity of the resultant load.

In addition, the PDA data can be used to estimate the compaction energy applied to the specimen. The gyratory compaction energy ($E_{gyratory}$) is the work done per unit volume by the vertical applied pressure and the moment induced by the vertical pressure and shear stress, which can be calculated using the equipment operational parameters (Table 6.2) and the measured shear resistance of the specimen as

$$E_{gyratory} = \frac{PA(H_0 - H_N) + 4\theta \sum_0^N \tau_{G(i)} V_i}{V_i} \quad (6.3)$$

where $E_{gyratory}$ is the gyratory compaction energy (kJ/m³), P is the vertical applied pressure (kPa), A is the cross-sectional area of the mold (m²), H_0 is the initial specimen height (m), H_N is the height after the final gyration (m), θ is the angle of gyration (radians), V_i is the specimen volume after gyration number i (m³), and $\tau_{G(i)}$ is corresponding shear resistance of the specimen (kPa) (see Delrio-Prat et al. 2011, Li et al. 2015b).

6.4 Image Analysis

In this study, before the gyratory test the specimen was separated into two portions using a No. 4 sieve. A high-speed optical scanner (Canon 9000F Mark II, Figure 6.2[a]) with a dust and scratch removal image processing feature was used to capture 2D color images of the gravel-size portions (retained on the No. 4 sieve) of the granular specimens. The coarse particles of the specimens were washed, oven dried at 110°C for 24 hours, and scanned for image analysis. To determine the particle size (i.e., the equivalent sieve opening size) and 2D sphericity of each aggregate using the image analysis, the coarse particles were manually distributed on top of the scanner platen with their maximum projection areas facing down, as shown in Figure 6.2(b). After scanning, the coarse and fine portions of the specimen were thoroughly mixed back together and transferred into the gyratory compactor. After the gyratory compaction test, the washing, drying, and scanning procedures were repeated on the coarse fractions to analyze the changes in gradation and morphology caused by the gyratory compaction load during the test.

Depending on the gravel content, the number of coarse particles varied from 1,000 to 3,200 per specimen, with individual scans containing up to several hundred aggregate particles each. However, the scanning process was easy to perform and took less than two hours per specimen.

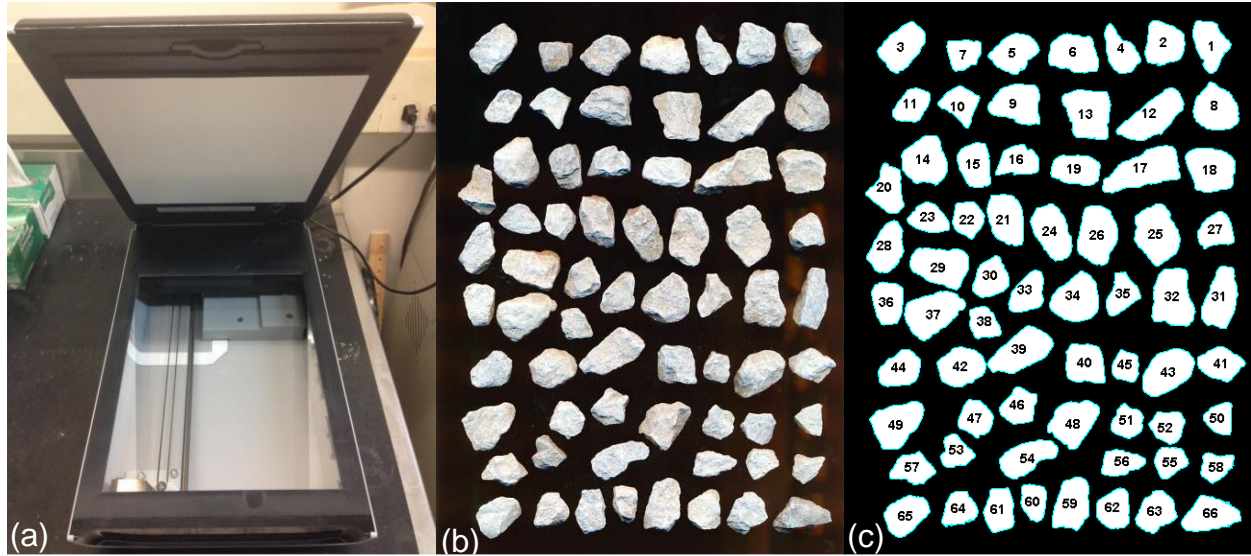


Figure 6.2. (a) Optical scanner used in this study, (b) example original scanned color image of gravel-size aggregates, (c) converted binary image with aggregate edges detected

To quantify the abrasion and morphology changes caused by the gyratory compaction, the images were then processed using a public domain image-processing program named ImageJ, developed by the National Institutes of Health, to quantify the size and shape of the individual aggregates (Schneider et al. 2012). A series of image processing techniques, including noise reduction, contrast enhancement, thresholding, background removal, local maxima detection, and hole filling, were performed to convert the original scanned color images to binary images, examples of which are shown in Figure 6.2(b) and (c).

6.5 Image-Based Particle Size Analysis

Using the 2D image analyses results, nearly continuous particle size distribution curves of the gravel-size aggregates could be generated. Several different methods could be used to estimate the particle sizes on the x-axis (i.e., the sieve size through which a particle would pass), including the minimum bounding rectangle, best-fit ellipse, or minimum Feret diameter, which is the minimum distance between two parallel lines tangential to the projections of an aggregate particle (Igathinathane et al. 2008, Yue et al. 1995).

For the present study, the percentages finer than a given size on the y-axis were calculated using the ratio of each individual particle's area to the total area of all particles. This approach assumes that all particles have the same specific gravity and that the ratios of their 2D projections are equal to the ratios of their volumes. The resulting PSD curves determined by the three methods mentioned above are compared in Figure 6.3.

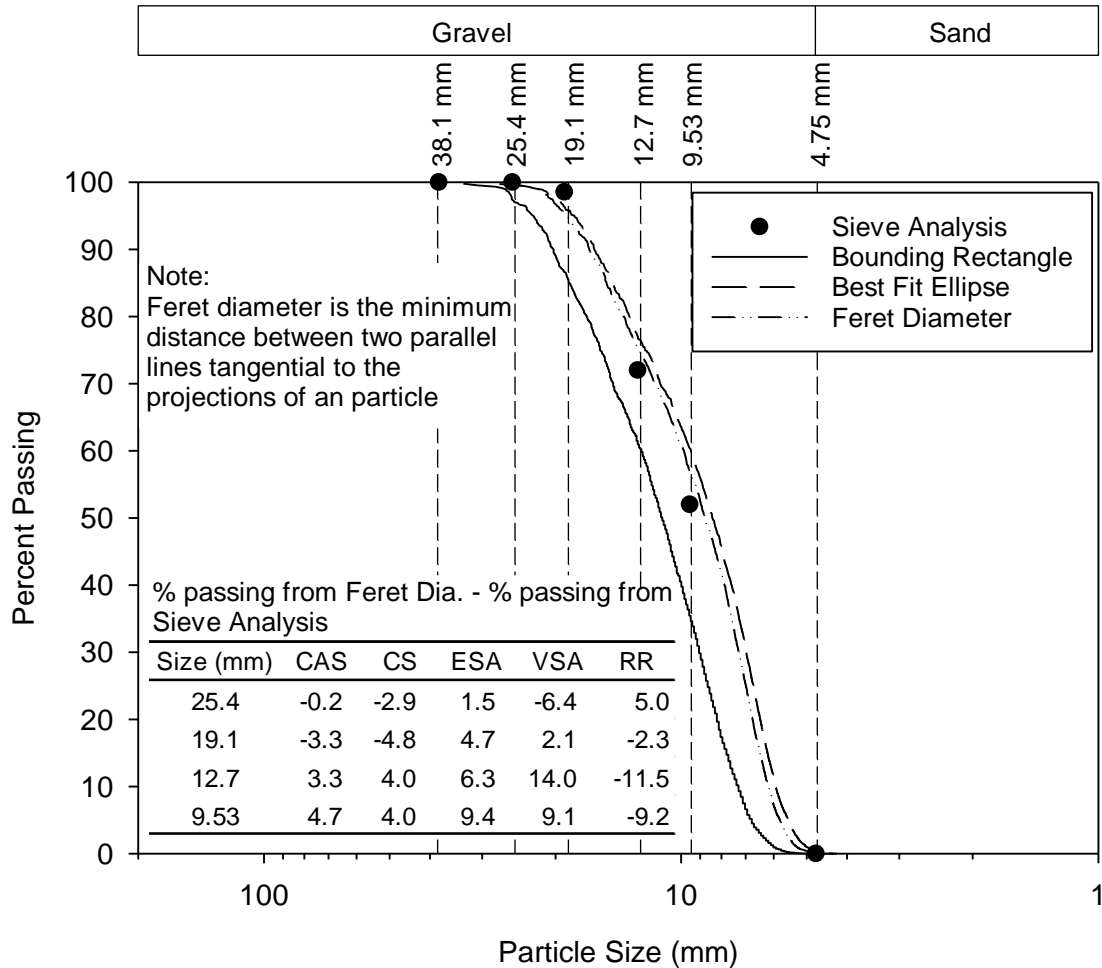


Figure 6.3. Comparison of PSD curves for ESA material determined by sieve analysis and 2D image analysis using three different methods for estimating particle sizes, with tabulated data for other materials

For all specimens tested in this study, similar comparisons revealed that the PSD curves determined by the minimum Feret diameter consistently showed the best agreement with actual sieve analysis results, with typically less than 6% difference at any given particle size. However, as particle size decreases, the difference between the Feret diameter and the sieve analysis results can increase to as much as 14%. The differences between the PSD curves from sieving versus those obtained from the 2D image analyses are mainly caused by the image analyses being based on area fractions rather than mass fractions (Ohm and Hryciw 2013, Tutumluer et al. 2000). Previous studies also demonstrated that the difference could be minimized by estimating the size of the intermediate dimension obtained from the three orthogonal 2D projections of the aggregate particle (Kumara et al. 2012, Ohm and Hryciw 2013, Rao et al. 2001). However, the PSD curves before and after gyratory compaction tests in this study were both generated based on the 2D image analyses and can therefore be compared directly, so the short-axis correction was not performed.

To quantify the particle shapes for the various specimens, the 2D sphericity of a particle defined in Wadell (1932) was calculated using the binary image data as

$$\text{Sphericity} = \frac{r_i}{r_c} \quad (6.4)$$

where r_i is the diameter of the largest inscribed circle of the aggregate projection area and r_c is the diameter of the smallest circle circumscribing the projection area.

6.6 Shortcomings of LA abrasion test

According to ASTM C131 for the LA abrasion test, depending on the original gradation of the material, the specimen must be washed and prepared to a standard grading before being tested in a rotating steel drum containing steel spheres. After the test (500 revolutions with 30 to 33 revolutions per minute), the specimen is washed and sieved through a No. 12 sieve, and the percent passing is reported as the LA abrasion loss or percent loss of the material. Because the specimen is first prepared to a standard grading, the influence of the material's original gradation on the actual abrasion performance in the field is eliminated.

In this study, additional sieve analyses beyond those required by the ASTM standard were performed on each specimen to determine the gradation change of the specimens during the LA abrasion test. Interestingly, it was found that specimens of the different material types (see Table 6.1) with the same initial grading yielded very similar gradations after the test despite the different geological sources and mineral components, as shown in Figure 6.4. This phenomenon may indicate that the mechanical impact and attrition caused by the steel spheres may not sensitively evaluate the effects of a material's intrinsic properties (i.e., mineral components, initial gradation, and morphology) on the abrasion characteristics of that material.

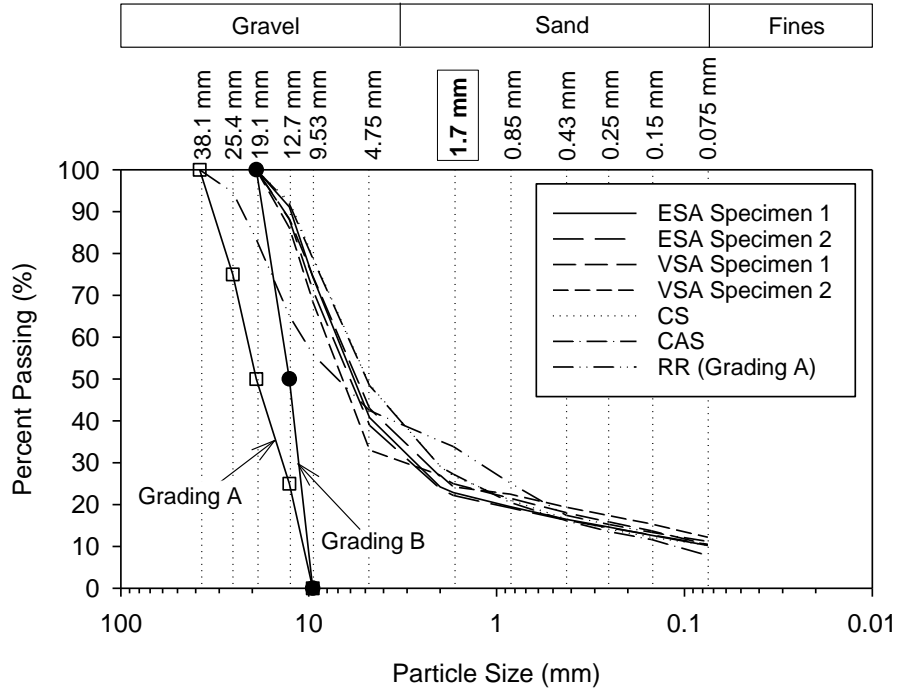


Figure 6.4. Standard initial Gradings A and B of the LA abrasion test and gradations of specimens after testing

For comparison with the LA abrasion loss values, a similar parameter can be calculated for each specimen based on the initial and final PSD curves generated using the image analysis data. To examine this idea, the parameter was taken as the difference between the initial and final PSD curves at the 4.75 mm sieve size (the smallest size available from the image analyses). Using this parameter, the gyratory compaction test results are compared with LA abrasion loss calculated using the 1.7 and 4.75 mm sieves in Figure 6.5. The figure shows that the percent losses determined by the two testing methods are significantly different, which is expected because of the different testing mechanisms and initial gradations of the specimens.

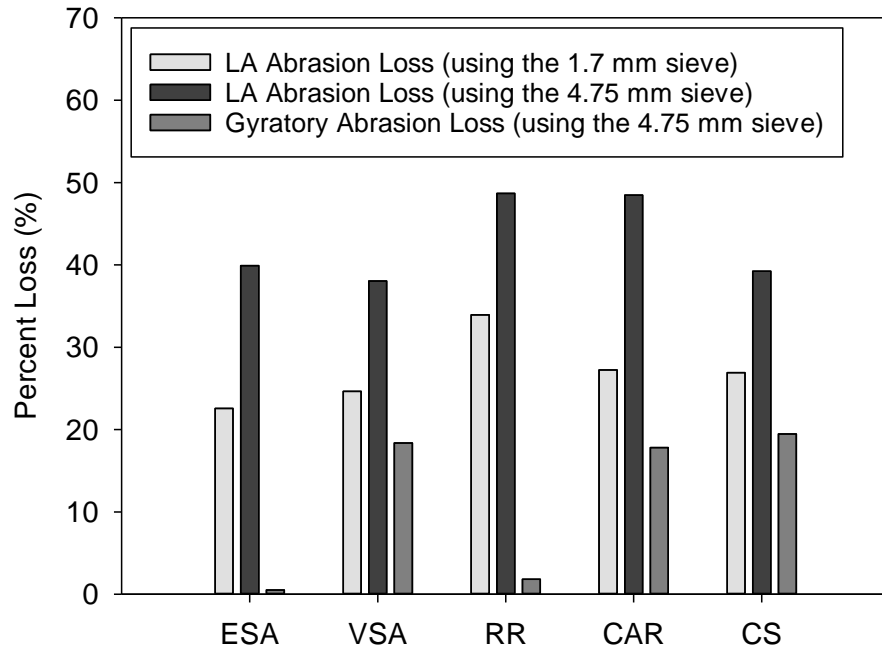


Figure 6.5. Comparison of percent abrasion loss in LA abrasion tests and gyrotory compaction tests for the five specimens

However, comparison of the PSD curves before and after the gyrotory compaction test demonstrates that using a single arbitrary sieve size to quantify the degradation of a material can be misleading. This is demonstrated in Figure 6.6, in which the road rock specimen (which has the highest LA abrasion loss of 34% in Figure 6.5) exhibited a significant difference between the initial and final PSD curves but yielded an increase of only 1.8% in the percent passing the No. 4 sieve after the gyrotory compaction test. Therefore, the total breakage (B_t), originally proposed by Hardin (1985) and defined as the area enclosed by the initial and final PSD curves of a material and the line of the No. 200 sieve, was adapted. In this study, the total breakage index (B_t) is determined only for the gravel-size portions (> No. 4 sieve) of the specimens, so the No. 4 sieve is used instead of the No. 200 sieve, as shown in Figure 6.6.

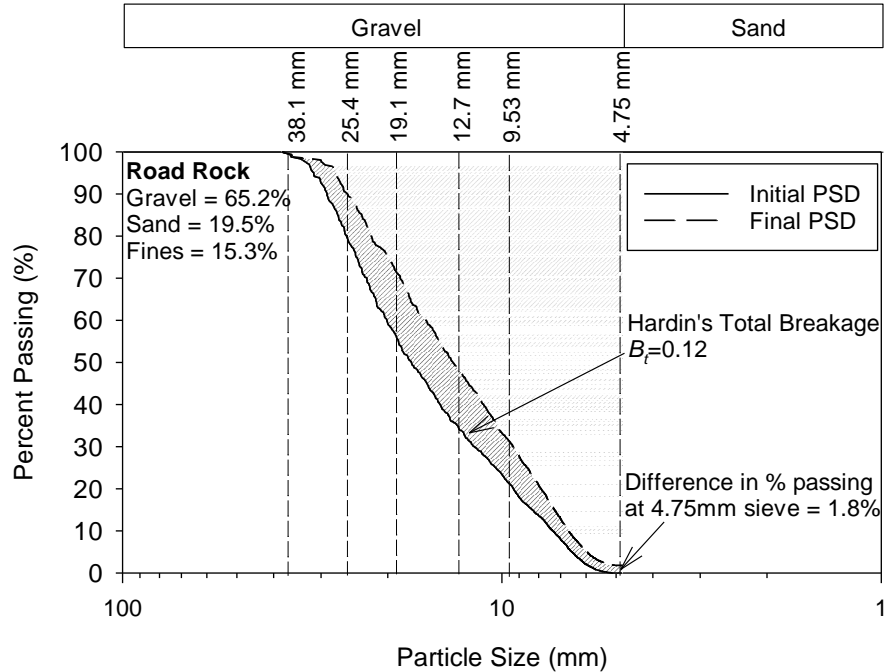


Figure 6.6. PSD curves of gravel fraction of road rock specimen before and after gyratory compaction test, as determined by 2D image analyses

For the different material types tested in this study, a strong linear relationship was observed between the total breakage (B_t) and initial gravel content of the specimens (Figure 6.7). This strong correlation indicates that particle size distribution or particle packing significantly influences the degradation of a material. Note that this relationship does not mean that gravel content is the only parameter that governs the mechanical degradation. To predict the mechanical degradation of a granular material, its gradation, morphology, void ratio, and loading condition need to be carefully considered. In addition, the correlation needs to be verified by field studies.

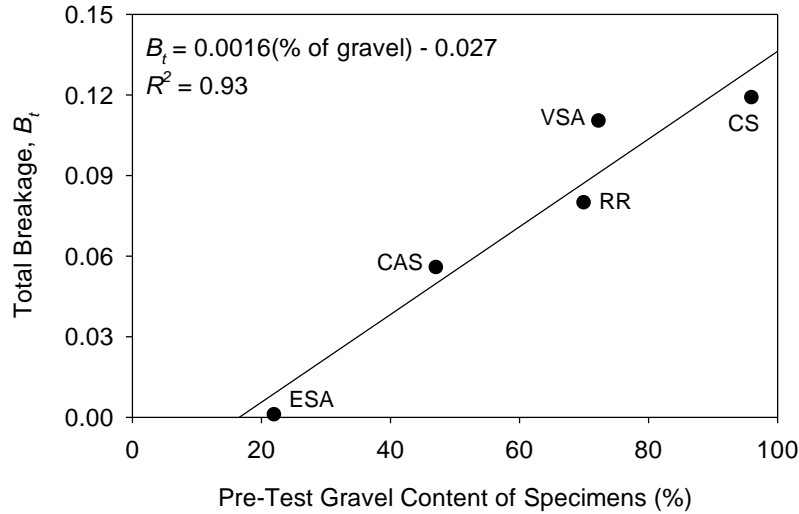


Figure 6.7. Correlation between initial gravel content of specimens and their total breakage caused by gyratory compaction tests, as measured by image analysis

6.7 Particle Degradation and Morphology Changes Quantified by the GAIA Test

The proposed GAIA testing method enables the mechanical gradation and morphology changes after compaction to be quantified relatively quickly and enables a void ratio (or density)-strength-compaction energy relationship to be established for each specimen. This section demonstrates how such GAIA test results can be used to (1) better understand how the large-size aggregate fraction of a material abrades during compaction and (2) set performance-based specifications for the field compaction of granular materials.

In this study, the concrete stone material had the highest gravel content (96%) among the five material types tested (Table 6.1). During the gyratory compaction test on the CS specimen, approximately 20% of the initial gravel-size aggregates degraded to sand-size particles or fines, as shown by the final PSD curve in Figure 6.8(a).

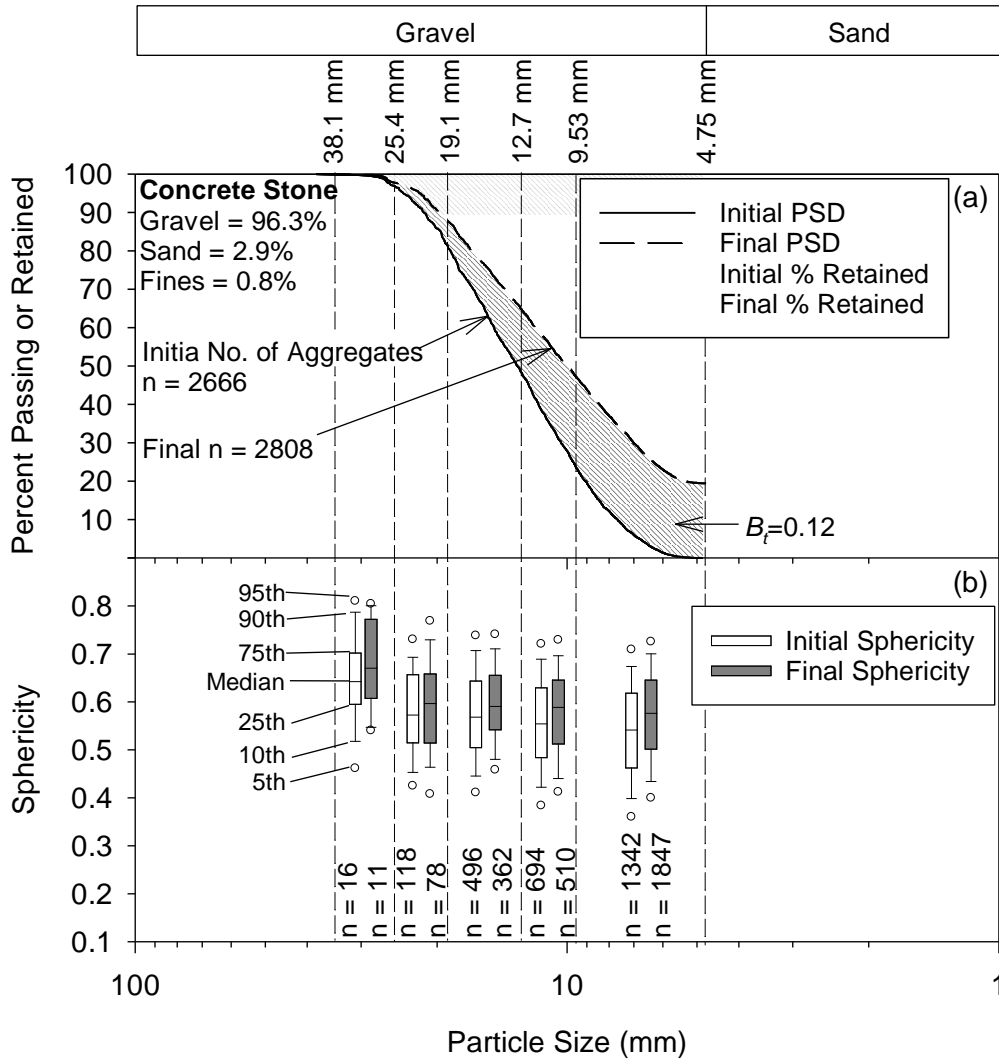


Figure 6.8. (a) Pre- and post-test gradations and (b) sphericities of the gravel-size aggregates of the concrete stone specimen determined by 2D image analysis

To further identify which size ranges of the gravel fraction degraded the most during the test, the percent retained on several commonly used sieves are also presented as a histogram in Figure 6.8(a). The histogram shows that the percent retained on all the sieves decreased after the test, except for the No. 4 to 3/8 in. sieve range. This indicates that a wide range of aggregate sizes comprised the skeleton of the initial specimen and played an important structural role under compaction loading, because almost all size ranges experienced similar abrasion.

From the image analysis data, changes in the particle shape (sphericity) of the aggregate were also calculated, giving the results shown in Figure 6.8(b). The sphericity spanned a wide range from 0.4 to 0.8, so use of only a single value (e.g., median or mean) to describe the morphology of the material may not be sufficient. Therefore, box plots of sphericity in Figure 6.8(b) are used to show the distribution of sphericity for each specimen before and after gyratory compaction. As shown in these results, the median sphericity increased very slightly in all of the CS gravel

size ranges examined because small asperities and corners fractured off the aggregates from abrasion during the gyratory compaction.

Compared to the concrete stone, the existing surface aggregate material had a much lower gravel content (24%) because this material had already been abraded by traffic for some time. The image analyses of the gravel-size fractions before and after the gyratory compaction test showed almost no change in the PSD curves and percent retained (Figure 6.9[a]), with slight changes in sphericity for the 3/4 in. to 1 in. range (Figure 6.9[b]). It can therefore be concluded that the mechanical behavior under loading was mostly governed by the sand-size particles and fines, which can not only bridge between the larger particles, thus creating more contact points and thereby reducing contact stresses, but also be reoriented more easily relative to the gravel-size particles. Both of these behaviors would reduce abrasion.

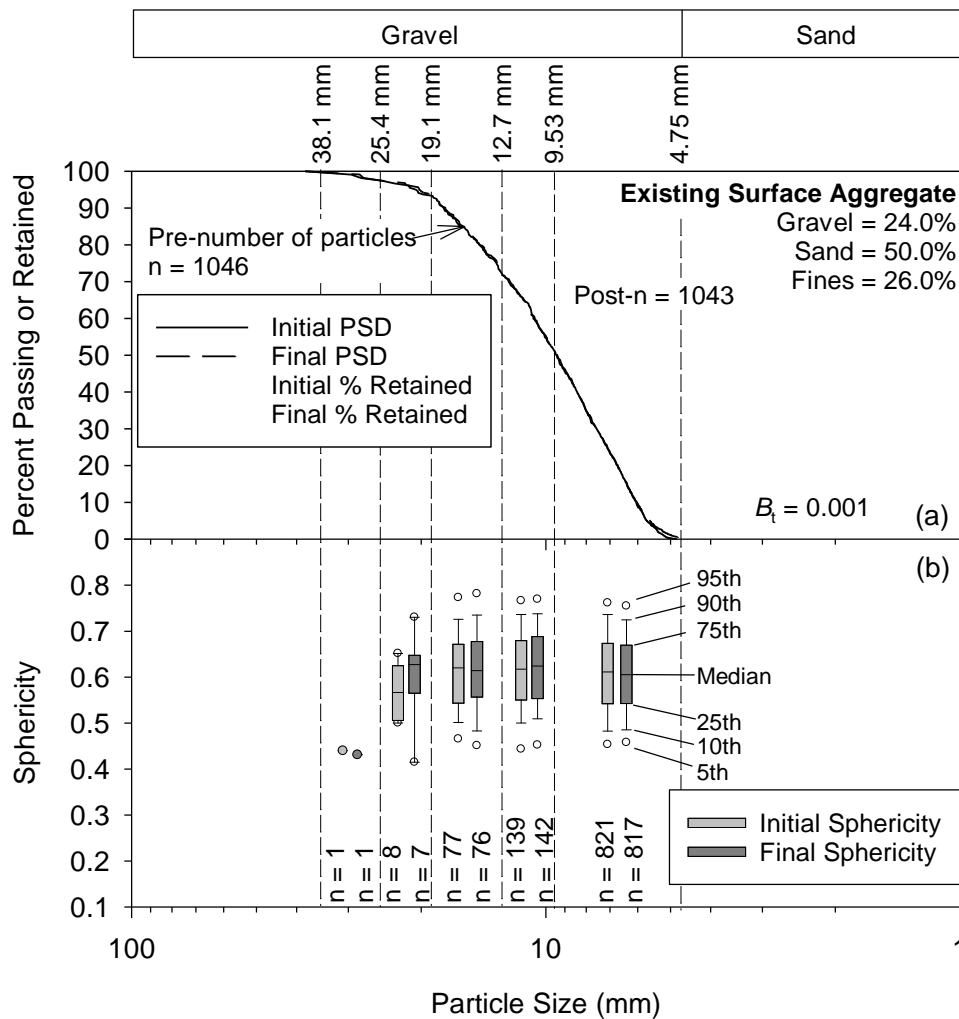


Figure 6.9. (a) Pre- and post-test gradations and (b) sphericities of the gravel-size aggregates of the existing surface aggregate specimen determined by 2D image analysis

6.8 Compaction Characteristics and Changes in Shear Strength of the Five Materials

The shear resistances and void ratios of the five specimens throughout the gyratory compaction tests were also calculated. To calculate the void ratio, a specific gravity of 2.75 was assumed for all the five materials in this study. Both the shear resistance and void ratio show similar trends for the different specimens, with rapid increases in the first 20 to 60 gyration cycles, followed by much slower rates of change in the remaining cycles, as shown in Figure 6.10. One explanation for this behavior is that the loose specimens with relatively large initial void ratios before compaction had few point-to-point contacts between aggregates, but the kneading-shearing mechanism induced by the gyratory compactor effectively reoriented the aggregates while causing corner abrasions, resulting in a rapid reduction in void ratio. As the void ratio decreased, further movement of the aggregates was limited by the rigid mold, causing contact stresses between the aggregates to rapidly increase. Once contact stresses increased beyond the aggregate strengths, particle breakage and additional corner abrasions occurred, further decreasing the void ratio at a much slower rate.

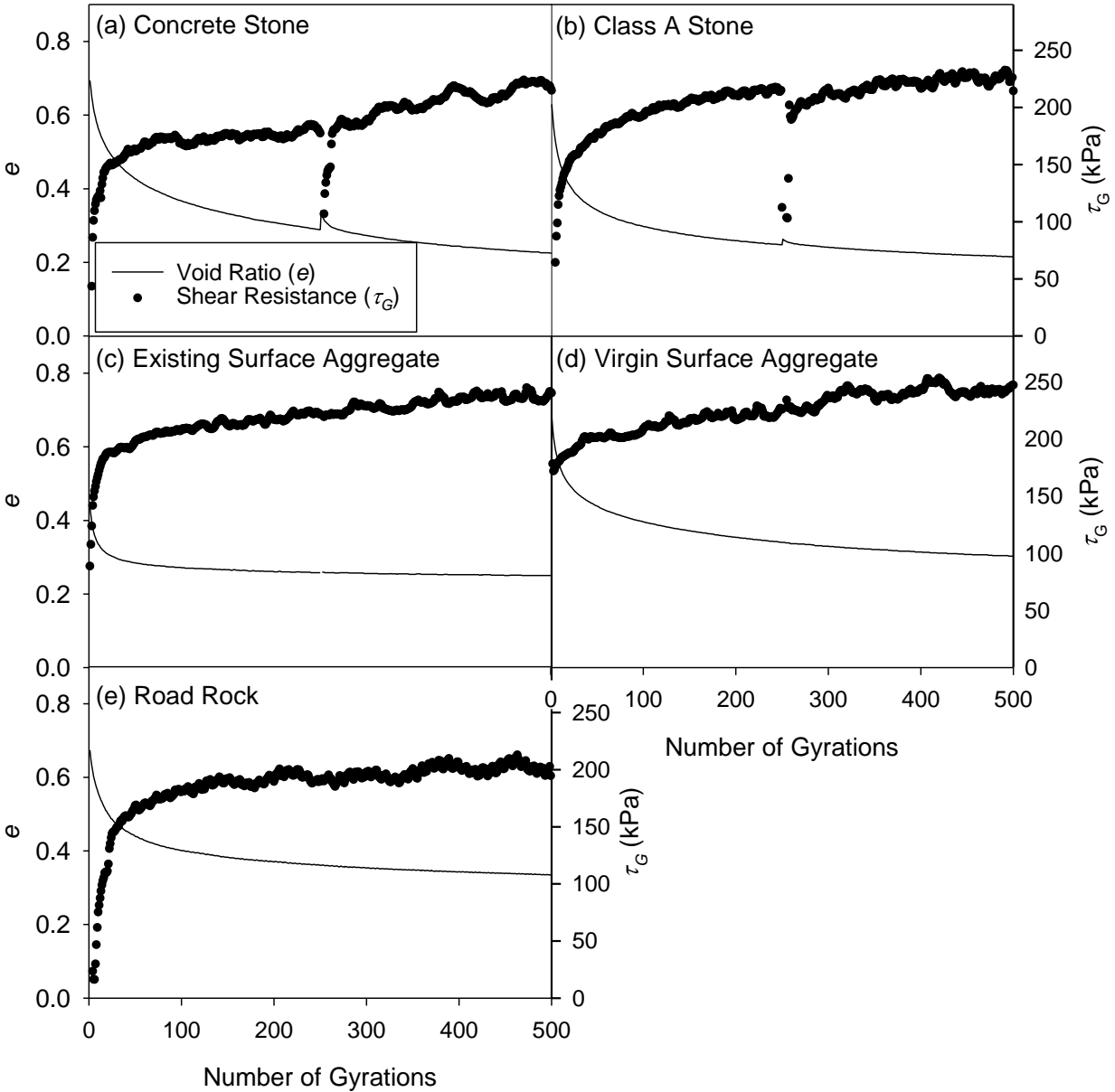


Figure 6.10. Changes in void ratio and shear resistance of the five material types during gyratory compaction tests

The shear resistances of all of the specimens in Figure 6.10 show noticeable fluctuations beyond the points of maximum curvature, whereas the void ratio curves are relatively smooth. The fluctuations in shear resistance may be due to fracture or frictional stick-slip behavior between aggregates, as well as slight dilation induced by the kneading-shearing movement of the compactor. The fluctuations also indicate that a small change in void ratio can result in a significant change in shear resistance. As mentioned above, the gyratory compactor was stopped after 250 gyrations and two dwell gyrations were applied to the specimen before restarting, which could have caused a slight degree of dilation, as shown by the jumps in void ratio at 250 gyrations for two specimens (Figure 6.10[a] and [b]). For the concrete stone specimen, a small

increase of 14% in void ratio was accompanied by a significant reduction of 33% in shear resistance, but both values quickly returned towards the previous trends with additional gyrations.

Based on the test results from the range of material types presented herein, the behavior of the specimens during the gyratory compaction test can potentially be divided into two stages. Stage I shows a rapid decrease in void ratio primarily due to particle reorientations, which results in a significant increase in shear resistance, while Stage II yields much slower changes in both void ratio and shear resistance, which may be caused primarily by particle breakage and abrasion. This indicates that the point of maximum curvature of the gyratory compaction curves has an important physical meaning and can be used to help prevent the overcompaction of granular materials, which can cause significant degradation without greatly improving the mechanical properties.

The gyratory compaction test data can also be used to establish relationships between density, shear resistance, and compaction energy for a given granular material. An example is shown for the road rock in Figure 6.11.

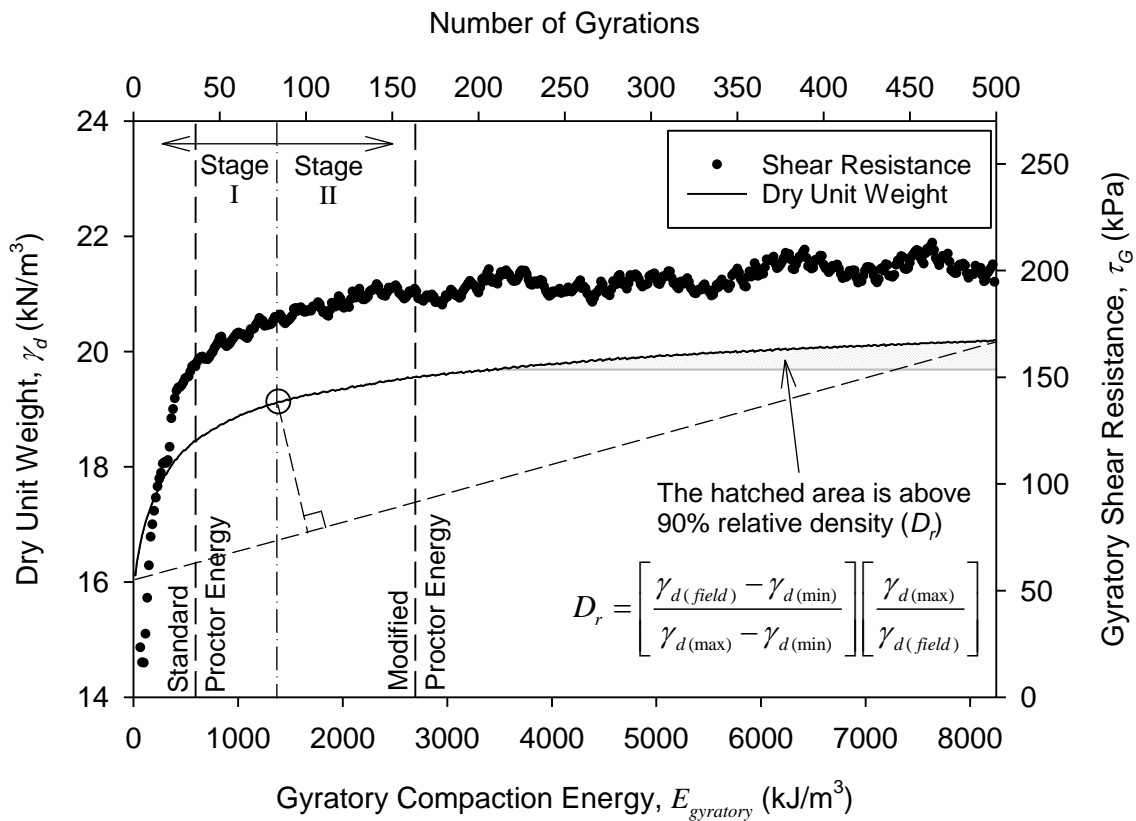


Figure 6.11. Density-shear resistance-compaction energy relationship for the road rock specimen

For the road rock specimen, both shear resistance and dry unit weight increase at a much slower rate beyond the boundary between Stage I and II, corresponding to a threshold compaction

energy level. Additionally, as discussed above, significantly more aggregate breakage may occur during Stage II. In this study, the turning point of the dry unit weight curve was used to define Stages I and II. The turning point was defined as the longest distance from the curve perpendicular to the line connecting the two ends of the curve (i.e., the minimum and maximum dry unit weights of the specimen), as shown in Figure 6.11.

As an improvement over current field specifications, which typically simply require granular material to be compacted to a certain minimum relative density (D_r), the density-shear resistance-compaction energy relationships established by the GAIA test can be used to set performance-based specifications that can give an optimum balance between compaction effort, material preservation, and performance of the compacted material, thus potentially saving significant amounts of time and energy. Further studies involving the measurement of such relationships against observations of field performance for demonstration sections of different material types and gradations is recommended.

6.9 Conclusions

In this study, the newly proposed GAIA laboratory testing method was developed and applied to five different granular materials to quickly evaluate their mechanical degradation, morphology, and shear strength under gyratory compaction.

Comparisons between GAIA and the commonly used LA abrasion test revealed four main shortcomings of the latter: (1) the standard specimen gradings of the LA abrasion test may only cover a very small range of the actual material gradation used in the field, (2) the testing mechanism that involves using steel spheres to impact or crush the aggregate in a rotating steel drum does not simulate the true field compaction or loading conditions, (3) test results determined based on an arbitrary sieve size instead of accounting for the entire gradation's change could be misleading, and (4) the testing method may not sensitively reflect the influence of a material's intrinsic properties on the abrasion characteristics of that material.

Based on the results presented herein, the newly proposed GAIA test can address all of the above issues. In addition, various parameters determined by the proposed test can be used to better understand the behavior of granular materials during compaction. The density-shear resistance-compaction energy relationship established based on the test results enables performance-based field specifications to be readily developed for the compaction of granular materials, which can ensure good performance and save time and energy.

CHAPTER 7. CONCLUSIONS AND RECOMMENDATIONS

This chapter summarizes the key findings from the laboratory study, field study, and statistical evaluations of the laboratory testing methods. Based on these key findings, a complete set of testing, design, and construction procedures is recommended for building or reconstructing and recycling granular road systems with improved performance and durability. Recommendations for future research and implementation of the results of this study are also provided.

7.1 Key Findings of the Laboratory Study

The laboratory study was conducted to evaluate the effects of gradation and plasticity on the mechanical performance of granular road surfacing materials. The laboratory soaked CBR test results showed that the undrained bearing capacity of granular surface materials does not simply increase with increasing gravel content or decreasing fines content. Instead, there is an optimum gradation (or particle size distribution and packing) that can achieve the greatest soaked bearing capacity. The multiple regression analysis conducted on the laboratory test results indicated that an optimal gradation in terms of the soaked CBR of a well-graded granular material can be predicted based on its top size and Fuller's model shape parameter (n) of the PSD curve.

Based on the laboratory test results and statistical analyses, a performance-based method for designing or specifying the gradation of granular road surface materials was proposed. Comparing the proposed method to the gradation band of the current DOT specifications, the proposed method is more performance related and can be used to develop specifications with more precise targets.

To evaluate the effects of plasticity on the performance of granular-surfaced road materials, laboratory UCS and slaking tests were conducted on samples of minus No. 40 sieved crushed limestone materials treated with different percentages of bentonite clay. For the materials tested in this study, the optimum range of plasticity index was determined to be 7 to 15 to give the best tradeoff between shear strength and slaking characteristics. The laboratory test results showed that adding plastic fines such as powdered bentonite to nonplastic granular surface materials can reduce the shear strength under wet conditions but greatly improve the slaking performance and thereby minimize loss of fines.

7.2 Key Findings of the Field Study

The field study was conducted to validate the proposed testing, design, and construction methods developed based on the laboratory study. Field granular-surfaced road and shoulder test sections were designed and constructed using the proposed methods. To help local roads agencies implement the proposed design methods and recycle existing degraded surface materials, a Microsoft Excel-based program was developed to optimize proportions of existing surface materials and two or three available fresh quarry materials to reach the target optimal gradation in terms of soaked CBR strength. Performance-based field tests were performed on the test sections following construction and after the 2016-2017 seasonal freeze-thaw period to compare

the as-constructed performance and freeze-thaw durability of the various test sections. Several groups of survey photos were also taken to visually compare the surface conditions of the various test and control sections.

The field test results further validated the performance of the proposed gradation optimization/recycling method. The test section constructed with the optimal gradation without bentonite exhibited better performance than the control section and yielded the smallest reductions in stiffness and strength among all the test sections. The test section with the optimal gradation and plasticity (with bentonite) yielded the best overall performance and the lowest dust emissions. However, visual observations and laboratory plasticity tests conducted on field samples collected periodically revealed that the bentonite decreased significantly after one freeze-thaw season. For the shoulder test sections, the field and laboratory test results also showed that precipitation and traffic can quickly wash and blow away the small amount of incorporated bentonite, significantly reducing its beneficial binding effects.

7.3 Key Findings from the Statistical Evaluation of the Laboratory Testing Methods

In this study, the commonly used laboratory testing methods for determining plasticity, gradation, morphology, and quality of granular surface materials were evaluated. Limitations and issues with the conventional tests were discussed, and alternative testing methods were evaluated and developed.

For the Atterberg limits tests, the conventional Casagrande cup and fall cone tests were evaluated and statistically compared. The analysis showed that the liquid limit determined using the fall cone test correlates very well ($R^2 = 0.98$) with that determined using the Casagrande cup test. In addition, the two-way ANOVA-based repeatability and reproducibility analysis revealed that the fall cone test exhibits much smaller overall variations than the Casagrande cup test, which is more strongly affected by the inter-operator errors. Therefore, use of the fall cone test is recommended for local roads agencies to more easily and reliably determine liquid limit compared to the Casagrande cup test. For the plastic limit test, the ASTM-recommended roller performs satisfactorily in terms of repeatability and reproducibility and eliminates one source of error in the test (i.e., variation and non-uniformity in thread diameter between different operators).

To evaluate the quality of granular surface materials, the newly proposed GAIA testing method was developed in this study and applied to five different granular materials to quickly evaluate their mechanical degradation, morphology, and shear strength under simulated field loading conditions. Comparisons between the GAIA test and the commonly used LA abrasion test revealed four main shortcomings of the latter: (1) the standard specimen gradings of the LA abrasion test may only cover a very small range of the actual material gradation used in the field; (2) the testing mechanism involves using steel spheres to impact or crush the aggregate in a rotating steel drum, which does not simulate the true field compaction or loading conditions; (3) test results are determined based on an arbitrary sieve size instead of accounting for the entire gradation's change, which could be misleading; and (4) the testing method may not sensitively reflect the influence of a material's intrinsic properties on the abrasion characteristics of that

material. Based on the evaluation results, the newly proposed GAIA test can address all of the above issues. In addition, various parameters determined by the proposed test can be used to better understand the behavior of granular materials during compaction.

7.4 Recommendations for Implementation of Research Results into Testing, Design, and Construction Procedures

Based on the key findings of the laboratory and field studies, the following complete set of testing, design, and construction procedures for building and reconstructing granular-surfaced roads is recommended:

1. Determine the road geometry and the thickness, gradation, and plasticity of the existing surface aggregate layer. To collect the design inputs, the DCP test can be used to rapidly determine the average thickness of the existing surface aggregate layer and the in situ DCP-CBR values of the surface and subgrade materials.
2. Design the thickness of the aggregate surface layer based on the in situ DCP-CBR values and traffic information. The thickness of the surface layer can be designed following the AASHTO (1993), Giroud and Han (2004), or other methods.
3. Determine the optimal PSD shape factor (n) based on the top size of the material using the proposed statistical model in Figure 3.10. Note that the statistical model was developed based on crushed limestone materials and needs further validation for other materials having significantly different particle shapes (e.g., river gravels).
4. Calculate the optimized design proportions of the existing surface materials and two or three available quarry materials using the Microsoft Excel-based program (Figure 4.20). Most quarries either do not produce custom gradations or charge extra for them, so blending two or three available quarry materials with the existing surface material is a more feasible solution to achieve the target gradation. The program will optimize the proportions of the quarry materials and calculate the needed quantity in tons per mile for each material type. Note that the quarry gradations used for the optimization should be representative.
5. For construction, the aggregate materials can be mixed in a quarry or onsite using motor graders, full-depth reclaimers, or tractor-powered reclaimers. Conventional equipment is sufficient to implement the proposed method, although compaction at optimum moisture content by a smooth drum vibratory roller is highly recommended. Quality control tests may be required to check the gradations of the quarry materials and the blended mixtures.
6. If bentonite or a local clay will be incorporated to increase the plasticity of the surface material, determine the liquid limit and plastic limit of the minus No. 40 fraction of the treated mixture using the fall cone device and ASTM plastic limit roller, respectively. It is recommended to mix the plastic fines into the top 2 to 3 in. of the roadway because they can greatly reduce shear strength of granular materials under prolonged wet conditions. When mixed into the top few inches of the surface course, the fines perform the desired function of binding the larger aggregates to reduce material loss while preserving the shear strength of the deeper aggregates in the lower part of the surface course. However, the field study showed that the small amounts of incorporated bentonite did not last more than one freeze-thaw season, so adding a larger proportion of locally available low-plasticity natural clay may be a more cost-effective solution.

7.5 Recommendations for Future Research and Further Implementation

The recommended testing, design, and construction procedures can provide state secondary roads departments with more cost-effective solutions to build or reconstruct granular road systems with improved performance and durability while optionally recycling existing surface course and subgrade materials. Some recommendations for future research activities and implementation are provided below:

- Validate or calibrate the statistical model (Figure 3.10) developed for predicting the optimum gradation of crushed limestone granular surface materials for other aggregate morphologies and mineralogy, for example, river gravel having more rounded particle shapes, or higher strength aggregates such as dolomitic limestone.
- Develop field testing equipment to more rapidly determine the gradation and morphology of granular materials, which can help to implement performance-based material selection specifications.
- Evaluate the performance and durability of using locally available low-plasticity natural clays, or clay slurries from quarrying operations, to adjust the plasticity of granular surface materials instead of using a small amount of high-plasticity bentonite clay powder.
- Construct field test sections using the proposed design and construction methods with different materials in different Iowa counties and monitor their long-term performance to assess the maintenance requirements, estimate service lifespans, and conduct life-cycle cost analyses.

To aid dissemination and implementation of the project results, the following presentations were given by the research team at various conferences and meetings throughout the project duration:

- *Stabilization and Recycling of Granular-Surfaced Roadways*. 2016. Iowa Streets and Roads Conference, Ames, IA, September 20, presented by J. C. Ashlock.
- *ISU Research on Stabilization and Recycling of Granular-Surfaced Roadways*. 2016. 70th Iowa County Engineers Conference, Ames, IA, December 7, presented by J. C. Ashlock.
- *Granular-Surfaced Road Research Results, Implementation, and Proposals*. 2017. 7th Annual County Engineers Research Focus Group, Ames, IA, February 15, presented by J. C. Ashlock.
- *Performance-Based Design and Testing Methods for Unpaved Road Surface Materials (IHRB Project TR-685)*. 2017. Mid-Continent Transportation Research Symposium, Ames, IA, August 16, presented by C. Li.
- *Summary of IHRB Project TR-685: Feasibility of Granular Road and Shoulder Recycling*. 2017. Workshop: Cost Savings and Sustainability Impacts of Using Recycled Materials along Unpaved Roadways, Institute for Transportation (InTrans), Ames, IA, September 28, presented by J. C. Ashlock.
- *Performance of Unpaved Road Construction with Recycled Materials in Council Bluffs, Iowa*. 2017. 71st Iowa County Engineers Conference, Ames, IA, December 6, presented by J. C. Ashlock.

- *Performance-Based Design Method for Gradation and Plasticity of Granular Road Surface Materials (Paper No. 18-05314)*. 2018. Transportation Research Board (TRB) Annual Meeting, Washington, DC, January 8, presented by J. C. Ashlock.

Additionally, the contents of Chapter 6 were published as a journal paper, and the January 2018 TRB conference paper mentioned above was recommended and accepted for publication in the *Transportation Research Record: Journal of the Transportation Research Board*.

The project was also featured in the *InTrans En Route* e-news story, Researchers seeking new way for counties to recycle gravel on roads, available at <http://www.intrans.iastate.edu/enroute/?action=main.item&newsID=381>.

A related research project was funded by the U.S. Environmental Protection Agency Region 7 to analyze the sustainability and costs of the field test sections in this project (US EPA Project No. 12237299, *Sustainability Analysis of Unpaved Road Construction with Recycled Materials in Council Bluffs, IA*. PI: Bora Cetin, Co-PIs: Kristen Cetin and Jeramy Ashlock). A workshop was held for this project on September 28, 2017 at InTrans in Ames, Iowa. The final report for this project will be published in 2018.

The gradation optimization spreadsheet developed in this project was posted on the Iowa County Engineers Association Service Bureau (ICEASB) website for access by all Iowa county engineers. Several county engineers have begun using the spreadsheet and providing feedback. Laboratory tests and gradation optimization analyses were also performed at ISU for trial sections constructed by Iowa county engineers for their own studies in Cass, Hamilton, and Wapello. Based on the feedback received and the requirements for those studies, an option to incorporate subgrade soils into the granular surface course mixture was added to the spreadsheet. The optimization spreadsheet was also used to design test sections in the ongoing Iowa Highway Research Board (IHRB) projects TR-704, *Performance Based Evaluation of Cost-Effective Aggregate Options for Granular Roadways*, and TR-721, *Low-Cost Rural Surface Alternatives Phase III: Demonstration Project*.

The presentation at the 2018 TRB conference also garnered significant interest from engineers from other states. Upon request, the optimization spreadsheet was sent to representatives of the Minnesota Department of Transportation and the North Dakota Local Technical Assistance Program / Upper Great Plains Transportation Institute (NDLTAP/UGPTI). The latter program also requested a two-hour webinar to convey the results of this project and demonstrate application of the optimization spreadsheet.

Several possible next steps that can be taken to help further implement the research results are given below:

1. The project team can develop a training workshop in coordination with the Iowa Local Technical Assistance Program at InTrans to describe the research project and provide hands-on demonstrations on how to use the optimization spreadsheet. County engineers would be

encouraged to bring gradations from local quarries and to have gradations from an existing granular road tested by the Iowa DOT materials laboratory, ISU, or other commercial laboratories ahead of time and bring the results with them for analysis. During the workshop, the participants would receive assistance on entering these gradations into the spreadsheet to determine the optimum mixing ratios for recycling the existing granular materials with the fresh quarry materials.

2. A short instructional video can be created to explain how the gradation optimization program was developed and demonstrate how to use it. Personnel in the Department of Civil, Construction, and Environmental Engineering at ISU who are experienced in professional video production for online course delivery can assist with this task. The video can be posted on the InTrans project webpage that will contain the final report and spreadsheet.
3. As requested by the NDLTAP/UGPTI, the PI will be conducting a one- to two-hour webinar describing the project and explaining how to use the gradation optimization program.
4. Given the interest expressed by engineers from surrounding states, a pooled-fund study could be proposed to extend the statistical model of Figure 3.10 to predict the optimum gradation of other types of granular surface materials beyond those used in this study and to develop field testing equipment to more rapidly determine the gradation and morphology of granular materials in the field.

REFERENCES

- AASHTO. 1993. *AASHTO Guide for Design of Pavement Structures*. American Association of State Highway and Transportation Officials, Washington, DC.
- Airey, G. D., A. E. Hunter, and A. C. Collop. 2008. The Effect of Asphalt Mixture Gradation and Compaction Energy on Aggregate Degradation. *Construction and Building Materials*, Vol. 22, No. 5, pp. 972–980.
- Al-Rousan, T., E. Masad, E. Tutumluer, and T. Pan. 2007. Evaluation of Image Analysis Techniques for Quantifying Aggregate Shape Characteristics. *Construction and Building Materials*, Vol. 21, No. 5, pp. 978–990.
- Anon. 1988. Gravel Road Maintenance Innovations. *Better Roads*, Vol. 58, No. 12, pp. 27–28.
- ASTM C131/C131M-14. 2014. Standard Test Method for Resistance to Degradation of Small-Size Coarse Aggregate by Abrasion and Impact in the Los Angeles Machine. *Annual Book of ASTM Standards*. ASTM International, West Conshohocken, PA.
- ASTM D2216-10. 2010. Standard Test Methods for Laboratory Determination of Water (Moisture) Content of Soil and Rock by Mass. *Annual Book of ASTM Standards*. ASTM International, West Conshohocken, PA.
- ASTM D4318-10. 2010. Standard Test Methods for Liquid Limit, Plastic Limit, and Plasticity Index of Soils. *Annual Book of ASTM Standards*. ASTM International, West Conshohocken, PA.
- ASTM E177-13. 2013. Standard Practice for Use of the Terms Precision and Bias in ASTM Test Methods. *Annual Book of ASTM Standards*. ASTM International, West Conshohocken, PA.
- ASTM E691-15. 2015. Standard Practice for Conducting an Interlaboratory Study to Determine the Precision of a Test Method. *Annual Book of ASTM Standards*. ASTM International, West Conshohocken, PA.
- Atterberg, A. 1911. Über Die Physikalische Bodenuntersuchung und Über Die Plastizität Der Tone. *Internationale Mitteilungen für Bodenkunde*, Vol. 1, Berlin, Germany.
- Bahia, H. U., and A. F. Faheem. 2007. Using the Superpave Gyratory Compactor to Estimate Rutting Resistance of Hot-Mix Asphalt. *Transportation Research E-Circular (E-C124)*. Transportation Research Board, Washington, DC.
- Barrett, P. J. 1980. The Shape of Rock Particles, A Critical Review. *Sedimentology*, Vol. 27, No. 3, pp. 291–303.
- Bauer, E. E. 1960. *History and development of the Atterberg limits tests*. ASTM STP, No. 254. ASTM International, West Conshohocken, PA.
- Belviso, R., S. Ciampoli, V. Cotecchia, and A. Federico. 1985. Use of the cone penetrometer to determine consistency limits. *Ground Engineering*, Vol. 18, No. 5, pp. 21–22.
- Bergeson, K. L., J. W. Waddingham, S. G. Brocka, and R. K. Lapke. 1995. *Bentonite Treatment for Economical Dust Reduction on Limestone Surface Secondary Roads*. Engineering Research Institute, Iowa State University, Ames, IA.
- Bergeson, K. L. and A. M. Wahbeh. 1990. *Development of an Economic Dust Palliative for Limestone Surfaced Secondary Roads*. Engineering Research Institute, Iowa State University, Ames, IA.

- Berthelot, C. and A. Carpentier. 2003. Gravel Loss Characterization and Innovative Preservation Treatments of Gravel Roads: Saskatchewan, Canada. *Eighth International Conference on Low-Volume Roads 2003*, June 22–June 25, Reno, NV, Transportation Research Record Vol. 1819, No. 2, pp. 180–184.
- British Standard (BS) 1337. 1990. Methods of tests for the classification of soil and for the determination of basic physical properties. <https://shop.bsigroup.com/ProductDetail/?pid=000000000000793481>.
- Butcher, M. 1998. Determining Gyrotory Compaction Characteristics Using Servopac Gyrotory Compactor. *Transportation Research Record: Journal of the Transportation Research Board*, No.1630, pp. 89–97.
- Casagrande, A. 1958. Notes on the Design of the Liquid Limit Device. *Géotechnique*, Vol. 8, No. 2, pp. 84–91.
- Cerni, G., and S. Camilli. 2011. Comparative Analysis of Gyrotory and Proctor Compaction Processes of Unbound Granular Materials. *Road Materials and Pavement Design*, Vol. 12, No. 2, pp. 397–421.
- Chen, X. and J. Zhang. 2016. Effect of Load Duration on Particle Breakage and Dilative Behavior of Residual Soil. *Journal of Geotechnical and Geoenvironmental Engineering*, Vol. 142, No. 9, pp. 06016008-1–06016008-7.
- Cheung, L. W. and A. Dawson. 2002. Effects of Particle and Mix Characteristics on Performance of Some Granular Materials. *Transportation Research Record: Journal of the Transportation Research Board*, Vol. 1787, pp. 90–98.
- Cho, G.-C., J. Dodds, and J. C. Santamarina. 2006. Particle Shape Effects on Packing Density, Stiffness, and Strength: Natural and Crushed Sands. *Journal of Geotechnical and Geoenvironmental Engineering*, Vol. 132, No. 5, pp. 591–602.
- DelRio-Prat, M., A. Vega-Zamanillo, D. Castro-Fresno, and M. A. Calzada-Perez. 2011. Energy Consumption during Compaction with a Gyrotory Intensive Compactor Tester. Estimation Models. *Construction and Building Materials*, Vol. 25, No. 2, pp. 979–986.
- De Vries, S. W. 2012. *Financial Needs of Iowa's County Roads*. Iowa County Engineers Association Service Bureau, West Des Moines, IA.
- Di Matteo, L. 2012. Liquid limit of low-to medium-plasticity soils: comparison between Casagrande cup and cone penetrometer test. *Bulletin of Engineering Geology and the Environment*, Vol. 71, No. 1, pp. 79–85.
- Dragoni, W., N. Prosperini, and G. Vinti. 2008. Some observations on the procedures for the determination of the liquid limit: an application on Plio-Pleistocenic clayey soils from Umbria region (Italy). *Italian Journal of Engineering Geology and Environment*, Special Issue 1, pp. 185–197.
- Fay, L., A. Kroon, K. Skorseth, R. Reid, and D. Jones, D. 2016. *NCHRP Synthesis 485: Converting Paved Roads to Unpaved*. National Cooperative Highway Research Program, Washington, DC.
- FHWA. 2014. Highway Statistics 2014. Federal Highway Administration, Washington, DC, <https://www.fhwa.dot.gov/policyinformation/statistics/2014/>.
- FHWA. 2015. *Gravel Roads Construction and Maintenance Guide*. Federal Highway Administration. <https://www.fhwa.dot.gov/construction/pubs/ots15002.pdf>.
- Fletcher, T., C. Chandan, E. Masad, and K. Sivakumar. 2003. Aggregate Imaging System for Characterizing the Shape of Fine and Coarse Aggregates. *Transportation Research Record: Journal of the Transportation Research Board*, No. 1832, pp. 67–77.

- Fojtová, L., M. Marschalko, R. Franeková, and L. Kovář, L. 2009. Study of compatibility of methods for liquid limit measurement according to Czech State Standard and newly adopted European Standard. *GeoScience Engineering*, Vol. LV, No. 1, pp. 55–68.
- Fuller, W. B. and S. E. Thompson. 1907. The laws of proportioning concrete. *ASCE Transactions*, Vol. 59, No. 2, pp. 67–143.
- Guler, M., H. U. Bahia, P. J. Bosscher, and M. E. Plesha. 2000. Device for Measuring Shear Resistance of Hot-Mix Asphalt in Gyratory Compactor. *Transportation Research Record: Journal of the Transportation Research Board*, No.1723, pp. 116–124.
- Haigh, S. K. 2012. Mechanics of the Casagrande liquid limit test. *Canadian Geotechnical Journal*, Vol. 49, No. 9, pp. 1015–1023.
- Hansbo, S. 1957. *A new approach to the determination of the shear strength of clay by the fall-cone test*, Royal Swedish Geotechnical Institute, Stockholm, Sweden.
- Hardin, B. 1985. Crushing of Soil Particles. *Journal of Geotechnical Engineering*, Vol. 111, No. 10, pp. 1177–1192.
- Harman, T., J. R. Bukowski, F. Moutier, G. Huber, and R. McGennis. 2002. History and Future Challenges of Gyratory Compaction 1939 to 2001. *Transportation Research Record: Journal of the Transportation Research Board*, No. 1789, pp. 200–207.
- Hudson, S. W., B. F. McCullough, and R. F. Carmichael, III. 1986. *Aggregate and Paved Surface Design and Rehabilitation Manual for Low-Volume Roads*. Federal Highway Administration, Washington, DC.
- Huntington, G. and K. Ksaibati. 2015. Visual Assessment System for Rating Unsealed Roads. *Transportation Research Record: Journal of the Transportation Research Board*, No. 2474, pp. 116–122.
- Igathinathane, C., L. O. Pordesimo, E. P. Columbus, W. D. Batchelor, and S. R. Methuku. 2008. Shape Identification and Particles Size Distribution from Basic Shape Parameters using ImageJ. *Computers and Electronics in Agriculture*, Vol. 63, No. 2, pp. 168–182.
- Indraratna, B., J. Lackenby, and D. Christie. 2005. Effect of Confining Pressure on the Degradation of Ballast under Cyclic Loading. *Géotechnique*, Vol. 55, No. 4, pp. 325–328.
- Indraratna, B., Y. Sun, and S. Nimbalkar. 2016. Laboratory Assessment of the Role of Particle Size Distribution on the Deformation and Degradation of Ballast under Cyclic Loading. *Journal of Geotechnical and Geoenvironmental Engineering*, Vol. 142, No. 7, pp. 04016016-1–04016016-12.
- Iowa DOT. 2011. *Iowa County Traffic Map*. Iowa Department of Transportation, Ames, IA.
- Iowa DOT. 2012. *Standard Specification for Highway and Bridge Construction*. Iowa Department of Transportation, Ames, IA.
http://publications.iowa.gov/17478/1/IADOT_Standard_Specifications_Highway_Bridge_Construction_Series_2012.pdf.
- Jahren, C. T., D. Smith, J. Thorius, M. Rukashaza-Mukome, D. White, and G. Johnson. 2005. *Economics of Upgrading an Aggregate Road*. Minnesota Department of Transportation, St. Paul, MN.
- Jones, D. 2015. Development of Provisional Specification Language for Chemical Treatments for Unpaved Roads. *Transportation Research Record: Journal of the Transportation Research Board*, No. 2473, pp. 189–199.

- Jones, D., A. Kociolek, R. Surdahl, P. Bolander, B. Drewes, M. Duran, L. Fay, G. Huntington, D. James, C. Milne, M. Nahra, A. Scott, B. Vitale, and B. Williams. 2013. *Unpaved Road Dust Management: A Successful Practitioner's Handbook*. FHWA-CFL/TD-13-001. Federal Highway Administration, Lakewood, CO.
- Jones, D., and P. Paige-Green. 2015. Limitations of Using Conventional Unpaved Road Specifications for Understanding Unpaved Road Performance. *Transportation Research Record: Journal of the Transportation Research Board*, No. 2474, pp. 30–38.
- Kodikara, J., H. N. Seneviratne, and C. V. Wijayakulasooriya. 2006. Discussion of "Using a small ring and a fall-cone to determine the plastic limit by Tao-Wei Feng." *Journal of Geotechnical and Geoenvironmental Engineering*, Vol. 132, No. 2, pp. 276–278.
- Krumbein, W. C. 1941. Measurement and Geological Significance of Shape and Roundness of Sedimentary Particles. *Journal of Sedimentary Research*, Vol. 11, No. 2, pp. 64–72.
- Krumbein, W. C. and L. L. Sloss. 1951. *Stratigraphy and Sedimentation*. W. H. Freeman & Co., San Francisco, CA.
- Kumara, G. H. A. J., K. Hayano, and K. Ogiwara. 2012. Image Analysis Techniques on Evaluation of Particle Size Distribution of Gravel. *International Journal of GEOMATE*, Vol. 3, No. 1, pp. 290–297.
- Lackenby, J., B. Indraratna, G. McDowell, and D. Christie. 2007. Effect of Confining Pressure on Ballast Degradation and Deformation under Cyclic Triaxial Loading. *Géotechnique*, Vol. 57, No. 6, pp. 527–536.
- Lade, P., J. Yamamuro, and P. Bopp. 1996. Significance of Particle Crushing in Granular Materials. *Journal of Geotechnical Engineering*, Vol. 122, No. 4, pp. 309–316.
- Lees, G. and C. K. Kennedy. 1975. Quality, Shape and Degradation of Aggregates. *Quarterly Journal of Engineering Geology*, Vol. 8, No. 3, pp. 193–209.
- Légère, G. and S. Mercier. 2004. Improving Road Performance by Using Appropriate Aggregate Specifications for Wearing Course. *Proceedings of the 6th International Symposium on Pavements Unbound (UNBAR 6)*, July 6-8, Nottingham, England, 345–353.
- Li, C. and J. C. Ashlock. 2017. *Collection of Freeze-Thaw Performance Data on Vail Avenue*. Iowa DOT Project HR-3013. Institute for Transportation and Iowa Department of Transportation, Ames, IA.
- Li, C., J. C. Ashlock, S. Lin, and P. K. R. Vennapusa. 2017a. Layered Elastic Moduli of Stabilized Unpaved Roads by Multichannel Analysis of Surface Waves and Falling Weight Deflectometer Tests. Paper presented at the Transportation Research Board 96th Annual Meeting, January 8–12, Washington DC.
- Li, C., J. C. Ashlock, D. J. White, and P. Vennapusa. 2015a. *Low-Cost Rural Surface Alternatives: Demonstration Project*. Institute for Transportation, Iowa State University, Ames, IA.
- Li, C., P. K. R. Vennapusa, J. Ashlock, and D. White, D. J. 2017b. Mechanistic-Based Comparisons for Freeze-Thaw Performance of Stabilized Unpaved Roads. *Cold Regions Science and Technology*, No. 141, pp. 97–108.
- Li, C., D. White, and P. Vennapusa. 2015b. Moisture-Density-Strength-Energy Relationships for Gyrotory Compacted Geomaterials. *Geotechnical Testing Journal*, Vol. 38, No. 4, pp. 461–473.

- Liu, Y., W. Sun, H. Nair, D.S. Lane, and L. Wang. 2016. Quantification of Aggregate Morphologic Characteristics with the Correlation to Uncompacted Void Content of Coarse Aggregates in Virginia. *Construction and Building Materials*, Vol. 124, pp. 645–655.
- Marsal, R. J. 1967. Large-Scale Testing of Rockfill Materials. *Journal of the Soil Mechanics and Foundations Division*, Vol. 93, No. 2, pp. 27–43.
- Mokwa, R. and E. Cuelho. 2008. Laboratory Testing of Soil Using the Superpave Gyrotory Compactor. Paper presented at the Transportation Research Board 87th Annual Meeting, January 13–17, Washington, DC.
- Nurmikolu, A. 2005. Degradation and Frost Susceptibility of Crushed Rock Aggregates Used in Structural Layers of Railway Track. Doctoral Thesis. Publication Vol. 567. Tampere University of Technology, Tampere, Finland.
- Oflaherty, C. A., C. E. Edgar, and D. T. Davidson. 1963. Iowa State Compaction Apparatus for Measurement of Small Soil Samples. *Highway Research Record*, No. 22, pp. 48–63.
- Ohm, H. and R. Hryciw. 2013. Translucent Segregation Table Test for Sand and Gravel Particle Size Distribution. *Geotechnical Testing Journal*, Vol. 36, No. 4, pp. 592–605.
- Özen, M. 2007. *Investigation of Relationship Between Aggregate Shape Parameters and Concrete Strength Using Imaging Techniques*. Master of Science Thesis. Middle East Technical University, Ankara, Turkey.
- Özer, M. 2009. Comparison of liquid limit values determined using the hard and soft base Casagrande apparatus and the cone penetrometer. *Bulletin of Engineering Geology and the Environment*, Vol. 68, No.3, pp. 289–296.
- Paige-Green, P. 1989. The influence of geotechnical properties on the performance of gravel wearing course materials. Doctoral Thesis. University of Pretoria, South Africa.
- Paige-Green, P. 1998. *Material selection and quality assurance for labour-based unsealed road projects*. International Labour Organisation, Advisory Support, Information Services, and Training, Nairobi, Kenya.
- Paige-Green, P. and D. Ventura. 1999. The Bar Linear Shrinkage Test – More Useful Than We Think! *Geotechnics for Developing Africa: Proceedings of the 12th Regional Conference for Africa on Soil Mechanics and Geotechnical Engineering Africa*. A.A. Balkema, Rotterdam, Netherlands.
- Pan, T., E. Tutumluer, and J. Anochie-Boateng. 2006. Aggregate Morphology Affecting Resilient Behavior of Unbound Granular Materials. *Transportation Research Record: Journal of the Transportation Research Board*, No. 1952, pp. 12–20.
- Ping, V. W., Z. Yang, M. Leonard, and S. Putcha. 2002. Laboratory Simulation of Field Compaction Characteristics on Sandy Soils. *Transportation Research Record: Journal of the Transportation Research Board*, No. 1808, pp. 84–95.
- Ping, W. V., G. Xing, M. Leonard, and Z. Yang. 2003. Evaluation of Laboratory Compaction Techniques for Simulating Field Soil Compaction (Phase II). Florida Department of Transportation, Tallahassee, FL.
- Rao, C., E. Tutumluer, and J. Stefanski. 2001. Coarse Aggregate Shape and Size Properties Using a New Image Analyzer. *Journal of Testing and Evaluation*, Vol. 29, No. 5, pp. 461–471.
- Rittenhouse, G. 1943. A Visual Method of Estimating Two-Dimensional Sphericity. *Journal of Sedimentary Petrology*, Vol. 13, No. 2, pp. 79–81.

- Sampson, L. R., D. F. C. Ventura, and D. K. Kalombo. 1992. *Linear shrinkage test: justification for its reintroduction as a standard South African test method*. National Department of Transport, Pretoria, Republic of South Africa.
- Sanders, T. G. and J. Q. Addo. 2000. Experimental road dust measurement device. *Journal of Transportation Engineering*, Vol. 126, No. 6, pp. 530–535.
- Satterthwaite, F. E. 1946. An Approximate Distribution of Estimates of Variance Components. *Biometrics Bulletin*, Vol. 2, No. 6, pp. 110–114.
- Schneider, C. A., W. S. Rasband, and K. W. Eliceiri. 2012. NIH Image to ImageJ: 25 Years of Image Analysis. *Nature Methods*, Vol. 9, No. 7, pp. 671–675.
- Sherwood, P. T., and M. D. Ryley. 1970. An Investigation of a Cone-Penetrometer Method for the Determination of the Liquid Limit. *Géotechnique*, Vol. 20, No. 2, pp. 203–208.
- Skempton, A. W. and R. D. Northey. 1952. The Sensitivity of Clays. *Géotechnique*, Vol. 3, No. 1, pp. 30–53.
- Skorseth, K. and A. A. Selim. 2000. *Gravel Roads: Maintenance and Design Manual*. Federal Highway Administration, Washington, DC.
https://www.epa.gov/sites/production/files/2015-10/documents/2003_07_24_nps_gravelroads_gravelroads.pdf.
- South Africa Department of Transport. 1990. *The structural design, construction and maintenance of unpaved roads*. Department of Transport, National Institute for Transport and Road Research, Council for Scientific and Industrial Research, Pretoria, Republic of South Africa.
- Sowers, G. F., A. Vesic, and M. Grandolfi. 1960. Penetration tests for liquid limit. ASTM STP 254. ASTM International, West Conshohocken, PA.
- Spagnoli, G. 2012. Comparison between Casagrande and drop-cone methods to calculate liquid limit for pure clay. *Canadian Journal of Soil Science*, Vol. 92, No. 6, pp. 859–864.
- TMH-A4. n.d. *The determination of the linear shrinkage of soils*. South African Technical Methods for Highways (TMH1-A4), Pretoria, Republic of South Africa.
<http://asphalt.csir.co.za/tmh/A4.pdf>.
- Tutumluer, E., C. Rao, and J. A. Stefanski. 2000. Video Image Analysis of Aggregates. Illinois Cooperative Highway and Transportation Series 278. Federal Highway Administration and Illinois Department of Transportation, Springfield, IL.
- Vallejo, L., S. Lobo-Guerrero, and K. Hammer. 2006. Degradation of a Granular Base under a Flexible Pavement: DEM Simulation. *International Journal of Geomechanics*, Vol. 6, No. 6, pp. 435–439.
- Van Zyl, G., M. Henderson, and R. Uys. 2007. Applicability of existing gravel-road deterioration models questioned. *Transportation Research Record: Journal of the Transportation Research Board*, No. 1989, pp. 217–225.
- Vardeman, S. B. and M. Jobe. 1999. *Statistical Quality Assurance Methods for Engineers*. John Wiley & Sons, Inc, New York, NY.
- Vennapusa, P. K. R., D. J. White, J. Siekmeier, and R. A. Embacher. 2012. In situ mechanistic characterisations of granular pavement foundation layers. *International Journal of Pavement Engineering*, Vol. 13, No. 1, pp. 52–67.
- Wadell, H. 1932. Volume, Shape, and Roundness of Rock Particles. *The Journal of Geology*, Vol. 40, No. 5, pp. 443–451.
- Wasti, Y. and M. H. Bezirci. 1986. Determination of the consistency limits of soils by the fall cone test. *Canadian Geotechnical Journal*, Vol. 23, No. 2, pp. 241–246.

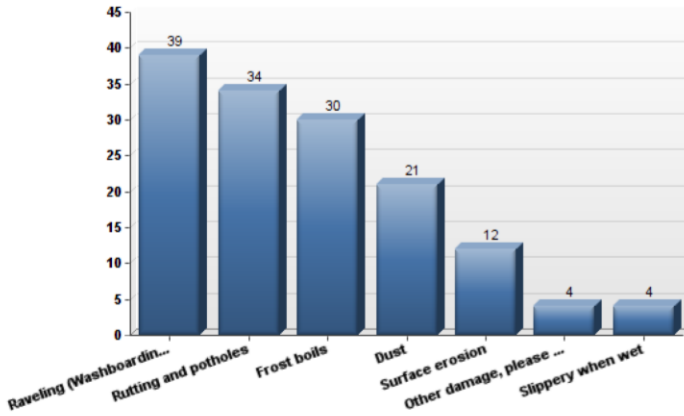
- White, D. and P. Vennapusa. 2014. Rapid In Situ Measurement of Hydraulic Conductivity for Granular Pavement Foundations. *Geo-Congress 2014 Technical Papers: Geo-Characterization and Modeling for Sustainability*. American Society of Civil Engineers, Reston, VA.
- White, D. J., P. Vennapusa, and C. T. Jahren. 2004. *Determination of the Optimum Base Characteristics for Pavements*. Center for Transportation Research and Education, Iowa State University, Ames, IA.
- Wroth, C. P. and D. M. Wood. 1978. The correlation of index properties with some basic engineering properties of soils. *Canadian Geotechnical Journal*, Vol.15, No. 2, pp. 137–145.
- Xiao, Y., E. Tutumluer, Y. Qian, and J. A. Siekmeier. 2012. Gradation Effects Influencing Mechanical Properties of Aggregate Base-Granular Subbase Materials in Minnesota. *Transportation Research Record: Journal of the Transportation Research Board*, No. 2267, pp. 14–26.
- Yue, Z. Q., W. Bekking, and I. Morin. 1995. Application of Digital Image Processing to Quantitative Study of Asphalt Concrete Microstructure. *Transportation Research Record: Journal of the Transportation Research Board*, No. 1492, pp. 53–60.
- Zeghal, M. 2009. The Impact of Grain Crushing on Road Performance. *Geotechnical and Geological Engineering*, Vol. 27, No. 4, pp. 549–558.
- Zheng, J. and R. D. Hryciw. 2015. Traditional Soil Particle Sphericity, Roundness and Surface Roughness by Computational Geometry. *Géotechnique*, Vol. 65, No. 6, pp. 494–506.

APPENDIX A. RESULTS OF SURVEY OF IOWA COUNTY ENGINEERS

Initial Report

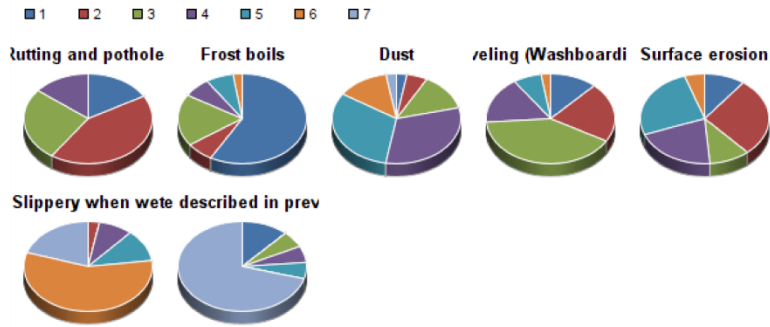
Last Modified: 09/01/2015

1. Which issues do the gravel roads suffer most in your county? (Please select the THREE most severe issues)



#	Answer	Bar	Response	%
4	Raveling (Washboarding)		39	85%
1	Rutting and potholes		34	74%
2	Frost boils		30	65%
3	Dust		21	46%
5	Surface erosion		12	26%
7	Other damage, please describe below		4	9%
6	Slippery when wet		4	9%

2. Which gravel road damage costs the most to maintain? (Please rank the damage with 1 being the most costly)



#	Answer	1	2	3	4	5	6	7	Total Responses
2	Frost boils	25	3	8	3	3	1	0	43
1	Rutting and potholes	7	18	11	6	0	0	0	42
4	Raveling (Washboarding)	5	9	17	7	3	1	0	42
5	Surface erosion	4	11	4	8	10	2	0	39
7	Other damage described in previous question	2	0	1	1	1	0	12	17
3	Dust	1	2	5	12	12	5	1	38
6	Slippery when wet	0	1	0	3	4	20	7	35
	Total	44	44	46	40	33	29	20	-

3. Based on your visual observation, typical existing surface material in your county have:

#	Answer	Bar	Response	%
1	Excessive fines caused by gravel degradation		26	59%
2	Excessive fines that have migrated from the subgrade Please describe the subgrade material (e.g., silt, clay, glacial till)		11	25%
3	Excessive fines from another source (Please identify):		6	14%
4	Loss of fines		8	18%

Excessive fines that have migrated from the subgrade Please describe the subgrade material (e.g., silt, clay, glacial till)	Excessive fines from another source (Please identify):
black mud	
We have a variety of soil types which include silt, clay and glacial till	
Loess Silty Clay	
A hilly area that the subgrade is a silty clay	
Silty clay	
clay and sandy-clay	mud from off-road sources
Silt and clay	
Clay	
	the rock is being crushed by the traveling public (particularly steel wheels and buggy traffic)
	The gravel source, the pit.
	As processed at the pit.
	Not sure of source

4. Which specifications do you currently follow to select surface course or shoulder materials for new construction or resurfacing of gravel roads in your county?

#	Answer	Bar	Response	%
1	Iowa DOT Class A Gravel Iowa DOT Class A Gravel Gradation Sieve No. Percent Passing 1 in. 100 3/4 in. 95-100 1/2 in. 70-90 No. 4 30-55 No. 8 15-40 No. 200 6-16 Plasticity Index NA Iowa DOT Class A Gravel Quality L.A. Abrasion loss 45% C Freeze 15% Clay Lumps and Friable Particles 4% Note: For shoulders only, abrasion limits may be raised to 55 if Alumina does not exceed 0.7 or A Freeze does not exceed 10.		23	55%
2	Iowa DOT Class B Gravel Iowa DOT Class B Gravel Gradation Sieve No. Percent Passing 1 in. 100 3/4 in. 95-100 1/2 in. 70-90 No. 4 30-55 No. 8 15-40 No. 200 6-16 Plasticity Index NA Iowa DOT Class B Gravel Quality L.A. Abrasion loss 55% C Freeze 15% Total of Abrasion & C Freeze 65% Clay Lumps and Friable Particles 4%		8	19%
3	Iowa DOT Class C Gravel Iowa DOT Class C Gravel Gradation Sieve No. Percent Passing 3/4 in. 100 No. 4 50-80 No. 8 25-60 No. 200 6 Plasticity Index NA Iowa DOT Class C Gravel Quality C Freeze 15% Shale (+ No. 4 (4.75mm) sieve) 10% Total of Clay Lumps and Friable Particles, plus % passing No. 200 (75µm) sieve 15% Total of Shale, Clay lumps and friable particles, plus % passing No. 200 (75 µm) sieve 20		5	12%
4	If you use other specifications for gradation, plasticity, abrasion, c freeze, or clay lumps and friable particles, please specify them below:		15	36%
5	If you provided an answer to the previous question, do you use the other specifications because of limited availability of materials in your county, or because you feel your specifications are optimum for your given materials?		13	31%
6	Are there any optimum gradations/specifications that you would recommend?		4	10%

If you use other specifications for gradation, plasticity, abrasion, c freeze, or clay lumps and friable particles, please specify them below:	If you provided an answer to the previous question, do you use the other specifications because of limited availability of materials in your county, or because you feel your specifications are optimum for your given materials?	Are there any optimum gradations/specifications that you would recommend?
1 inch 100 1/2 inch 85-100 #4 50-70 #8 25-55 #30 10-28 #200 0-10	Optimum for given pit sources	no
1 1/8-100,1-90-98, 3/4-70-90,1/2-40-70,#4 18-40,#8 10-30, #200 3-10	The pit we crush out of has shale seams and this gradation is the best we can achieve for the price we are willing to pay.	
We use both rock and gravel. This is our gravel spec. 100 passing 1"; 80-100 passing 3/4"; 68-91 passing 1/2"; 50-78 passing No. 4; 37-56 passing No. 8; 13-35 passing No. 40; 6-15 passing No. 200; Plasticity 4-12; Max Liquid Limit - 35 For rock, we use 1" Class A Roadstone	Optimum for materials. Spec was created by previous county engineer.	our gravel gradation produces good material
Gradation: 100% passing 1" 95 to 100% passing 3/4" 70-90% passing 1/2" 30-55% passing #4 15-40% passing #8 6-12% passing #200	To limit the fines and allow for a little bit larger aggregate.	
1 1/4" 100 3/4" 85-98 #4 50-67 #8 35-55 #30 10-28 #200 0-7	This is generally the type of material that can be economically produced from the naturally occurring deposits in this area. It also works well on the road. The only item we are not testing for is the plasticity of the fines.	
1" 98-100 3/4" 85-98 No.4 50-67 No.8 35-55 No.30 10-28 Finer than 200 4-10		
We use a modified class C gradation. We require that our gravel be run through a crusher to get some angularity on our large particles. Our gradation is as follows; Sieve Percent Passing 1 1/4" 100% 3/4" 80-95% #4 50-65% #8 35-50% #30 10-30%	We would like some clay fines for some plasticity in our gravel, especially in areas we treat for dust, but this material is just not available in our area.	Our gradation works for us, but the percent passing 200 is lower than we would like.
Guthrie County utilizes a "Modified" Class C gradation. 1" - 80-100%, #4 - 50-68%, #8 - 35-55%, #200 - 0-10% We do not test for plasticity, abrasion, or any of the other listed items. I should clarify that this is for gravel production only, for crushed limestone we utilize whatever the quarry produces for "road rock"	Gradation has the most quantifiable qualities for contractual purposes as well as indicator of quality. Plasticity can be indirectly quantified by experience, how it lays on the road, and physically handling the material.	
We use the materials as it comes from the pit. We do not buy material from a commercial pit.	limited availability of materials	
County 1" Road Stone Gradation: Percent passing the 1 1/4" sieve: 100% 1" sieve: 97-100% No. 4 sieve: 20-65% No. 8 sieve: 15-30% No. 200 sieve: 6-15% Max Percent Allowed Abrasion: 45% Max Percent Allowed C Freeze: 15% Max Clay Lumps and Friable Particles: 4%	With the larger truck traffic and lack of base we have tried a larger gradation on some of our roads.	
1 1/4" - 100% 1" - 90 - 100% #8 - 10 - 30% 200 - 5 - 12% Mudballs Max 4%	Optimum	
Gravel does not come from a producer, but from county leased pits. We use what we have available to us.	Limited availability of materials.	
Clinton County "Modified Class B" shall be defined as follows: 100% passing the 1-1/8" sieve, 15% to 30% passing the No. 8 sieve, 6% to 16% passing the No. 200 sieve and the abrasion shall not be more than 50%.	provides larger top size stone for soft conditions. Abrasion is more in line with what local quarries can produce	
100% passing 1-1/8" 15-30% passing #8 6-16% passing #200 Abrasion	Both	
45		Plasticity index to determine quality of fines.

5. Do the quarries provide abrasion test results for their materials?

#	Answer	Bar	Response	%
1	Yes		9	24%
2	No (If not, do you ask for their recent material abrasion tests results before purchasing?)		29	76%
Total			38	

No (If not, do you ask for their recent material abrasion tests results before purchasing?)	
not for maintenance gravel	
We have our own quarry	
But I have sent samples to DOT materials for testing.	
NO	
We have not asked. Due to limited sources of material, it becomes less relevant.	
Furnished by IDOT	
Haven't ever asked	
We do not ask for abrasion tests before purchasing.	
We do not purchase from private pits.	
We use the reports from the IDOT.	
We only have 1 quarry - so no real choice. It happens to have good material.	
no	
DOT testing as well	
yes	

6. Do most materials produced in your county (or quarries close to your county) meet the specifications?

#	Answer	Bar	Response	%
1	Yes		34	94%
2	No (If not, which part of the specifications cannot be met?)		2	6%
Total			36	

No (If not, which part of the specifications cannot be met?)	
I don't know	
We do not run tests on the materials.	

7. What is the name and location of the main quarry that you purchase gravel road materials from?

Text Response	
Hallett Materials - Cherokee LG Everistt - Washta, Akron	
County owns several gravel quarries. We also purchase from several commercial operations.	
Van Buren Co Quarry 5 miles northwest of Keosauqua in section 21-69-10	
Bruenings Brooks Quarry Nieman Gaffney Quarry	
Limestone rock comes from BMC in Fertile, IA.	
We have a source in which we crush our own. Also purchase from Martin Marietta and BMC.	
Schildberg Construction Atlantic-Crescent-- Martin Marrieta-- Fort Dodge	
Stone City Quarry	
Hallett Materials: Anthon, Wall Lake and Woodbine Our crushed limestone materials come from Martin Marietta in Fort Dodge	
Washta pit, by Washta Iowa	
We purchase from primarily county owned pits. We contract with an aggregate producer to mine our gravel pits.	
We purchase from multiple locations, depending on their proximity to the roads being rockcd. Douds Stone has two locations we purchase from in the county (West Chester & Copcock Quarries). River Products has four locations we purchase from (Keota & Young America Quarries are both in the county and Riverside Sand Plant and Columbus Junction Quarries are both right outside the county).	
Guthrie county has gravel produced from multiple sources. As of late, it's been mainly two sites. Davis Pit north of Jamaica along the N Raccoon River and the L&L Pit east of Monteith (unincorporated town).	
Stone Mill Quarry located southwest of Tipton, IA owned by Wendling Quarries	
Thomas Pit and Linien Pit	
Riverstone Group - LeClaire Quarry, McCausland Quarry, New Liberty Quarry Linwood Stone - Linwood Quarry	
River Products Wendling Quarries Martin Marrietta	
No main quarry	
Weber Stone Stone City Rd. Anamosa, IA 52205	
Schildberg's Jefferson quarry	
Martin Marietta - Dows and Ubben Quarries	
N/A	
Wendling Quarries and Preston Quarry	
Schilberg in Atlantic Iowa	
We have more than 10 quarries we use on a regular basis in the county.	
Greene County has two county owned quarries and buy from up to six (6) private suppliers.	
Jefferson County Quarry near Fairfield, IA	
Wendling Quarry - Moscow, IA	
Private sources within Boone county.	
Wendling Quarry, Montour, IA	
Milford east and west pits are both County owned. They are the two main gravel sources	
Martin Marietta in Gilmore City and Humboldt. Also Griffith Quarry (Stratford Gravel Inc.) near Humboldt. All materials Class A or 1" road stone.	
Coming Quarry, Coming	
Wendling Quarries	
Local Gravel pits at various locations	
Waterloo South	
Statistic	Value
Total Responses	36

8. What are your typical maintenance methods (e.g., dumping virgin gravel and motor grading, etc.)?

Text Response	
spreading material by truck and blading	
Gravel applied at 240-280 tons per mile every third year and spot graveling occurs on heavier traveled roads yearly.	
Yes dumping gravel and then motor grading it. In addition it is bladed on every 2-3 weeks	
Dumping new crushed limestone rock and blading.	
300 ton per mile added to 1/3 of granular roads. Regular blading with maintainer. Some roads are limestone rock, some are gravel. Rock roads are the more heavily traveled roads.	
Blading in spring to get roads in good condition. Re-rock roads with virgin material every 2 to 3 years depending on traffic.	
As described; Dumping and spreading with truck then motergrader	
roads with 100 vpd have been graded and have a macadam base placed with choke stone (6" total thickness 3" of clean 2" as macadam and 3" of Class A Road Stone as choke). Traffic below 100 vpd typically has 3" of choke stone placed every 8-10 years. We spot lodas as needed as normal maintenance. We use 6" clean base through sand or soft area as trench traetment when road is graded.	
We haul maintenance amounts (average 100 ton/mile) on the roadways each year then blade with Motor Grader. We have approximately 150 miles of roadway that we apply crushed limestone to with gravel on the remaining 700 miles.	
Spreading road gravel with a belly dump trailer. Then followed behind by a motor grader.	
We regravell roads as needed. Roads are bladed by maintainer (road grader) operators as needed.	
Blade roads with motor graders and haul virgin material (crushed limestone) to the roads. Sometimes we roll the material when it is placed.	
Spreading virgin gravel and 1" road rock from a limestone quarry with routine blading.	
Rock resurfacing, motor grading, Shoulder retrieving, etc.	
dumping gravel and/or motor grading	
Routine Blading mostly, Resurfacing every three years	
Tailgate spreading with a motor grader blading the material into the roadway.	
fly dump rock, blading as necessary	
Dumping virgin gravel and motor grading.	
dump/spread with a truck, blade when required	
Typically spot rock in the spring and then when roads firm up haul rock to each grader district. Typically 12-15 miles per year at a rate of 250-300 tons per mile. With hog confinements and grain facilities some roads have rock each year lengthening the time for other less use roads. Blading and maintenance with motor graders.	
Yes	
We re-rock every road at a minimum every fourth year at 400-600 tons per mile and haul spot rock as needed. Are standard of practice for maintenance blading is once every three weeks.	
Motor grading and placing more rock. We use mostly limestone	
Adding virgin gravel and motor grader. We have 900 miles of crushed rock road with 11 motor grader districts.	
Applying materials including virgin limestone, recycled concrete, and gravel starting early spring and maintaining with motor graders and pull behind truck drags. Begin applying yearly gravel in late spring and ending around July 4. Typical gravel road maintenance for the remaining summer.	
Dumping virgin gravel and motor grading is very typical. Regular motor grading of existing rock materials is also done.	
Dump rock and spread it. Blade road with grader.	
Dumping virgin gravel and blading with a maintainer. We use discs on shoulders to retrieve rock	
Spot rocking by placing virgin limestone and blading it in with the road.	
crushing, truck hauling and blading. On occasion, the county will repair frost boils by coring out a foot of material, placing geogrid, filling with crushed concrete and covering the "core out" with fresh gravel. While costly, this has been very successful.	
Truck spread and blade.	
Dump new rock, spread, compaction by traffic, regular blading	
roads get new rock every 3-4 years at 400 ton per mile. We haul around 140,000 tons per year for approx. 800 miles of aggregate roads (includes spot rock)	
Yes	
Statistic	Value
Total Responses	35

9. Have you tried to recycle, re-process or reclaim surface materials (other than dumping and motor-grading virgin aggregate) to rebuild or maintain existing gravel roads?

#	Answer	Bar	Response	%
1	No		26	68%
2	Yes (If yes, please briefly describe equipment you used and the performance of the roads built using recycled gravels)		12	32%
Total			38	

Yes (If yes, please briefly describe equipment you used and the performance of the roads built using recycled gravels)

Motorgrader and end loader. All that seemed to exist are fines.

We have used crushed recycled concrete in some areas. We have also used some geogrid material in unstable areas or truck haul roads.

When we are rebuilding a gravel road, we have used paddle wheel scrapers to help reclaim the existing surfacing material. This can either be done directly with the scraper cutting the material out or a motor grader blading the material in to a windrow and then picking it up with the scraper. This material is generally very high in the fines content and is a very loose/fluffy material that does not bind down real well. The material works to get landowners in and out as needed and to work in the base and help seal the top.

Minor section have been regarded to original profiles

We have a disk that is pulled with our motor grader that retrieves excess shoulder material built up over the past year. This material is dried then spread across the top of the road.

We have an Asphalt Zipper we used to process the road regrade the surface and compact. WE use recycled concrete and asphalt materials blended with the limestone without any problems.

Have used a reclaimer (looks like a short section of disk), mounted to the side of a tractor, to pull rock and earth off of the shoulder; then wind-rowed the material until the vegetation has dried and the soil has washed out of the rock, then the rock was spread with a motor grader.

Discs

We use 10-20,000 ton of crushed recycled concrete per year

10. Do you foresee any challenges for recycling surface materials for gravel roads?

Text Response

Recycling will probably involve too much clay mixed into the material

Gravel roads are not like limestone roads. They do not develop a substantial base. The subsoil must be adequate.

I would assume that the material will be on the fines size since the material has broken down and/or the larger material has been lost to the ditch.

Limited materials remain

Sounds cost prohibitive. Will it provide any benefit?

Area crushed lime stone in SW Iowa has always been soft and abrades terribly. Gravel in on the sandy side for pit run material.

in Linn County rock is cheap enough to make it impractical to process existing road instead of adding new surfacing layer.

have not had any experience with recycling

Depends on what you mean by recycling. We do not "mine" our foreslopes and ditches to reclaim lost gravel.

I'm curious as to how you are going to pick up the existing material without crushing it any further.

A few years ago I sampled gravel thicknesses around the whole county and determined that the vast majority of roads have 1.5" or less of material before hitting soil. With such thin material there appears to be no tangible value to recycling as there is very little material to recycle.

not enough material to recycle, potential cost challenge, public resistance

Typically with recycled material the fines content is higher and leave you with a slippery, muddy road.

there is no existing materials to reclaim or recycle. Most of our roads look like dirt roads.

The granite boulders buried by county crews and the contractor do not process through the mill.

Processing large amounts of subgrade material in order to recycle the aggregate. Depending on the depth of reclamation the compaction effort to restore the road bed density would be a concern as well. Aggregate prices would have to be quite high to justify the cost to reclaim aggregate from the road bed.

No

Time and money.

Dust and narrow ROW's.

Flat tire complaints if the material is too jagged. Impurities in the recycled material. Finding sufficient quantities of material to recycle in rural areas.

Yes what does the traffic drive on while you process the reclaimed material.

Not a lot to recycle. 1" limestone is beat to death and turns to lime dust.

At the cost per tone to place new rock due to the proximity of our local quarries I would think recycling aggregate from the road base would be cost prohibitive

Not at this time

Statistic	Value
Total Responses	24

11. If you have tried recycling gravel road materials, would you be willing to share your experience through a telephone interview?

Name	County	Email Address	Phone Number
Brian Keierleber	Iowa	engineer@co.buchanan.ia.us	3193346031
Jacob Thorius	Washington	engineer@co.washington.ia.us	319-653-7731
Jay Waddingham	IA	jwaddingham@co.franklin.ia.us	6414564671

Statistic	Value
Total Responses	3

12. Do you have any recommendations or ideas about this research topic? (e.g., equipment to recycle or sieve surface materials)

Text Response
no
We are going to purchase either the Asphalt Zipper or RoadHog to reclaim and help stabilize some existing roads. We will have the capability to add new material to the road and then mix the material together for hopefully an improved gradation.
I think that the volume of aggregate you would get from reclamation of the road bed would be small compared to the cost. I think that if you have that type equipment on the road and you are disturbing that much of the road bed you would want to chemically stabilize the roadbed after you recycle the aggregate to improve its strength.
No
I would start by determining what size of material is missing, add this material, then try to determine the best method for onsite/in place mixing.
No, but the topic sounds interesting.
No

Statistic	Value
Total Responses	7

13. Would you be willing to participate in the study by providing a short (1000 ft or less) section of gravel road with the problem of loss of fines, or a section of district roadway with a gravel shoulder exhibiting one of the problems mentioned above, and some equipment to assist in building the demonstration section? If yes, please provide the following information.

Name	County	Email Address	Phone Number	Roadway location for demonstration section
Brian Keierleber	Iowa	engineer@co.buchanan.ia.us	3193346031	
scott meinders	winnebago	scott.meinders@winnebagocountyiaowa.gov	641-585-2905	Forest City
Mary Kelly	Cerro Gordo	mkelly@co.cerro-gordo.ia.us	641-424-9037	Quail Ave between 130th and 140th Street
Steve Gannon	Linn County	steve.gannon@linncounty.org	319-892-6400	Linn Grove Road south from Highway 151 in 26,84,5
Patrick Mowu	Ida	idaengineer@frontiernet.net	7123642920	Many, lets visit first
Mark Nahra	Woodbury	mnahra@sioux-city.org	7128733215	in place location in county
Jacob Thorius	Washington	engineer@co.washington.ia.us	319-653-7731	
Jon Burgstrum	Scott	jon.burgstrum@scottcountyiaowa.com	563-326-8640	non specific
Greg Parker	Johnson	gparker@co.johnson.ia.us	319-356-6046	Open
Jay Waddingham	IA	jwaddingham@co.franklin.ia.us	6414564671	
Rafe Koopman	Clayton	rkoopman@claytoncountya.gov	563-245-1782	Many
Wade Weiss	Greene County	wweiss@co.greene.ia.us	5153865650	To be determined
Scott Kruse	Boone	Scottk@boonecounty.iowa.gov	515.433.0530	Do you want high or low traffic
dan eckert	dickinson	deckert@co.dickinson.ia.us	712-336-2944	any where near Milford
Todd Kinney	Clinton	tkinney@clintoncounty-ia.gov	563-244-0564	anywhere
Gary Mauer	Grundy	garym@gccourthouse.org		

Statistic	Value
Total Responses	16

APPENDIX B. FALL CONE LIQUID LIMIT AND BAR LINEAR SHRINKAGE TEST PROCEDURES

Sample Preparation (Same for Both Tests)

1. Air-dry the representative soil sample or oven-dry it at 40°C for 24 hours
2. Break down and sieve the sample through a No. 40 sieve to obtain approximately 300 g of material passing through the No. 40 sieve.
(Note: if the sample has a high clay content which cannot be easily broken down, the sample should be washed through a No. 40 sieve, and the soil slurry passing the No. 40 sieve should be oven-dried at 60°C before repeating Step 2.)
3. Add the necessary amount of distilled water to the sample and mix thoroughly to reach the consistency of a thick brownie batter.
4. Place the sample in a re-sealable zippered plastic bag and label it with the project and material names.
5. Cure the sample for at least 16 hours to allow the water uniformly distribute in the soil mass.

Fall Cone Liquid Limit Test

1. Record the dry mass and container ID of three empty moisture content containers with lids on the bottom.
2. Transfer the cured sample from the plastic bag into a mixing dish. If necessary, add water in small increments to reach a consistency of thick brownie batter, which would allow a 15 mm penetration depth of the fall cone.
3. Fill the testing cup (55 mm in diameter by 50 mm tall) with three or four lifts and push on the soil surface with a spatula and tap the testing cup on a hard surface to remove trapped air bubbles.
4. Strike off any excess material using a spatula to level the surface of the specimen.
5. Place the center of the testing cup directly under the cone and lower the cone until the tip of the cone just touches the surface of the specimen and barely marks the surface when moved slightly in the horizontal direction.
6. Lower the stem of the dial gauge until it contacts the cone shaft and zero the initial dial gauge reading.
7. Set a timer to count down 8 seconds. When the countdown timer reaches 5 sec, release the cone by pushing the release button and holding it down until the timer reaches zero to allow the cone to penetrate for a period of 5 sec.
(Note: do not bump or jerk the apparatus and make sure that your hands are not in contact with the cone shaft.)
8. After locking the cone by disengaging the release button, lower the stem of the dial gauge to contact the cone shaft and then record the final dial gauge reading to the nearest 0.1 mm.
9. The first penetration depth should be 15±2 mm, if it is not within this range, readjust the moisture content of the specimen by adding water to increase penetration or air drying to decrease penetration.
(Note: Adding dry material or oven drying the specimen is not allowed during the test.)
10. Take about 10 g of soil from the top of the specimen and place it into the moisture content container and record the total mass (container mass + wet soil).
11. Place the moisture content container in an oven at 105±5°C for at least 16h.

12. Return the rest of the material in the cup back to the mixing dish and clean the cone and the testing cup.
13. Add a small amount of water to the specimen and thoroughly mix.
14. Repeat Steps 3 through 13 to obtain two more penetration depths of 20 ± 2 mm and 25 ± 2 mm.
15. After drying the moisture content specimens for at least 16 h, cap the lid of the moisture content containers and record their total masses (container mass + dry soil).
16. Plot the moisture content versus the penetration depth using linear scales for both, and draw a best-fit straight line through the data points.
17. Using the best-fit line, record the moisture content to one decimal place as the value at which the cone penetration is 20 mm.
18. Report the LL as the moisture content recorded in the previous step rounded to the nearest whole number.

Bar Linear Shrinkage Test

1. When the penetration depth of the fall cone liquid limit specimen reaches 20 ± 2 mm, the sample can be used to conduct the bar linear shrinkage test.
2. Heat the bar linear shrinkage mold in an oven at $105 \pm 5^\circ\text{C}$ for few minutes.
3. Disassemble the mold and coat the inside wall with a paraffin wax bar.
(Note: the wax should be melted by the hot mold, so using heat gloves is required for this operation.)
4. Reassemble the mold after it cools down to room temperature.
5. Measure and record the initial length of the mold to the nearest 0.1 mm using calipers.
6. Place the mold on a glass plate and fill the trough with the soil. Remove the trapped air by pressing the soil against the inside wall of the mold.
7. Remove the excess material and level the surface of the specimen from one end to the other.
8. Flip the mold over carefully and fill up any holes and level the surface if necessary.
9. Place the mold on its side in the oven for at least 16 h, so that the soil is exposed on both vertical sides (see Figure 5.3e).
10. Take the mold out of the oven and let it cool to room temperature.
11. Remove the soil bar from the mold.
(Note: If the mold was waxed properly, the bar can be easily pushed out from one side of the mold. Otherwise, wax the inside wall of the mold more thoroughly and redo the test.)
12. If the bar appears to be straight, record three lengths of the bar to the nearest 0.1 mm using calipers.
13. If the bar is warped, place it on a white piece of paper and mark the two corners and longitudinal center of the bar, then measure the chord length and arc. Repeat for the longer side and calculate the average specimen arc length.
14. Calculate the BLS value as the percent shrinkage, i.e. 100 times the change in length divided by the original length.

**THE INSTITUTE FOR TRANSPORTATION IS THE FOCAL POINT FOR TRANSPORTATION
AT IOWA STATE UNIVERSITY.**

InTrans centers and programs perform transportation research and provide technology transfer services for government agencies and private companies;

InTrans manages its own education program for transportation students and provides K-12 resources; and

InTrans conducts local, regional, and national transportation services and continuing education programs.



**IOWA STATE
UNIVERSITY**

Visit www.InTrans.iastate.edu for color pdfs of this and other research reports.